NASA Contractor Report 3172

NASA-CR-3172
19800002784

# A Comparison of the Pitching and Plunging Response of an Oscillating Airfoil

F. O. Carta

CONTRACT NAS1-14012
OCTOBER 1979

NASA

NASA Contractor Report 3172

# A Comparison of the Pitching and Plunging Response of an Oscillating Airfoil

F. O. Carta
*United Technologies Research Center*
*East Hartford, Connecticut*

Prepared for
Langley Research Center
under Contract NAS1-14012

National Aeronautics
and Space Administration

**Scientific and Technical
Information Branch**

1979

# TABLE OF CONTENTS

TABLE OF CONTENTS (Cont'd)

# SUMMARY

Unsteady aerodynamic experiments were conducted on an oscillating SC1095 airfoil model in the United Technologies Research Center (UTRC) Oscillating Cascade Wind Tunnel, modified to perform these tests on an isolated airfoil. The model was oscillated in rigid body single-degree-of-freedom pitch about its quarter chord, and also in rigid body single-degree-of-freedom plunge to evaluate the ability of pitching data to model plunging motions. A one-to-one correspondence was established between pairs of pitching and plunging motions according to the potential flow transformation formula $\alpha = ikh$. The imposed variables of the experiment were mean incidence angle, amplitude of motion, free stream velocity, and oscillatory frequency. The unsteady aerodynamic loading was measured using pressure transducers along the chord. Numerical integrations of the unsteady pressure transducer responses were used to compute the normal force and pitching moment as functions of time.

The main objective of this program was to determine whether or not pitching and plunging data obtained according to the potential flow transformation formula were interchangeable via that formula. For convenience in performing this evaluation, the plunging data were transformed into equivalent pitching results. Over the range of parameters tested, it was found that significant differences exist between the aerodynamic responses to the two motions, particularly at high load conditions. This evaluation of the two motions was carried out by a direct comparison of force and moment loops, aerodynamic damping parameter variations, pressure time histories, pressure harmonic content, and hot film time histories.

The major finding of this study was that at high load conditions the normal force for equivalent pitch is significantly greater than that for true pitch at the same geometric incidence angle. In addition, the $C_N$ loops for equivalent pitch have higher slopes than those for true pitch. It appears that these differences are chordwise pressure manifestations of a major difference in the way in which stall flow breakdown occurs. For true pitch a conventional leading edge stall cell or vortex is formed which propagates downstream along the chord. However, there is indirect evidence to suggest that for equivalent pitch the stall cell is poorly organized and does not propagate downstream in an orderly fashion.

# INTRODUCTION

The dynamic analysis of a helicopter rotor blade involves combinations of blade pitching, plunging, and edgewise motions as well as variations in both magnitude and direction of the approach velocity vector. Although the complexity of these motions was known early in the development of helicopter rotor analyses, the initial approach to the solution of dynamic response problems customarily used quasi-steady aerodynamic inputs. This was adequate for the low performance rotor blades employed many years ago because only the 1-per-rev frequency of the cyclic motion was dominant in the dynamic system. Hence, the reduced frequency of any significant blade motion was small enough for quasi-steady data to provide a good approximation for the true (unsteady) aerodynamic response of the system.

Within the past two decades the combination of increased blade flexibility and higher performance led to increased blade torsional motions, both in elastic blade vibration and in cyclic pitch. The blade torsional vibration was of particular concern because it generally occurred over the retreating half of the rotor disk and gave every appearance of being a self-induced aerodynamic instability caused by a substantial penetration into the static stall regime. On occasion, dangerously high torsional root stresses were recorded, and, more infrequently, the mechanical couplings in the rotor hub were damaged. Consequently, a concentrated effort was begun by the helicopter industry in general and by the United Technologies Research Center (UTRC) in particular to generate a substantial body of data for airfoils oscillating in pitch about the quarter-chord, at large amplitudes of motion, and over a range of mean incidence angles sufficiently large to penetrate the static stall regime (Refs. 1 through 5). This large body of unsteady airload data has since been used extensively in computing the dynamic response of helicopter blades (Refs. 3 and 6). Moreover, it has been found (Ref. 7) that the inclusion of unsteady airloads into the stall regime can also improve the ability of the various performance analyses to predict overall disk and blade load characteristics.

Virtually all of the unsteady airload data available are for airfoil pitching motion, with the exception of a small body of data for vertical translation obtained more than ten years ago in Ref. 2, and an even smaller amount of plunging data thirty years ago in Ref. 8. However, a helicopter rotor blade is subject to a variety of motions and variable velocities including: 1) cyclic pitch at 1-per-rev, 2) pitch flexibility at approximately 4-per-rev to 8-per-rev, 3) rigid blade flapping (or plunging) at 1- and 2-per-rev, 4) elastic flatwise responses over a range of frequencies, 5) edgewise motions, 6) in-plane velocity variations from advancing to retreating sides of the disk at 1-per-rev, and 7) other variable inflow effects which introduce higher harmonics into the local approach velocity at each blade station. It is obvious that with most of the data limited to pitching motions it has been necessary to replace the variety of blade motions and air velocity changes with an equivalent pitching motion in even the most up-to-date blade response analyses. This is but one of the many assumptions made necessary by the complexity of the problem (see pp. 8-11 of Ref. 6 for an enumeration of these assumptions).

As with any analytical approach that is conditioned by a large number of assumptions, each of these assumptions can be considered suspect in the event that discrepencies occur. To date the theory has been generally successful for nominal flight conditions, but some discrepancies are occasionally found, and hence the validity of each assumption can be legitimately questioned. As shown below, the specific use of pitching data for plunging motions into the stall regime was open to question because of an apparent discrepancy in the interpretation of certain of the published results for this type of motion. Background material analytically comparing pitching and plunging motions, and the questions raised concerning the effects of stalled flow are discussed at length in the next section. The experimental program that resulted as a consequence of these doubts is the primary subject of this report and is described in detail in subsequent sections.

# LIST OF SYMBOLS

Note: Equation or figure numbers refer to the defining relationship or to the first use of the given symbol.

| | |
|---|---|
| $a$ | Dimensionless pivot axis location aft of midchord, in semichords, Fig. 1 |
| $b$ | Blade semichord, m, Fig. 1 |
| $C_M$ | Moment coefficient, Eq. (29) |
| $C_N$ | Normal force coefficient, Eq. (2) |
| $C_W$ | Work coefficient, Eq. (25) |
| $c$ | Blade chord, m, Eq. (20) |
| $E_{M_\alpha}$ | Moment magnitude error function, Eq. (50) |
| $E_{N_h}$ | Normal force magnitude error function, Eq. (16) |
| $F,G$ | Real and imaginary parts of Theodorsen function, Eq. (8) |
| $f$ | Frequency, cps, Fig. 21 |
| $h$ | Dimensionless plunging displacement, Eq. (1) |
| $h' = bh$ | Plunging displacement, m, Fig. 1 |
| $k = b\omega/U$ | Reduced frequency, Eq. (1) |
| $M$ | Moment, newton-m, Eq. (27), or Mach no., Fig. 6 |
| $M_h,M_\alpha$ | Unsteady moment functions, Eq. (41) |
| $N$ | Normal force, newton, Eq. (26) |
| $N_h,N_\alpha$ | Unsteady normal force functions, Eq. (4) |
| $n$ | Fourier integer |
| $p$ | Pressure, newton/m$^2$, Eq. (26) |

# LIST OF SYMBOLS (Cont'd)

| | |
|---|---|
| $q$ | Dynamic pressure, newton/$m^2$, Eq. (28) |
| $R$ | Rotor radius, m, Eq. (21) |
| $T$ | Period, sec, Eq. (60) |
| $t$ | Time, sec, Eq. (23) |
| $U$ | Freestream velocity, m/sec, Eq. (63) or Fig. 1 |
| $V_{TOT}$ | Rotor-tip velocity, m/sec, Eq. (20) |
| $V_w$ | Wave velocity, m/sec, Eq. (59) |
| $\bar{V}w$ | Dimensionless wave velocity, Eq. (63) |
| $X_\alpha$ | Dimensionless pivot axis location aft of quarter chord, in semichords, Eq. (4) |
| $x$ | Chordwise coordinate, m, Eq. (26) |
| $\alpha$ | Incidence angle, deg, Eq. (1) |
| $\alpha_M$ | Mean incidence angle, deg, Eq. (23) or Fig. 3 |
| $\beta = (a+1)/2$ | Dimensionless pivot axis location aft of leading edge, in chords, Eq. (27) |
| $\delta_h$ | Small quantity, Eq. (12) |
| $\epsilon_{N_h}$ | Normal force phase error function, Eq. (19) |
| $\mu$ | Rotor advance ratio, Eq. (21) |
| $\Xi$ | Aerodynamic damping parameter, Eq. (31) |
| $\phi$ | Phase angle, deg or rad, Eq. (60) |
| $\phi_M$ | Moment phase angle, deg or rad, Eq. (33) |
| $\phi_N$ | Normal force phase angle, deg or rad, Eq. (17) |

## LIST OF SYMBOLS (Cont'd)

| | |
|---|---|
| $\chi = x/c$ | Dimensionless chord |
| $\Psi$ | Rotor azimuth angle, deg or rad, Eq. (21) |
| $\Omega$ | Rotor angular velocity, rad/sec, Eq. (20) |
| $\omega$ | Frequency, rad/sec, Eq. (23) |

Subscripts, superscripts, and operators

| | |
|---|---|
| $(\ )_e$ | Equivalent motion, Eq. (1) |
| $(\ )_h$ | Plunging, Eq. (3) |
| $(\ )_I$ | Imaginary part, Eq. (2) |
| $(\ )_n$ | nth Fourier harmonic, Eq. (33) |
| $(\ )_R$ | Real part, Eq. (2) |
| $(\ )_S$ | Steady, Eq. (26) |
| $(\ )_u$ | Unsteady, Eq. (26) |
| $(\ )_\alpha$ | Pitching, Eq. (2) |
| $(\ )_{1p}$ | One-per-rev, Eq. (20) |
| $(\bar{\ })$ | Amplitude, Eq. (1) |
| $\mathrm{Re}(\ )$ | Real part of, Eq. (24) |
| $\Delta$ | Difference, Eq. (59) |
| $\oint$ | Cyclic integral, Eq. (25) |

# ANALYTICAL BACKGROUND

## Comparison of Pitching and Plunging Derivatives in Potential Flow

It will be shown in the following brief analysis that for an incompressible potential flow the normal force due to pitch and the normal force due to equivalent plunge approach the same limit as the reduced frequency becomes small. The meaning of equivalent plunge is depicted in Fig. 1 which contains the coordinate system for an oscillating airfoil in the upper portion of the figure, and which shows a pitching airfoil at some instantaneous angle of attack, $\alpha$, relative to the oncoming stream at velocity U in the lower portion. The component of U normal to the airfoil is U tan $\alpha \approx U\alpha$ for small $\alpha$, and this normal velocity component is equivalent to the normal velocity $b\dot{h}_e$ due to a plunging motion (where $h_e$ is the dimensionless equivalent plunging displacement of the airfoil). Hence $U\alpha = b\dot{h}_e$ and if $\alpha = \bar{\alpha}e^{i\omega t}$ and $h_e = \bar{h}_e e^{i\omega t}$ then the equivalence relationship is

$$\bar{\alpha} = ik\bar{h}_e . \tag{1}$$

In general, normal force due to pitch can be written in influence function form as

$$C_{N_\alpha} = (\bar{C}_{N_{\alpha R}} + i\bar{C}_{N_{\alpha I}})\,\bar{\alpha} , \tag{2}$$

and normal force due to plunge as

$$C_{N_h} = (\bar{C}_{N_{hr}} + i\bar{C}_{N_{hI}})\bar{h} , \tag{3}$$

where the barred quantities within the parentheses are the real and imaginary normal force amplitudes due to unit displacements, and where the left hand sides of Eqs. (2) and (3) are complex normal force functions associated with the specific displacements $\bar{\alpha}$ and $\bar{h}$.

For convenience, consider the traditional notation for a combined pitching and plunging motion, and write the normal force coefficient as (Refs. 9, 10, and 11)

$$C_N = -\pi k^2 \left\{ N_h\bar{h} + \left[N_\alpha - X_\alpha N_h\right] \bar{\alpha} \right\} = C_{N_\alpha} + C_{N_h} , \tag{4}$$

where $N_h$ and $N_\alpha$ are the normal force counterparts to the Smilg and Wasserman coefficients, $X_\alpha = 1/2 + a$ is the dimensionless distance in semichords of the pivot axis aft of the quarter chord, and where the right hand side of Eq. (4) shows that $C_N$ is the sum of Eqs. (2) and (3). Hence, Eqs. (2) and (3) can be replaced by

$$C_{N_\alpha} = -\pi k^2 \left[N_\alpha - X_\alpha N_h\right] \bar{\alpha} \; , \tag{5}$$

$$C_{N_h} = -\pi k^2 N_h \bar{h} \; . \tag{6}$$

Equation (5) is the normal force due to pitch and, in a potential flow, could be used to calculate the normal force due to pitch. If this normal force due to pitch were to be converted to an equivalent normal force due to plunge, the equivalence relationship of Eq. (1) would be inserted into the right hand side of Eq. (5) while the left hand side would be transformed to $C_{N_{he}}$, or

$$C_{N_\alpha} \rightarrow C_{N_{h_e}} = -i\pi k^3 \left[N_\alpha - X_\alpha N_h\right] \bar{h}_e \; . \tag{7}$$

The remainder of this section will be devoted to a comparison of Eqs. (6) and (7) for equal values of $\bar{h}$ and $\bar{h}_e$.

It can be shown (Refs. 9 and 10) that

$$k^2 N_h = k^2 + 2Gk - i2Fk \; , \tag{8}$$

$$k^2 N_\alpha = \frac{k^2}{2} + 2Gk - 2F - i(k + 2Fk + 2G) \; , \tag{9}$$

where F and G are the real and imaginary parts of the Theodorsen function (Ref. 12). When Eqs. (8) and (9) are substituted into Eqs. (6) and (7), the results are

$$C_{N_h} = -\pi k \left[2G + k - i2F\right] \bar{h} \; , \tag{10}$$

$$C_{N_{h_e}} = -\pi k \left\{ 2G + k(1 + 2F(1 - X_\alpha)) - i \left[2F - 2Gk(1 + X_\alpha) - k^2\left(\frac{1}{2} - X_\alpha\right)\right] \right\} \bar{h}_e \; . \tag{11}$$

These equations are best compared using magnitudes and phase angles of the complex numbers. For the specific application to the helicopter rotor blade, the pivot axis is at the quarter chord, so $X_\alpha = 0$. With this simplification, the normal force magnitudes can be rewritten in the form

$$|C_{N_h}| = 2\pi F k \bar{h} \sqrt{1+\delta_h} , \tag{12}$$

$$|C_{N_{h_e}}| = 2\pi F k \bar{h}_e \sqrt{1+\delta_{h_e}} , \tag{13}$$

where $\delta_h$ and $\delta_{he}$ are small quantities given by

$$\delta_h = \frac{1}{F^2} (G^2 + Gk + \frac{k^2}{4}) , \tag{14}$$

$$\delta_{h_e} = \frac{1}{F^2} \left[ G^2 + Gk + \frac{k^2}{4} (1 + 2F + 4F^2 + 4G^2) + \frac{1}{2} Gk^3 + \frac{k^4}{16} \right] . \tag{15}$$

It is seen that even the small quantities $\delta_h$ and $\delta_{he}$ differ only in terms of high order in k, and as $k \to 0$, $|C_{N_h}|$ and $|C_{N_{he}}|$ will approach one another. A magnitude error function can be defined as

$$E_{N_h} = \frac{|C_{N_h}| - |C_{N_{h_e}}|}{|C_{N_h}|} . \tag{16}$$

This function is plotted versus reduced frequency in Fig. 2, where it is shown that for $k < 0.1$ the relative magnitude error is less than one percent.

The normal force phase angle relative to true plunge and equivalent plunge can be obtained from Eqs. (10) and (11) (with $X_\alpha = 0$) as

$$\tan \phi_{N_h} = \frac{2F}{-(2G+k)} , \tag{17}$$

$$\tan \phi_{N_{h_e}} = \frac{2F-2Gk-k^2/2}{-(2G+k+2Fk)} . \tag{18}$$

Since $\phi_{N_h} \to \pi/2$ as $k \to 0$ it is possible to define a similar relative error function for phase angle having the form

$$\varepsilon_{N_h} = \frac{\phi_{N_h} - \phi_{N_{h_e}}}{\phi_{N_h}} , \tag{19}$$

which will be well behaved in the limit $k \to 0$. The results of this calculation are also plotted in Fig. 2, where it is shown that for $k < 0.1$ the relative phase angle error is less than seven percent.

Because the velocity relative to the blade varies around the rotor disk, the reduced frequency for a helicopter rotor blade also varies. A crude estimate of this variation for the 1-per-rev frequency is given by the formula

$$k_{1P} = \frac{c\Omega/2}{V_{TOT}} , \tag{20}$$

where $\Omega$ is rotor angular velocity and

$$V_{TOT} = \Omega R(1 + \mu \sin\psi) , \tag{21}$$

at the blade tip. Thus, on combining Eqs. (20) and (21),

$$k_{1P_{TIP}} = \frac{1}{\frac{2R}{c}(1 + \mu \sin\psi)} . \tag{22}$$

Typically $R/C \cong 18$ and for an advance ration of $\mu \cong 0.3$, values of $k_{1P_{TIP}}$ on the advancing and retreating sides ($\psi$ = 90 and 270 deg) lead to a 1-per-rev range of

$$\underset{\text{(advancing)}}{0.02} < k_{1P_{TIP}} < \underset{\text{(retreating)}}{0.04} .$$

Thus, according to Fig. 2, if the flow is unstalled (and hence the use of potential flow theory is justified) then pitching data (or theory) can be validly substituted with relatively little error for plunging data over the entire rotor disk for plunging motions having frequencies up to approximately 3-per-rev. However, the key statement here is the requirement for an unstalled, potential flow. The next section discusses the possible pitfalls of extending this substitution into a stalled flow regime.

## Effects of Stalling on Synthesized Plunging Response

At high angles of attack the available evidence leads to contradictory results for the analysis of plunging motions using pitching data. Consider the following facts. (1) In his now classical report on stall flutter (Ref. 8), Halfman measured the work per cycle for plunging motion for a variety of conditions including deep penetrations into the stall regime and showed that the airfoil always dissipates work to the surrounding air and hence is stable in the bending mode. (2) Rainey performed an abbreviated bending test at high $\alpha$ (Ref. 13) in which he also showed that the aerodynamic damping in bending was always positive, although the airfoil was found to respond to random buffeting. (3) A series of experiments performed at UTRC (unpublished) verified Rainey's results in that no coherent instability could be found, although the random buffeting response was observed. (4) In contrast to these results, Liiva (Ref. 14) measured the work per cycle in the plunging mode and found regions of instability for sufficiently high incidence angles. Thus, there is a basic disagreement in directly measured plunging response.

A brief analysis was performed at UTRC to determine the plunging response that would be predicted using the available pitching data from Refs. 3 and 6. The formula $U\alpha = b\dot{h}_e$ was used with the assumption of sinusoidal motion to establish the relationship

$$\alpha_R - \alpha_M = -k\bar{h}_e \sin\omega t \ , \tag{23}$$

where $\alpha_R$ is the real part of the pitching motion and where

$$h_{e_R} = \mathrm{Re}(\bar{h}_e e^{i\omega t}) = \bar{h}_e \cos\omega t \ , \tag{24}$$

is the real part of the equivalent plunging displacement which is 90 deg out of phase with respect to $\alpha_R$. (Note that $\bar{h}_e$ is the amplitude of the equivalent plunging displacement.) It can be seen from these equations that $h_{e_R} = 0$ whenever $\alpha_R - \alpha_M$ is a maximum or minimum, that $h_{e_R}$ is a positive maximum at $\alpha_R - \alpha_M = 0$ during a downward stroke and that $\bar{h}_{e_R}$ is a negative maximum at $\alpha_R - \alpha_M = 0$ during an upward stroke. This is depicted in the left-hand sketch in Fig. 3.

The right-hand sketch in Fig. 3 is a plot of $C_N$ versus $h_{e_R}$ obtained from the quasi-steady traverse of the $C_N$, $\alpha_R$ curve during one cycle of $\alpha_R$ motion, and equivalently, one cycle of $h_{e_R}$ motion. The arrow denotes the direction of increasing time. It is seen that a large loop is obtained in the

$C_N$, $h_{e_R}$ plane, even for quasi-steady motion. The area enclosed by this loop is related directly to the work per cycle done by the air on the airfoil. For the sign convention chosen here, with N positive up and h positive down, the formula for the work coefficient for plunging motion is

$$C_{W_h} = -\frac{1}{2}\oint C_{N_R} dh_R \,, \tag{25}$$

and it is seen that a clockwise enclosure, as in Fig. 3, represents negative work, which is stable.

Use was made of the UTRC α, A, B tables for a pitching airfoil (Refs. 3 and 6) and the formulas derived earlier to compute $C_N$ versus $h_{e_R}$ for a range of mean angle of attack, $\alpha_M$. Both unsteady data at k = 0.068 and quasi-steady data were used. The results of this computation are shown in Fig. 4. At low angle of attack ($\alpha_M$ = 4 deg) and in the vicinity of static stall ($\alpha_M$ = 14 deg) all loops are traversed in the clockwise direction, implying stable motion. However, at $\alpha_M$ = 18 deg, which is deeply into the stall regime, the loops, both unsteady and quasi-steady, are traversed counterclockwise, implying unstable motion. This is qualitatively in agreement with Liiva's result (Ref. 14) although a much higher mean incidence angle was necessary to attain the instability (note that Liiva's sign convention for plunge is opposite to that used here so his loops are also traversed in the reverse sense). This is shown in Fig. 5 in which Liiva's loop for $\alpha_M$ = 14.65 deg is reproduced and compared with two of the synthesized UTRC loops of Fig. 4, for $\alpha_M$ = 14 deg in the left panel and for $\alpha_M$ = 18 deg in the right panel. However, despite this qualitative agreement with Liiva's work a number of troublesome questions arise which must be answered.

The first question is concerned with the lack of consistency between the apparently contradictory experimental results in which both stable and unstable work cycles have been measured. These results are summarized in Fig. 6 in which the work per cycle for a plunging motion, normalized with respect to the theoretical value, has been plotted versus mean angle of attack. The two upper panels have been plotted from Halfman's tabulated results (Ref. 8) for the intermediate and the sharp blades, both 12 percent thick. Halfman had a fixed amplitude of 0.9 in., which can be expressed in semichords as $\bar{h}$ = 0.155, and his tests were performed over a range of reduced frequencies from k = 0.09 to k = 0.33. None of his measurements showed an instability, although the sharp blade at k = 0.09 had a much smaller stable margin than the other conditions. The lower left panel was extracted from Rainey's plot (Ref. 13) for his 10 percent thick blade. His amplitude range was smaller than Halfman's, $.015 < \bar{h} < .055$, and his maximum reduced frequency was greater, up to k = 0.45. His system increased its stability as the angle of attack was increased. The lower right panel is taken from Liiva's paper, Ref. 14, for a 10 percent thick blade. His reduced frequency was fixed at k = 0.068, which is smaller than the other cited work, and his amplitude range, $0.31 < \bar{h} < 0.62$, is greater. Here a strong penetration into the unstable range has been measured, in contrast to the results of the other investigators. Liiva acknowledges these differences and suggests that his higher Mach number and larger amplitudes may be the reasons. While these may be contributing factors, it may also be possible that the small value of reduced frequency in Ref. 14 could account for this unstable behavior. Note the trend toward lowered stability in the upper right panel as k is decreased. It is also possible that the higher Mach numbers have a more complicated effect than that cited by Liiva. In Ref. 14 the result for $M = 0.6$ appears to have the same stability boundary, but becomes unstable less precipitously. Thus, it appears that many more questions are raised than are answered by these few available pieces of information.

A second important factor is that there is no known experimental evidence in the available literature for free flutter of an isolated airfoil in single degree-of-freedom plunging motion. There is ample evidence that such an airfoil will buffet if $\alpha_M$ is sufficiently large but this is a random response phenomenon and cannot be classified in the same sense as single-degree-of-freedom torsional stall flutter. This second consideration implies that a more complete investigation must be made into the meaning of the "unstable" work cycles to determine if this apparent instability is manifested as buffet or if it simply does not exist. In this connection, note that the right-hand panel of Fig. 4 shows both the unsteady and quasi-steady plunging loops obtained from pitching data to be unstable. The generation of an unstable quasi-steady loop in plunging at $\alpha_M$ beyond stall can be simply explained by referring to Fig. 3 and repeating the process for a steady $C_N$, $\alpha_R$ curve with negative slope (typical of steady operation beyond the stall angle). However, the meaning of such a quasi-steady loop is more difficult to interpret in view of the implied instability as zero frequency is approached. This is in contrast to the more physically palatable neutral stability limit in torsional stall flutter as reduced frequency approaches zero (Ref. 15). Thus, the analysis of plunging motions using pitching data leads to further possible inconsistencies when dynamic loops and quasi-steady loops are compared.

Underlying all of these questions is the fact that current analytical procedures for rotor blades must rely on these same tables of pitching data (or on equivalent pitching results) to predict plunging response. The complexity of the possible motions which must be synthesized was outlined earlier. These motions have both large amplitudes at low frequencies and small amplitudes at high frequencies, and can occur in potential flow on the advancing blade and in stalled flow on the retreating blade. In short, the necessity to synthesize these motions may, in many cases, lead to parameter values which lie outside the region where such a synthesis is valid, particularly in the high incidence angle regime. Furthermore, the only known data presently available for plunging motions do not form a self-consistent set, nor do any individual data sets cover large enough parameter ranges to be useful.

## Examination of Existing Plunging Data

It could be argued that the existing body of plunging data (in Refs. 2, 8 and 13) could be used to serve the needs of designers who wish to account for the separate pitching and plunging movements of rotor blades. However, the issue is not the availability of such data but the validity of the customary practice of using pitching data to predict plunging response. Thus, the primary requirement of this investigation is a direct one-to-one comparison of pitching and plunging data in which as many individual aspects of the data as possible are compared under identical external conditions. Not only is it necessary to compare lift and pitching moment time histories, but pressure distributions and separation behavior as well must be compared on a timewise basis. Furthermore, the requirement for identical external conditions encompasses not only free stream Mach number and mean incidence angle, but it also requires satisfaction of the equivalence relationship in Eq. (1).

The work reported in Ref. 8 can be immediately discarded since it cannot satisfy the requirements cited above. These results were measured using a balance and only lift and moment data are available. Furthermore, only average or first harmonic data were tabulated so it is impossible to reconstruct the time history of either lift or moment. Rainey's results (Ref. 13) are even more limited.

Liiva's tabulated data in Ref. 2 offered some hope of meeting these requirments but a careful examination of his tabulated parameter values showed that none of the plunging amplitudes produced equivalent pitching amplitudes that coincided with any of the actual pitching amplitudes. This is acknowledged in Ref. 16 in which Liiva's pitching and plunging data were compared. Here the authors concluded that although several cases were found in which a reasonable match existed there were no sets of data in which all conditions ($\alpha_M$, k, equivalent amplitudes) coincided with sufficient accuracy. Furthermore, of the sets selected for examination there was not systematic parameter variation from which trends could be established (cf. Table I of Ref. 16). (Obviously, at the time Liiva obtained his results there was no reason to expect that it would be important to provide such a one-to-one correspondence in pitch and plunge.) Thus, although the results in Ref. 16 point to significant differences between pitching and plunging responses, it is not clear that these are solely ascribed to the dissimilarity in the generating motions.

The experimental program described below was designed with the specific objective of satisfying the one-to-one correspondence of Eq. (1). It will be shown in subsequent sections that in most cases, sufficient accuracy was achieved to permit a valid and rational comparison to be made between the pitching and plunging responses. Further, the parameters of the problem were varied systematically and it was possible to examine these results for trends.

# WIND TUNNEL AND EXPERIMENTAL EQUIPMENT

## Wind Tunnel and Air Supply

The experimental program was carried out in the UTRC Oscillating Cascade Wind Tunnel (OCWT) which was modified to perform these tests on an isolated airfoil. In its cascade configuration it is completely described in Ref. 17. The main test section of this facility is 25.4 cm (10 in.) wide and 63.5 cm (25 in.) high. It receives its air from atmosphere through an upstream bellmouth and discharges downstream through two centrifugal compressors operating in a vacuum mode. Sidewall boundary layer slots are located 34.3 cm (13.5 in.) ahead of the blade quarter chord bearing mount. For a 15.24 cm (6 in.) chord blade the slots are 30.5 cm (or 2 chord lengths) ahead of the blade leading edge. Each slot opens to its own plenum and each plenum is separately vented to a common line which is evacuated by an auxiliary vacuum pump. Adequate vacuum was obtained at a free stream speed of 61 m/sec (200 ft/sec) and below to produce a boundary layer thickness of approximately 2 percent of the tunnel width on either wall, based on recovery to within 98 percent of free stream velocity.

## Test Airfoil and Drive Systems

The airfoil used in this test was a 15.24 cm (6 in.) chord Sikorsky SC1095 profile, having a span of 25.4 cm (10 in.). Its coordinates, in dimensionless form, are presented in Table I, and a cross section view is shown in Fig. 7. (Also shown in Fig. 7 are coordinate locations of the blade instrumentation which will be discussed presently.) A photograph of the disassembled model prior to transducer installation is shown in Fig. 8. It is seen that the model consisted of two primary parts: a steel nose region, including the cylindrical pivot shafts at the quarter chord, and a magnesium region aft of the quarter-chord. Cylindrical tungsten slugs were inserted in the nose region to balance the model about its quarter-chord pivot axis. (The measured center of gravity location was 0.7 percent chord aft of the pivot axis.) Also shown are the channels cut into the blade surfaces to house the pressure transducers and their lead wires. A view of the model after all instrumentation was installed and assembly was completed is found in Fig. 9.

The airfoil was driven in a sinusoidal motion, either pitching or plunging, by a constant speed, 5600 watt (7.5 hp) electric motor with a continuously variable speed transmission through a timing belt and pulleys. For pitching motions a four-bar linkage (described in detail in Ref. 17 and shown here in Fig. 10) was used to drive the blade from one side. Three cams were used to produce the three pitching amplitudes of 2, 5, and 8 deg, each with less than

0.6 percent second harmonic waveform distortion. Plunging motions were accomplished by driving the blade vertically in sealed sidewall slots with a similar cam-push-rod arrangment, as depicted in Fig. 11. Here an eccentric cam was directly linked to the blade shaft on both sides of the tunnel through two connecting rods, and the blade shaft was constrained to move vertically along slide bars mounted vertically on the tunnel wall. Again three cams were used to produce the three plunging amplitudes of 2.54, 3.81, and 5.08 cm (1, 1.5, and 2 in.), or in semichords, $\bar{h}$ = 1/3, 1/2, 2/3. No second harmonic distortion was present in the plunging motion.

## Instrumentation

Conventional pneumatic wind tunnel instrumentation was used to measure flow properties in the test section, as described in Ref. 17. In addition to the measurements cited there, an upstream wedge probe, located midway between the blade leading edge and the sidewall suction slot leading edge, was used to insure correct alignment of the inlet flow relative to the model attitude.

As shown in Figs. 8 and 9, ten miniature pressure transducers were mounted on each airfoil surface along the center span, from 1.2 to 91 percent chord (cf. Table II) in a Gaussian array (Ref. 17). All of these devices were single surface absolute transducers rated at ± 0.34 atmospheres (± 5 psi) relative to ambient pressure, with nominal sensitivities of 0.68 mV/atmos (10 mV/psi) at 10 V excitation. Each transducer output was ac-coupled to yield only the oscillatory component, and a pneumatic orifice located next to each transducer was used to record the time-mean pressure distribution. Further details on specifications and installation will be found in Ref. 4. In addition, ten hot films were applied to the suction surface in a staggered array from 2.5 to 91.7 percent chord (cf. Table II for location and Ref. 4 for details). A plan view of the model showing the locations of all suction surface measuring stations is presented in Fig. 12.

Airfoil pitching motion was measured using a linear transformer fixed to the 4-bar linkage. Plunging motion output voltage was produced by the variable overlap of two faces of a rectangular capacitor fixed to the tunnel sidewall and to the vertical plunge mechanism.

# TEST PROGRAM AND COMPUTATIONAL PROCEDURES

## Calibration Procedures

Prior to testing, all pressure transducers were individually calibrated. A vacuum line was applied to each location and the diaphragm of each transducer was subjected to pressures approximately 84 cm $H_2O$ (33 in. $H_2O$) below atmosphere. The calibration curves are essentially linear. In addition to static calibrations, no-flow dynamic tare tests were performed, with emphasis on plunge, at the highest expected frequency. Transducer output was negligible.

## Test Plan

A test plan was conceived, governed by Eq. (1) and the principles of one-to-one correspondence and systematic variation discussed above, but tempered by several constraints involving tunnel operating limits and model drive system load limits. The resulting program was therefore bounded by a maximum free stream velocity of 61 m/sec (200 ft/sec), a maximum plunging acceleration of 31 g's, and a maximum frequency of 16.67 cps. The original test plan contained 30 points each in pitch and plunge which are listed in Tables III and IV. In each table the left column is sequentially numbered to define the table item number, the right column contains the corresponding item number from the other table (one-to-one correspondence), and the subscript e denotes the equivalent amplitude. All other headings are self-explanatory. In the course of the experiment several additional points in the pitching mode were run to extend some data trends, and these will be discussed presently.

## Unsteady Data Acquisition

Two FM tape recorders were employed to record the data for subsequent digitizing and computer processing. Virtually the same system was used in this test as in Ref. 4 which contains further details and a system block diagram.

## Force and Moment Computation Procedure

The unsteady aerodynamic normal force and pitching moment are obtained by integrating the time-dependent pressure distribution on each surface independently and then taking the difference between the upper and lower surface loads. The equations are

$$N(t) = -\underbrace{\int_0^c (p_u(x,t) + p_s(x))dx}_{\text{suction surface}} + \underbrace{\int_0^c (p_u(x,t) + p_s(x))dx}_{\text{pressure surface}} \qquad (26)$$

and

$$M(t) = -\underset{\text{suction surface}}{\int_0^c} (p_u(x,t) + p_s(x))(\beta c - x)dx + \underset{\text{pressure surface}}{\int_0^c} (p_u(x,t) + p_s(x))(\beta c - x)dx \; , \qquad (27)$$

where subscripts u and s represent the unsteady and steady-state values, respectively. The quantity c is the airfoil chord length and $\beta c$ is the pivot axis location relative to the leading edge (where $\beta = (a+1)/2$). In the present case, $\beta = 0.25$. Equations (26) and (27) were numerically computed from the recorded data using the Gaussian quadrature procedure with extrapolation to the trailing edge (Ref. 3). The conventional dimensionless coefficients were obtained from the formulas

$$C_N(t) = N(t)/qc \; , \qquad (28)$$

$$C_M(t) = M(t)/qc^2 , \qquad (29)$$

where $q = 0.5\ \rho U^2$ is the free stream dynamic pressure.

The sign convention in Eqs. (26) through (29) defines the normal force to be positive upward and the moment to be positive in the nose up direction. These integrations are performed with the tacit assumption that the flow is two-dimensional near the instrumented mid-span region and that, as a result, the quantities $C_N(t)$ and $C_M(t)$ are per-unit-span values.

## Aerodynamic Damping Computation Procedure

The prediction of airfoil stability for either pitching or plunging motions is related to the prediction of the transfer of energy between either of these motions and the surrounding unsteady flow environment. The energy transfer is computed in terms of the work per cycle coefficient, given by

$$C_{W_\alpha} = \oint C_{M_R} d\alpha_R \; , \qquad (30)$$

for pitching motions and by Eq. (25) for plunging motions. When the motion is purely sinusoidal the corresponding aerodynamic damping parameter for each motion is obtained from the expressions

$$\Xi_\alpha = - \frac{C_{W_\alpha}}{\pi \bar{\alpha}^2} , \tag{31}$$

$$\Xi_h = - \frac{C_{W_h}}{\frac{\pi}{2} \bar{h}^2} . \tag{32}$$

When $\Xi$ is positive (work done by the airfoil) there is a net transfer of energy from the airfoil to the airstream and the motion is stable. Conversely, a negative value of $\Xi$ represents an unstable motion.

If $C_{M_R}$ and $C_{N_R}$ are expressed in terms of their Fourier coefficient representations,

$$C_{M_R} = \sum_n C_{M_n} \sin (n\omega t + \phi_{M_n}) , \tag{33}$$

$$C_{N_R} = \sum_n C_{N_n} \sin (n\omega t + \phi_{N_n}) , \tag{34}$$

then the integrals of Eqs. (25) and (30) simplify through orthogonality to yield the formulas

$$\Xi_\alpha = - \frac{C_{M_1}}{\bar{\alpha}} \sin \phi_{M_1} , \tag{35}$$

$$\Xi_h = \frac{C_{N1}}{\bar{h}} \sin \phi_{N1} , \tag{36}$$

where $C_{M_n}$ and $C_{N_n}$ are the nth harmonic components of the moment and normal force amplitudes, and $\phi_{M_n}$ and $\phi_{N_n}$ are their corresponding phase angles relative to $\alpha$ and h (positive for the moment or force leading the blade motion). It is seen from Eqs. (35) and (36) that for simple harmonic motions, only the first harmonic component of the response is relevant to the stability of the motion. Furthermore, stability is determined only by the algebraic sign of the phase angle. (Note that there is a sign difference between the two expressions because normal force and plunging deflection are defined to be positive in opposite directions.) These equations were used in the present report to evaluate the experimentally measured damping parameters. For convenience in comparing theory with experiment the evaluation of these equations using the potential flow analysis yields the theoretical expressions

$$\Xi_\alpha = \frac{\pi k}{2} , \tag{37}$$

$$\Xi_h = 2\pi kF . \tag{38}$$

## STEADY-STATE RESULTS

Steady-state tests were conducted at free stream speeds of $U = 30.5$ and 61 m/sec (100 and 200 ft/sec) using only the pneumatic instrumentation in the model, and computations of normal force and moment coefficient were obtained via Eqs. (26) through (29). These results are presented in Figs. 13 and 14. Although stall occurs at approximately the same incidence angle (16 deg for $C_N$ and $C_M$) for both speeds, it is seen that at 61 m/sec both the slope and the maximum value of $C_N$ are higher than at 30.5 m/sec. This may be ascribed to the Reynolds number range over which these tests were run; namely, $Re \cong 3.15 \times 10^5$ at 30.5 m/sec and $Re = 6.3 \times 10^5$ at 61 m/sec. Since the critical Reynolds number for transition is approximately $Re \cong 5 \times 10^5$ (cf. Ref. 18) this difference in $C_N$ behavior is not unexpected. However, this is not likely to affect the basic purpose of this investigation since the comparisons to be made invariably involve pitching and plunging cases run at the same free stream conditions, and hence at the same Reynolds number.

# UNSTEADY RESULTS

## General Considerations

It is useful in the present study to begin the examination of pitch versus plunge with a discussion of the aerodynamic damping characteristics of the motions. This is because such an examination can be performed globally on all cases at once and can immediately highlight the specific conditions to be studied and compared in detail. This is the approach which will be used herein.

In the earlier sections of this report use was made of Eq. (1) to transform pitching theory into equivalent plunge since the usual practice in load calculations is to use pitching data to predict plunging response, and it was useful to examine the theoretical results from that vantage point. It makes no difference, however, which motion is transformed, and in this section the measured plunging data will be transformed via Eq. (1) to equivalent pitch. This is done because the existing literature on unsteady pitching data has made dynamic stall in pitch familiar to most researchers in this field, whereas no comparable familiarity exits for plunging effects. Nevertheless, actual plunging response will also be discussed.

Before proceeding with this study, the reader is cautioned that any stability results obtained for equivalent pitching motions are not "true" results in the sense that a pitching instability could or could not happen. Rather, the transformed results are presented only for comparison so a judgment can be made on the validity of the transformation.

## Discussion of Aerodynamic Damping

The aerodynamic damping parameter was computed for all test points run. Equation (31) was used directly for pitching cases, and with the transformation of Eq. (1) applied to the motion, was also used to compute the equivalent pitch damping for all plunging cases. Equation (32) was used directly for plunging motions. The results of these calculations are found in Tables V and VI in which blocks of data are arranged for increasing amplitude from left to right and increasing incidence angle from top to bottom. Within each block are found values of reduced frequency and their associated values of damping parameter. The number in parentheses to the left of the reduced frequency is the appropriate item number for pitch or plunge to permit these values to be referred back to the original test plans in Tables III and IV.

In Table V there are two columns of values of damping parameter, labeled $\Xi_\alpha$ and $\Xi_{\alpha e}$ for damping in pitch and equivalent pitch, respectively. Each has its own reduced frequency and item number. Also, appended to the bottom of this table are several additional points not originally included in the test plan. It will be seen that these values are useful in extending the curves to be discussed presently. Table VI contains only the damping in plunge values.

The values of damping in pitch and in equivalent pitch from Table V are plotted in Figs. 15 through 18. First consider Fig. 15 which is arranged in four parts, one for each value of mean incidence angle, $\alpha_M = 2, 9, 12, 15$ deg. Each part has three panels, one for each value of amplitude, $\bar{\alpha} = 2, 5, 8$ deg. In this set the circled points are for actual pitch and the triangular points are for equivalent pitch. The solid line is the theoretical variation from Eq. (37). It is seen that in several panels there is local agreement between $\Xi_\alpha$ and $\Xi_{\alpha e}$ in the neighborhood of $k = 0.12$, but there is a strong disagreement between the two at virtually all other values of k. For the three lowest incidence angles and for the smallest amplitude at $\alpha_M = 15$ deg, the damping in pitch tends to follow the theoretical curve. This is further illustrated in Fig. 16 in which all damping in pitch measurements, including extra points, have been plotted. In sharp contrast to these results, the damping in equivalent pitch plotted in Fig. 15 tends to be negative for small values of k, positive for large values of k, and appears to follow a trend line that is considerably steeper than the theory. More will be said about this presently.

The behavior of the damping in pitch, shown in Fig. 16, carries no surprises compared with results of previous investigations. At low incidence angle, the measured values follow the theory, and at high incidence, if the amplitude is sufficiently large to penetrate stall, the values trend toward negative damping. Note, for example, that at $\alpha = 15 \pm 2$ deg (left panel) there is little or no stall penetration and the results still follow the theory. In contrast to this, at $\alpha = 15 \pm 5$ deg (center panel) and $\alpha = 15 \pm 8$ deg (right panel), sufficient stall penetration has occurred to produce negative damping (dashed curves).

Figure 17 is the equivalent pitch damping counterpart to Fig. 16. With the exception of the values for $\alpha_e = 15 \pm 5$ deg and $\alpha_e = 15 \pm 8$ deg (diamond points in center and right panels), all of the plotted points trend strongly from lower left to upper right. This is verified in Fig. 18 in which all points except those for $\alpha_e = 15 \pm 5$ deg and $\alpha_e = 15 \pm 8$ deg have been plotted in a composite form. It is seen that the values here are well correlated from lower left to upper right, and since each value represents an independent measurement made over a wide variety of parameter values, this correlation lends credence to the validity of the observed behavior. There are two theoretical damping curves in Fig. 18; the solid curve is for true pitch, computed from Eq. (37), and the dashed curve is for equivalent pitch which is shown in Appendix I to be significantly different from Eq. (37). The sharp disagreement between pitching theory and equivalent pitch measurements is indicative of the inability to transform analytically from one motion to another, at least with respect to damping in pitch. However, this is only one aspect of the transformation problem, and other factors must also be considered.

The damping in plunge values from Table VI have been plotted in Figs. 19 and 20. Figure 19 is comparable to Fig. 15 in that it is comprised of four parts with three panels on each such that all combinations of incidence angle and plunging amplitude are displayed separately. The solid line is the theoretical variation from Eq. (38). Here it is seen that there is no obvious evidence of stall in that there is no departure of any of the points from the trend established by all points. In virtually every case, the measured value is in reasonable agreement with but is somewhat greater than theory, and the difference between theory and experiment grows with reduced frequency. This is further emphasized by the composite plot of Fig. 20 in which all points are included. As in Fig. 18, there is a coherent trend of all the data, but here even the results that are associated with stall penetration are well correlated.

It would appear, based on these results, that normal force due to plunge is less sensitive to stall effects than moment due to pitch, since these are the constituent parts of the aerodynamic damping just discussed, and only damping in pitch shows any effect of stall. However, it will be seen in the next section that although the large departures from the quasi-steady moment usually associated with stall are not necessarily present in the unsteady normal force due to plunge, there is, nevertheless, a sufficient disparity between actual and equivalent total load to cast some doubt on the validity of the pitch-plunge transformation.

Finally, the question of plunging instability must be considered. Unlike the lower right panel of Fig. 6 (from Ref. 14), the results in Fig. 20 show no tendency for an instability to occur as incidence angle is increased. Although the amplitude range of both experiments was substantially the same, it should be noted that there was a significant difference in Mach number. The higher Mach number of Ref. 14 was cited in an earlier section as a possible explanation for the emergence of an unstable region in Fig. 6, and without an equivalently high Mach number in the present experiment, this question must remain moot.

## Normal Force and Pitching Moment Loops

As in Ref. 4, all loops described in this report were the result of integrating the chordwise pressures (Eqs. (26) and (27)), converting to coefficient form (Eqs. (28) and (29)), and cycle-averaging over five complete cycles of data. Loops of normal force and pitching moment coefficient versus incidence angle for both pitch and equivalent pitch are found in Figs. 21 through 49, arranged according to the order of the columnar items in Table V. For example, Figs. 21 through 30 are for $\bar{\alpha}$ = 2 deg, increasing in incidence from $\alpha_M$ = 9 deg (Figs. 21-24), through 12 deg (Figs. 25 and 26), to 15 deg (Figs. 27-30), and for increasing k within each block. Similarly, Figs. 31-46 are for $\bar{\alpha}$ = 5 deg and Figs. 47-49 are for $\bar{\alpha}$ = 8 deg. Note that items 27-pitch and 22-plunge ($\bar{\alpha}$ = 8 deg and $\alpha_M$ = 9 deg) are not included in these figures, because a large difference in frequency prevents them from being comparable on a one-to-one basis as all other pairs of loops are.

In each figure the solid curve denotes the pitching loop and the dashed curve denotes the equivalent pitching loop. Arrows indicate the direction of increasing time. A tabulation on each figure lists the item number and the actual values of the run parameters for each motion. In the following discussion, each amplitude will be considered separately.

In general, for the low amplitude runs (Figs. 21-30), the shapes of the loops for pitch and equivalent pitch are substantially the same, but with some notable exceptions. In Figs. 21, 22, 27, and 28 for example, the moment for equivalent pitch is traversed clockwise, indicating an unstable motion (Refs. 1-4), while the moment for actual pitch is traversed counterclockwise, indicating stability. In several of the figures the normal force loop for equivalent pitch is significantly distorted relative to the traditional shape, and in virtually every case the $C_N$ loop for equivalent pitch has a greater slope than that for true pitch. Nevertheless, the shapes of the loops are not significantly altered in going from pitch to equivalent pitch, and this is probably because there is little or no penetration into stall for a pitching amplitude of $\bar{\alpha} = 2$ deg. (Note that the negative damping in equivalent pitch occurs only at low reduced frequency and accounts for all four unstable points in Fig. 18.)

Before proceeding further, the reader should note that throughout the set of data shown in Figs. 21 through 49 there are occasional displacements between the mean values of the equivalent pitch loops and the true pitch loops. The source of these discrepancies is not known at this time. One possibility is the tendency for the pneumatic tubing used for time-mean pressure measurements to suffer fatigue failures during the early portion of the plunging test. Under these circumstances, it was necessary to fair the pressure distribution through the few missing values to arrive at an estimated integrated load. However, this explanation is not entirely satisfying since in several cases a vertical displacement is noted for $C_N$ and not for $C_M$ (or vice versa), and in several cases, discrepancies exist for runs in which all pneumatic tubes were intact. Hence, the observed effect may actually be associated with an alteration of the flow characteristics over the airfoil due to change in motion and may not be an error.

The next group of data to be considered, in Figs. 31 through 46, is for $\bar{\alpha} = 5$ deg and constitutes the largest part of the data obtained herein. Thus, it is useful to study these results in separate groups of constant mean incidence angle. First, in Figs. 31-33, for $\alpha_M = 2$ deg, all the loops for equivalent pitch increase in size more rapidly than those for true pitch as k increases. Also, for the two lowest values of k, the slopes of the $C_N$ loops for equivalent pitch are greater than those for true pitch. In particular, in Fig. 31, the discrepancy in peak $C_N$ is approximately 40 percent of the $C_N$ due to true pitch, and this type of load difference occurs repeatedly throughout the data set.

In the cases for $\alpha = 9 \pm 5$ deg (Figs. 34-38) and $\alpha = 12 \pm 5$ deg (Figs. 39-41), the same basic trend is observed; namely, the equivalent normal force slope is increased, the width of each loop (both $C_N$ and $C_M$) for equivalent pitch is greater than that for true pitch, and there is a significant load discrepancy between equivalent and true pitching response. Note that in all of these cases there is little or no penetration into the stall regime, and the loop shapes are still similar although differing in size.

This situation is considerably altered in Figs. 42 through 46 for $\alpha = 15 \pm 5$ deg in which stall penetration is achieved. At low reduced frequency (Figs. 42-44) the $C_N$ loops are no longer similar in shape, and the size comparison is reversed in that the true pitch $C_N$ loop is now larger than that for equivalent pitch. Inspection of the figures shows that there is evidence that dynamic stall has occurred for true pitch but is not manifested in the transformed loop. (This is also implied by Fig. 20 in which no significant changes in normal force damping occur with stall penetration.) However, the moment loops for true and equivalent pitch at low k are similar in that both have the traditional figure-eight behavior. In contrast to this, at high k in Fig. 46, the $C_N$ loops are now in better agreement while the $C_M$ loops are in complete disagreement. Throughout this set, the $C_N$ loops for equivalent pitch have larger mean slopes than those for true pitch, and the differences in local values of $C_N$ for the two motions are significant.

The largest amplitude loops in Figs. 47-49 clearly show large differences between pitching and plunging responses. In all three figures, the equivalent pitch $C_N$ loops exhibit the same increased mean slope relative to the loops for true pitch. As before, there are large differences in value between the two, and in Fig. 48, in the neighborhood of the mean incidence angle, the discrepancy between the two is nearly 50 percent during the upstroke, and as much as 70 percent during the downstroke.

Although these are probably the largest differences observed, the entire set of data consistently has significant disagreement between the normal force due to true pitch and that due to equivalent pitch. The original objective of this study was to assess the ability of pitching data to predict the load due to plunging, and it is clear that in the majority of cases considered here, this predictive ability fails. The remainder of this report is devoted to a detailed examination of surface measurements for a few selected examples of the data just discussed. Although this will not be an in-depth study, it will serve to illustrate some of the sources of the differences between the responses to the two motions. (A brief discussion of the original plunging loops, plotted versus plunging displacement, will be found in Appendix II.)

## Unsteady Suction Surface Pressure Distributions and Time Histories

Some selected cases have been chosen from the previous set of loop data to examine in some detail the suction surface pressure time histories and the chordwise pressure distributions. Many other cases were also studied but of those examined it was found that the set included here was representative enough to display the more important characteristics of the pressure response to the pitching and plunging motions, and to indicate the circumstances under which significant differences appeared.

There are six cases considered here, contained in Figs. 50 through 55. Each figure consists of four parts, arranged as follows. Parts a) and b) are cycle-averaged suction surface pressure time histories over one period of motion for pitch and plunge, respectively, expressed in coefficient form. Each curve consists of the sum of the unsteady and the time mean pressures acting at the given location. Three different lines (solid, dashed, dash-dot) are interspersed to help separate the curves. At the top of each figure are time histories of either true pitch or equivalent pitch to permit a direct comparison of results. Parts c) and d) of each figure contain the chordwise harmonic distributions for both pitch (left columns) and plunge (right columns). Circled points are for first harmonic results, triangular points are for second harmonics, and occasionally the third harmonic is displayed as a square point. Part c) is the harmonic pressure coefficient amplitude distribution and part d) is the harmonic phase angle distribution. At the top of all four parts of each figure is complete documentation of the run conditions, including item number, to permit ease in crosschecking with data from previous figures and tables.

Figures 50 and 51, for $\alpha = 9\pm5$ deg and $\alpha = 12\pm5$ deg show substantially the same behavior in most respects. There are minor differences between the wave forms of the two sets, both from pitch to plunge and from $\alpha_M = 9$ deg to $\alpha_M = 12$ deg. However, the similarities far outweigh the differences, and this is true also of the loops associated with these two conditions (cf. Figs. 36 and 40). The harmonic amplitudes in part c) show some differences in magnitude and the only substantial changes appear in part d) for the harmonic phase angles. However, the largest differences are in the first harmonic distributions near the trailing edge, where amplitudes are low, and throughout the second harmonic distributions, where the amplitudes are low over the entire chord.

One persistent and characteristic behavior that reappears throughout this entire set (and was also observed in several cases not included here) is the appearance of a jump in the first harmonic pressure phase angle for plunge in the neighborhood of $\chi = 0.5$. A similar jump also appears in the second harmonic phase angle for plunge, but it is never observed in the cases for pitch.

A comparison of these figures with Fig. 52 for $\alpha$ = 15±5 deg shows the substantial change that occurs when stall is penetrated. Within Fig. 52 the pitch and plunge time histories are significantly different, and they differ also from those at lower incidence in Figs. 50 and 51. Note that now the response to true pitch (part a) has a strong second harmonic behavior, as seen in the amplitude distributions of part c). A measurable third harmonic is also present near the leading edge. In part b) for plunge it is seen that the second harmonic is lower near the leading edge, and that a third harmonic behavior exists primarily at the second measuring station ($\chi$ = .062) and is small everywhere else. Finally, in part d) the first and second harmonic wave forms for pitch have consistent negative slopes over most of the chord, characteristic of the propagation of a stall cell or vortex along the chord. (See Appendix III for a brief discussion in which wave velocity is derived as a function of phase angle slope. Here it is shown that negative slope implies propagation from front to rear, and that large slope magnitudes imply low propagation rates.) Such a strong coherence is not present for the plunge case, but the trend is similar. In contrast, the wave propagation is forward in the vicinity of the leading edge in both Figs. 50 and 51. Large differences between pitch and plunge are also seen in the associated loop plots for this 15 deg case in Fig. 42.

A comparison will now be made of the results in Figs. 52, 53 and 54, all for $\alpha$ = 15±5 deg but for increasing values of k. Part a) for all three figures shows the strong similarity of all pitching cases at this condition as k is varied. In all three a characteristic secondary peak, indicative of vortex shedding, appears at $\chi$ = .062 after stall has been penetrated but before maximum incidence angle is reached, and progresses downstream as time increases. Recovery from stall appears to initiate first at the leading edge during the downstroke and this too propagates downstream with increasing time. There is essentially no comparison between these results and those for plunging in part b) of each figure. In Fig. 52b) for k = .131 the penetration into stall is not evident until the second station ($\chi$ = .062) is reached, and no organized propagation downstream appears. At k = .176 in Fig. 53b) the leading edge region is similar to its pitching counterpart, but the depth of the stall collapse is not as great, no secondary peaks exist in the aft stations, and hence no strong stall cell or vortex appears to have been formed. The highest frequency condition in Fig. 54b) bears no resemblance to either of the other two results for 15±5 deg, and in fact, is more closely related to the results in Fig. 51b) for 12±5 deg. No stall is evident here in sharp contrast to its own related pitch result and to its lower frequency plunge counterparts. (In this case there were transducer failures at $\chi$ = .392 and .661 and no data were taken at those stations.) It should be noted that in Fig. 46 for this set of conditions the moment loop for true pitch is traversed mostly in the clockwise direction, implying instability, and that for equivalent pitch is entirely counterclockwise and represents a stable pseudo-motion. An examination of the harmonic amplitude distributions in parts c) and phase angles in parts d) further heightens these observations. Except for minor changes in amplitude, all three pitching amplitude distributions are similar for first, second, and third harmonics, and all three phase angle distributions are nearly identical. A similar agreement in harmonic behavior exists at the two lower values of k for plunge (Figs. 52c,d) and Figs. 53c,d)), but these differ from their pitching counterparts. Also, the harmonic content of the plunge response at high reduced frequency (Fig. 54c,d) is in substantial disagreement with the other two 15 deg cases, primarily in its lack of any substantial second harmonic content. Here the amplitude and phase angle distributions resemble those of Fig. 51 for 12±5 deg.

Finally, there are the results for 15±8 deg to be examined. These curves are contained in Fig. 55. The values of k here are comparable to those in Fig. 54 so a comparison between these two figures is in order. As before, pitching behavior is similar between the two figures in parts a) c) and d). A secondary peak is formed, indicating the presence of a vortex, and its propagation downstream is signaled by the well-ordered phase angle distributions in first and second harmonics. However, the plunge for 15±8 deg appears to have a mixed chordwise behavior, agreeing with neither the lower amplitude plunge (Fig. 54b) or its own pitching counterpart. Although no leading edge stall breakdown is evident, a secondary peak appears after maximum stall penetration at the downstream stations, but no organized propagation is observed. Both harmonic amplitude and phase angle distributions for the plunge case are in complete disagreement with pitch for all harmonics, and this is further borne out by the differences observed in the force and moment loops of Fig. 49.

It would appear that the unsteady flow at high load for these two motions differs primarily in the way in which stall cells form and propagate over the chord. Although there are no visual observations to confirm this surmise, the quantitative evidence contained in these figures, and in particular in the harmonic phase behavior, points strongly to support this thesis. Thus, in brief, stall cells or vortices form at the leading edge and propagate downstream during dynamic stall penetration in a true pitching oscillation. However, in a plunging oscillation stall cells do not appear to form as strongly as in pitch, or if they do, the plunging motion is not conducive to a downstream propagation as in the case of pitch.

## Unsteady Hot Film Time Histories

Hot film data were taken at all test conditions. However, it is beyond the scope of the present document to consider all of these cases, and only four pairs of results for pitching and plunging have been chosen for examination. These correspond to the conditions already discussed in Figs. 51 through 54 and have been selected to be representative of the data available.

Although hot films have been used in the past by many investigators (e.g. Refs. 19, 20) and the principles involved have been well documented, it is useful to outline these principles and to use the schematic in Fig. 56 to assist the reader in the interpretation of the results that follow. In brief, laminar flow is associated with low heat transfer and hence low output voltage. Further, the response will be smooth and somewhat rounded with time, as characterized in the first three curves of Fig. 56. Curve No. 1 also contains transition to turbulence, associated with high heat transfer, high output voltage, and noisy response followed by relaminarization. Curves 2 and 3 are characteristic of a laminar-turbulent-separated flow combination. For separated flow the heat transfer varies over a wide range, indicated by large response fluctuations. In curve 2 the flow reattaches turbulently before relaminarization while in curve 3 it goes directly from a separated to a laminar condition. Finally, in curve 4, there is no laminar flow and the distinction between turbulent and separated flow can only be made by the intensity of the fluctuations. These events are related to the incidence angle variation, $\alpha$, and the plunging displacement, $-h$, at the bottom of the figure. In this and the several figures that follow the plunging motion is plotted as the physical displacement which is equal and opposite to the defined displacement, $h$. Thus, in Fig. 56, maximum angular displacement corresponds to the condition of maximum downward velocity in the dashed curve. (Note that a blank page has been inserted between Figs. 56 and 57 to provide facing page comparisons in the remaining figures.)

Before examining the selected cases in detail, some general statements can be made relative to the overall sampling of results that resulted in the choices for this report. All low incidence cases were virtually the same, with pitching and plunging responses showing negligible differences. This was also true for higher incidence runs in which the amplitude was sufficiently small to preclude penetration into the stall regime, such as 9 ±2 deg, 9 ± 5 deg, 12 ± 5 deg, and 15 ± 2 deg. However, when the steady stall was penetrated, significant differences were observed which are briefly described below. In each figure that follows, the raw, self-scaled (cf. Ref. 4, p.29) hot film time histories are plotted as a function of time. The measuring station for each trace is indicated by the appended value of X and the displacement time history is plotted at the bottom of each page. As in Fig. 56, the plunging displacement is the quantity $-h$, and for direct comparison between the two parts of each figure, the $-h$ wave form must be shifted one-quarter cycle ahead of the $\alpha$ wave form. Finally, the first group of five traces on each plot were taken at a different time than the second group of five traces, so individual disturbances can only be tracked within each group. Furthermore, the hot films were staggered on either side of the span centerline (cf. Fig. 12), so such tracking is only possible for spanwise-correlated disturbances. Occasionally a hot film circuit failed during a test run and these "dead" channels are indicated by a flat response.

Figure 57 for $\alpha = 12 \pm 5$ deg is typical of many of the cases with little or no static stall penetration. A standard laminar-turbulent pattern exists over the forward 10 percent of the chord for both pitch and plunge. Between 15 and 25 percent chord there appears to be a breakdown to completely turbulent flow with some vestiges of possible separation appearing at peak incidence or maximum downward displacement at the quarter chord. Figure 51 is the pressure time history counterpart to Fig. 57, and it is seen that the pitch and plunge pressure wave forms are substantially the same also.

Figures 58, 59, and 60, for $\alpha = 15 \pm 5$ deg, show substantial differences between the pitching and plunging hot film time histories, as do the corresponding pressure time histories in Figs. 52, 53, and 54. In all three cases the hot film results for pitch are similar to one another over the entire chord, as are the pressure time histories for pitch. However, the hot film responses for plunge differ from one another, and bear no resemblance to the pitch results, in keeping with previous observations for the pressure time histories. A brief examination of each case will not be made.

First, in Fig. 58a), a combination of laminar, turbulent, and separated flows exist near the leading edge, followed by a typical turbulent-separated flow pattern from approximately 15 percent chord aft to the trailing edge. It is seen that the region of separated flow appears to exist over a larger time interval as the trailing edge is approached. In contrast to this, Fig. 58b) for plunge shows that the leading edge region is either laminar or turbulent, at least back to the 7.5 percent chord location. At 10 percent chord there is some separation, and from 15 percent chord aft to the trailing edge there is a turbulent-separated flow pattern similar to that in Fig. 58a), although the temporal extent of the separation is more limited in plunge than in pitch as the trailing edge is approached.

Figure 59a) for pitch at a higher frequency is virtually the same as Fig. 58a), and can be described in the same terms. The hot film response for plunge in Fig. 59b) shows a predominantly laminar-turbulent pattern near the leading edge, but it has intrusions of separated flow near peak equivalent incidence (near $-\dot{h} = 0$) that grow in intensity as one moves aft along the chord. From approximately 50 percent chord to the trailing edge the pitching and plunging responses are nearly indistinguishable.

As before, the hot film response for pitching at the highest frequency, in Fig. 60a), is similar to the previous two results. However, the response for plunge has reverted to a dominant laminar-turbulent pattern as far back as the 10 percent chord with no significant separation in evidence forward of the quarter chord. It appears that the corresponding pressure time history in Fig. 54b) is also devoid of any apparent stalling effects in regions of high load near the leading edge.

## CONCLUSIONS AND OBSERVATIONS

The following is a list of the more significant findings of this test program. Items 1 through 4 and 6 through 8 are based on direct evidence, quantitatively established in the text. Items 5 and 9, while based on quantitative evidence, also include some speculation on the nature of the dynamic stall processes for the two motions. The term "equivalent pitch" denotes a plunge motion having the same aerodynamic incidence angle time history as the corresponding true pitch case. The terms mean load and mean incidence angle are used interchangeably.

1. For low oscillation amplitudes, $\bar{\alpha} = 2$ deg, the loops for both true and equivalent pitch have the same general shape. However, at low k the moment loops for equivalent pitch are traversed in the clockwise direction whereas the loops for true pitch are traversed in the counterclockwise direction. Also, in general, the normal force loops for equivalent pitch have a greater slope than those for true pitch.

2. For modest oscillation amplitudes, $\bar{\alpha} = 5$ deg, there are three regimes to be considered:

    a) At low mean load the loops for equivalent pitch increase in size more rapidly with increasing k than those for true pitch.
    b) At modest mean load, but below the point of stall penetration, the observed behavior is similar to that of the low mean load regime.
    c) At high mean load, involving stall penetration, a reversal in trend is noted in that the normal force loops are no longer similar in shape, and the loops for true pitch are now larger than those for equivalent pitch. This appears to be related to the occurrence of dynamic stall (and accompanying load collapse) in true pitch, while the equivalent pitch loops exhibit no apparent effects of dynamic stall.
    d) Also at high mean load the moment loops for both true and equivalent pitch have the characteristic figure-eight behavior associated with stall instability at low k, but the equivalent pitch loop at high k returns to a stable, single-valued behavior while the true pitch loop does not.
    e) For the entire set of modest amplitude oscillations the $C_N$ loops for equivalent pitch have higher slopes than those for true pitch.

3. For large oscillation amplitudes, $\bar{\alpha} = 8$ deg, there are large differences in both shape and magnitude between true pitch and equivalent pitch responses. As before the equivalent pitch $C_N$ loops generally have higher slopes than those for true pitch.

4. As a consequence of the consistently higher $C_N$ slopes due to equivalent pitch, there is a $C_N$ magnitude discrepancy ranging from approximately 30 percent at modest load to values greater than 50 percent at high load between normal force due to equivalent pitch and normal force due to true pitch.

5. At high loading conditions into the stall regime the time histories and harmonic distributions are substantially different for pitch and plunge.

   a) A strong second harmonic amplitude and phase angle for true pitch indicates the formation and downstream propagation of stall cells or vortices, consistent with past experience.
   b) A relative lack of phase coherence for equivalent pitch is verified by examination of the time history and indicates no orderly downstream propagation of the stall cell.

6. Aerodynamic damping in pitch generally follows the theoretical curve except for high loading cases that penetrate the stall regime which indicate an unstable tendency at high k.

7. Aerodynamic damping in equivalent pitch is well correlated and follows a linear trend, but disagrees with potential flow theory. The experimental data indicate an instability for all loading at low k and stability for all but the highest loading at high k.

8. Aerodynamic damping in plunge is in reasonable agreement with, but is somewhat greater than, the theoretical curve and is well correlated for all loadings. There is no deviation from the general behavior even for significant penetration of the stall regime. There is no evidence of a plunging instability over the range of parameters tested.

9. The hot film time history results are in general agreement with pressure time histories. At high mean incidence angle and with sufficient amplitude for stall penetration, there are significant differences between pitching and plunging response; i.e., dynamic stall effects are present near the leading edge during pitch but are largely absent during plunge. The responses are generally similar for both motions over the aft portion of the airfoil.

## RECOMMENDATIONS FOR FURTHER STUDY

Long Term:

- Additional tests should be conducted over a similar range of $\alpha_M$ and $\alpha$ but at higher M, and at higher f to maintain the same range of k. This should be done to examine the effects of compressibility, which is expected to be important.

- Simple low speed water tunnel or airflow tests should be performed with flow visualization to reveal the observed differences in the stall cell propagation behavior of the two motions.

Short Term:

- A more exhaustive analytical study should be performed of the existing data to examine in detail the several variations discussed herein. In particular, quantitative comparisons of the pressure harmonics, both amplitude and phase angle, should be conducted with a view toward the ultimate construction of an empirical or analytical model of the dynamic stall process in plunge and a determination of how it differs from the reasonably well documented phenomenon in pitch.

## APPENDIX I

## MOMENT AND AERODYNAMIC DAMPING FOR EQUIVALENT PITCH

The derivation of the pitching moment behavior and the aerodynamic damping for equivalent pitch that follows is included for completness. Although it is brief, the procedure is relatively straightforward and the reader should have little or no difficulty in supplying the missing steps. To begin with, the moments due to pitch and plunge are given by the two formulas

$$C_{M_\alpha} = (\bar{C}_{M_{\alpha R}} + i\,\bar{C}_{M_{\alpha I}})\,\bar{\alpha}\ , \tag{39}$$

$$C_{M_h} = (\bar{C}_{M_{h_R}} + i\,\bar{C}_{M_{hI}})\,\bar{h}\ , \tag{40}$$

in parallel with the earlier normal force development in Eqs. (1) and (2), et. seq. As before, these are written in the Smilg and Wasserman notation as

$$C_{M\alpha} = \frac{\pi k^2}{2}\left[M_\alpha - X_\alpha\,(N_\alpha + M_h) + X_\alpha^2\,N_h\right]\bar{\alpha}\ , \tag{41}$$

$$C_{M_h} = \frac{\pi k^2}{2}\left[M_h - X_\alpha\,N_h\right]\bar{h}\ . \tag{42}$$

However, in contrast to the earlier derivation, the emphasis here will be to convert the moment due to plunge into an equivalent moment due to pitch by using Eq. (1) in the form

$$\bar{h} = -\frac{i\bar{\alpha}_e}{k}\ , \tag{43}$$

and transforming Eq. (42) to read

$$C_{M_h} \rightarrow C_{M\alpha e} = -\frac{i\pi k}{2}\left[M_h - X_\alpha\,N_h\right]\bar{\alpha}_e\ . \tag{44}$$

In Ref. 9 it is shown that

$$M_h = \frac{1}{2}$$

$$M_\alpha = \frac{3}{8} - \frac{i}{k} \tag{45}$$

and after sufficient manipulation and the use of Eqs. (8) and (9), Eqs. (41) and (44) become

$$C_{M_\alpha} = \frac{\pi}{2}\left\{ \frac{3k^2}{8} - X_\alpha\,(k^2 + 2Gk-2F) + X_\alpha^2\,(k^2+2Gk) \right.$$
$$\left. + i\left[ -k + X_\alpha\,(k + 2Fk + 2G) - 2Fk\,X_\alpha^2\right] \right\} \bar{\alpha}\ , \qquad (46)$$

$$C_{M_{\alpha e}} = \frac{\pi}{2}\left\{ 2FX_\alpha + i\left[ -\frac{k}{2} + X_\alpha\,(k + 2G)\right]\right\} \bar{\alpha}_e\,. \qquad (47)$$

A comparison of these two equations with Eqs. (10) and (11) shows a fundamental difference in the arrangement of the terms. For the normal force, the pivot axis location, $X_\alpha$, always appeared in combination with a constant such that no difficulties were encountered for quarter-chord pivot with $X_\alpha \equiv 0$. Specifically, the relationships between first order terms and ascending powers of k were unaffected in the limit as k became vanishingly small, and the approximate results were continuous in the neighborhood of $X_\alpha = 0$. However, in Eqs. (46) and (47), $X_\alpha$ appears as a direct muliplier of first order terms and it can be shown that the behavior of the equations in the neighborhood of $X_\alpha = 0$ is discontinuous if the same approximations are attempted. For example, if the pivot axis is at the quarter chord and $X_\alpha \equiv 0$, then Eqs. (46) and (47) reduce to

$$C_{M_\alpha} = \frac{\pi k}{2}\left(\frac{3k}{8} - i\right) \bar{\alpha}\ , \qquad (48)$$

$$C_{M_{\alpha e}} = \frac{\pi k}{2}\left(0 - \frac{i}{2}\right) \bar{\alpha}_e\,. \qquad (49)$$

If an error function such as Eq. (16) is constructed and the limit k → 0 is taken the result is

$$E_{M_\alpha} \rightarrow \frac{1}{2} \quad (X_\alpha \equiv 0)\ . \qquad (50)$$

However, this result may be meaningless since the quasi-steady moment for $X_\alpha \equiv 0$ is also theoretically zero.

In contrast, for $X_\alpha \neq 0$, Eqs. (46) and (47) can be written in ascending orders of k in the form

$$C_{M_\alpha} = \pi F X_\alpha \left\{ 1 + \frac{Gk}{F} (X_\alpha - 1) + \frac{k^2}{2F} (X_\alpha - 1 + \frac{3}{8X_\alpha}) + i \left[ \frac{G}{F} + k (1 + \frac{1}{2F} - X_\alpha - \frac{1}{2FX_\alpha}) \right] \right\} \bar{\alpha} , \tag{51}$$

$$C_{M\alpha_e} = \pi F X_\alpha \left\{ 1 + i \left[ \frac{G}{F} + k (\frac{1}{2F} - \frac{1}{4FX_\alpha}) \right] \right\} \bar{\alpha}_e . \tag{52}$$

If the procedures in Eqs. (12) through (16) are followed it is possible to arrive at the approximate formula for the error,

$$E_{M_\alpha} \cong - \frac{Gk}{4F^2 X_\alpha} \quad (X_\alpha \neq 0) . \tag{53}$$

To obtain the aerodynamic damping for equivalent pitch, use is made of analogy to simplify the derivation (although a formal procedure yields the same results). Only the case for quarter chord pivot, $X_\alpha \equiv 0$, will be considered. First, it can be shown that Eq. (35) for aerodynamic damping in pitch can be rewritten in terms of the imaginary part of the moment due to pitch as

$$\Xi_\alpha = - \bar{C}_{M_{\alpha I}} . \tag{54}$$

A comparison of Eqs. (39) and (48) shows that

$$\bar{C}_{M_{\alpha I}} = - \frac{\pi k}{2} , \tag{55}$$

so Eq. (54) becomes

$$\Xi_\alpha = \frac{\pi k}{2} . \tag{56}$$

Similarly, for equivalent pitch, Eq. (49) yields

$$\bar{C}_{M_{\alpha_{eI}}} = - \frac{\pi k}{4} , \tag{57}$$

and hence

$$\Xi_{\alpha_e} = \frac{\pi k}{4} . \tag{58}$$

# APPENDIX II

## PLUNGING LOOPS

For convenience, all of the plunging loops, both $C_N$ and $C_M$ versus $h/\overline{h}$, have been included here in Figs. 61 through 75. They have been arranged in ascending order of item number, as listed in Table IV, with normal force in the left hand column and moment in the right hand column.

# APPENDIX III

# WAVE VELOCITY

Assume that a sinusoidal response to a given motion is measured at two points on an airfoil, say at $x_1$ and $x_2 > x_1$, and that the wave at $x_1$ leads the wave at $x_2$ by a time interval $\Delta t$, as shown schematically in Fig. 76. Then the wave velocity, defined to be positive for propagation in the direction of increasing x, is given by

$$V_w = \frac{x_2 - x_1}{t_2 - t_1} = \frac{\Delta x}{\Delta t} . \tag{59}$$

Now each of these response waves is related to the primary motion by a phase angle $\phi_1$ and $\phi_2$, and the usual convention will be adopted that $\phi$ is positive for the response leading the motion. Thus, if $\phi$ increases positively from $x_1$ to $x_2$ such that $\phi_2 > \phi_1$, this represents a forward propagation, and to conform to the definition for positive Vw in Eq. (59), use will be made of the negative difference, $-\Delta\phi = -(\phi_2 - \phi_1)$, to represent rearward propagation. A relationship between time interval and phase difference can be established as

$$\frac{\Delta t}{T} = -\frac{\Delta\phi}{2\pi} , \tag{60}$$

and since $T = 2\pi/\omega$, then

$$\omega \Delta t = -\Delta\phi . \tag{61}$$

When this is divided by $\Delta x$ and the limit as $\Delta x \to 0$ is taken, Eq. (59) may be rewritten as

$$V_w = -\frac{\omega}{d\phi/dx} . \tag{62}$$

Finally, if $x = c\chi$ and $\omega = Uk/b$ are substituted, the normalized wave velocity is obtained in the form

$$\bar{V}_w = \frac{V_w}{U} = -\frac{2k}{d\phi/d\chi} . \tag{63}$$

It should be noted that this is valid only for pure sinusoidal response, or can be related only to the harmonic components in a Fourier decomposition of a non-sinusoidal response. In the present case this result is useful in Figs. 50-55 in relating the slope of the phase angle distribution to the propagation of the harmonic component being considered, and will not, in general, yield a result that corresponds to the calculations made in Ref. 21.

# REFERENCES

1. Carta, F. O.: Experimental Investigation of the Unsteady Aerodynamic Characteristics of an NACA 0012 Airfoil. United Aircraft Research Laboratories Report M-1283-1, August 1960.

2. Liiva, J., et al: Two-Dimensional Tests of Airfoils Oscillating Near Stall. Vol. 1, Summary and Evaluation of Results, USAAVLABS TR 68-13A, Vol. 2, Data Report, USAAVLABS TR 68-13B, U. S. Army Aviation Material Laboratories, Fort Eustis, Virginia, April 1968.

3. Carta, F. O., G. L. Commerford, R. G. Carlson, and R. H. Blackwell: Investigation of Airfoil Dynamic Stall and Its Influence on Helicopter Control Loads. USAAMRDL Technical Report 72-51, U. S. Army Air Mobility Research and Development Laboratory, Fort Eustis, Virginia, September 1972.

4. St. Hilaire, A. O., F. O. Carta, M. R. Fink, and W. D. Jepson: The Influence of Sweep on the Aerodynamic Loading of an Oscillating NACA 0012 Airfoil. Vol. I - Technical Report, NASA Contractor Report CR-3092, February 1979.

5. St. Hilaire, A. O. and F. O. Carta: The Influence of Sweep on the Aerodynamic Loading of an Oscillating NACA 0012 Airfoil. Vol. II - Data Report, NASA Contractor Report CR-145350, February 1979.

6. Carta, F. O., L. M. Casellini, P. J. Arcidiacono, and H. L. Elman: Analytical Study of Helicopter Rotor Stall Flutter. American Helicopter Society Preprint No. 413, June 1970.

7. Bellinger, E. D.: Analytical Investigation of the Effects of Blade Flexibility, Unsteady Aerodynamics, and Variable Inflow on Helicopter Rotor Stall Characteristics. NASA CR-1769, September 1971.

8. Halfman, R. L., H. C. Johnson, and S. M. Haley: Evaluation of High-Angle-of-Attack Aerodynamic Derivative Data and Stall-Flutter Prediction Techniques. NACA TN 2533, November 1951.

9. Smilg, B. and L. S. Wasserman: Application of Three-Dimensional Flutter Theory to Aircraft Structures, AAF Technical Report 4798, July 1942.

10. Scanlan, R. H. and R. Rosenbaum: Introduction to the Study of Aircraft Vibration and Flutter. MacMillan, New York, 1951.

## REFERENCES (Cont'd)

11. Bisplinghoff, R. L., H. Ashley, and R. L. Halfman: Aeroelasticity. Addison- Wesley, Reading, Mass., 1955.

12. Theodorsen, T.: General Theory of Aerodynamic Instability and the Mechanism of Flutter. NACA Report 496, 1934.

13. Rainey, A. G.: Measurement of Aerodynamic Forces for Various Mean Angles of Attack on an Airfoil Oscillating in Pitch and on Two Finite-Span Wings Oscillating in Bending with Emphasis on Damping in Stall. NACA Report 1305, 1957.

14. Liiva, J.: Unsteady Aerodynamic and Stall Effects on Helicopter Rotor Blade Airfoil Sections. AIAA Journal of Aircraft, Vol. 6, No. 1, pp. 46-51 January-February 1969.

15. Carta, F. O. and C. F. Niebanck: Prediction of Rotor Instability at High Forward Speeds. Vol. III, Stall Flutter. USAAVLABS Technical Report 68-18C, U. S. Army Aviation Material Laboratories, Fort Eustis, Virginia, February 1969.

16. Fukushima, T. and L. U. Dadone: Comparison of Dynamic Stall Phenomena for Pitching and Vertical Translation Motions. NASA Contractor Report CR-2793, July 1977.

17. Carta, F. O. and A. O. St. Hilaire: An Experimental Study on the Aerodynamic Response of a Subsonic Cascade Oscillating Near Stall. Project SQUID Technical Report UTRC-2-PU, July 1976.

18. Perkins, C. D. and R. E. Hage: Airplane Performance, Stability and Control. John Wiley & Sons, New York, 1949.

19. McCroskey, W. J. and E. J. Durbin: Flow Angle and Shear Stress Measurements Using Heated Films and Wires. Trans. ASME, Journal of Basic Engineering, Vol. 94, No. 1, pp. 46-52, March 1972.

20. Carta, F. O.: Unsteady Surface Flow Behavior on a Cascade of Airfoils Oscillating Below Stall. Project SQUID Technical Report UTRC-1-PU, September 1975.

21. Carta, F. O.: Analysis of Oscillatory Pressure Data Including Dynamic Stall Effects. NASA Contractor Report CR-2394, May 1974.

## TABLE I

## SC1095 AIRFOIL COORDINATES

| X/C | Y/C Upper | Y/C Lower | Camber Line Location $\frac{Y_u + Y_l}{2C}$ | Thickness Distribution $\frac{Y_u - Y_l}{C}$ |
|---|---|---|---|---|
| 0.0000 | 0.00000 | 0.0000 | .0000 | .0000 |
| 0.0125 | 0.01770 | -0.01450 | .0016 | .0322 |
| 0.0250 | 0.02640 | -0.02100 | .0027 | .0474 |
| 0.0500 | 0.03677 | -0.02843 | .00417 | .0652 |
| 0.0750 | 0.04275 | -0.03225 | .00525 | .075 |
| 0.1000 | 0.04680 | -0.03460 | .0061 | .0814 |
| 0.1500 | 0.05170 | -0.03740 | .00715 | .0891 |
| 0.2000 | 0.05447 | -0.03883 | .00782 | .0933 |
| 0.2500 | 0.05550 | -0.03940 | .00805 | .0949 |
| 0.3000 | 0.05524 | -0.03916 | .00804 | .0944 |
| 0.4000 | 0.05299 | -0.03761 | .00769 | .0906 |
| 0.5000 | 0.04854 | -0.03446 | .00704 | .083 |
| 0.6000 | 0.04212 | -0.02988 | .00612 | .072 |
| 0.7000 | 0.03375 | -0.02384 | .00496 | .05759 |
| 0.8000 | 0.02362 | -0.01658 | .00352 | .0402 |
| 0.9000 | 0.01235 | -0.00864 | .00186 | .02099 |
| 0.9500 | 0.00640 | -0.00450 | .00095 | .0109 |
| 0.9750 | 0.00329 | -0.00232 | .00049 | .00561 |
| 1.0000 | 0.00329 | -0.00232 | .00049 | .00561 |

Leading Edge Radius, upper surface 0.0100 c
Leading Edge Radius, lower surface 0.0066 c

## TABLE II

## CHORDWISE MEASURING STATIONS
## (PERCENT CHORD)

| Pressure Transducers | Hot Films |
|---|---|
| 1.2 | 2.5 |
| 6.2 | 5.0 |
| 14.8 | 7.5 |
| 26.1 | 10.0 |
| 39.2 | 15.0 |
| 53.0 | 25.0 |
| 66.1 | 40.0 |
| 77.4 | 50.0 |
| 86.0 | 66.7 |
| 91.0 | 91.7 |

## TABLE III

## ORIGINAL PITCH TEST PLAN

| Pitch Item Number | $\bar{\alpha}$ (deg) | $\alpha_M$ (deg) | V (m/sec) | f (cps) | k | $\bar{h}e$ | Corresponding Plunge Item Number |
|---|---|---|---|---|---|---|---|
| 1 | 2° | 9° | 45.7 | 10.00 | .1047 | .333 | 3 |
| 2 | ↓ | ↓ | 61.0 | 6.67 | .0524 | .667 | 25 |
| 3 | ↓ | ↓ | 61.0 | 8.89 | .0698 | .500 | 15 |
| 4 | ↓ | ↓ | 61.0 | 13.33 | .1047 | .333 | 4 |
| 5 | ↓ | 12° | 45.7 | 10.00 | .1047 | .333 | 6 |
| 6 | ↓ | ↓ | 61.0 | 13.33 | .1047 | .333 | 7 |
| 7 | ↓ | 15° | 45.7 | 10.00 | .1047 | .333 | 9 |
| 8 | ↓ | ↓ | 61.0 | 6.67 | .0542 | .667 | 30 |
| 9 | ↓ | ↓ | 61.0 | 8.89 | .0698 | .500 | 20 |
| 10 | ↓ | ↓ | 61.0 | 13.33 | .1047 | .333 | 10 |
| 11 | 5° | 2° | 30.5 | 8.33 | .1309 | .667 | 21 |
| 12 | ↓ | ↓ | 30.5 | 16.67 | .2618 | .333 | 1 |
| 13 | ↓ | ↓ | 36.6 | 13.33 | .1745 | .500 | 11 |
| 14 | ↓ | 9° | 30.5 | 8.33 | .1309 | .667 | 23 |
| 15 | ↓ | ↓ | 30.5 | 11.11 | .1745 | .500 | 13 |
| 16 | ↓ | ↓ | 30.5 | 16.67 | .2618 | .333 | 2 |
| 17 | ↓ | ↓ | 36.6 | 10.00 | .1309 | .667 | 24 |
| 18 | ↓ | ↓ | 36.6 | 13.33 | .1745 | .500 | 14 |
| 19 | ↓ | 12° | 30.5 | 8.33 | .1309 | .667 | 26 |
| 20 | ↓ | ↓ | 30.5 | 11.11 | .1745 | .500 | 16 |
| 21 | ↓ | ↓ | 30.5 | 16.67 | .2618 | .333 | 5 |
| 22 | ↓ | 15° | 30.5 | 8.33 | .1309 | .667 | 28 |
| 23 | ↓ | ↓ | 30.5 | 11.11 | .1745 | .500 | 18 |
| 24 | ↓ | ↓ | 30.5 | 16.67 | .2618 | .333 | 8 |
| 25 | ↓ | ↓ | 36.6 | 10.00 | .1309 | .667 | 29 |
| 26 | ↓ | ↓ | 36.6 | 13.33 | .1745 | .500 | 19 |
| 27 | 8° | 9° | 24.4 | 10.67 | .2094 | .667 | 22 |
| 28 | ↓ | ↓ | 24.4 | 14.22 | .2793 | .500 | 12 |
| 29 | ↓ | 15° | 24.4 | 10.67 | .2094 | .667 | 27 |
| 30 | ↓ | ↓ | 24.4 | 14.22 | .2793 | .500 | 17 |

# TABLE IV

## ORIGINAL PLUNGE TEST PLAN

| Plunge Item Number | $\bar{h}$ | $\alpha_M$ (deg) | V (m/sec) | f (cps) | k (deg) | $\bar{\alpha}_e$ | Corresponding Pitch Item Number |
|---|---|---|---|---|---|---|---|
| 1 | 0.333 | 2° | 30.5 | 16.67 | .2618 | 5° | 12 |
| 2 | ↓ | 9° | 30.5 | 16.67 | .2618 | 5° | 16 |
| 3 | ↓ | ↓ | 45.7 | 10.00 | .1047 | 2° | 1 |
| 4 | ↓ | ↓ | 61.0 | 13.33 | .1047 | 2° | 4 |
| 5 | ↓ | 12° | 30.5 | 16.67 | .2618 | 5° | 21 |
| 6 | ↓ | ↓ | 45.7 | 10.00 | .1047 | 2° | 5 |
| 7 | ↓ | ↓ | 61.0 | 13.33 | .1047 | 2° | 6 |
| 8 | ↓ | 15° | 30.5 | 16.67 | .2618 | 5° | 24 |
| 9 | ↓ | ↓ | 45.7 | 10.00 | .1046 | 2° | 7 |
| 10 | ↓ | ↓ | 61.0 | 13.33 | .1047 | 2° | 10 |
| 11 | 0.500 | 2° | 36.6 | 13.33 | .1745 | 5° | 13 |
| 12 | ↓ | 9° | 24.4 | 14.22 | .2793 | 8° | 28 |
| 13 | ↓ | ↓ | 30.5 | 11.11 | .1745 | 5° | 15 |
| 14 | ↓ | ↓ | 36.6 | 13.33 | .1745 | 5° | 18 |
| 15 | ↓ | ↓ | 61.0 | 8.89 | .0698 | 2° | 3 |
| 16 | ↓ | 12° | 30.5 | 11.11 | .1745 | 5° | 20 |
| 17 | ↓ | 15° | 24.4 | 14.22 | .2793 | 8° | 30 |
| 18 | ↓ | ↓ | 30.5 | 11.11 | .1745 | 5° | 23 |
| 19 | ↓ | ↓ | 36.6 | 13.33 | .1745 | 5° | 26 |
| 20 | ↓ | ↓ | 61.0 | 8.89 | .0698 | 2° | 9 |
| 21 | 0.667 | 2° | 30.5 | 8.33 | .1309 | 5° | 11 |
| 22 | ↓ | 9° | 24.4 | 10.67 | .2094 | 8° | 27 |
| 23 | ↓ | ↓ | 30.5 | 8.33 | .1309 | 5° | 14 |
| 24 | ↓ | ↓ | 36.6 | 10.00 | .1309 | 5° | 17 |
| 25 | ↓ | ↓ | 61.0 | 6.67 | .0524 | 2° | 2 |
| 26 | ↓ | 12° | 30.5 | 8.33 | .1309 | 5° | 19 |
| 27 | ↓ | 15° | 24.4 | 10.67 | .2094 | 8° | 29 |
| 28 | ↓ | ↓ | 30.5 | 8.33 | .1309 | 5° | 22 |
| 29 | ↓ | ↓ | 36.6 | 10.00 | .1309 | 5° | 25 |
| 30 | ↓ | ↓ | 61.0 | 6.67 | .0524 | 2° | 8 |

# TABLE V

## AERODYNAMIC DAMPING IN PITCH AND EQUIVALENT PITCH

| | $\bar{\alpha} \cong 2^\circ$ | | | | $\bar{\alpha} \cong 5^\circ$ | | | | $\bar{\alpha} \cong 8^\circ$ | | | |
|---|---|---|---|---|---|---|---|---|---|---|---|---|
| $\alpha_M$ | ITEM | k | $\Xi_\alpha$ | $\Xi_{\alpha e}$ | ITEM | k | $\Xi_\alpha$ | $\Xi_{\alpha e}$ | ITEM | k | $\Xi_\alpha$ | $\Xi_{\alpha e}$ |
| $2^\circ$ | | | | | 11 | .124 | .224 | - | | | | |
| | | | | | 21 | .129 | - | .192 | | | | |
| | | | | | 13 | .166 | .224 | - | | | | |
| | | | | | 11 | .165 | - | .474 | | | | |
| | | | | | 12 | .247 | .372 | - | | | | |
| | | | | | 1 | .272 | - | .642 | | | | |
| $9^\circ$ | 2 | .050 | .079 | - | 14 | .126 | .200 | - | 27 | .150* | .214 | - |
| | 25 | .051 | - | -.318 | 23 | .130 | - | .231 | 22 | .218 | - | .523 |
| | 3 | .065 | .093 | - | 17 | .126 | .208 | - | 28 | .271 | .364 | - |
| | 15 | .071 | - | -.065 | 24 | .129 | - | .243 | 12 | .263 | - | .823 |
| | 1 | .096 | .148 | - | 15 | .168 | .243 | - | | | | |
| | 3 | .103 | - | .138 | 13 | .174 | - | .480 | | | | |
| | 4 | .099 | .147 | - | 18 | .165 | .234 | - | | | | |
| | 4 | .102 | - | .066 | 14 | .173 | - | .489 | | | | |
| | | | | | 16 | .246 | .329 | - | | | | |
| | | | | | 2 | .262 | - | .608 | | | | |
| $12^\circ$ | 5 | .099 | .169 | - | 19 | .126 | .153 | - | | | | |
| | 6 | .104 | - | .191 | 26 | .130 | - | .195 | | | | |
| | 6 | .097 | .154 | - | 20 | .166 | .264 | - | | | | |
| | 7 | .103 | - | .078 | 16 | .166 | - | .396 | | | | |
| | | | | | 21 | .249 | .355 | - | | | | |
| | | | | | 5 | .261 | - | .616 | | | | |
| $15^\circ$ | 8 | .049 | .085 | - | 22 | .123 | -.147 | - | 29 | .201 | -.075 | - |
| | 30 | .052 | - | -.341 | 28 | .131 | - | .009 | 27 | .213 | - | -.041 |
| | 9 | .066 | .111 | - | 25 | .124 | -.147 | - | 30 | .263 | -.110 | - |
| | 20 | .070 | - | -.180 | 29 | .128 | - | .014 | 17 | .280 | - | .298 |
| | 7 | .100 | .186 | - | 23 | .164 | -.169 | - | | | | |
| | 9 | .101 | - | .138 | 18 | .176 | - | -.061 | | | | |
| | 10 | .099 | .190 | - | 26 | .169 | -.207 | - | | | | |
| | 10 | .104 | - | .075 | 19 | .173 | - | .102 | | | | |
| | | | | | 24 | .248 | -.202 | - | | | | |
| | | | | | 8 | .246 | - | .530 | | | | |

*wrong frequency in pitch

TABLE V (concl.)

AERODYNAMIC DAMPING IN PITCH
AND EQUIVALENT PITCH

| | $\bar{\alpha} \cong 2^\circ$ | | | $\bar{\alpha} \cong 5^\circ$ | | | $\bar{\alpha} \cong 8^\circ$ | | |
|---|---|---|---|---|---|---|---|---|---|
| $\alpha_M$ | k | $\Xi_\alpha$ | $\Xi_{\alpha e}$ | k | $\Xi_\alpha$ | $\Xi_{\alpha e}$ | k | $\Xi_\alpha$ | $\Xi_{\alpha e}$ |
| | Additional values, pitch only | | | | | | | | |
| 9° | | | | | | | .070 | .023 | |
| | | | | | | | .094 | .079 | |
| | | | | | | | .118 | .139 | |
| | | | | | | | .121 | .074 | |
| 15° | | | | .101 | .111 | - | .071 | .082 | |
| | | | | | | | .095 | .082 | |
| | | | | | | | .117 | .057 | |
| | | | | | | | .118 | .012 | |

# TABLE VI

## AERODYNAMIC DAMPING IN PLUNGE

| | $\bar{h} = .333$ | | | $\bar{h} = .5$ | | | $\bar{h} = .667$ | | |
|---|---|---|---|---|---|---|---|---|---|
| $\alpha_M$ | ITEM | k | $\Xi_h$ | ITEM | k | $\Xi_h$ | ITEM | k | $\Xi_h$ |
| 2° | 1 | .272 | 1.027 | 11 | .165 | .876 | 21 | .129 | .722 |
| 9° | 3 | .103 | .733 | 15 | .071 | .508 | 25 | .051 | .370 |
| ↓ | 4 | .102 | .763 | 13 | .174 | 1.036 | 23 | .130 | .808 |
| | 2 | .262 | 1.427 | 14 | .173 | .990 | 24 | .129 | .763 |
| | | | | 12 | .263 | 1.413 | 22 | .218 | 1.275 |
| 12° | 6 | .104 | .770 | 16 | .166 | 1.040 | 26 | .130 | .781 |
| ↓ | 7 | .103 | .785 | | | | | | |
| | 5 | .261 | 1.447 | | | | | | |
| 15° | 9 | .101 | .694 | 20 | .070 | .445 | 30 | .052 | .316 |
| ↓ | 10 | .104 | .803 | 18 | .176 | 1.020 | 28 | .131 | .780 |
| | 8 | .246 | 1.458 | 19 | .173 | .996 | 29 | .128 | .731 |
| | | | | 17 | .280 | 1.549 | 27 | .213 | 1.247 |

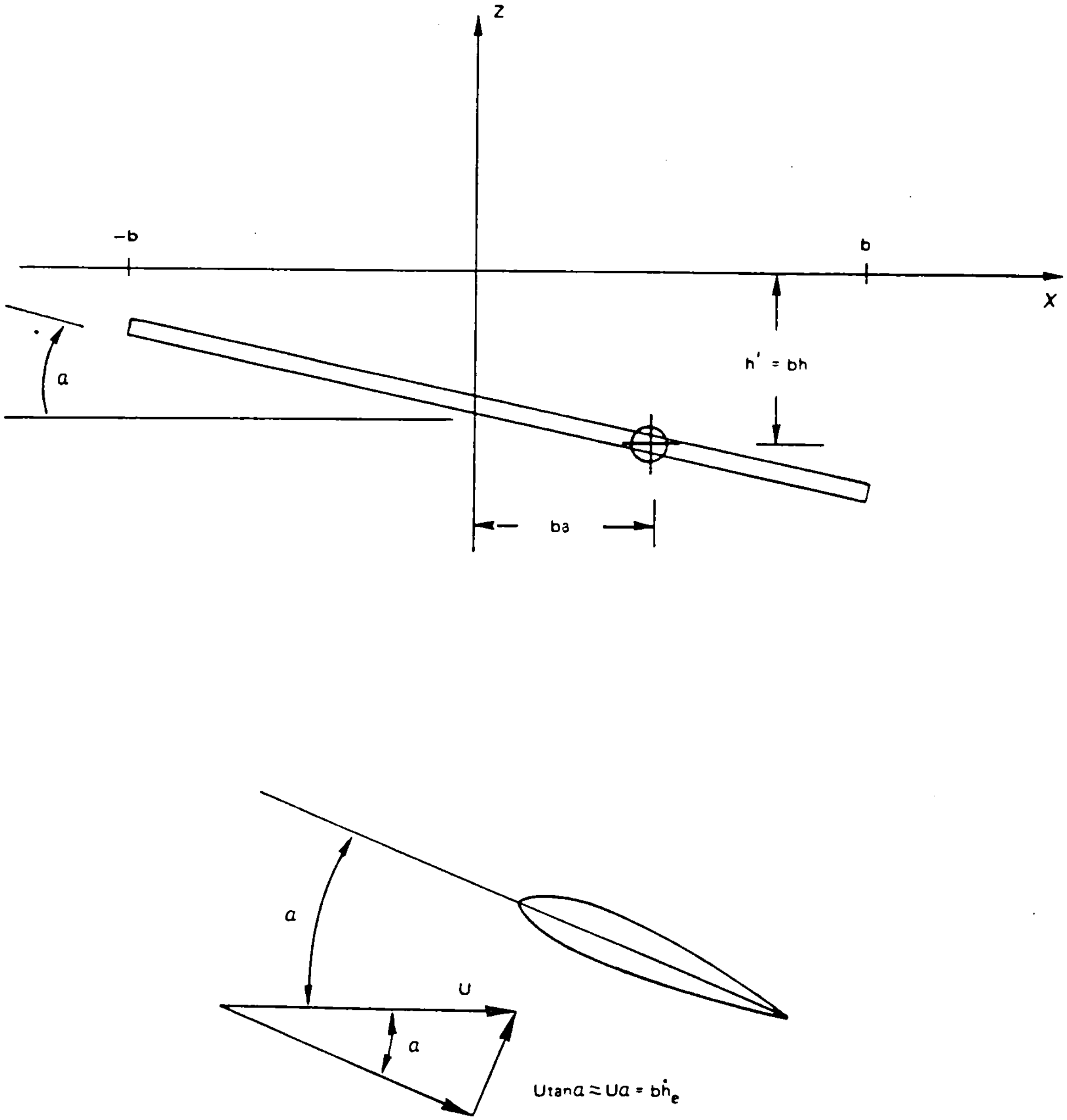

Figure 1 Coordinate System and Equivalent Plunging Motion

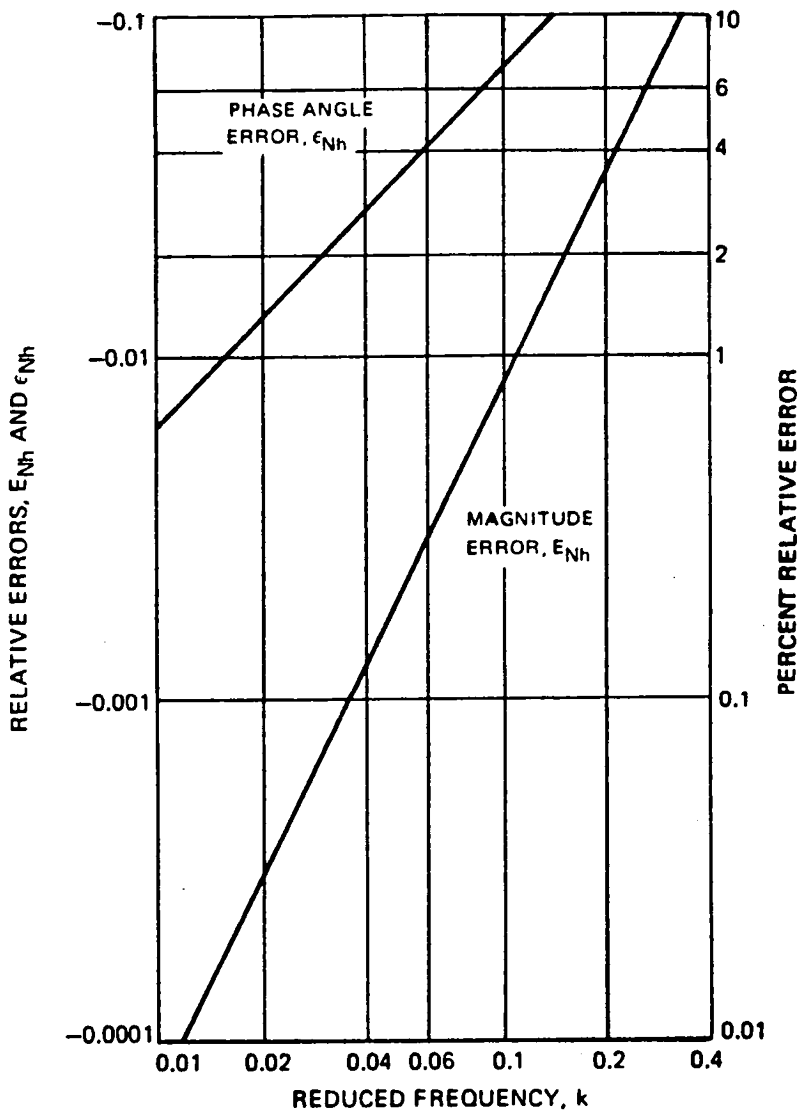

**Figure 2** Variation in Normal Force Amplitude and Phase Angle Error with Reduced Frequency for Plunging Motion

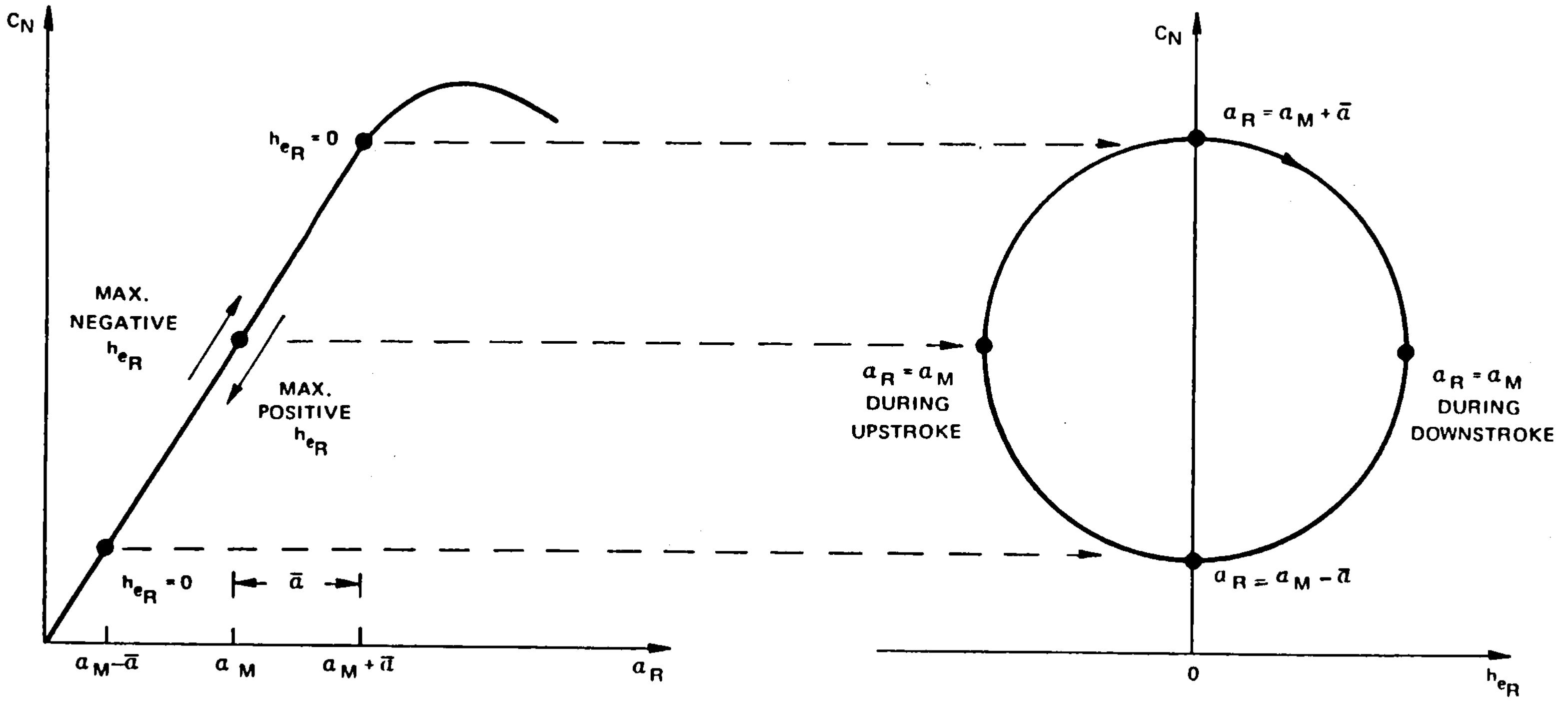

Figure 3 Schematic Showing Generation of Work Per Cycle in Bending During Quasi–Steady Motion

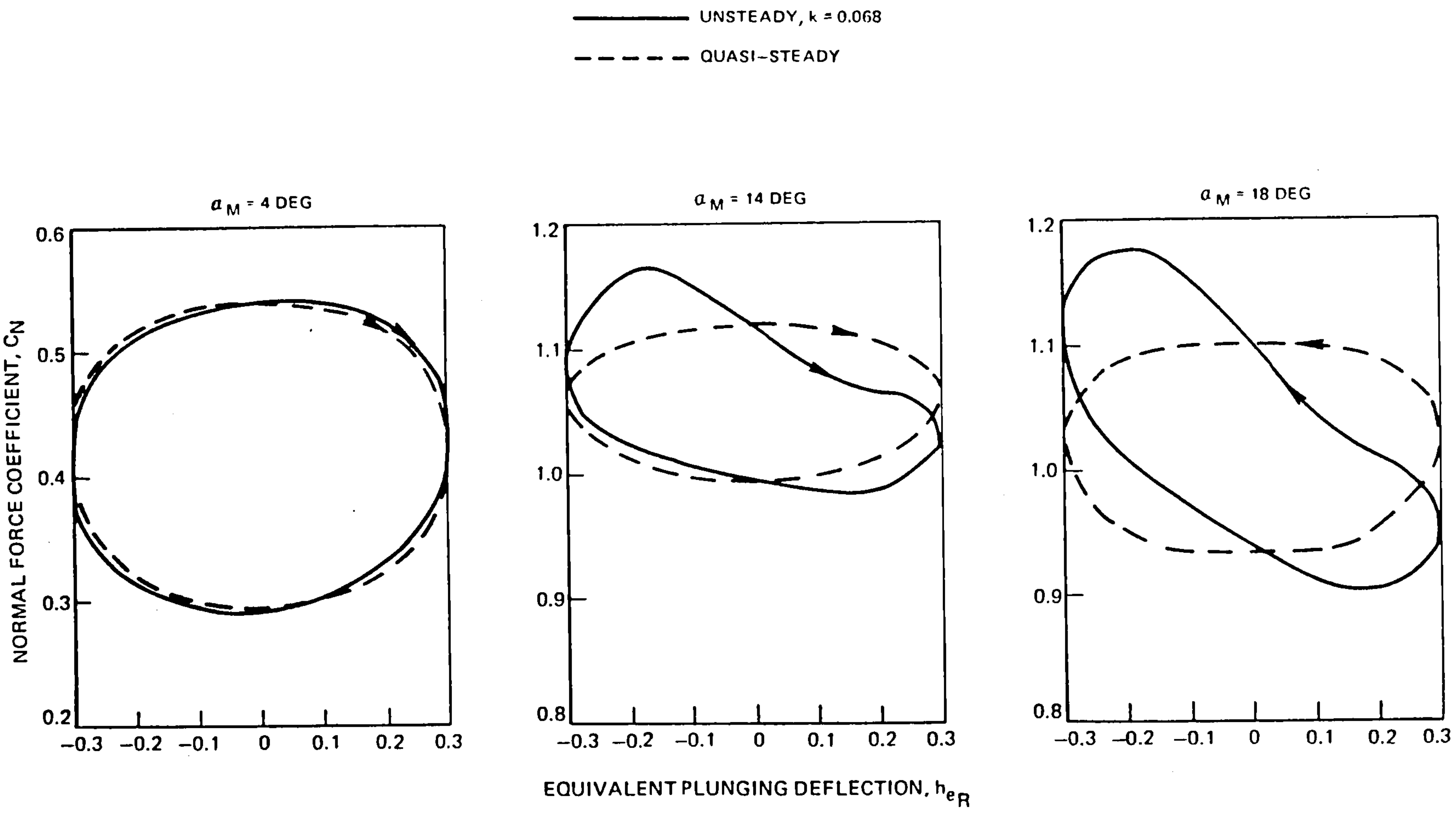

Figure 4 Normal Force Due to Equivalent Plunge Obtained from UTRC Pitching Airfoil Data

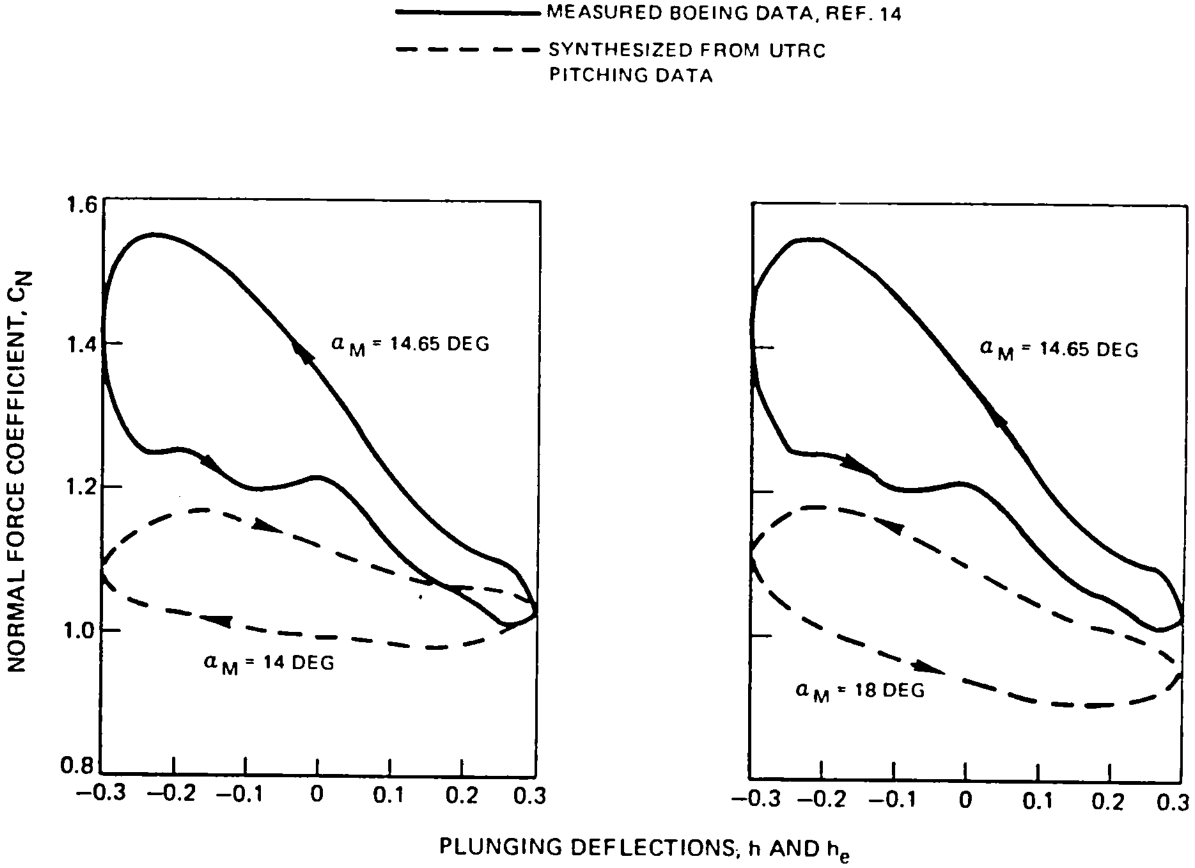

Figure 5 Comparison Between Measured and Synthesized Normal Force Loops for Plunging Motions, k = 0.068

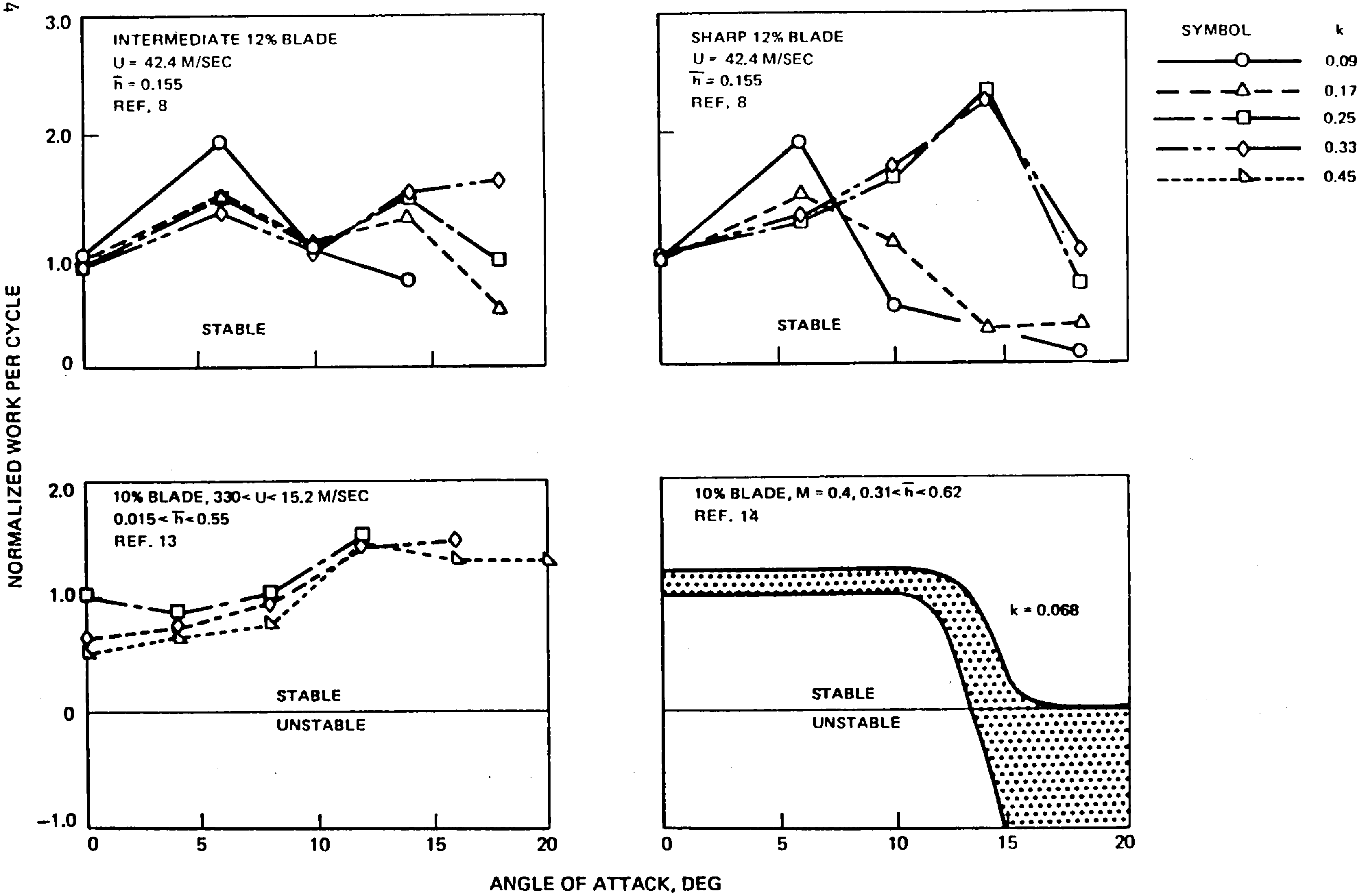

Figure 6 Normalized Work Per Cycle for Plunging Motion

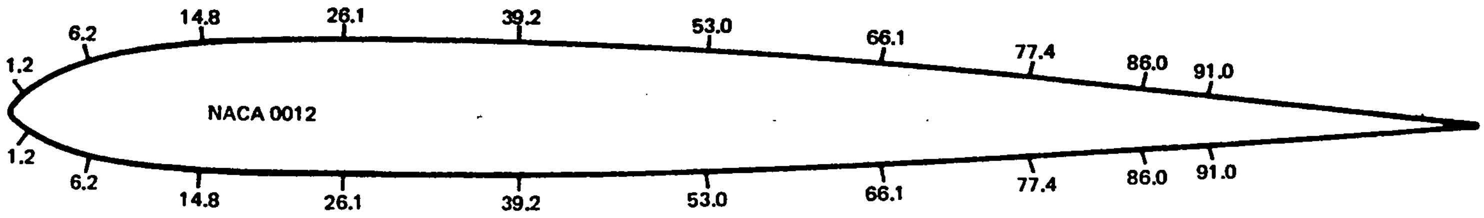

PRESSURE MEASURING STATIONS, PERCENT CHORD

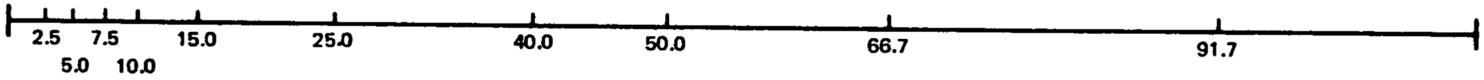

HOT FILM LOCATIONS, PERCENT CHORD

Figure 7 Airfoil Cross Section Showing Measuring Stations

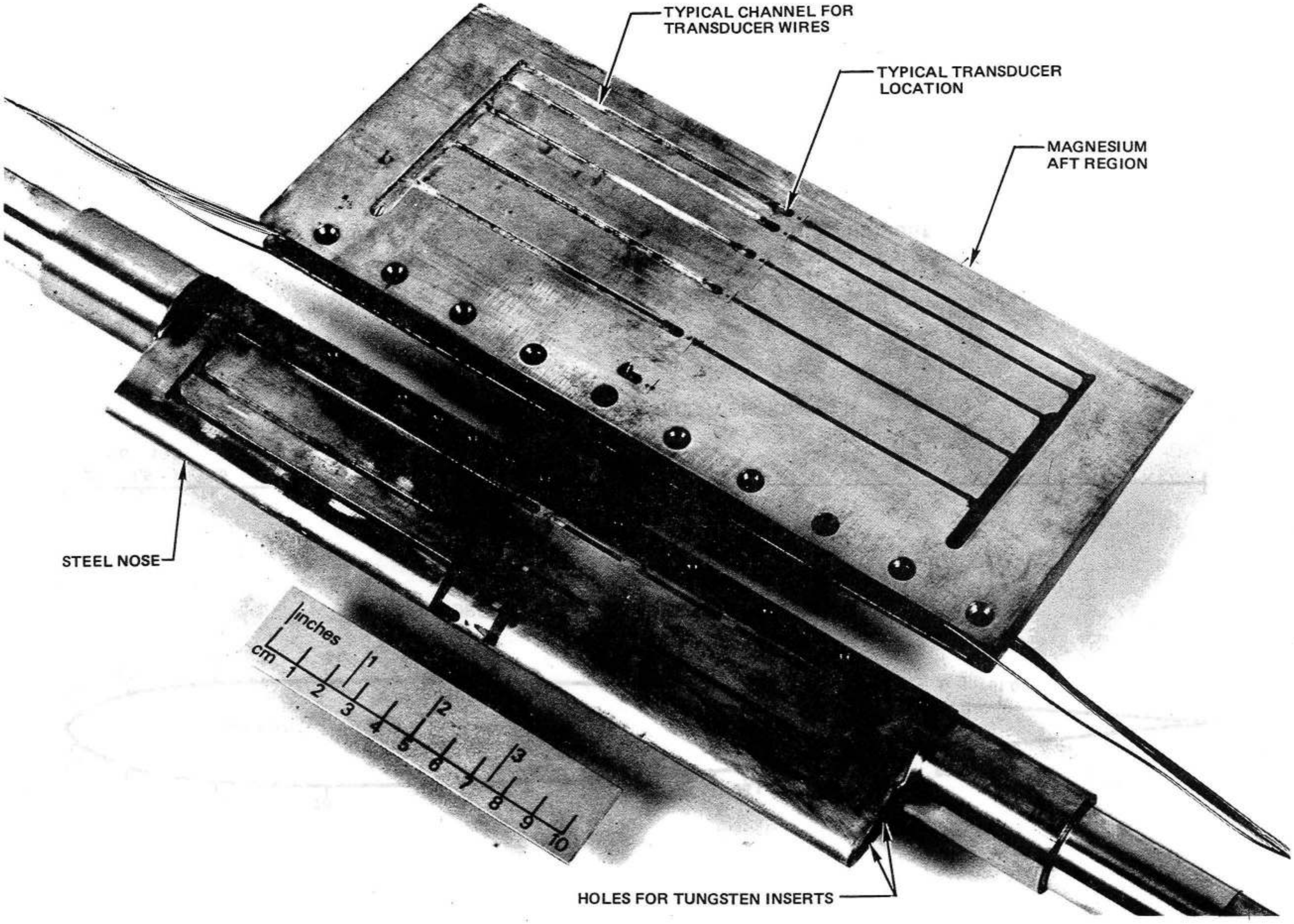

Figure 8 Disassembled Model Airfoil

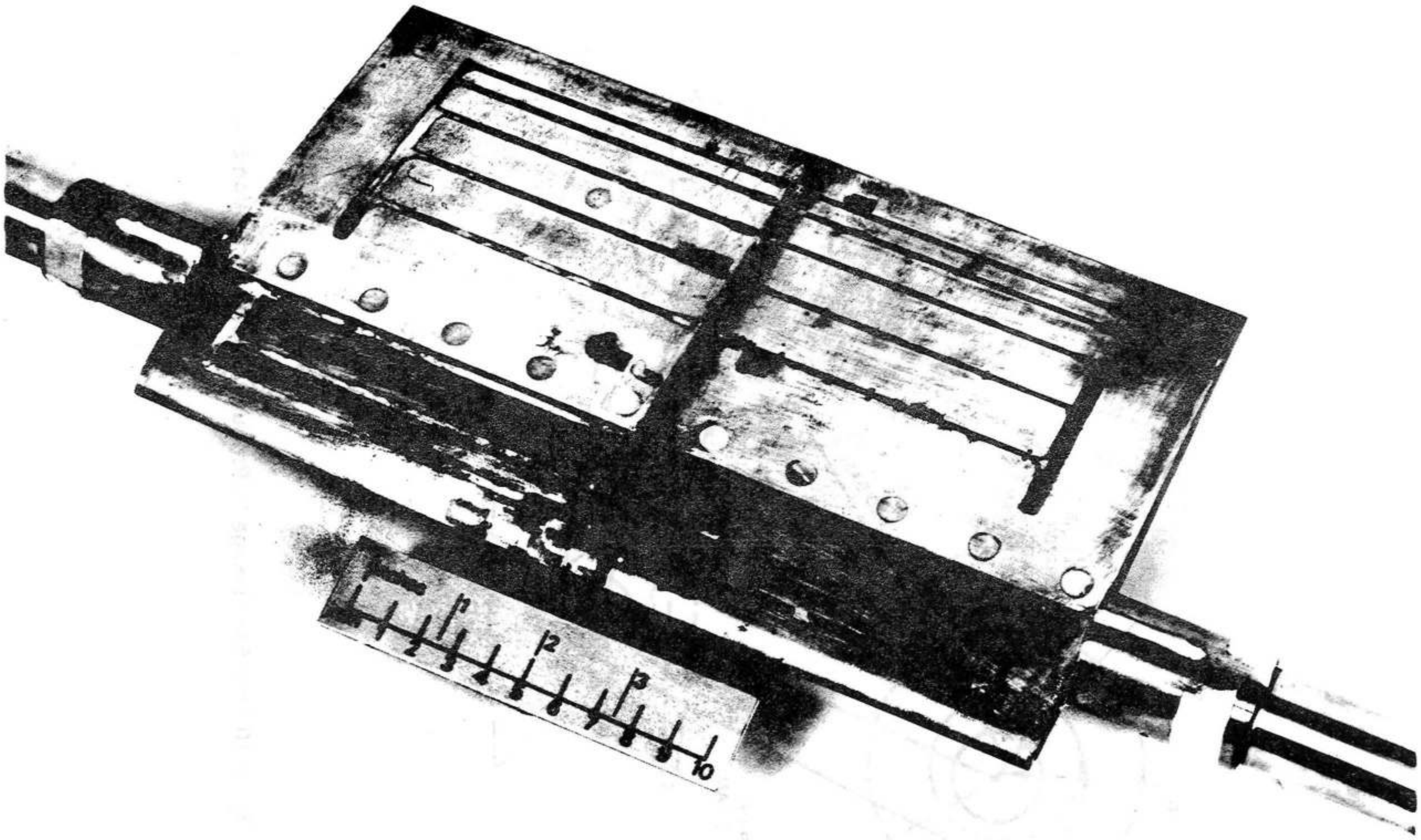

Figure 9 Assembled and Instrumented Model Airfoil

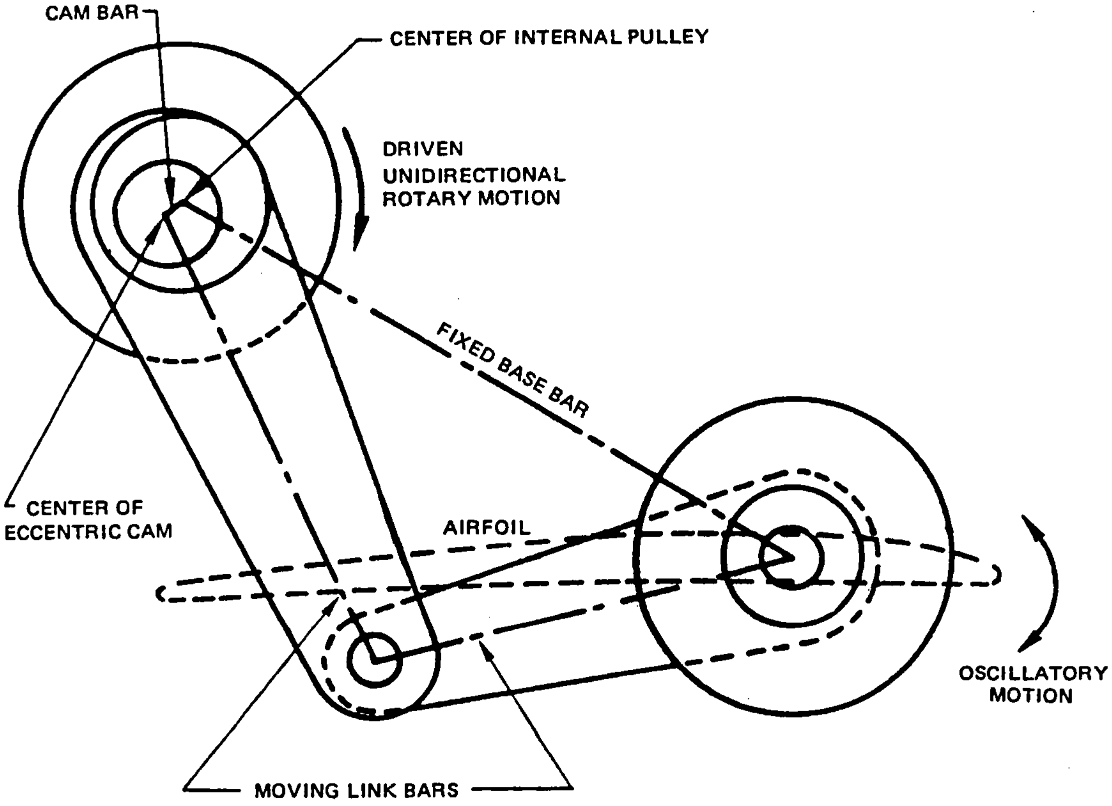

Figure 10 Four-Bar Linkage to Produce Sinusoidal Motion-Schematic

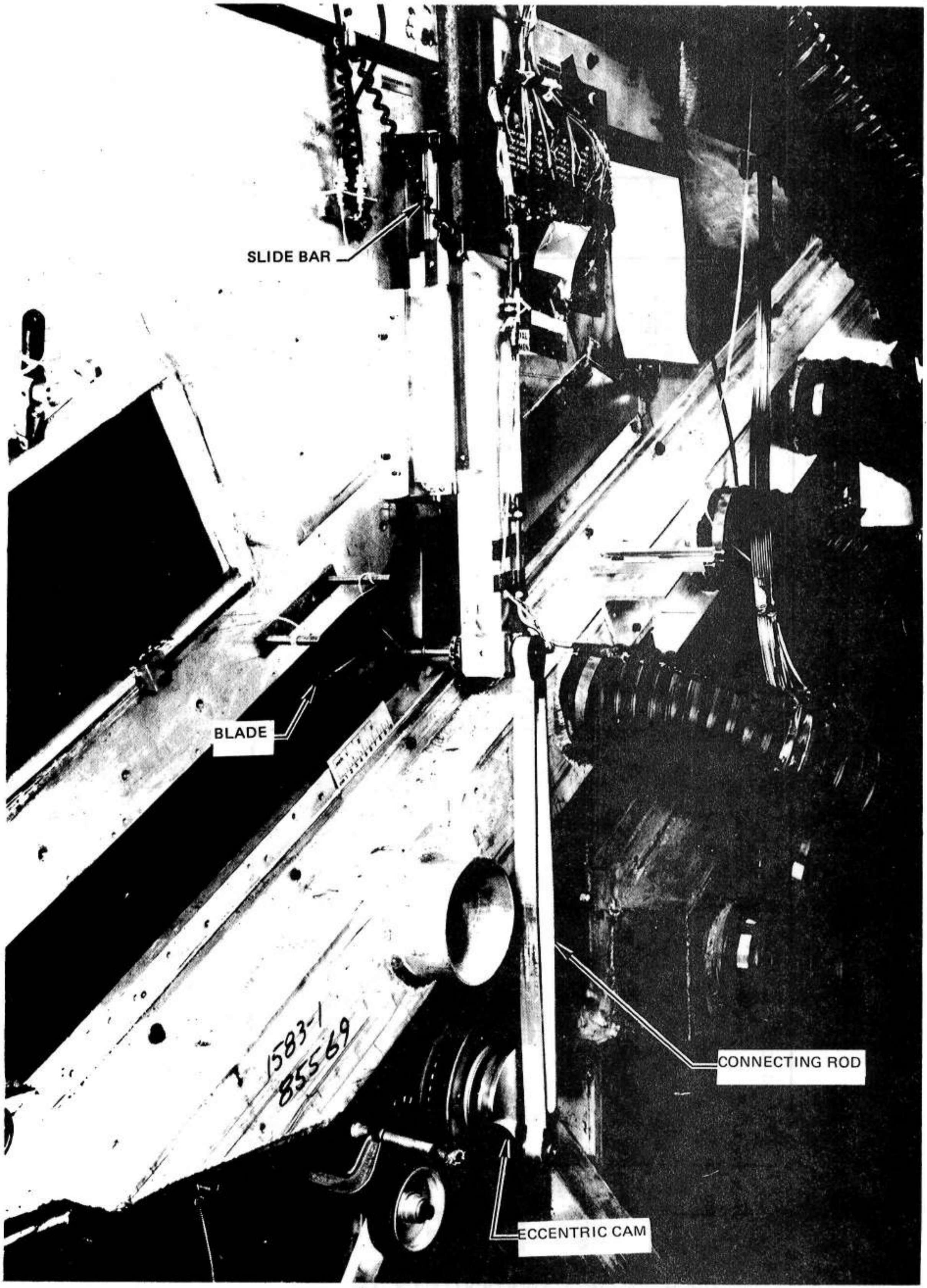

Figure 11 Plunging Drive System

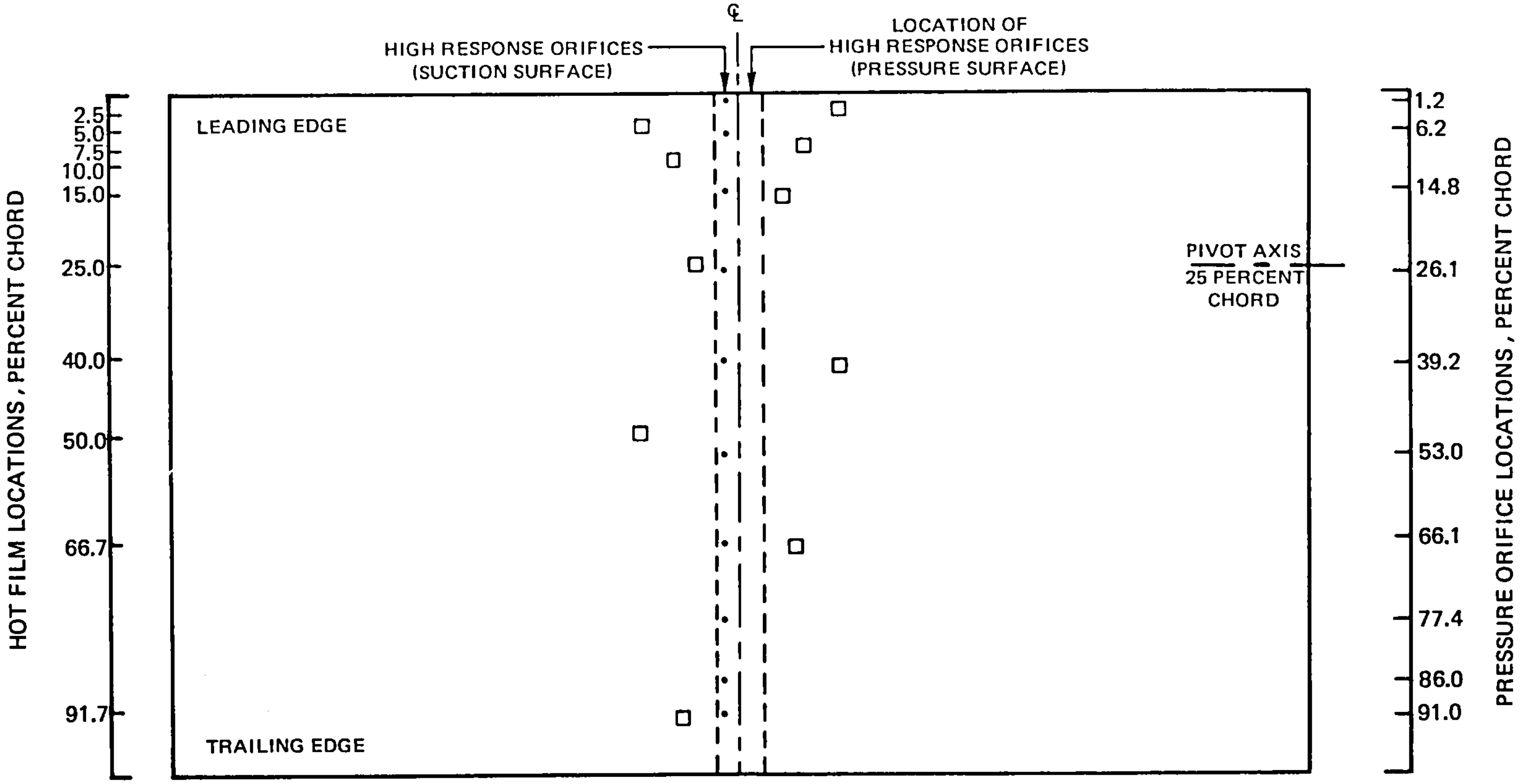

Figure 12 Suction Surface Plan View of Instrumented Airfoil

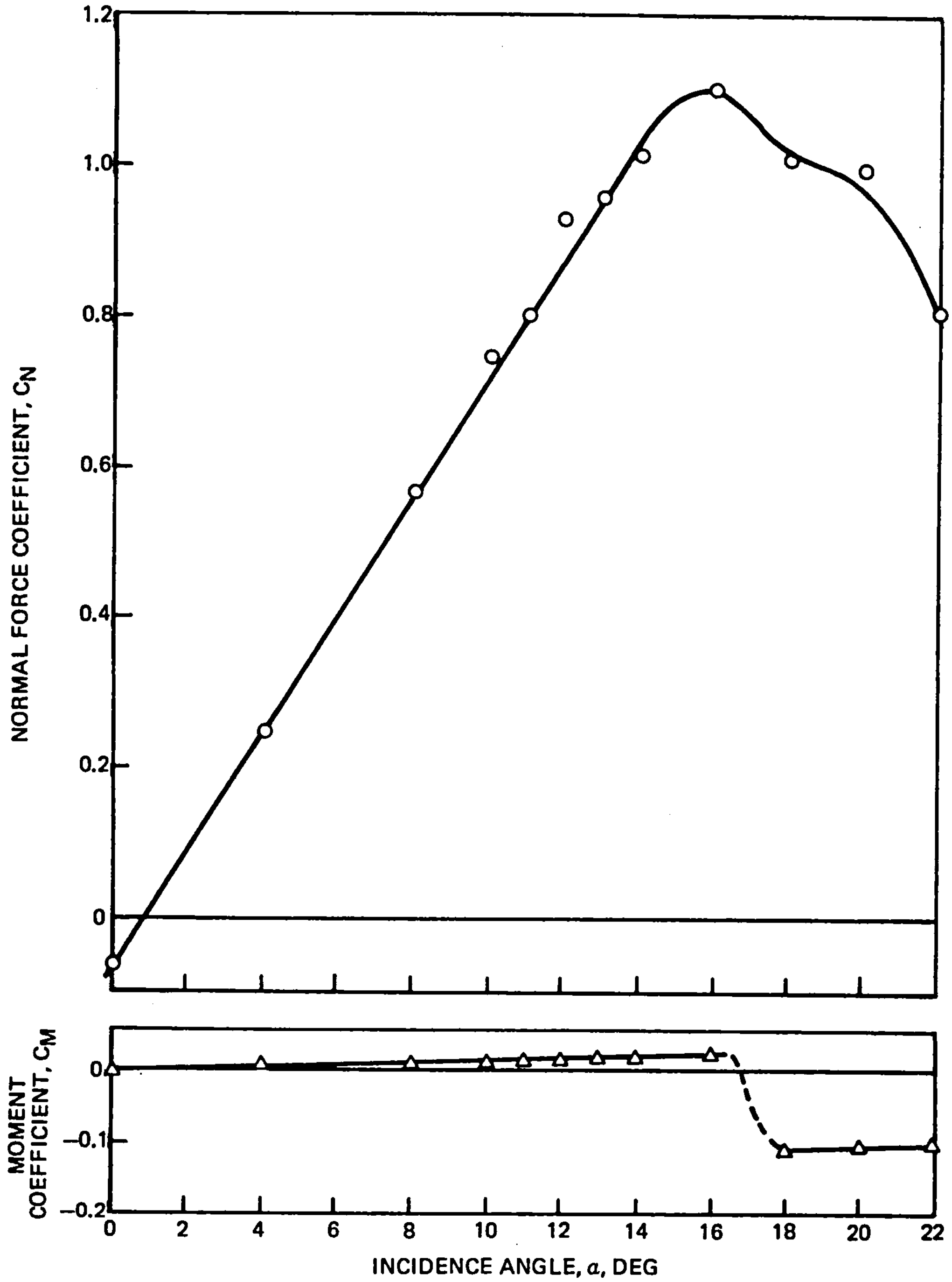

**Figure 13 Steady-State Normal Force and Pitching Moment Coefficient for U = 30.5 m/sec (100 ft/sec)**

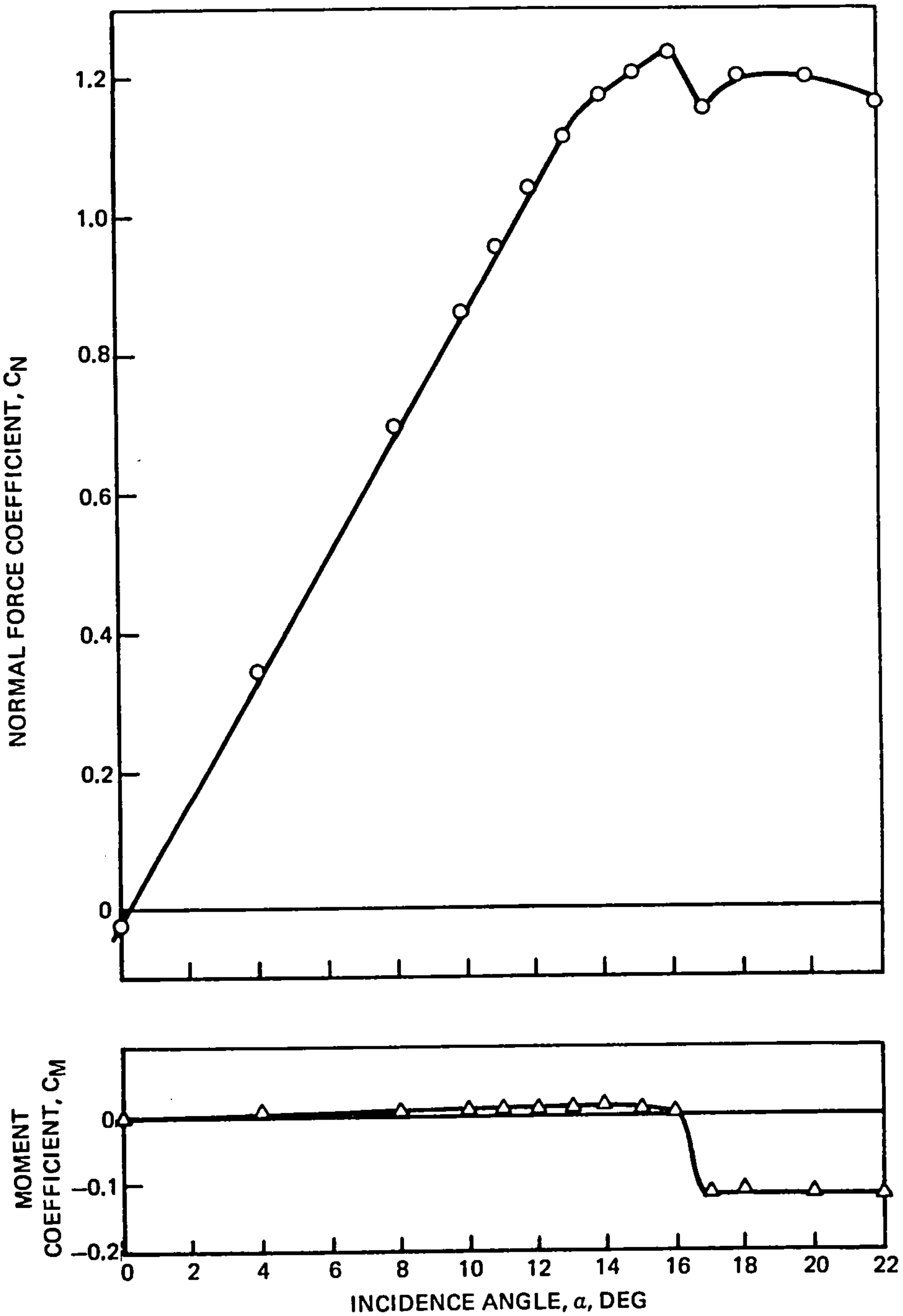

**Figure 14 Steady-State Normal Force and Pitching Moment Coefficient for U = 61 m/sec (200 ft/sec)**

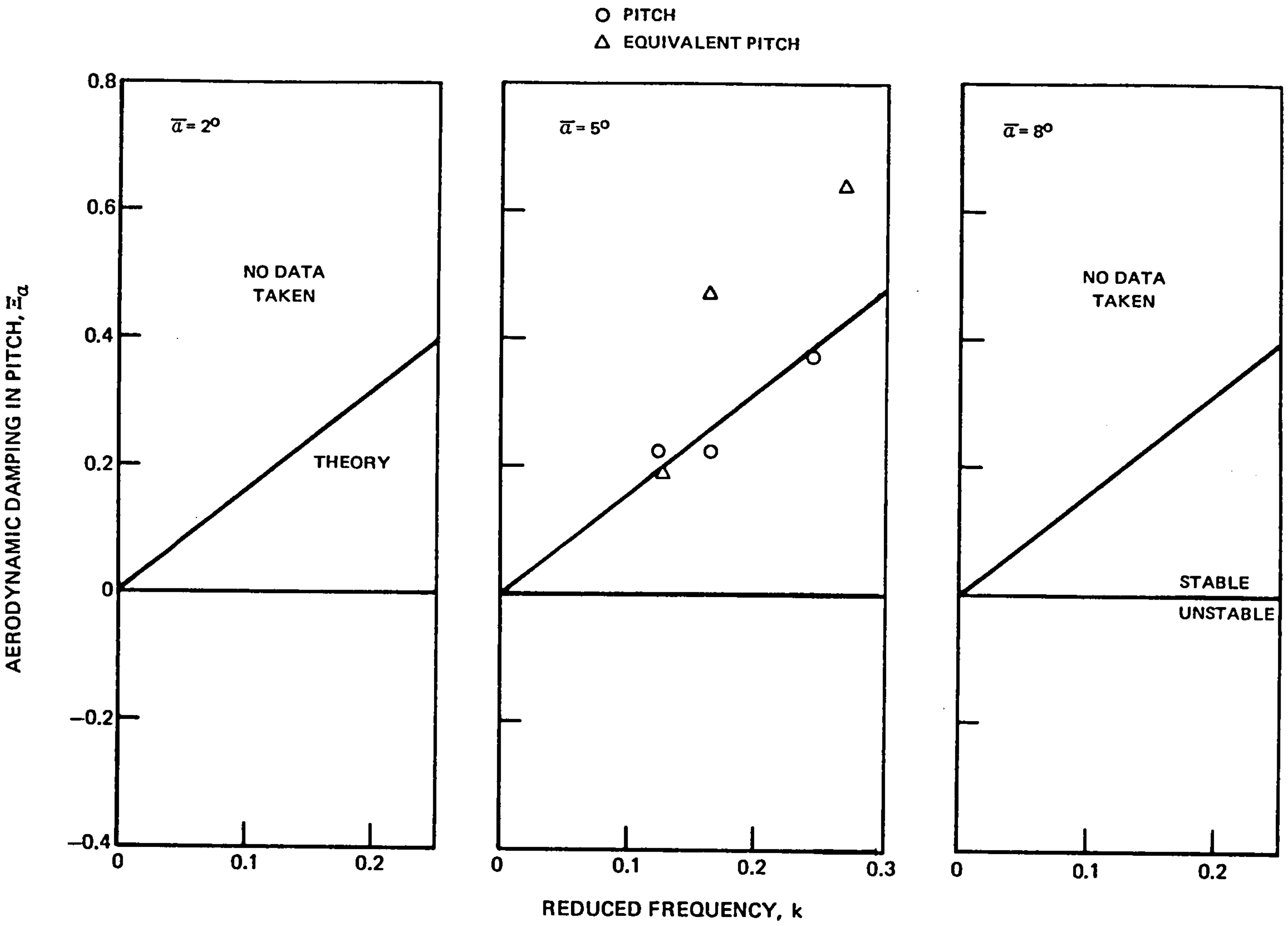

**Figure 15 Aerodynamic Damping in Pitch and Equivalent Pitch**
**a)Mean Incidence Angle $\alpha_M$ = 2 Deg.**

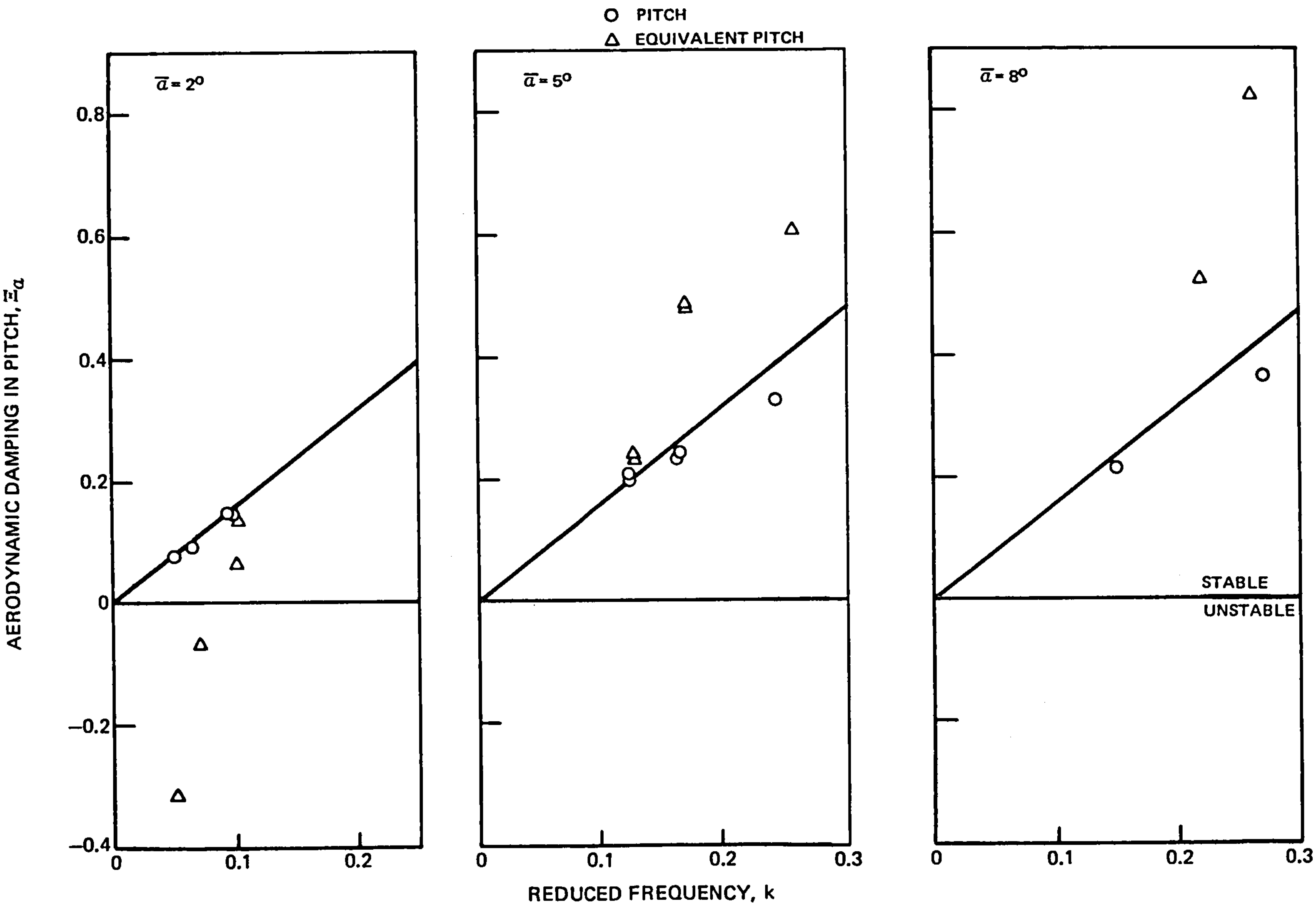

**Figure 15 (continued)**
**b) Mean Incidence Angle $\alpha_M$ = 9 Deg.**

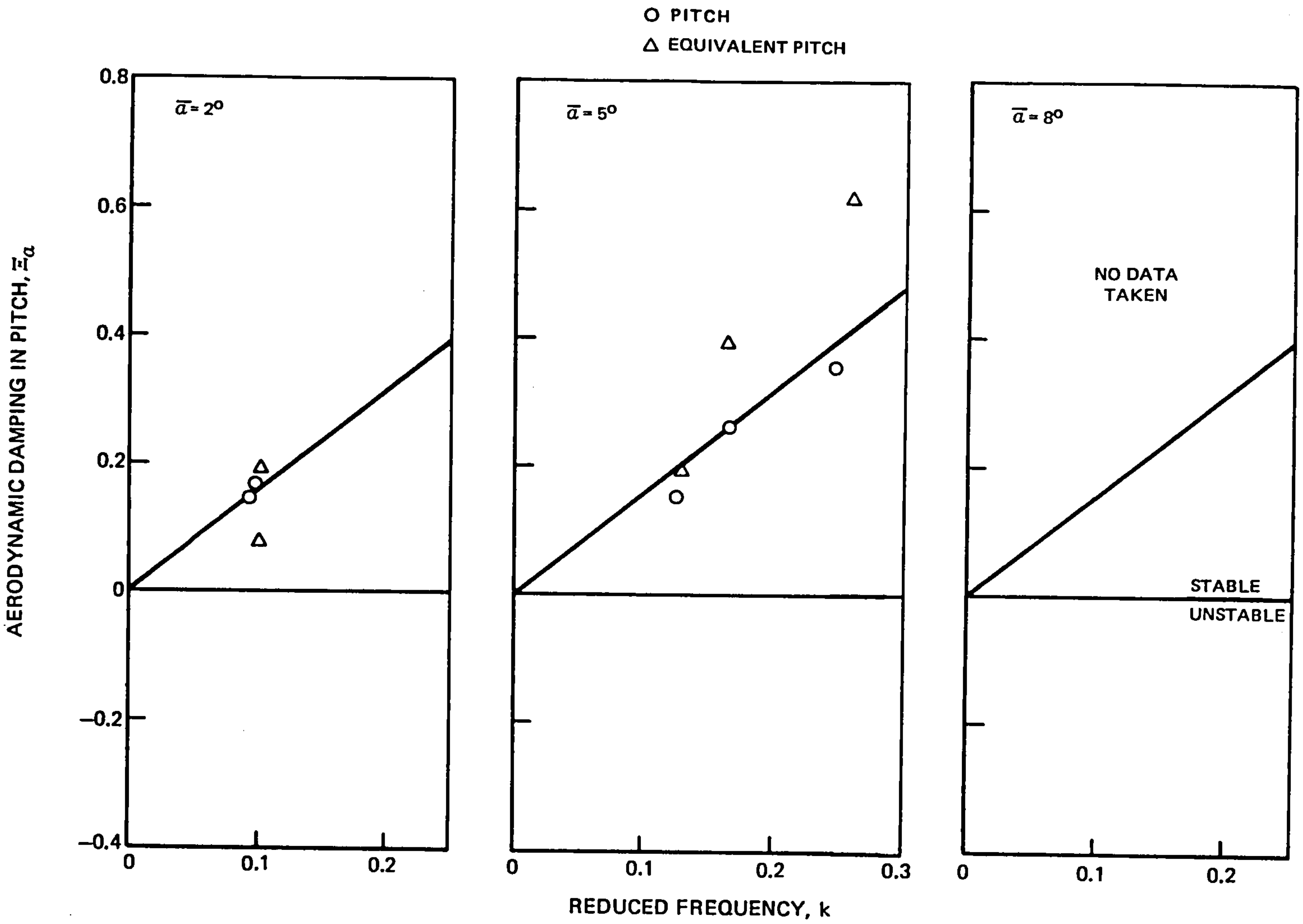

Figure 15 (continued)
c) Mean Incidence Angle $\alpha_M$ = 12 Deg.

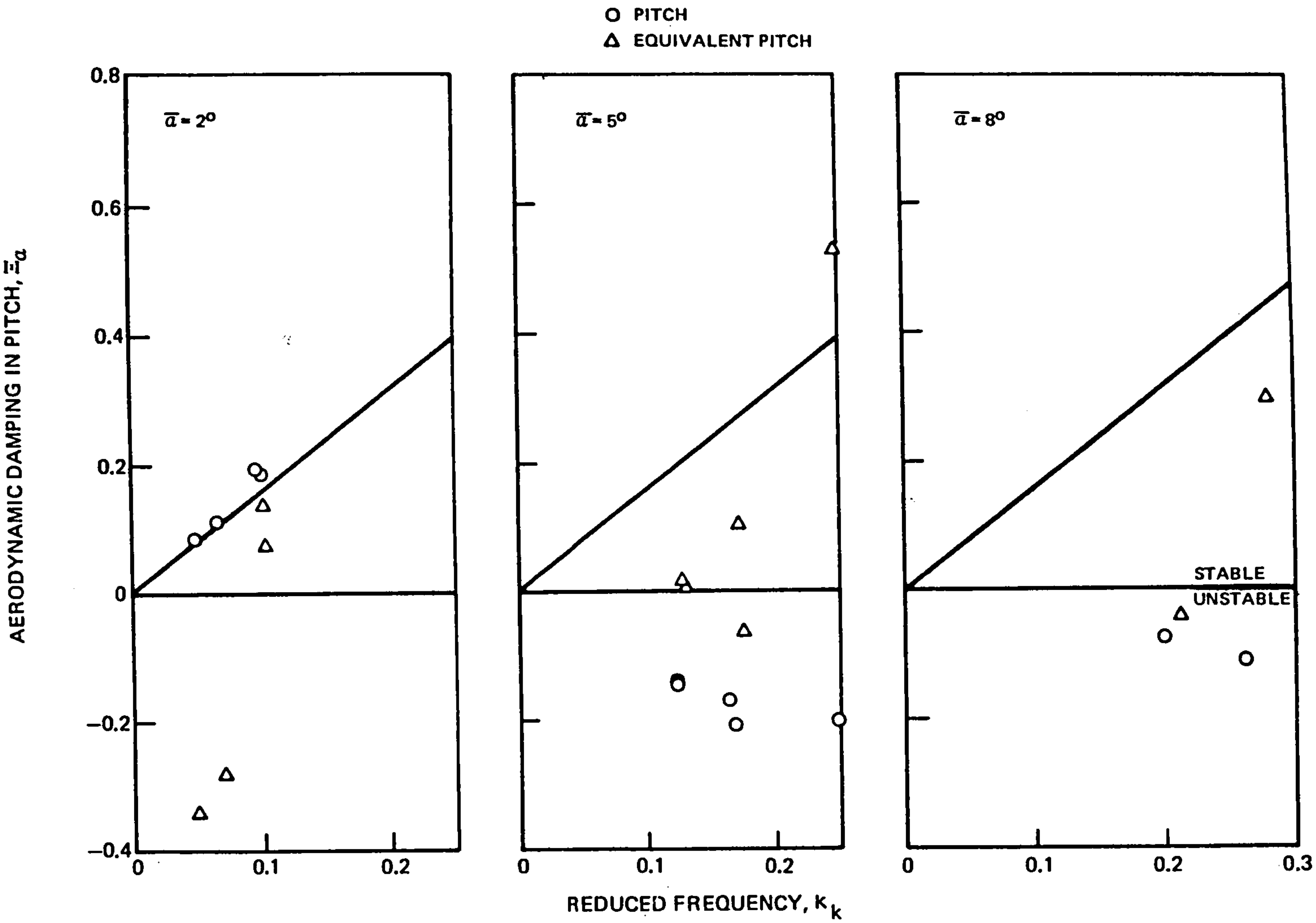

Figure 15 (concluded)
d) Mean Incidence Angle $\alpha_M$ = 15 Deg.

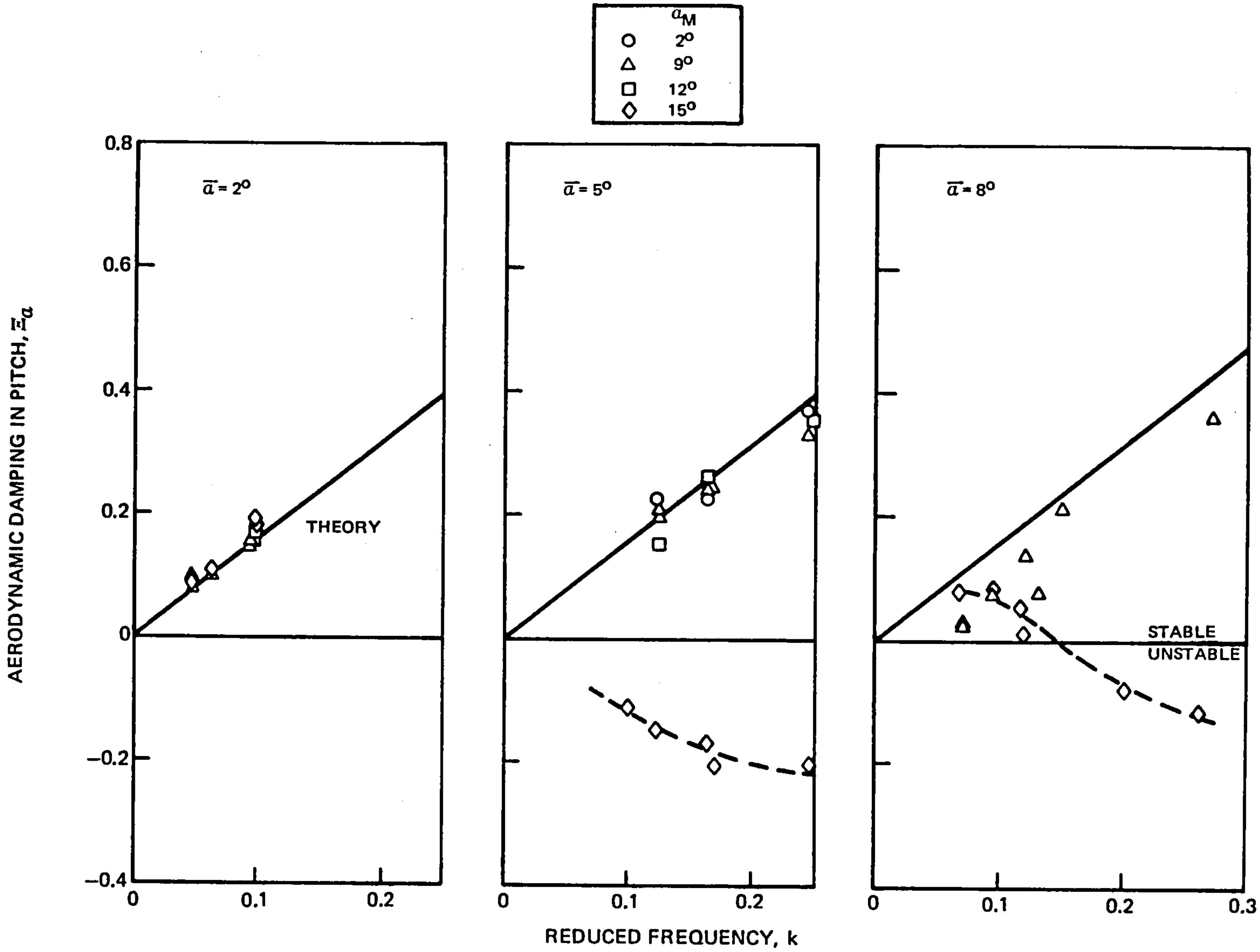

Figure 16 Aerodynamic Damping in Pitch for All Incidence Angles

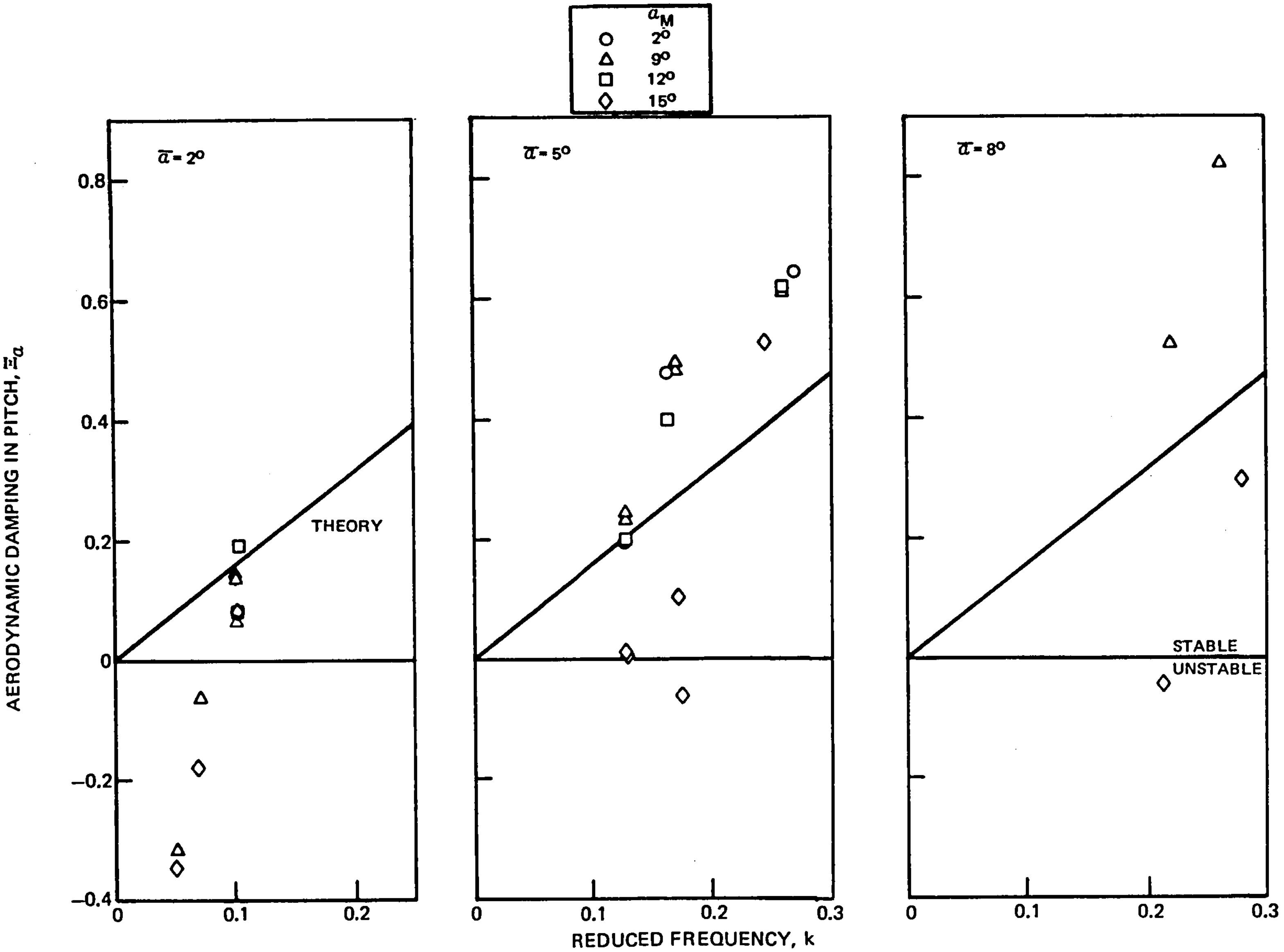

**Figure 17 Aerodynamic Damping in Equivalent Pitch for All Incidence Angles**

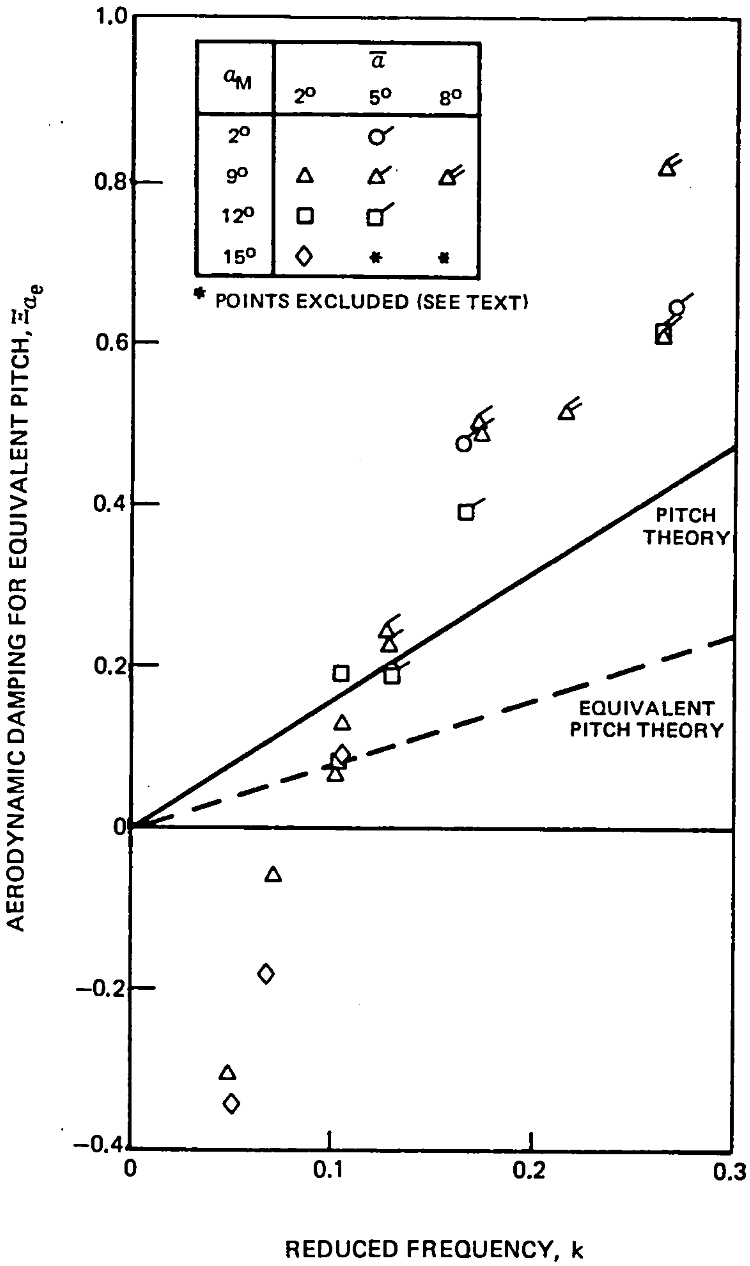

Figure 18 Composite Aerodynamic Damping for Equivalent Pitch

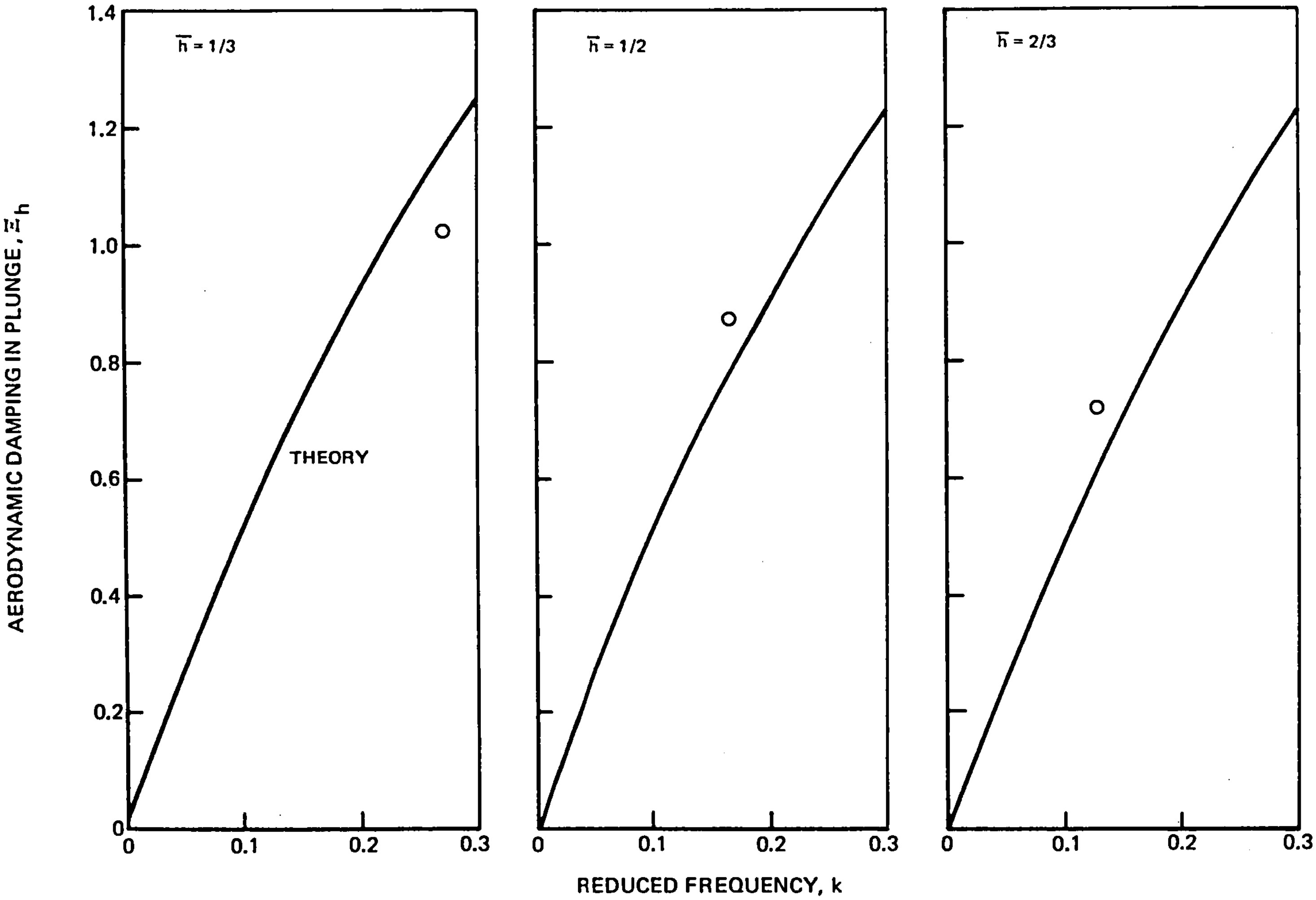

Figure 19 Aerodynamic Damping in Plunge
a) Mean Incidence Angle $\alpha_M$ = 2 Deg.

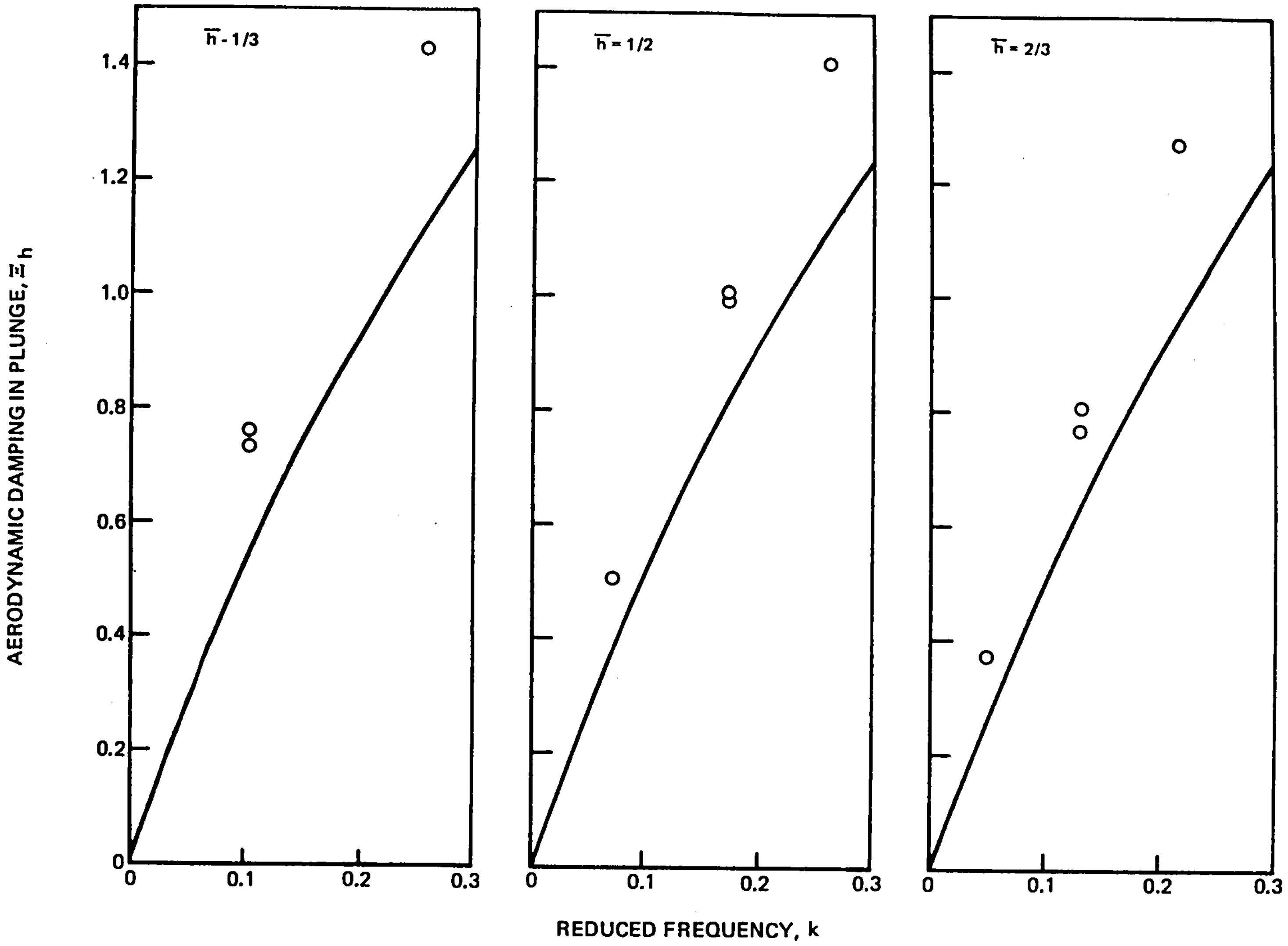

Figure 19 (continued)

b) Mean Incidence Angle $\alpha_M$ = 9 Deg.

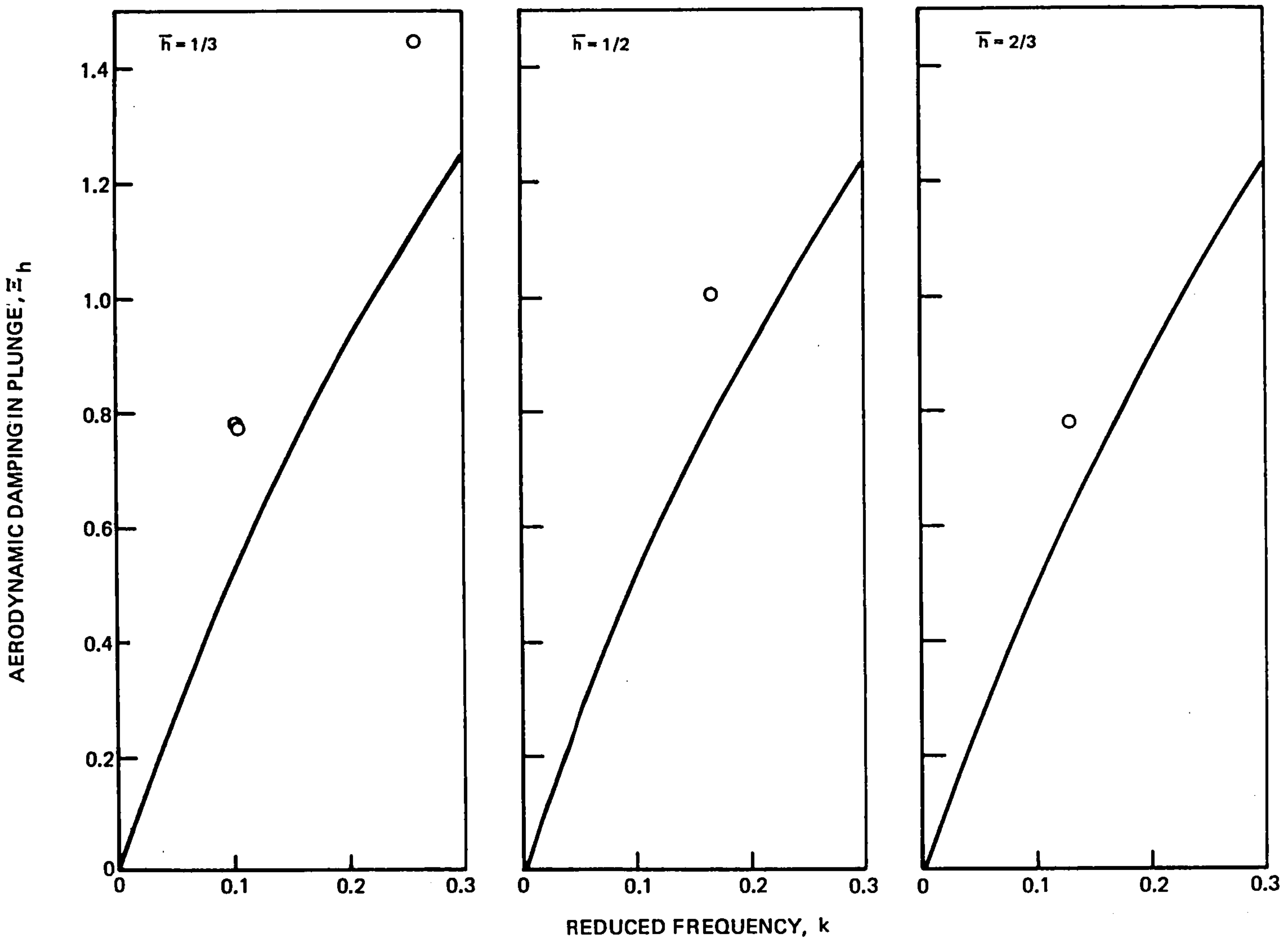

Figure 19 (continued)

c) Mean Incidence Angle $\alpha_M$ = 12 Deg.

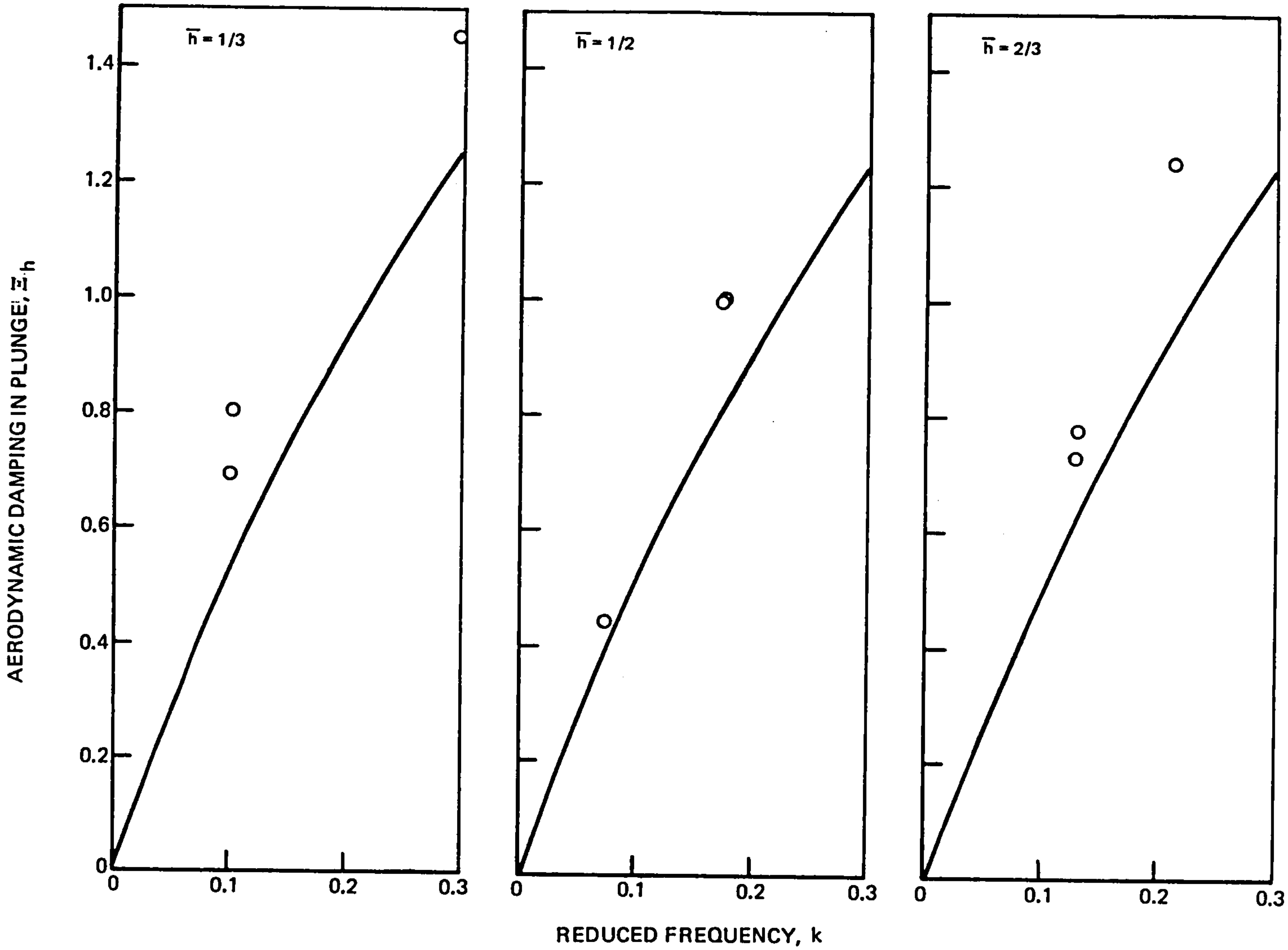

**Figure 19 (concluded)**
**d) Mean Incidence Angle $\alpha_M$ = 15 Deg.**

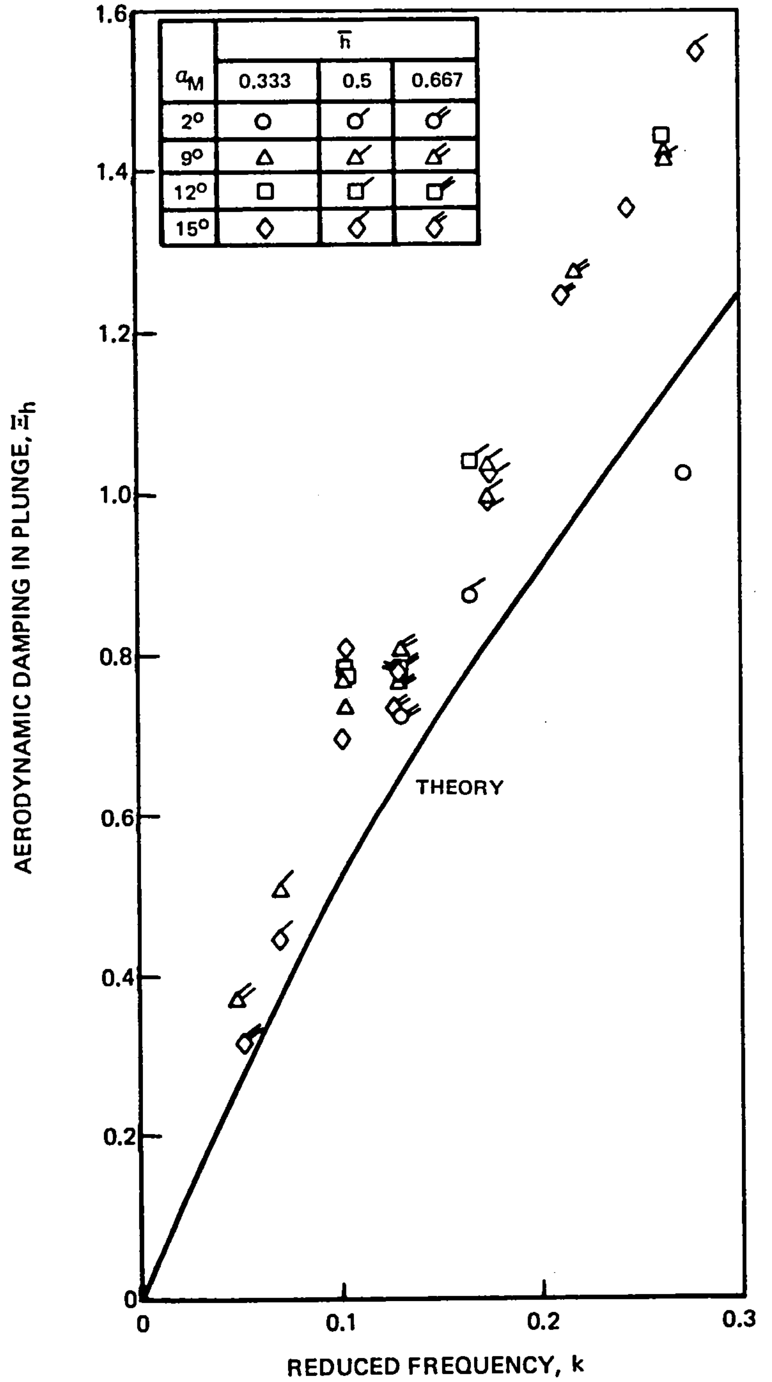

Figure 20 Composite of Aerodynamic Damping for Plunge

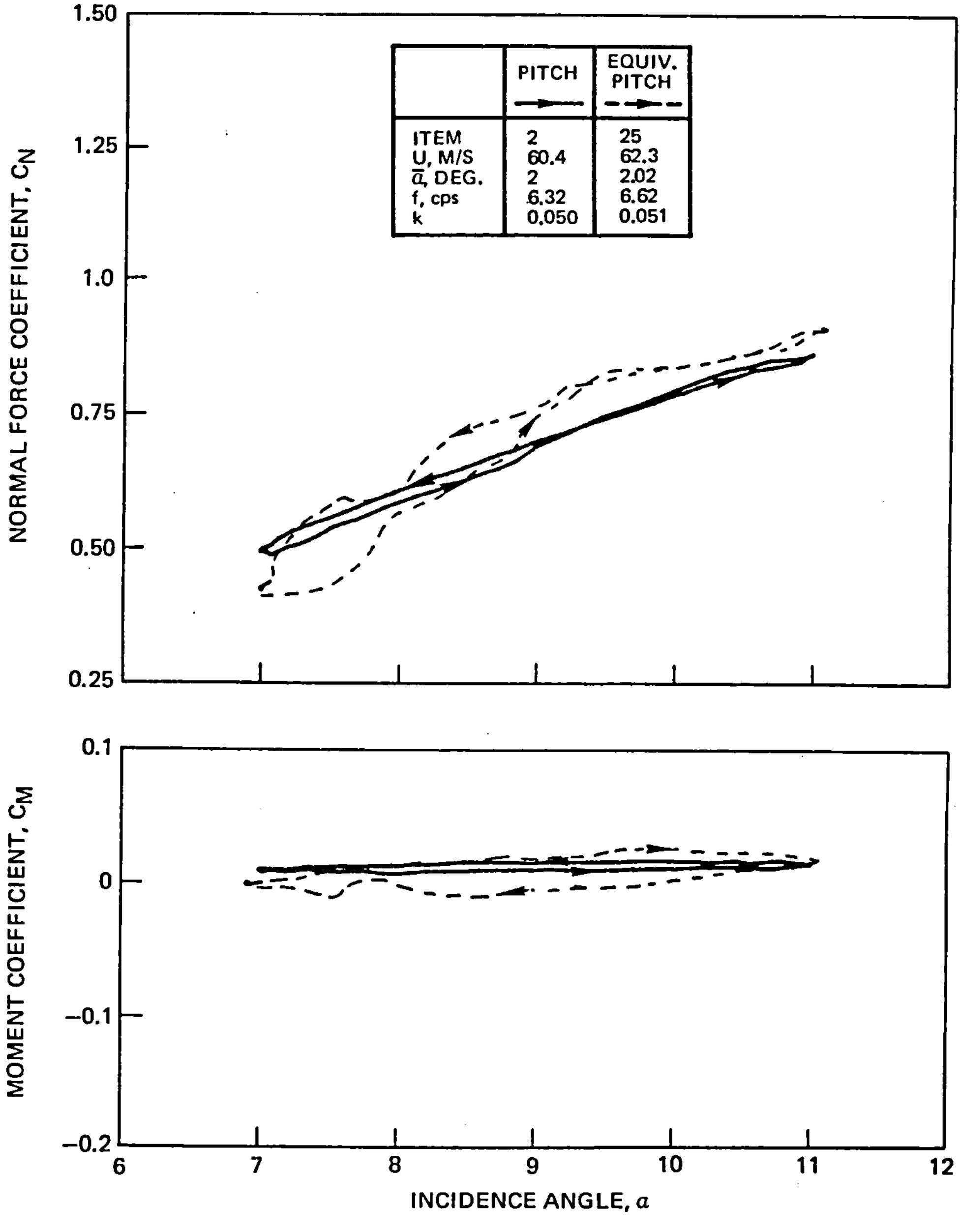

Figure 21 Normal Force and Pitching Moment Coefficient Loops for $a_M = 9^\circ, \bar{a} \cong 2^\circ, k \cong 0.05$

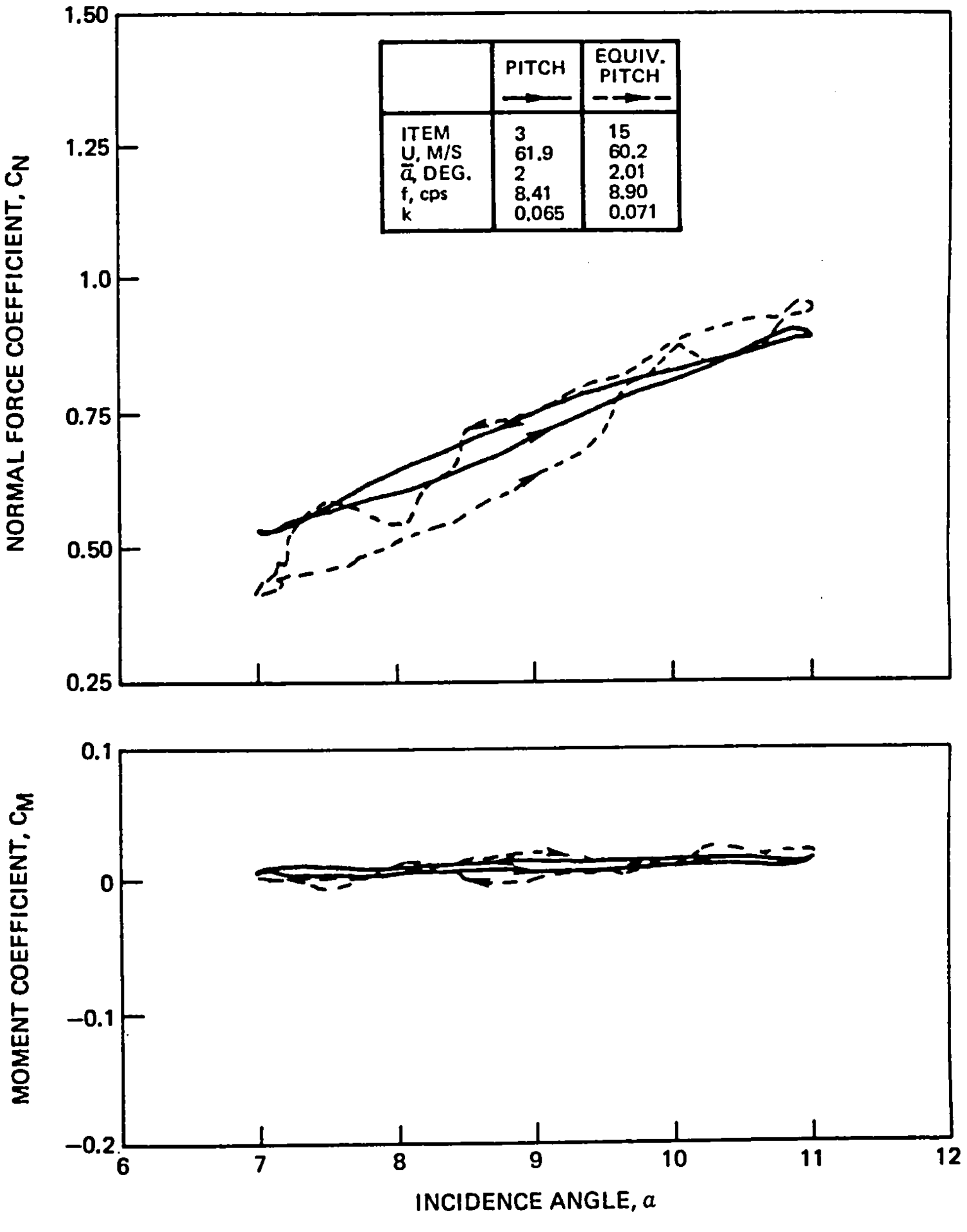

Figure 22 Normal Force and Pitching Moment Coefficient Loops for $\alpha_M = 9^\circ, \bar{\alpha} \cong 2^\circ, k \cong 0.07$

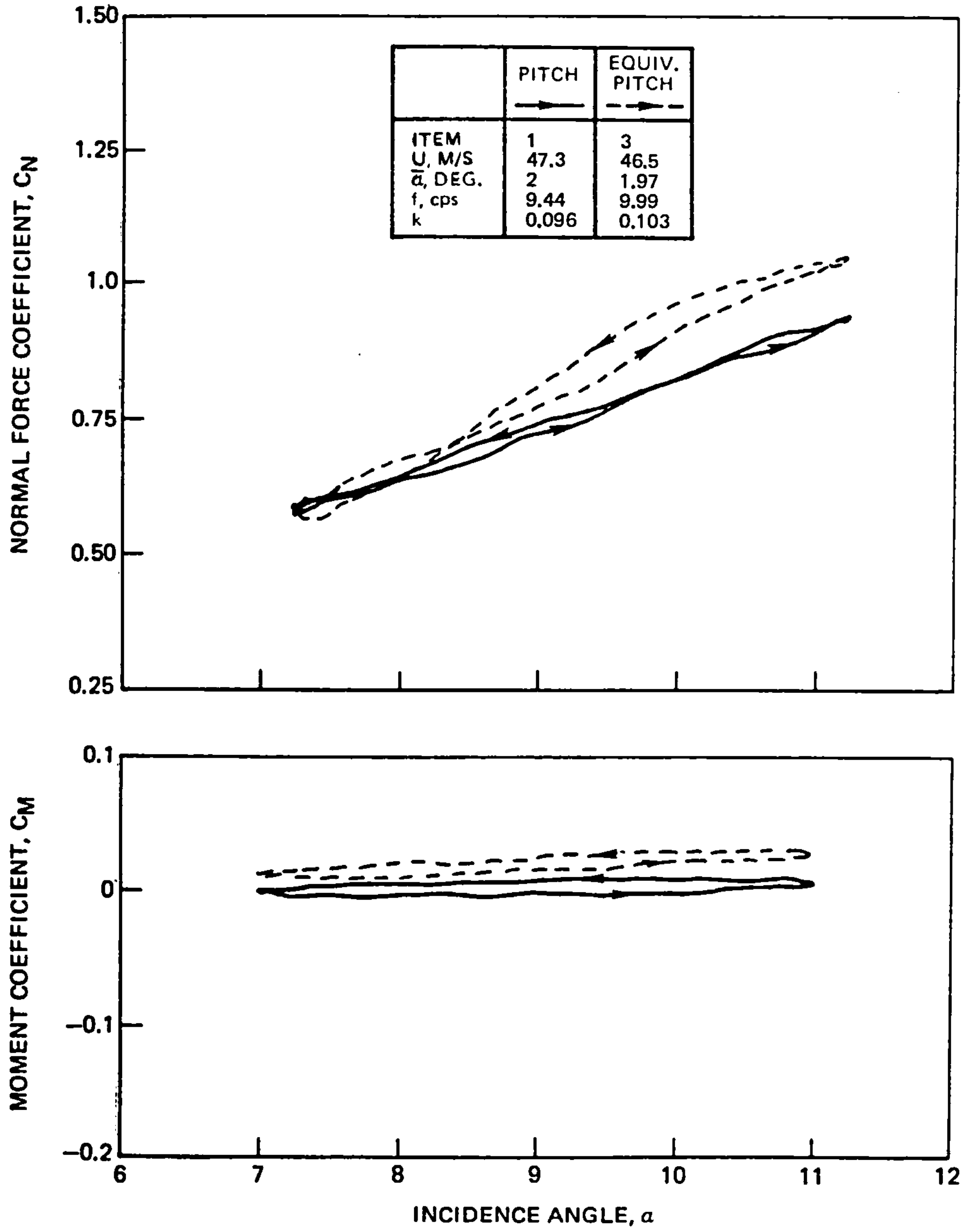

Figure 23 Normal Force and Pitching Moment Coefficient Loops for $a_M = 9^o, \bar{a} \cong 2^o, k \cong 0.10$

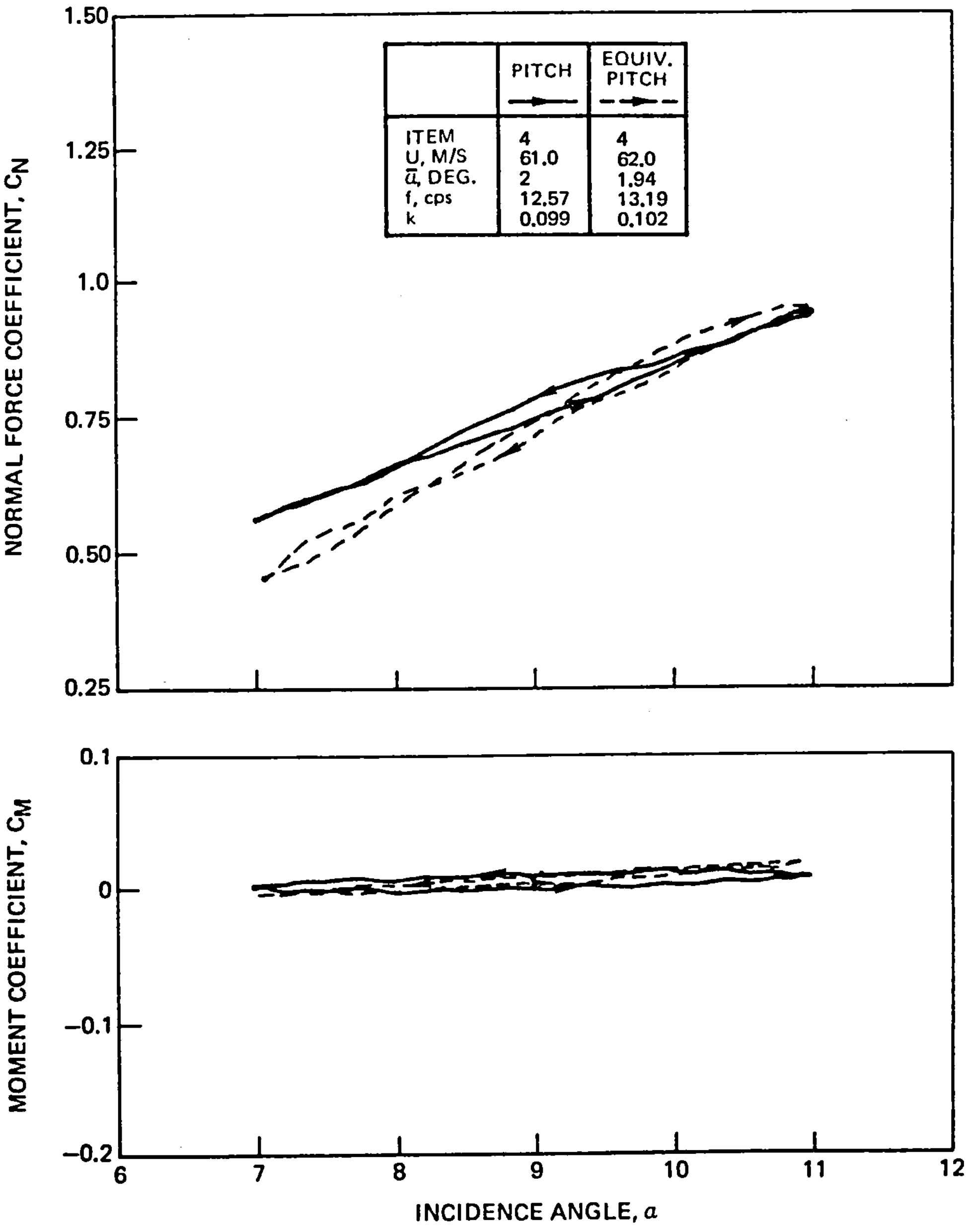

Figure 24 Normal Force and Pitching Moment Coefficient Loops for $\alpha_M = 9^o, \bar{\alpha} \cong 2^o, k \cong 0.10$

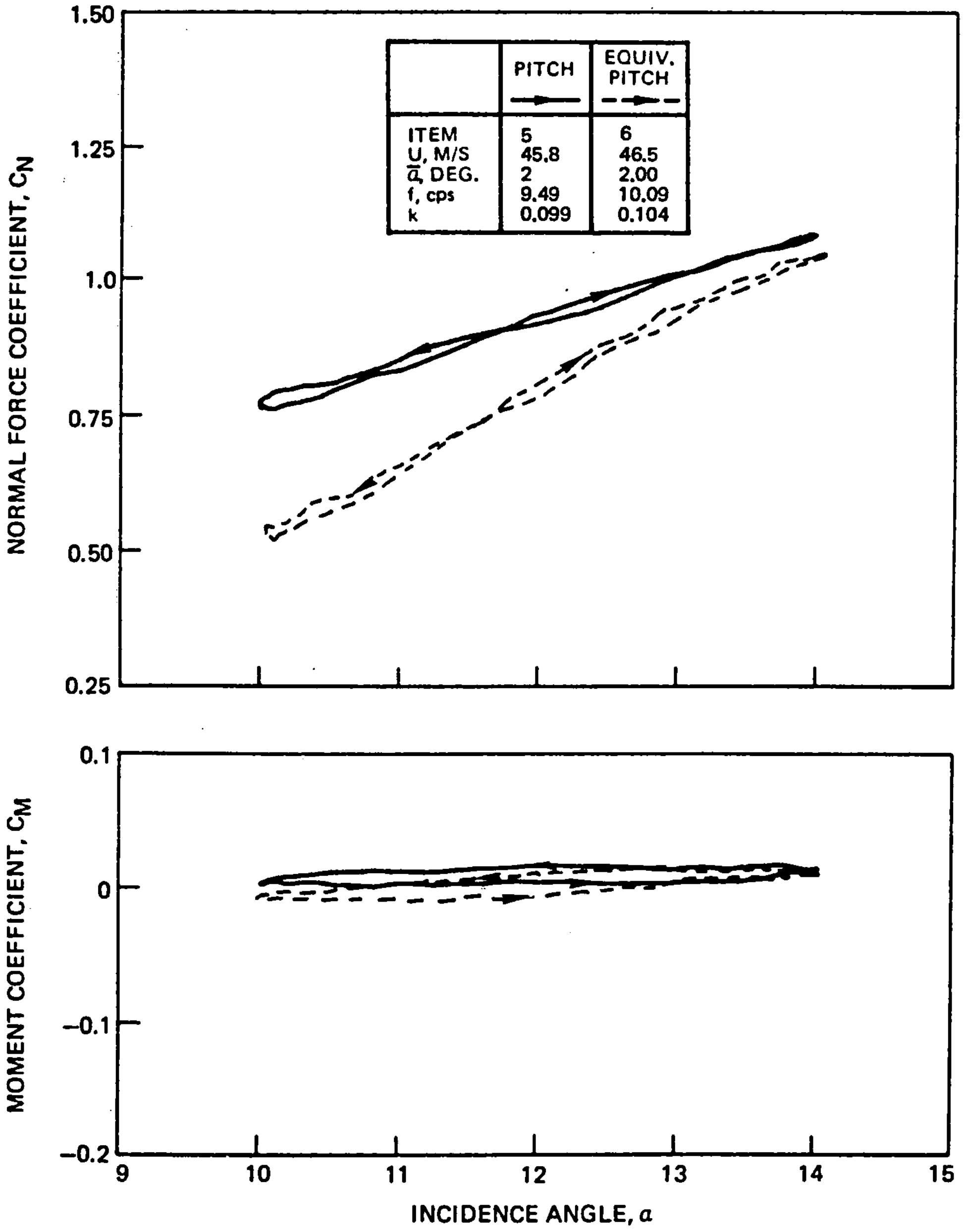

Figure 25 Normal Force and Pitching Moment Coefficient Loops for $a_M = 12^o, \bar{a} \cong 2^o, k \cong 0.10$

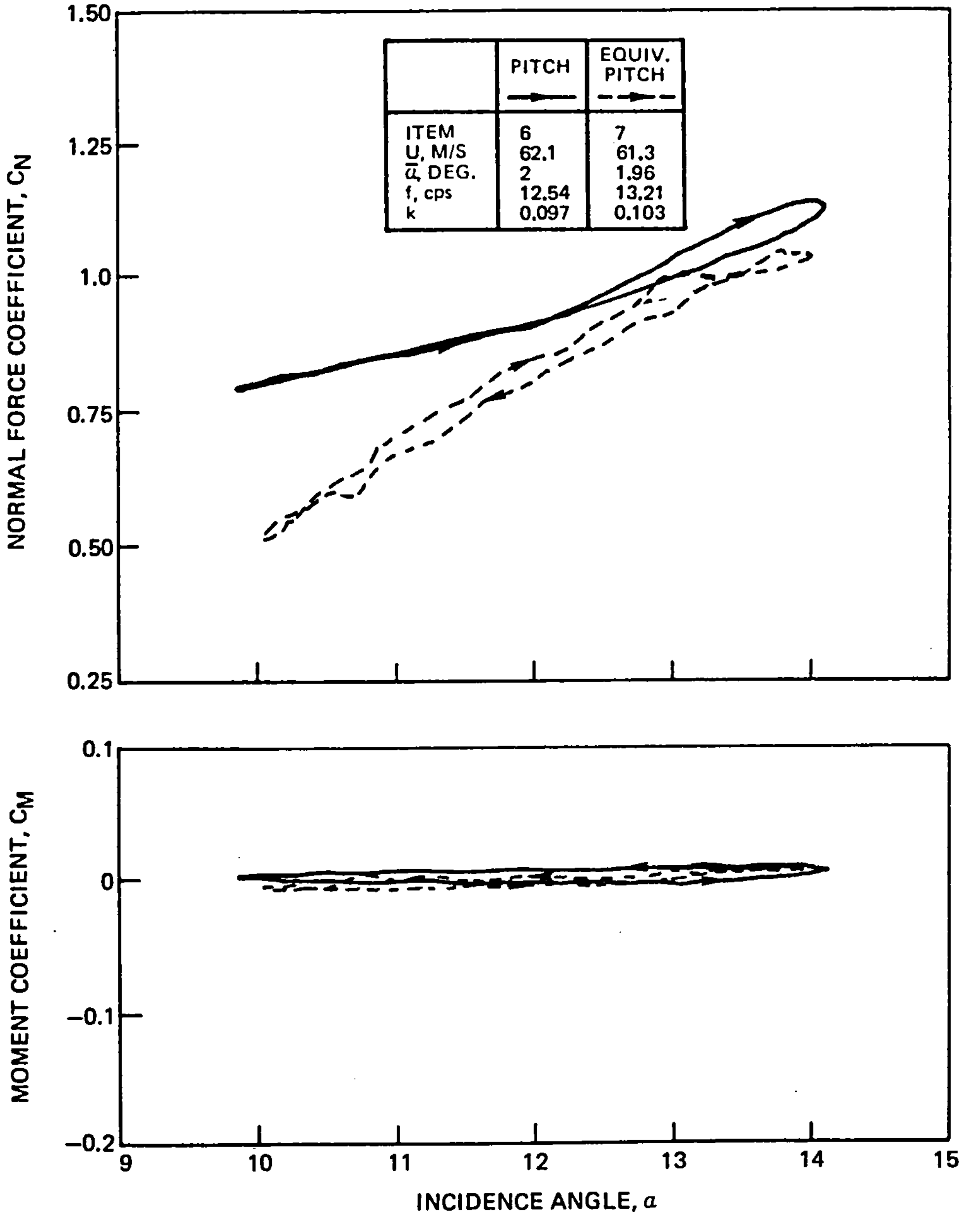

Figure 26 Normal Force and Pitching Moment Coefficient Loops for $\alpha_M = 12^o, \bar{\alpha} \cong 2^o, k \cong 0.10$

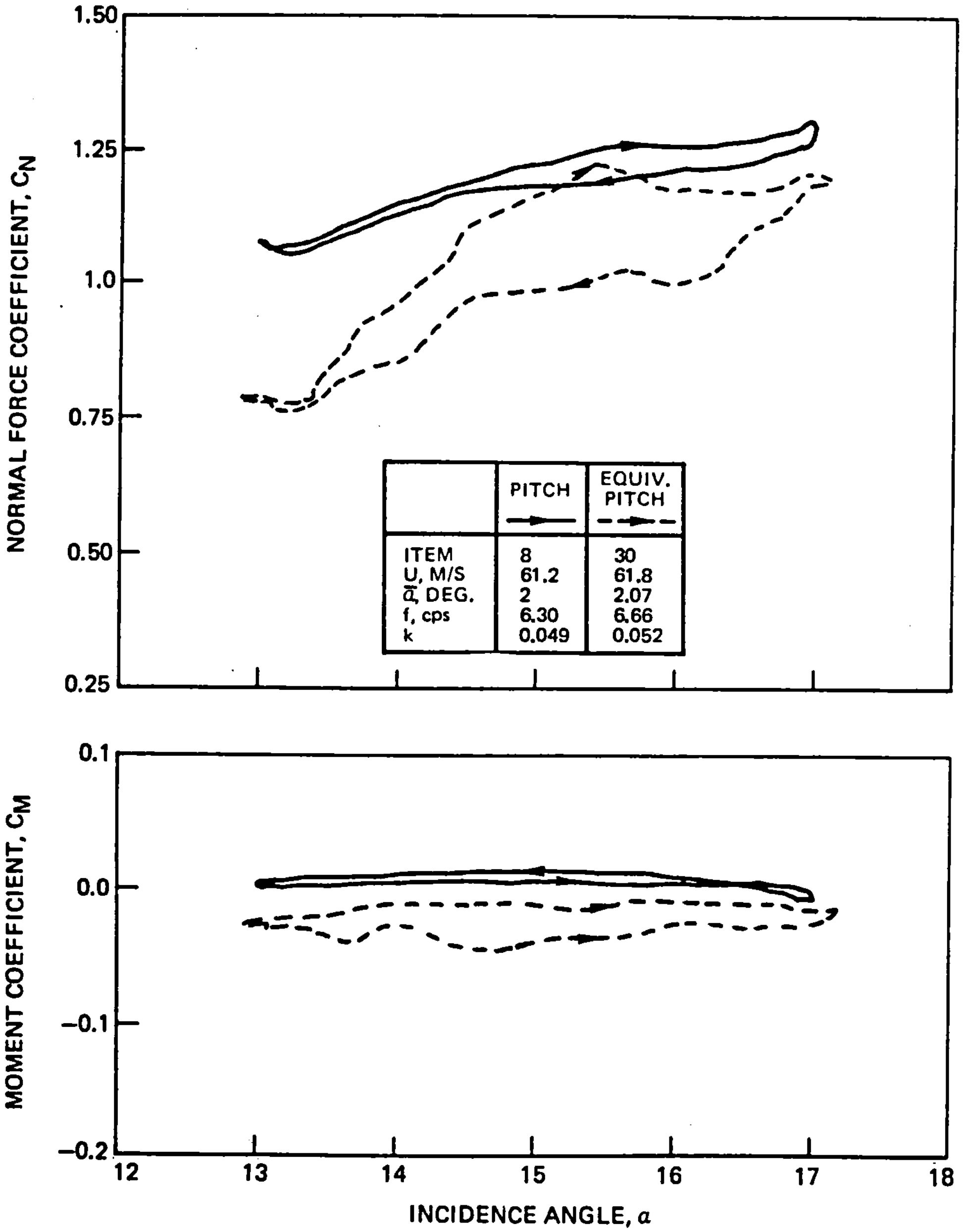

**Figure 27** Normal Force and Pitching Moment Coefficient Loops for $\alpha_M = 15^\circ, \bar{\alpha} \cong 2^\circ, k \cong 0.05$

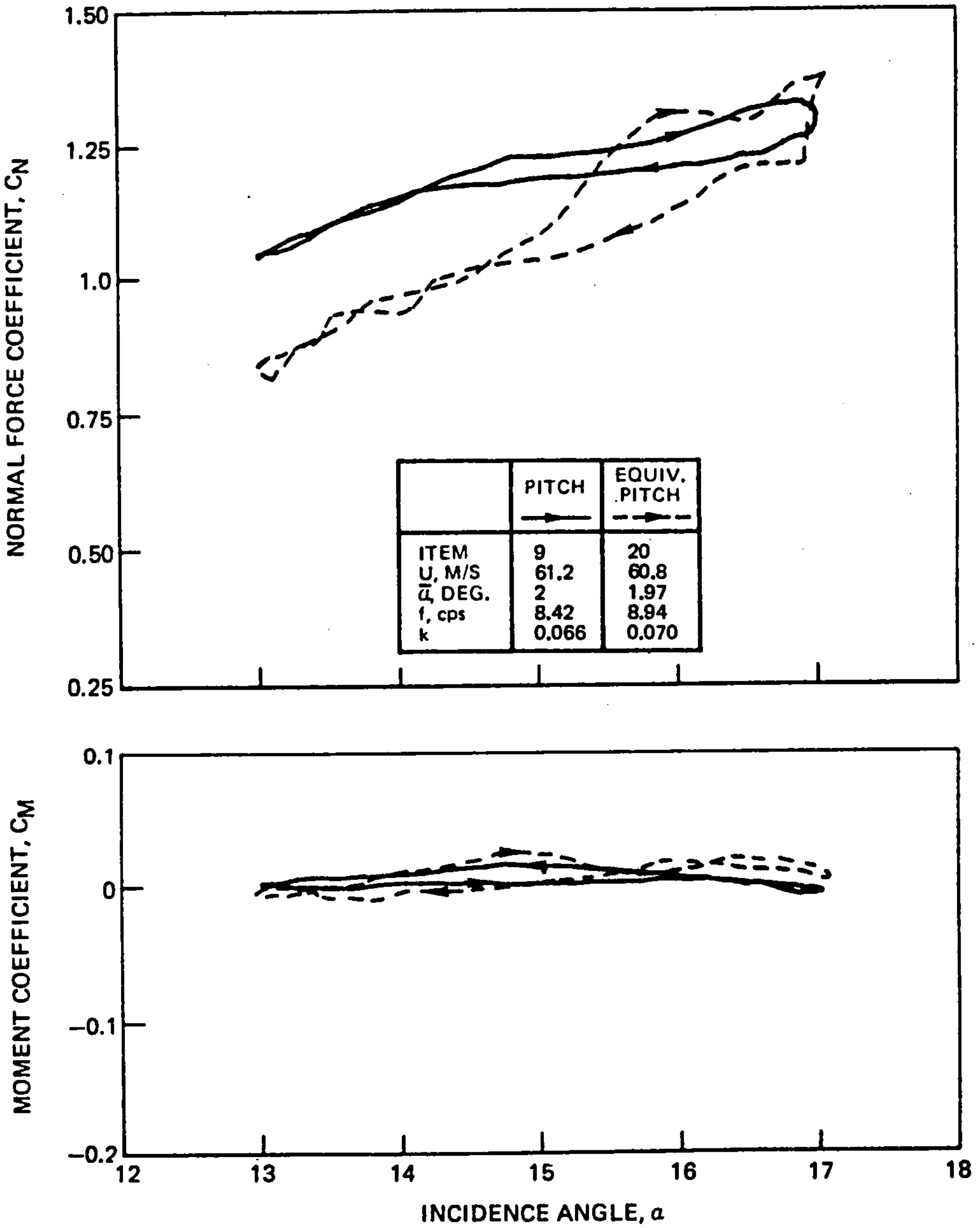

| | PITCH ——▶—— | EQUIV. PITCH – –▶– – |
|---|---|---|
| ITEM | 9 | 20 |
| U, M/S | 61.2 | 60.8 |
| $\bar{\alpha}$, DEG. | 2 | 1.97 |
| f, cps | 8.42 | 8.94 |
| k | 0.066 | 0.070 |

**Figure 28** Normal Force and Pitching Moment Coefficient Loops for $\alpha_M = 15^o, \bar{\alpha} \cong 2^o, k \cong 0.07$

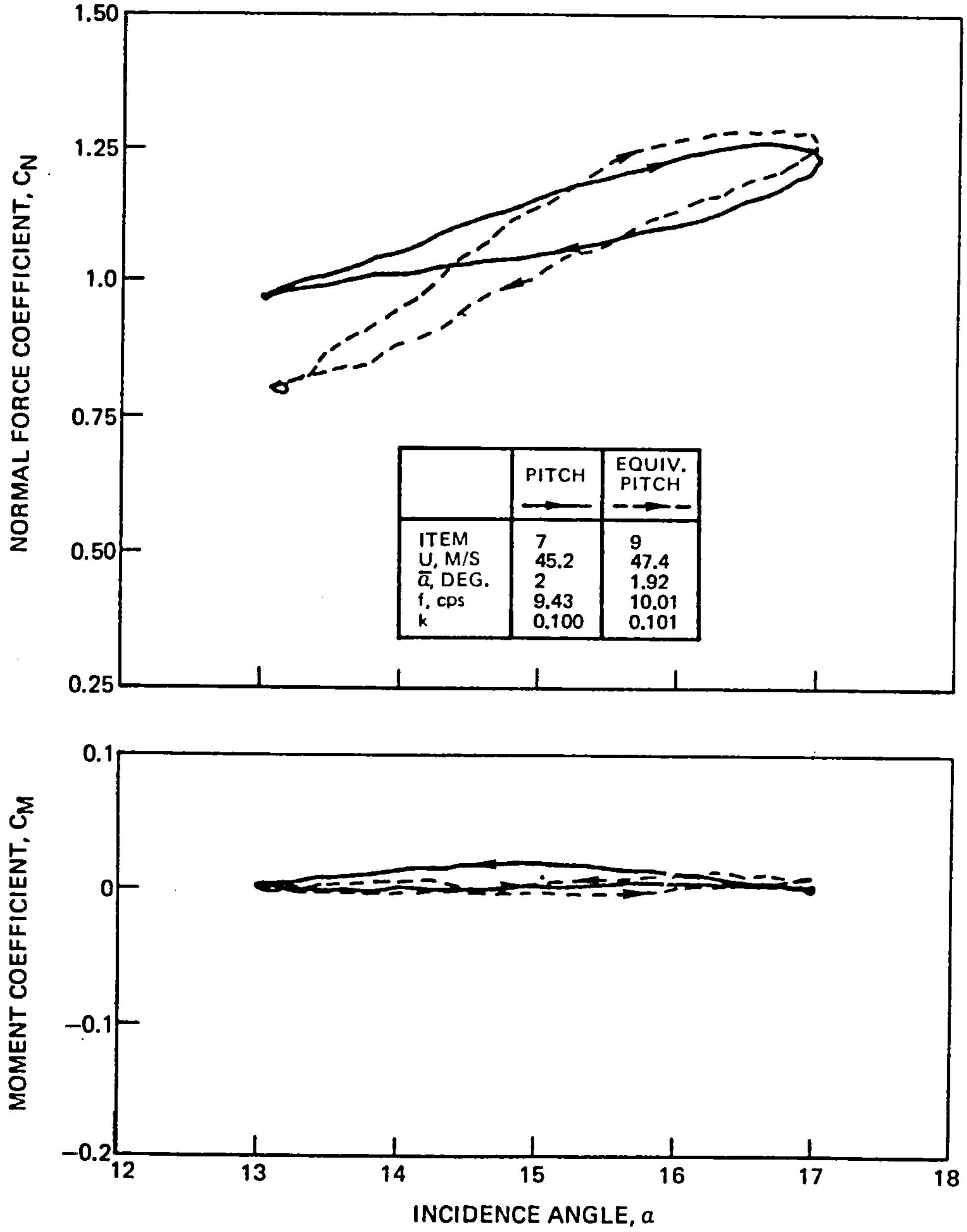

Figure 29 Normal Force and Pitching Moment Coefficient Loops for $\alpha_M = 15^o, \bar{\alpha} \cong 2^o, k \cong 0.10$

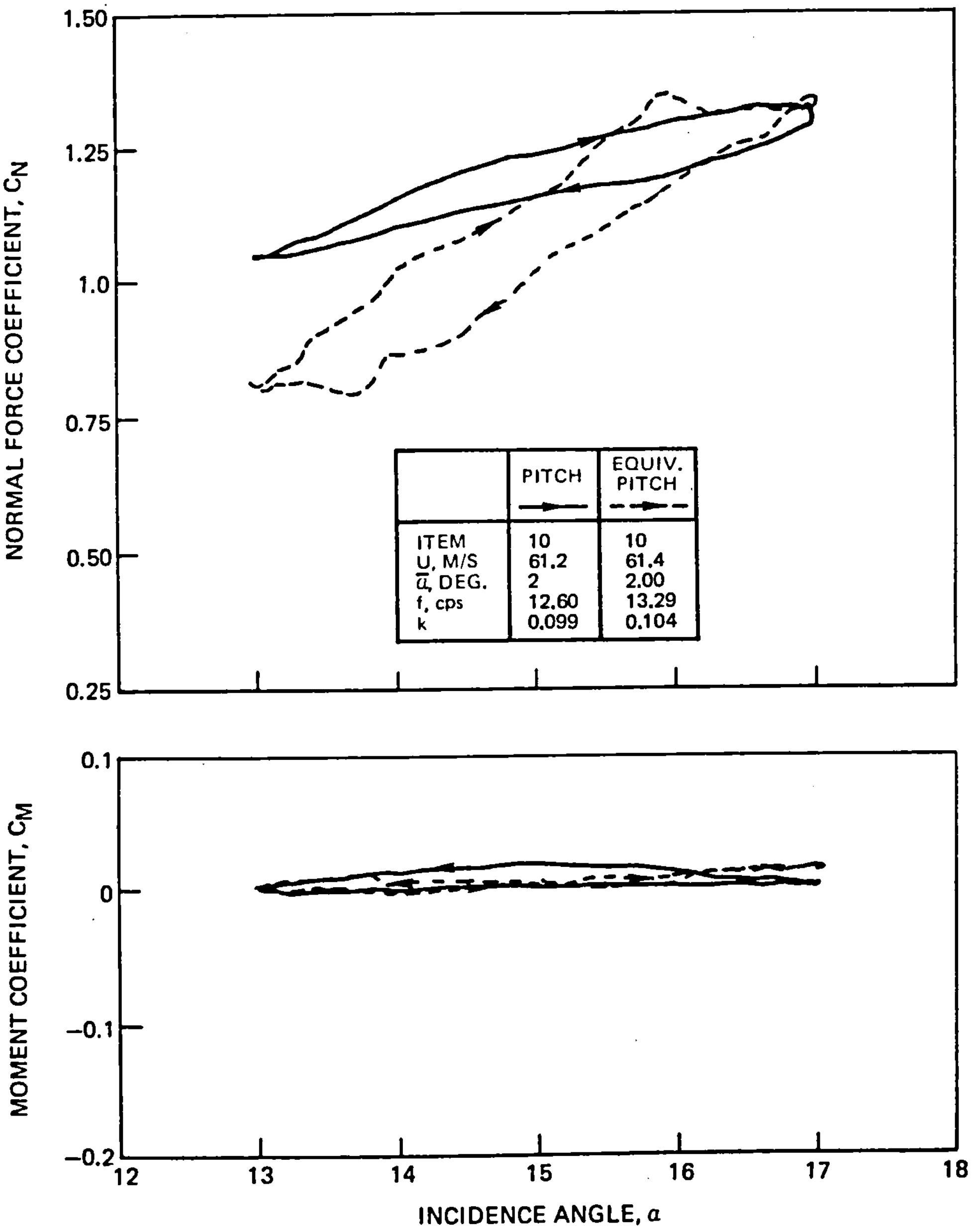

| | PITCH<br>——▶—— | EQUIV. PITCH<br>– – ▶ – – |
|---|---|---|
| ITEM | 10 | 10 |
| U, M/S | 61.2 | 61.4 |
| $\bar{\alpha}$, DEG. | 2 | 2.00 |
| f, cps | 12.60 | 13.29 |
| k | 0.099 | 0.104 |

**Figure 30** Normal Force and Pitching Moment Coefficient Loops for $\alpha_M = 15^\circ, \bar{\alpha} \cong 2^\circ, k \cong 0.10$

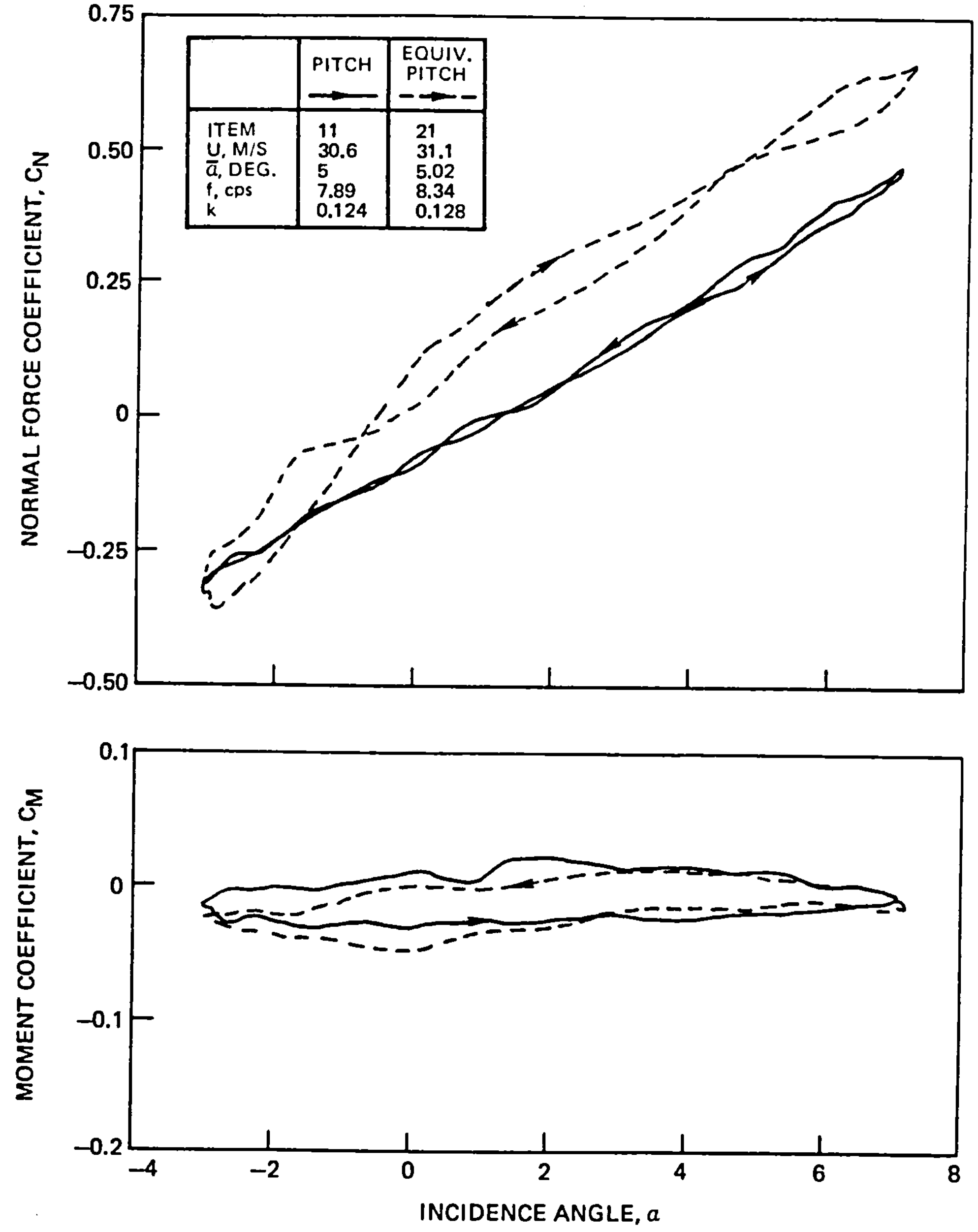

Figure 31 Normal Force and Pitching Moment Coefficient Loops for $\alpha_M = 2^\circ, \bar{\alpha} \cong 5^\circ, k \cong 0.12$

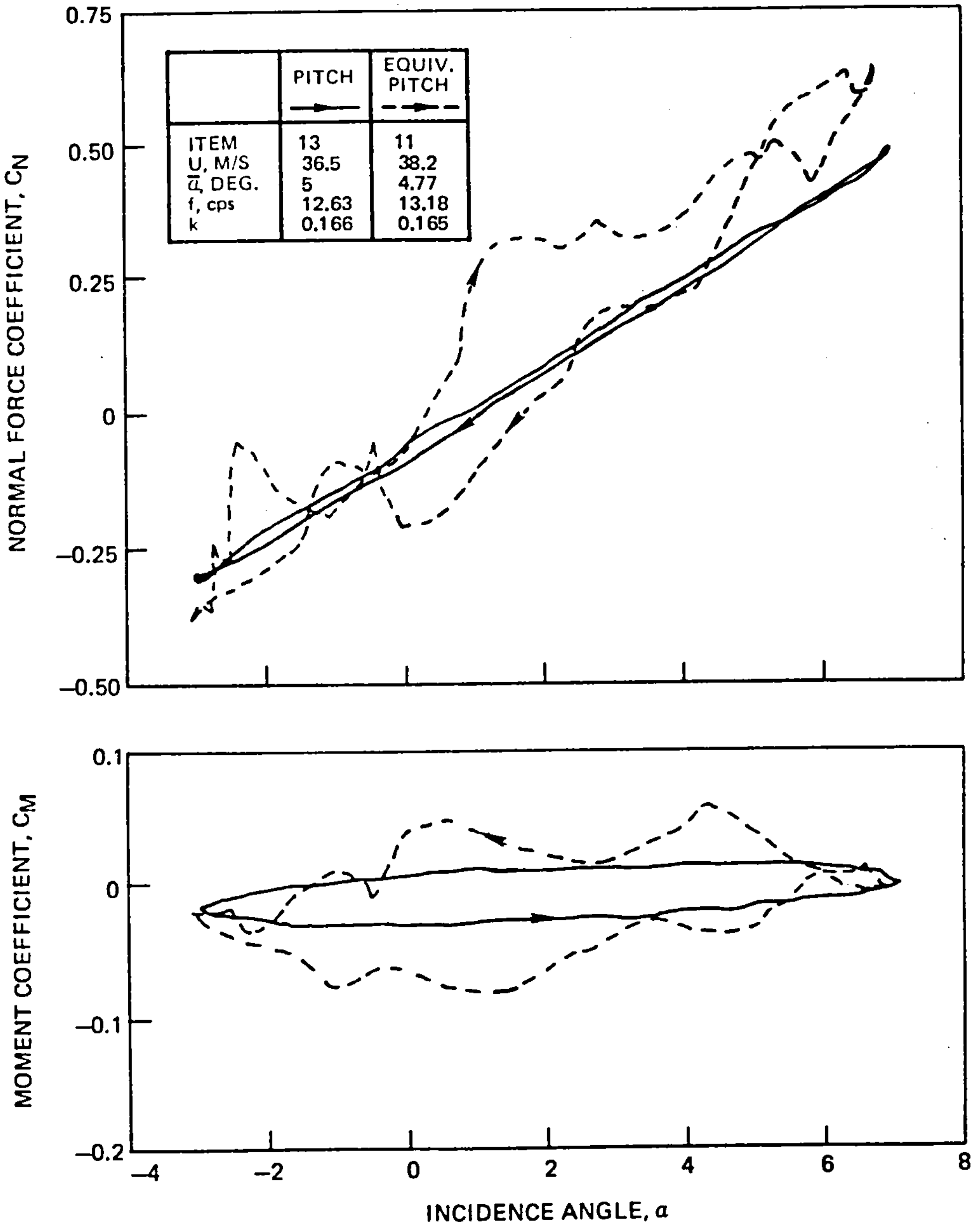

**Figure 32** Normal Force and Pitching Moment Coefficient Loops for $\alpha_M = 2^o, \bar{\alpha} \cong 5^o, k \cong 0.17$

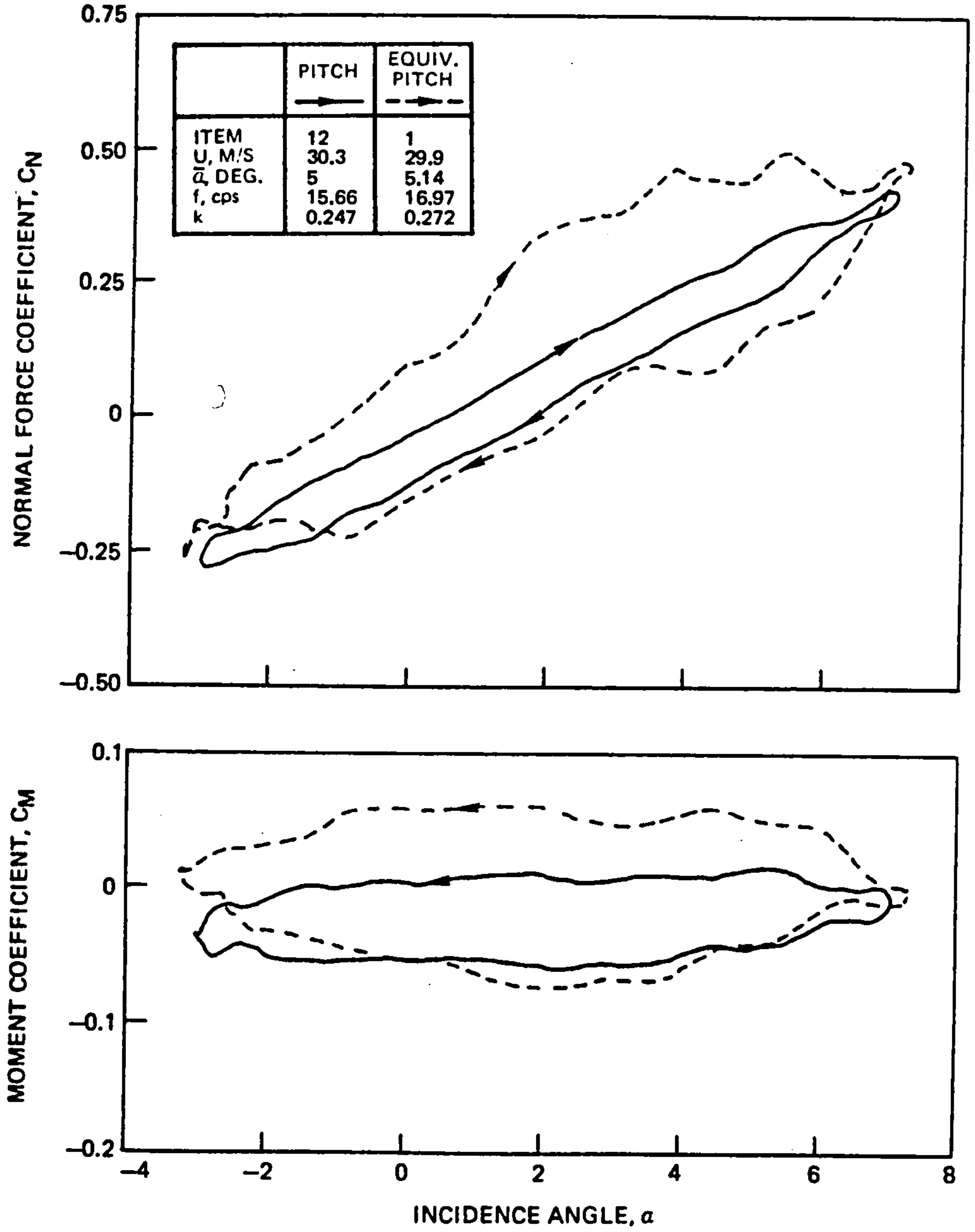

Figure 33 Normal Force and Pitching Moment Coefficient Loops for $\alpha_M = 2^o, \bar{\alpha} \cong 5^o, k \cong 0.25$

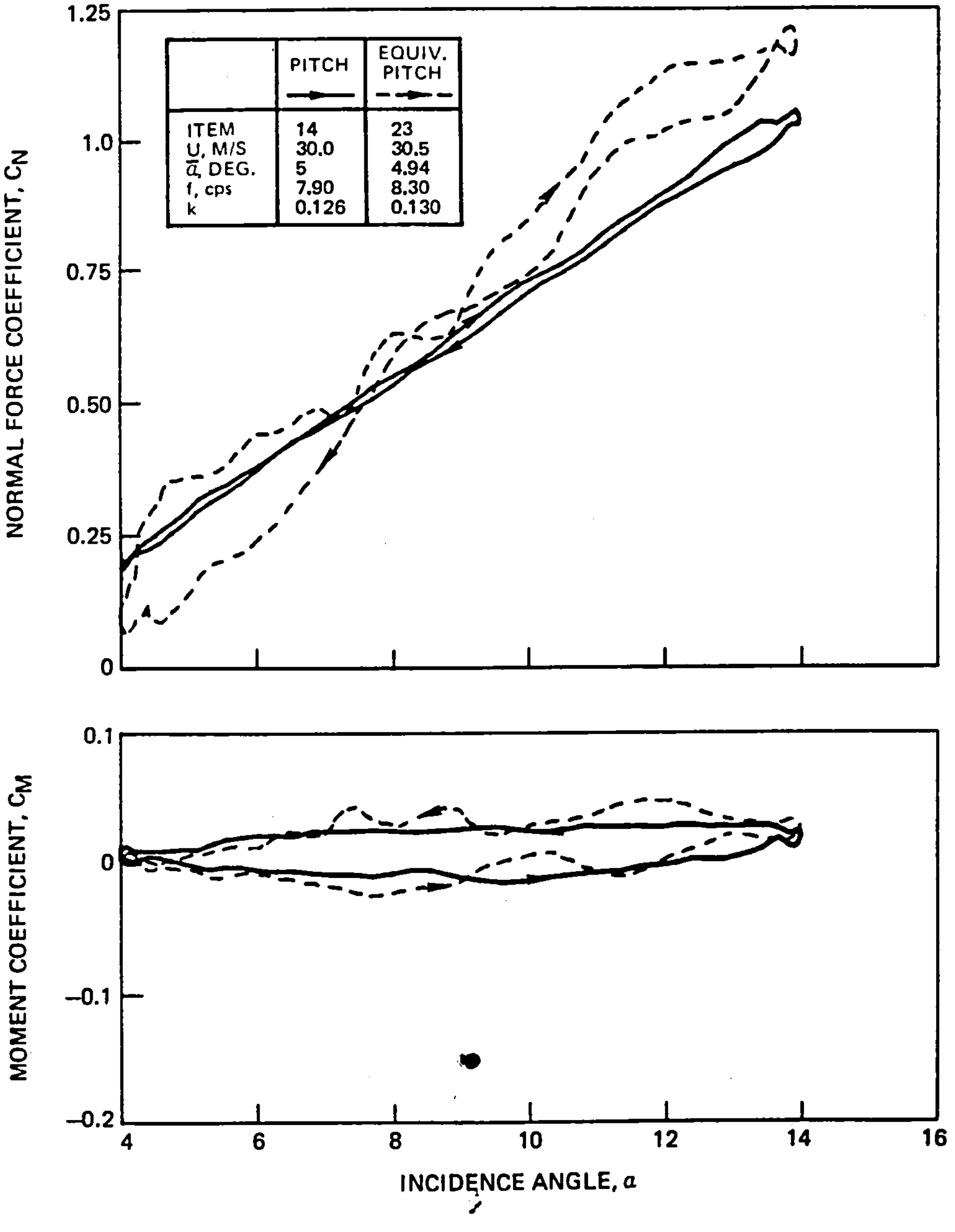

Figure 34 Normal Force and Pitching Moment Coefficient Loops for $\alpha_M = 9^o, \bar{\alpha} \cong 5^o, k \cong 0.13$

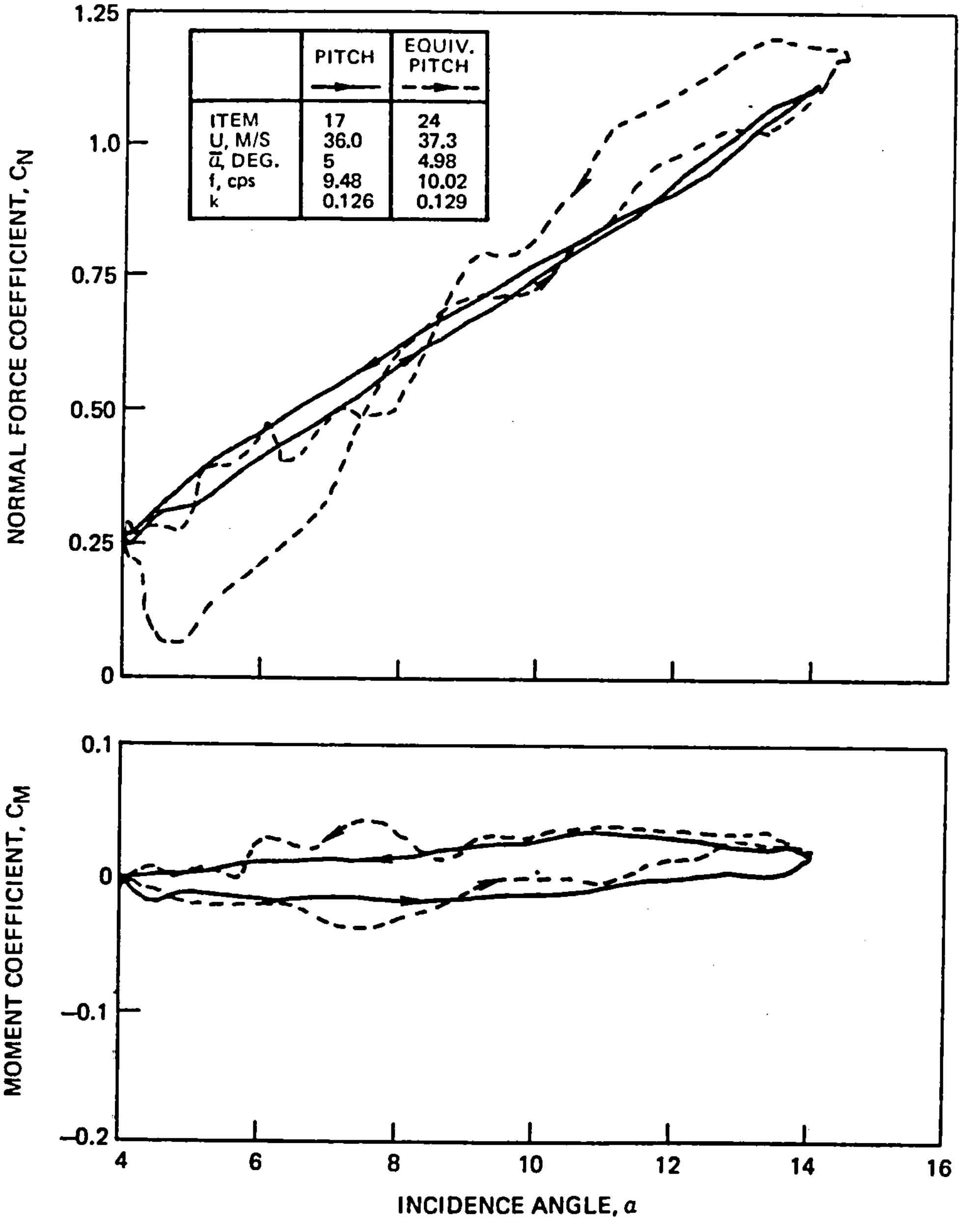

Figure 35 Normal Force and Pitching Moment Coefficient Loops for $\alpha_M = 9^o, \bar{\alpha} \cong 5^o, k \cong 0.13$

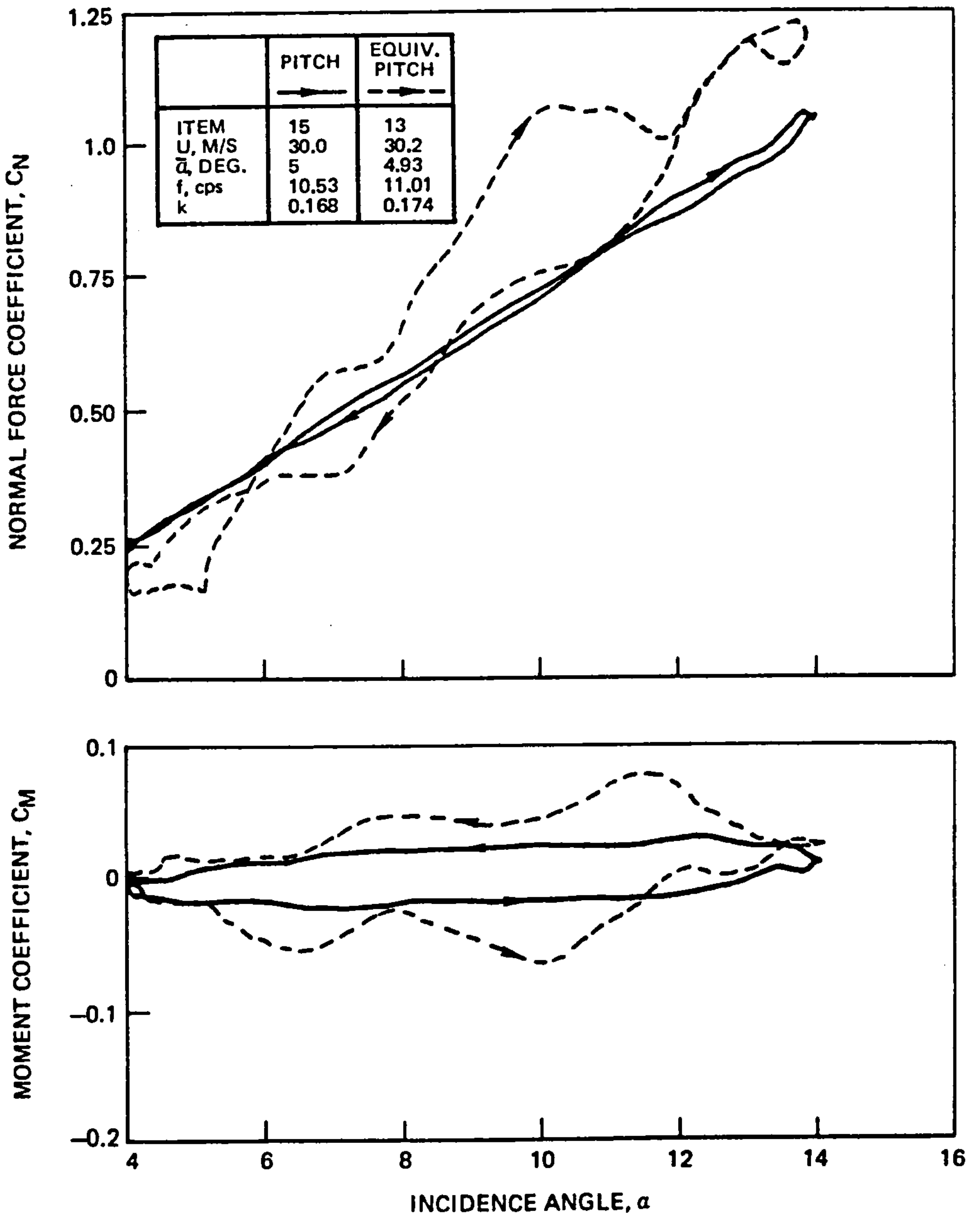

**Figure 36** Normal Force and Pitching Moment Coefficient Loops for $\alpha_M = 9^\circ, \bar{\alpha} \cong 5^\circ, k \cong 0.17$

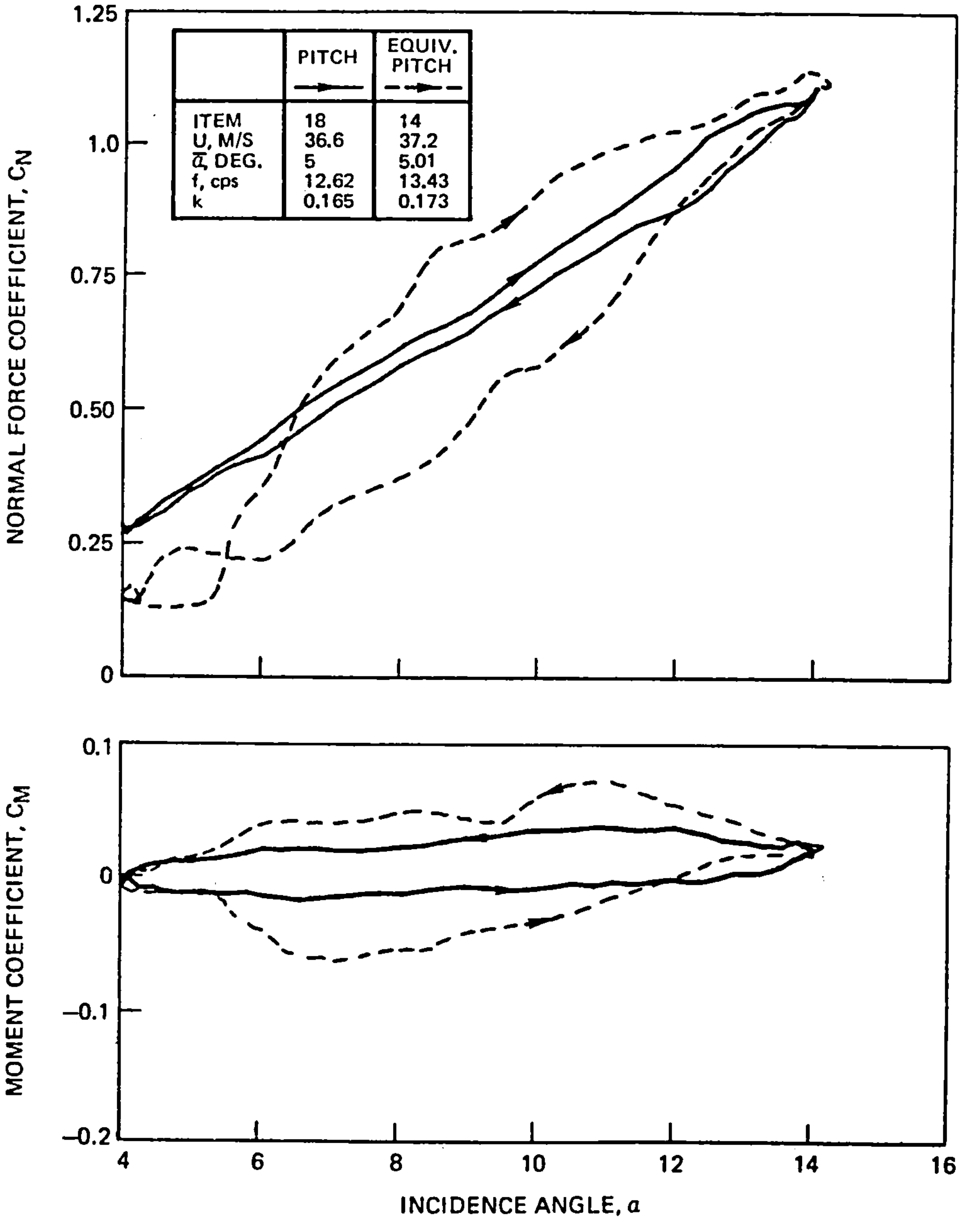

Figure 37 Normal Force and Pitching Moment Coefficient Loops for $a_M = 9^o, \bar{a} \cong 5^o, k \cong 0.17$

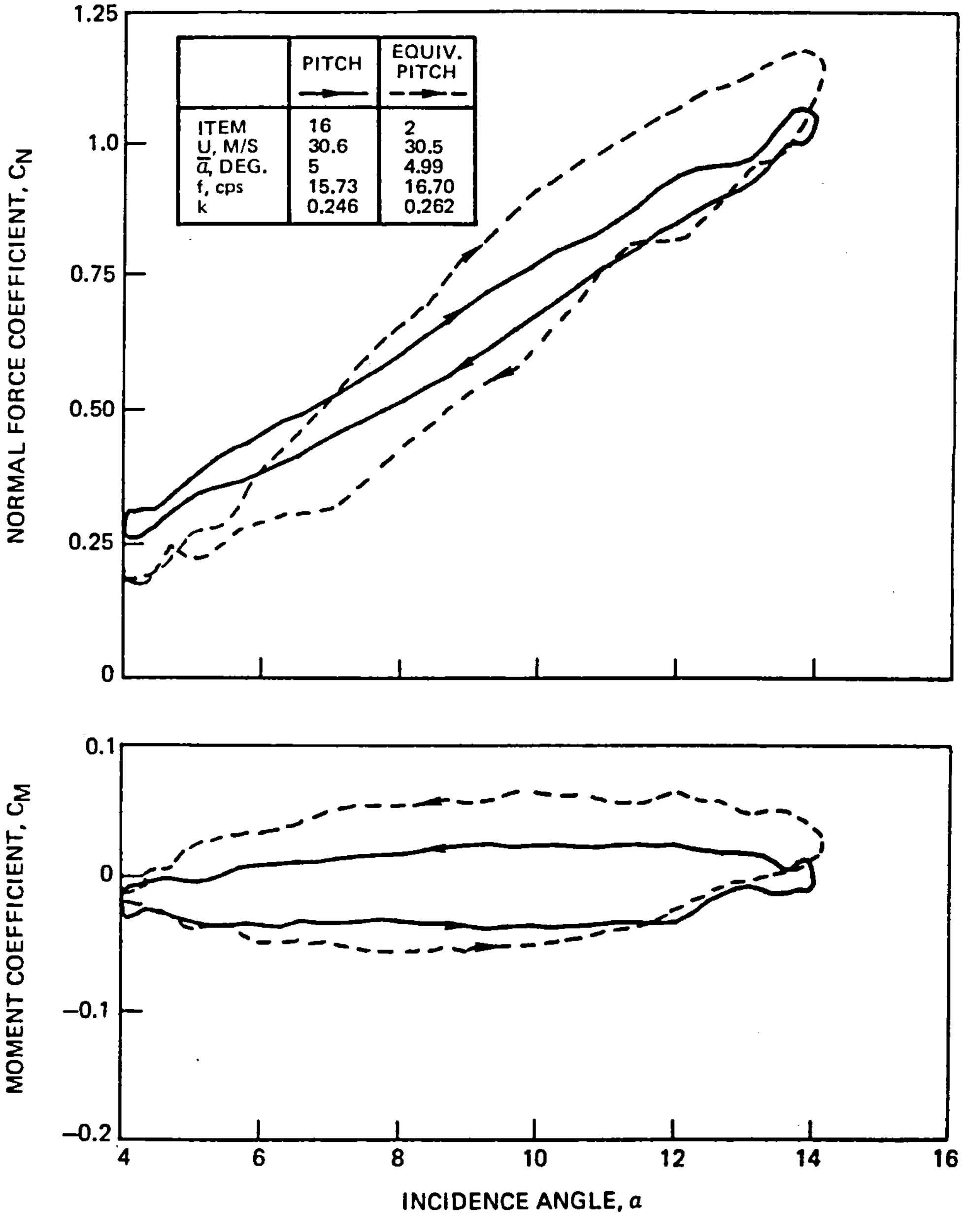

**Figure 38** Normal Force and Pitching Moment Coefficient Loops for $\alpha_M = 9^\circ, \bar{\alpha} \cong 5^\circ, k \cong 0.25$

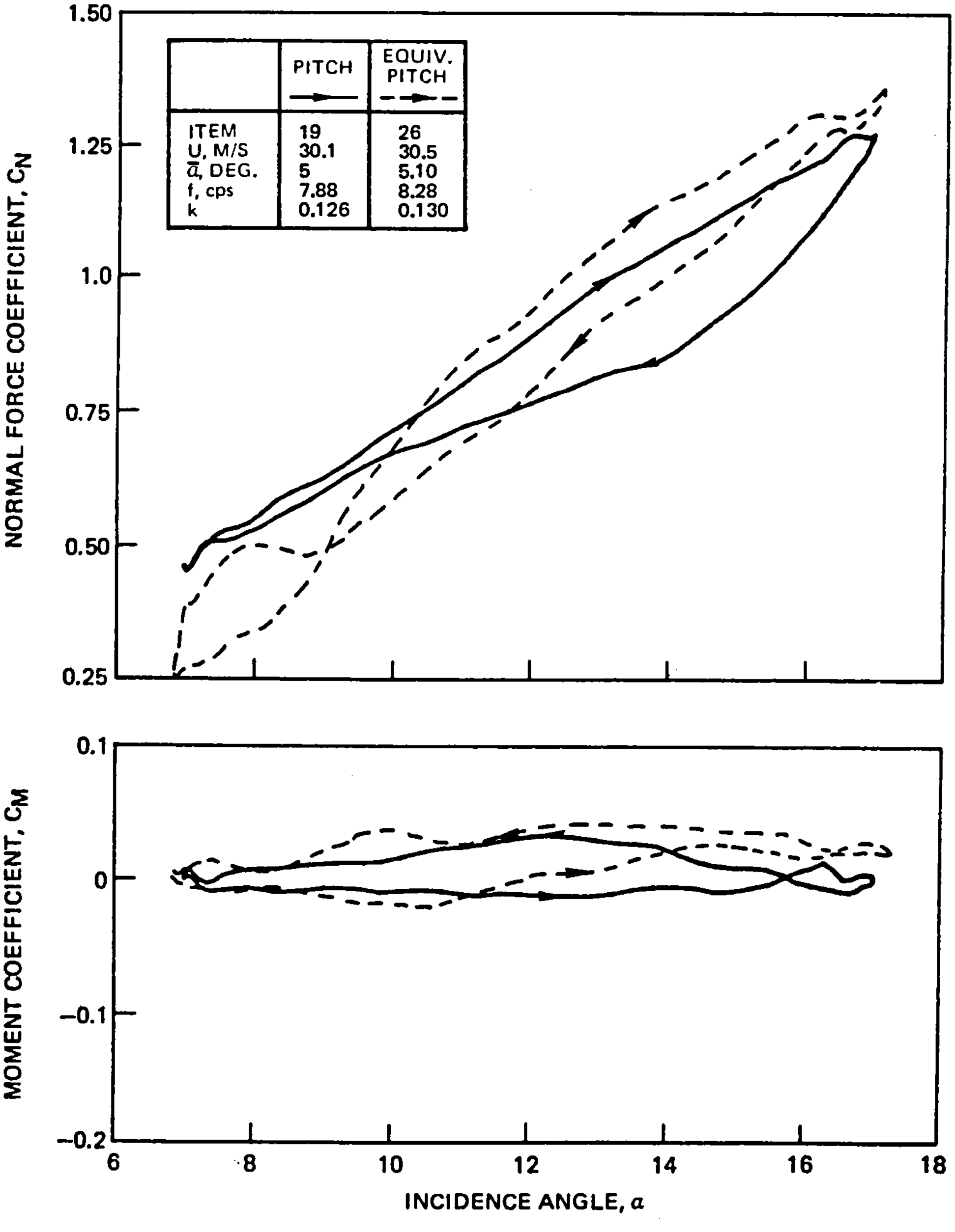

**Figure 39** Normal Force and Pitching Moment Coefficient Loops for $\alpha_M = 12^o, \bar{\alpha} \cong 5^o, k \cong 0.13$

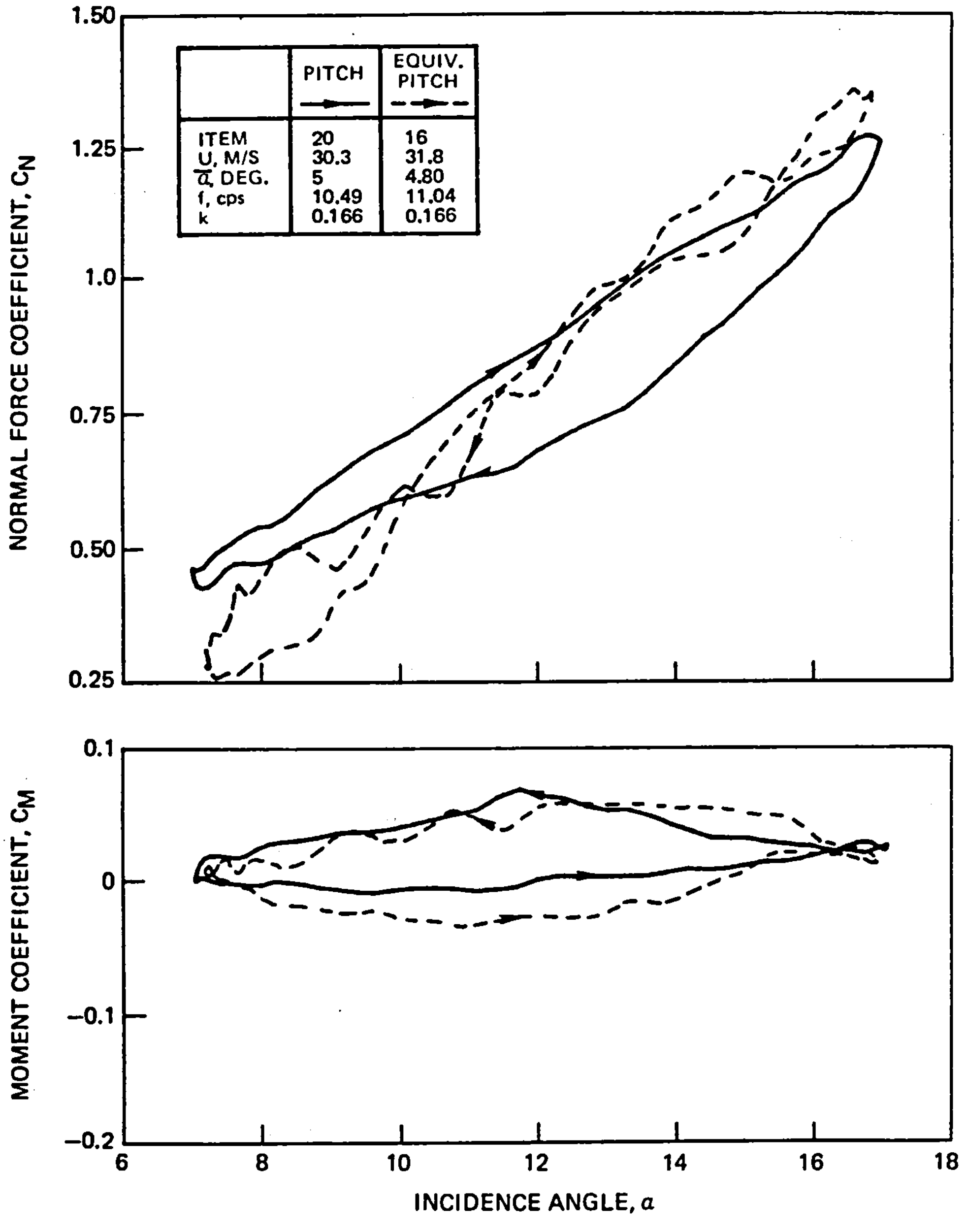

| | PITCH<br>——▶—— | EQUIV. PITCH<br>– –▶– – |
|---|---|---|
| ITEM | 20 | 16 |
| U, M/S | 30.3 | 31.8 |
| $\bar{\alpha}$, DEG. | 5 | 4.80 |
| f, cps | 10.49 | 11.04 |
| k | 0.166 | 0.166 |

**Figure 40** Normal Force and Pitching Moment Coefficient Loops for $\alpha_M = 12^o, \bar{\alpha} \cong 5^o, k \cong 0.17$

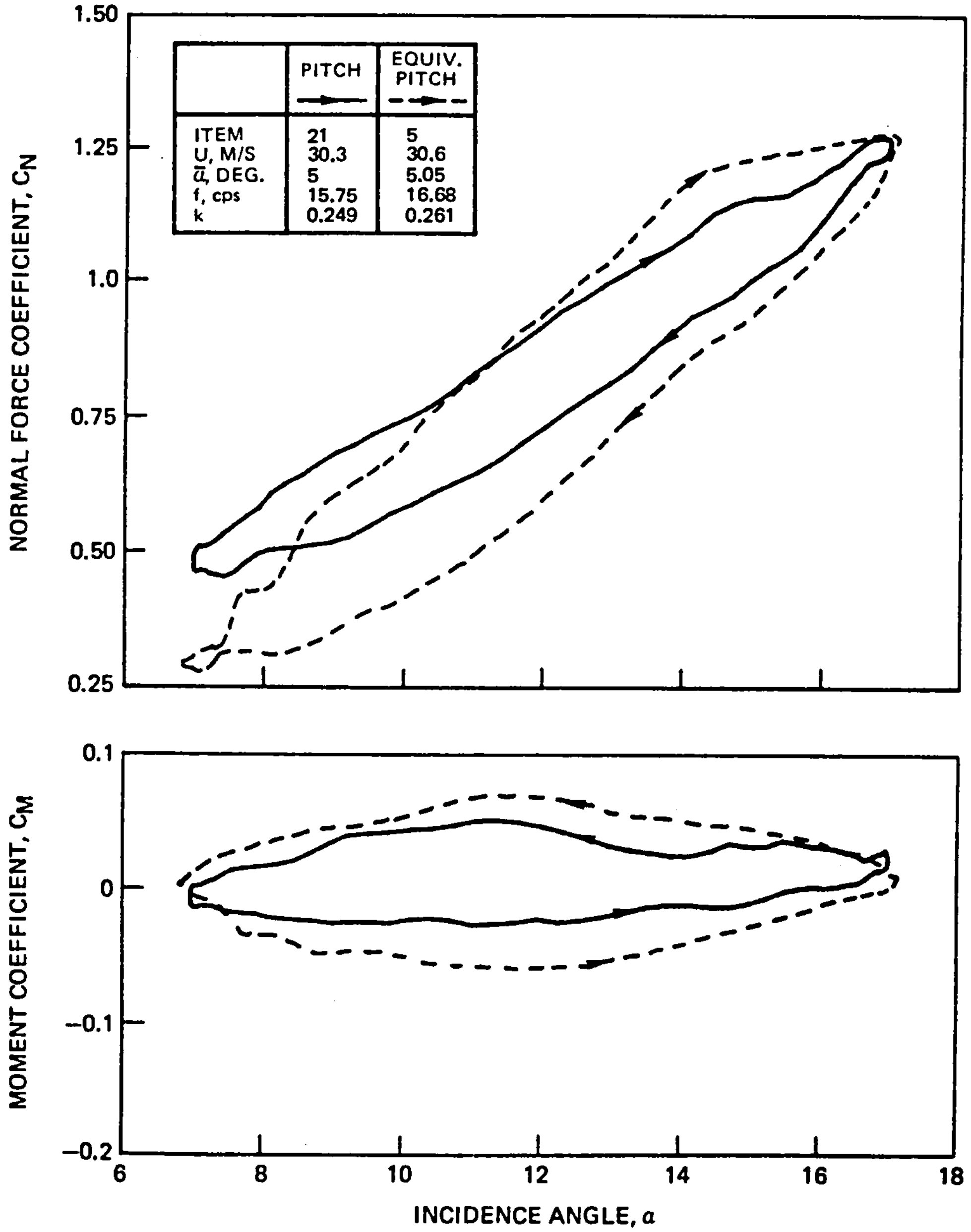

Figure 41 Normal Force and Pitching Moment Coefficient Loops for $\alpha_M = 12^\circ, \bar{\alpha} \cong 5^\circ, k \cong 0.25$

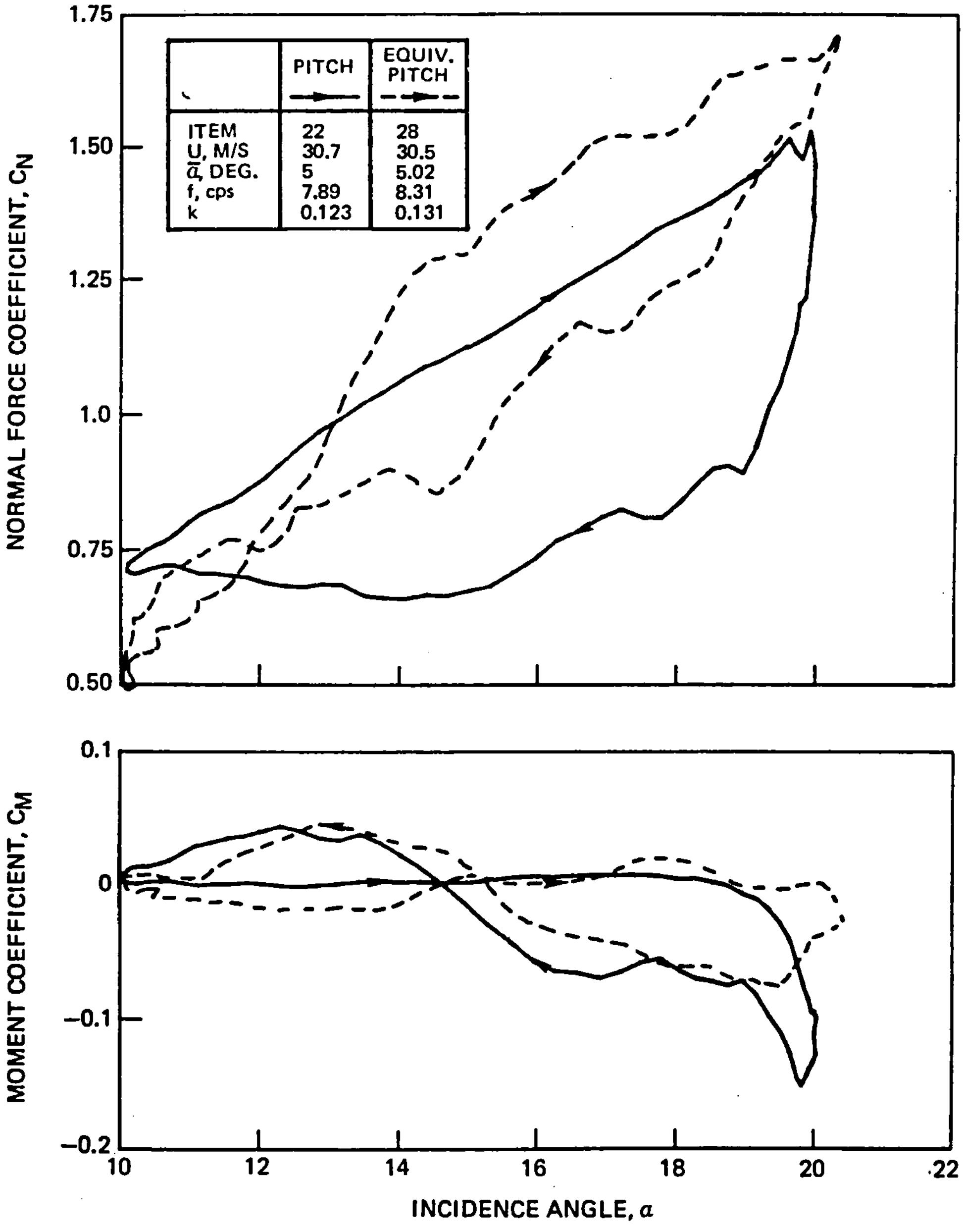

Figure 42 Normal Force and Pitching Moment Coefficient Loops for $a_M = 15^o, \bar{a} \cong 5^o, k \cong 0.12$

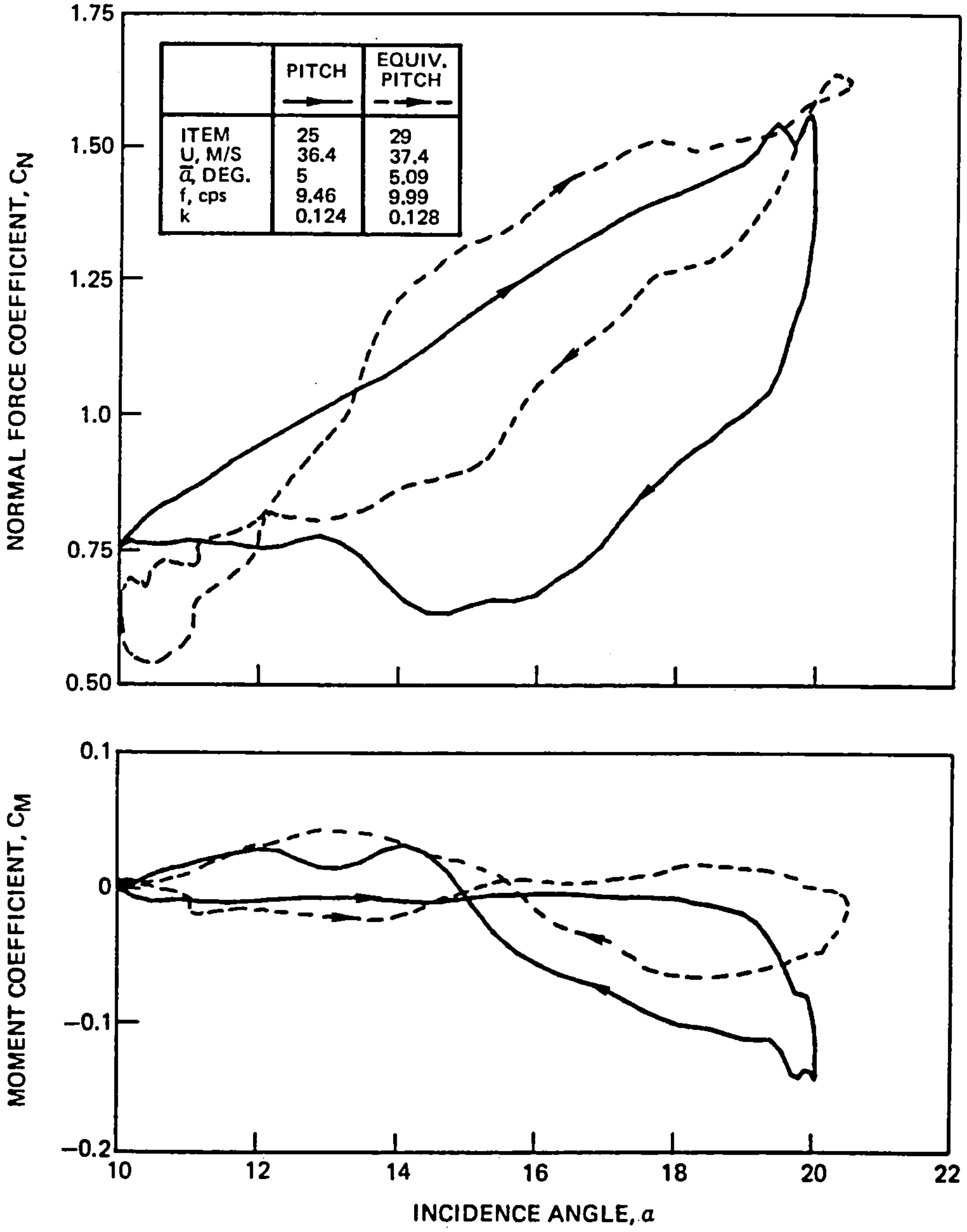

Figure 43 Normal Force and Pitching Moment Coefficient Loops for $a_M = 15^o, \bar{a} \cong 5^o, k \cong 0.12$

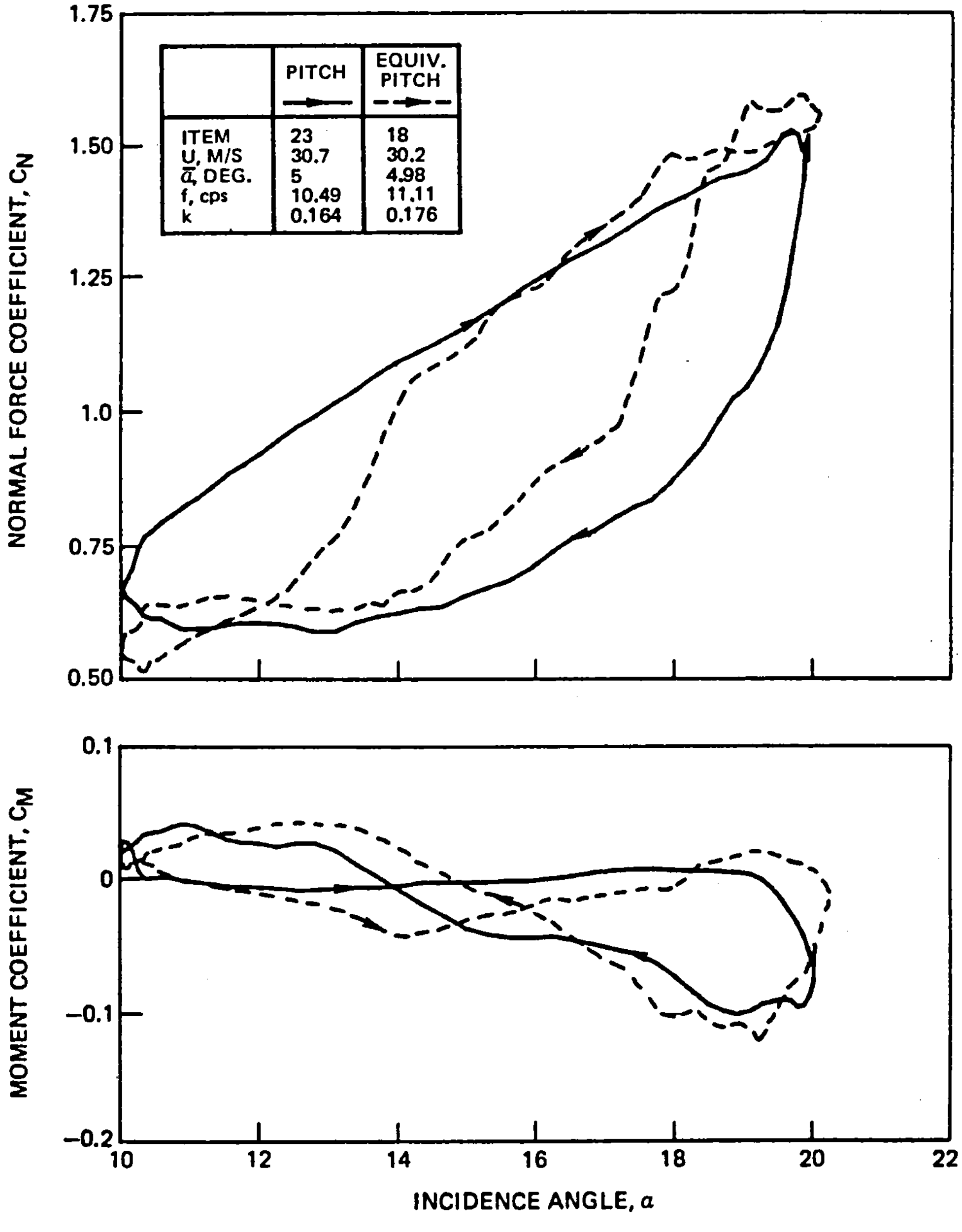

**Figure 44** Normal Force and Pitching Moment Coefficient Loops for $\alpha_M = 15^o, \bar{\alpha} \cong 5^o, k \cong 0.16$

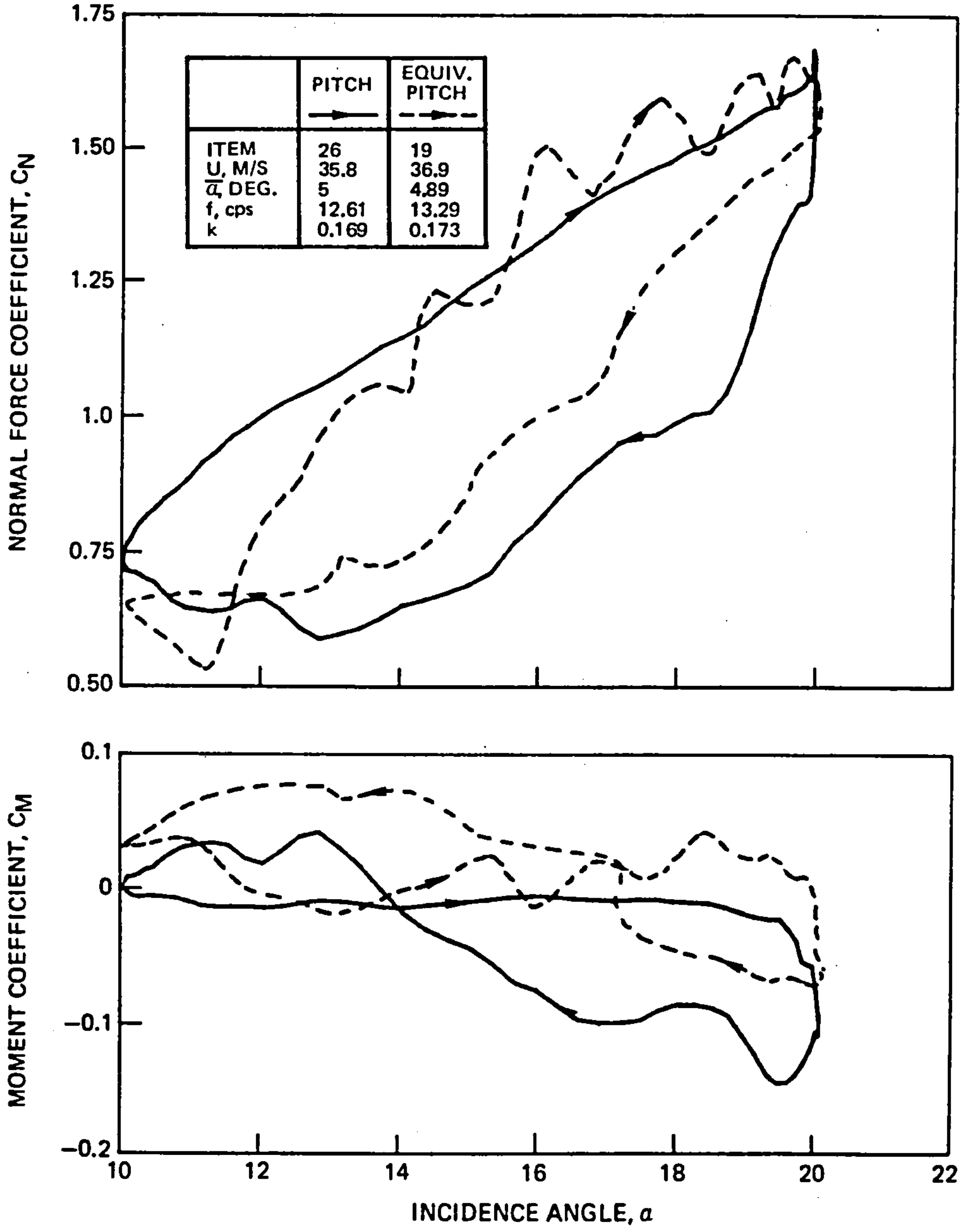

Figure 45 Normal Force and Pitching Moment Coefficient Loops for $\alpha_M = 15^o, \bar{\alpha} \cong 5^o, k \cong 0.17$

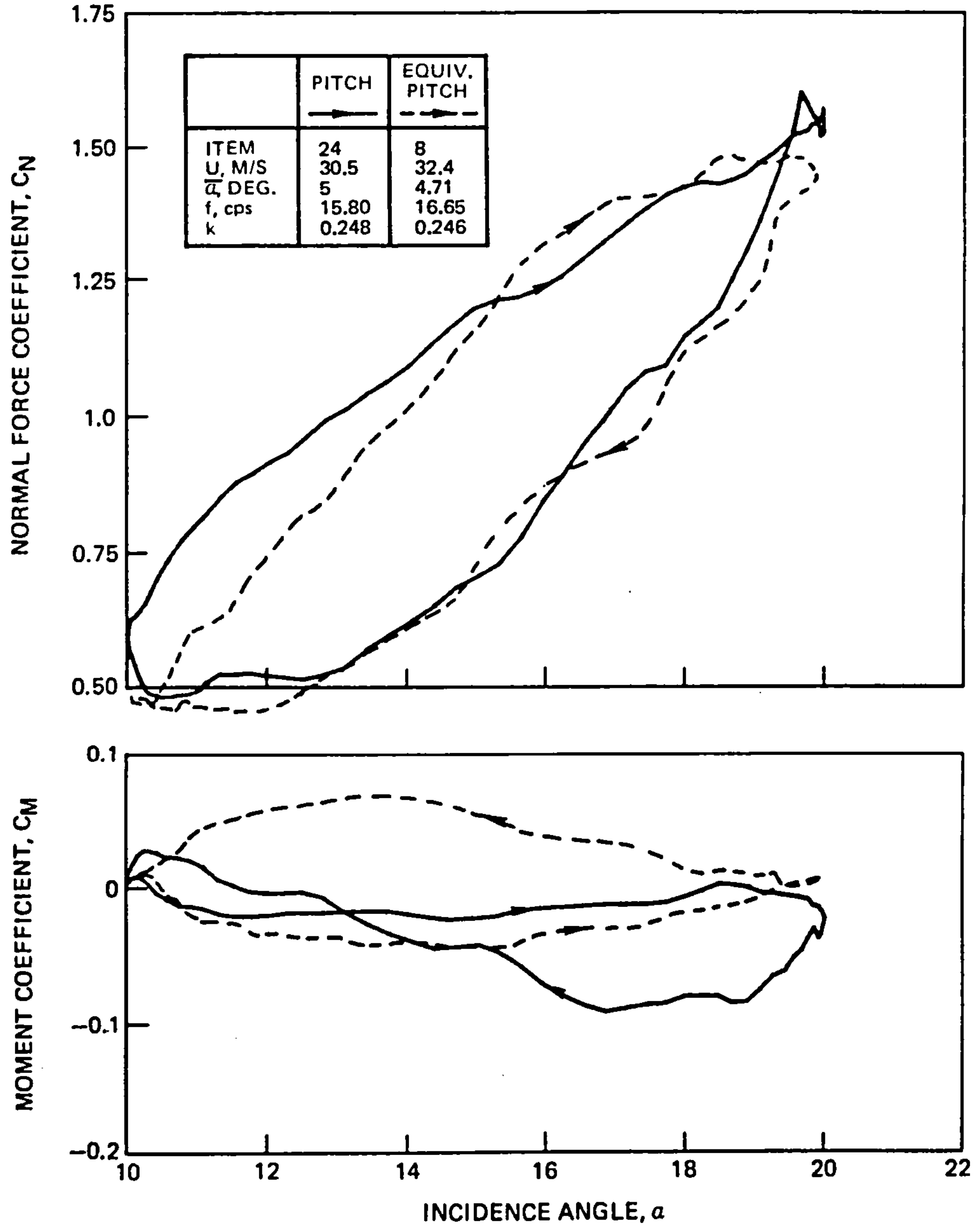

**Figure 46** Normal Force and Pitching Moment Coefficient Loops for $\alpha_M = 15°, \bar{\alpha} \cong 5°, k \cong 0.25$

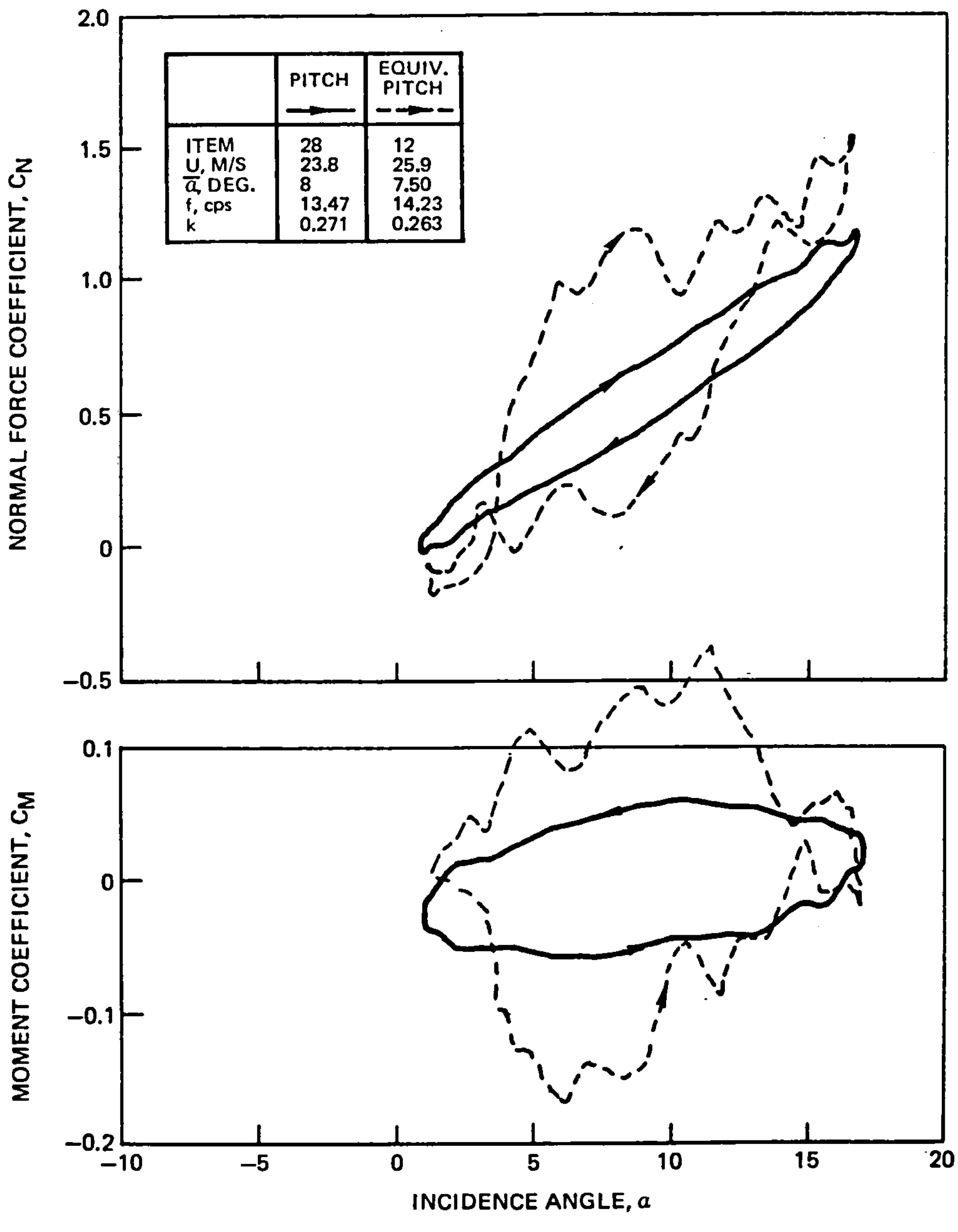

Figure 47 Normal Force and Pitching Moment Coefficient Loops for $\alpha_M = 9^\circ, \bar{\alpha} \cong 8^\circ, k \cong 0.27$

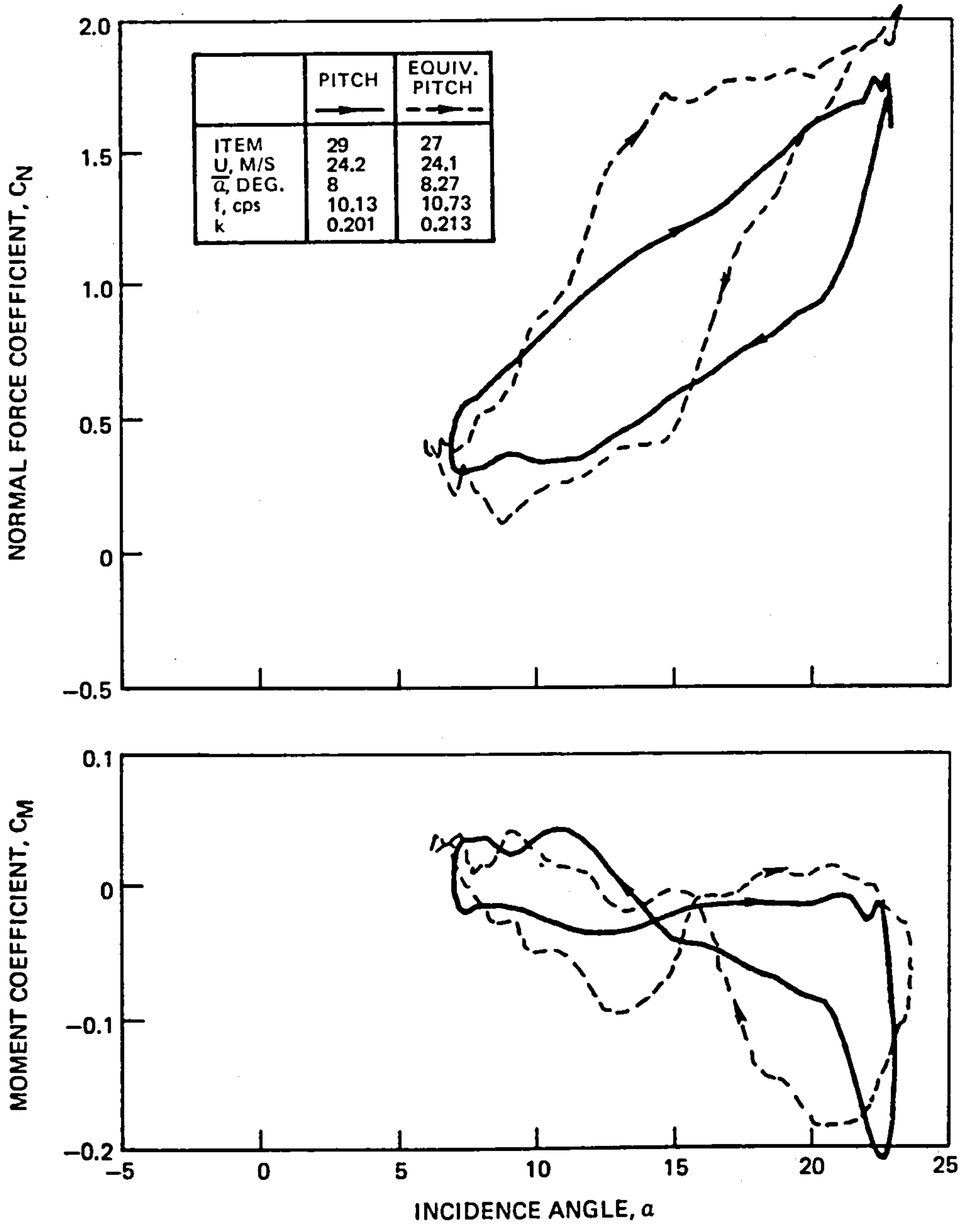

**Figure 48** Normal Force and Pitching Moment Coefficient Loops for $\alpha_M = 15°, \overline{\alpha} \cong 8°, k \cong 0.20$

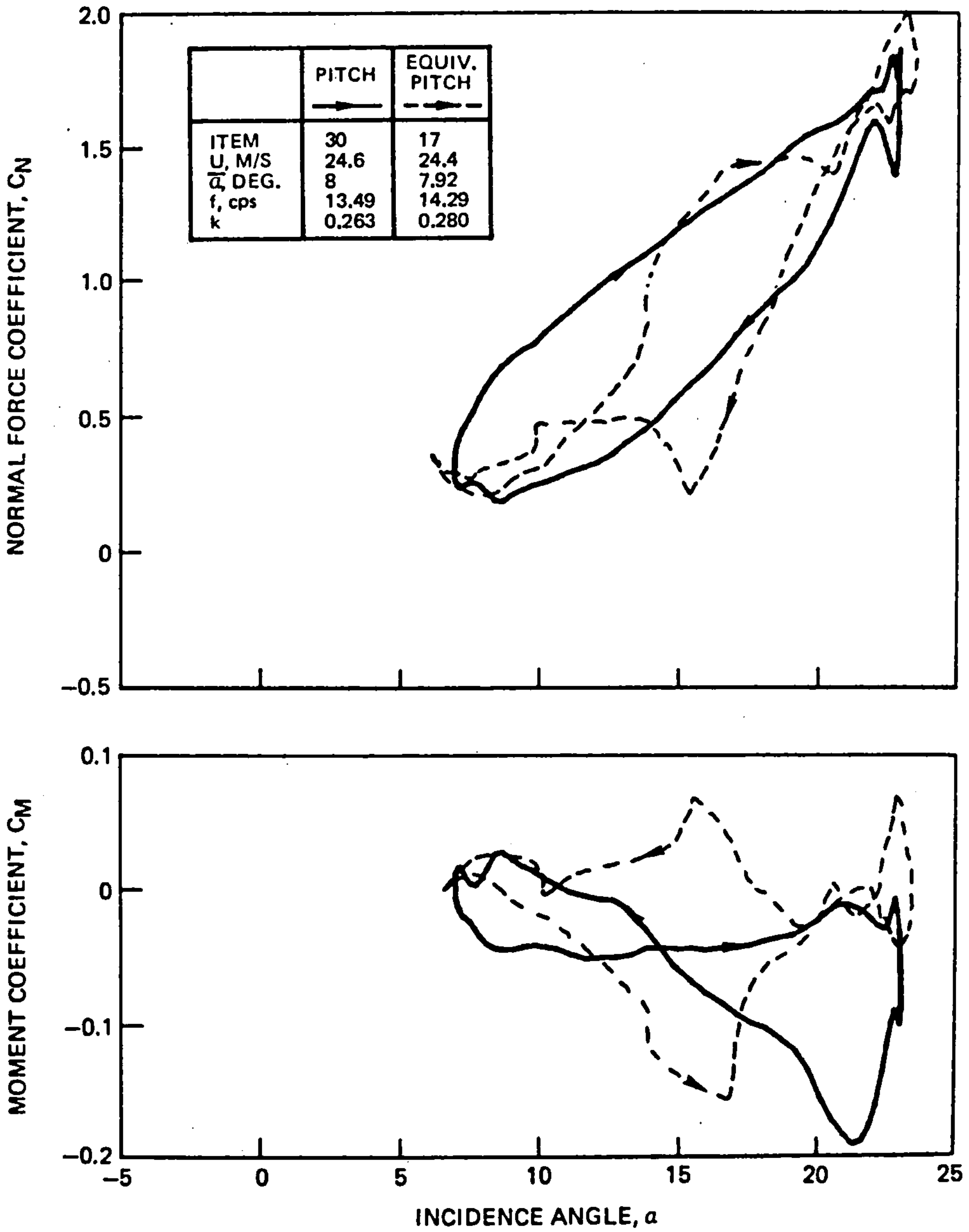

Figure 49 Normal Force and Pitching Moment Coefficient Loops for $\alpha_M$ = 15°, $\bar{\alpha} \cong$ 8°, k ≅ 0.26

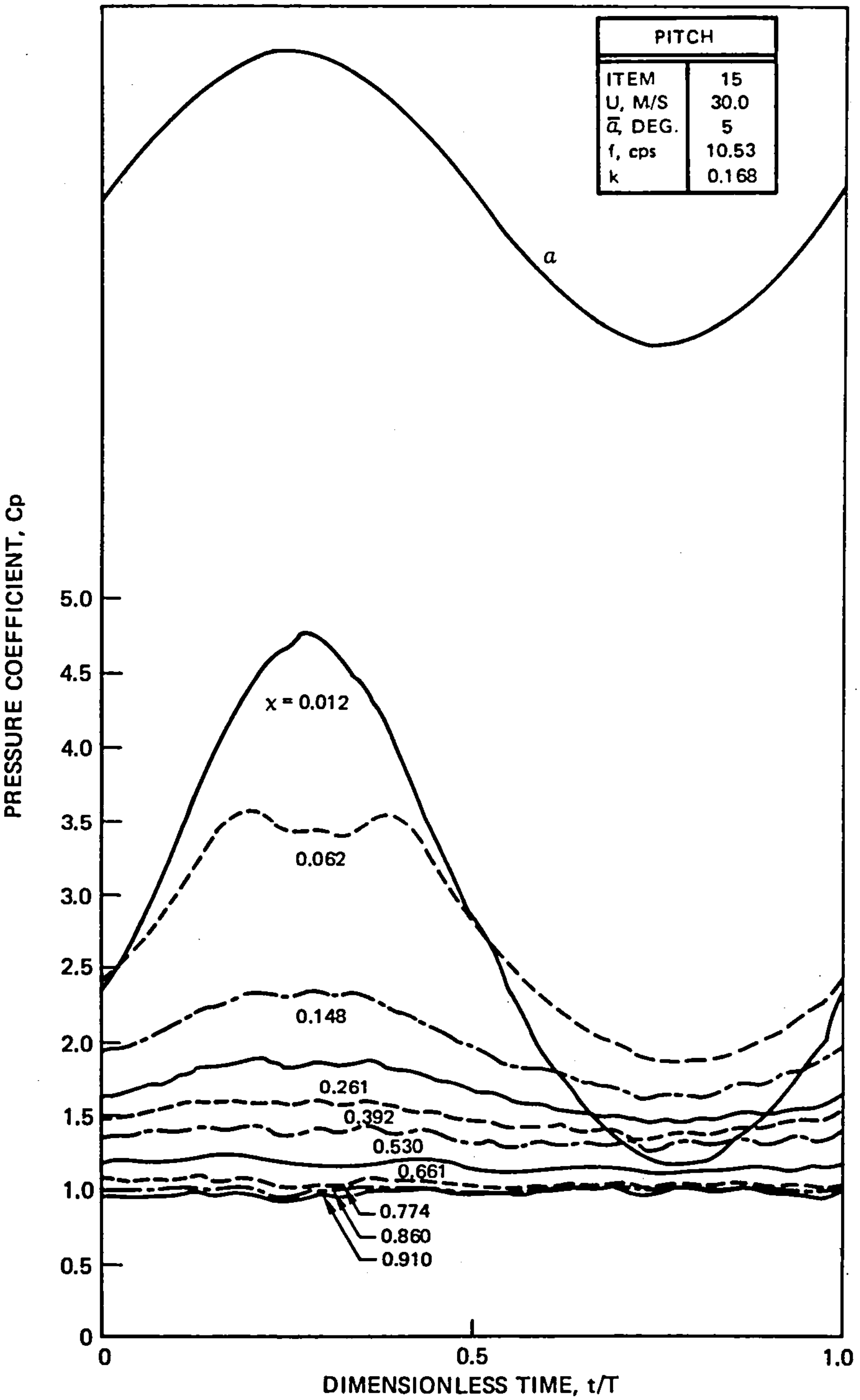

**Figure 50** Pressure Comparisons for $\alpha = 9 \pm 5°$ at $k \cong 0.17$
a) Pitch Time History

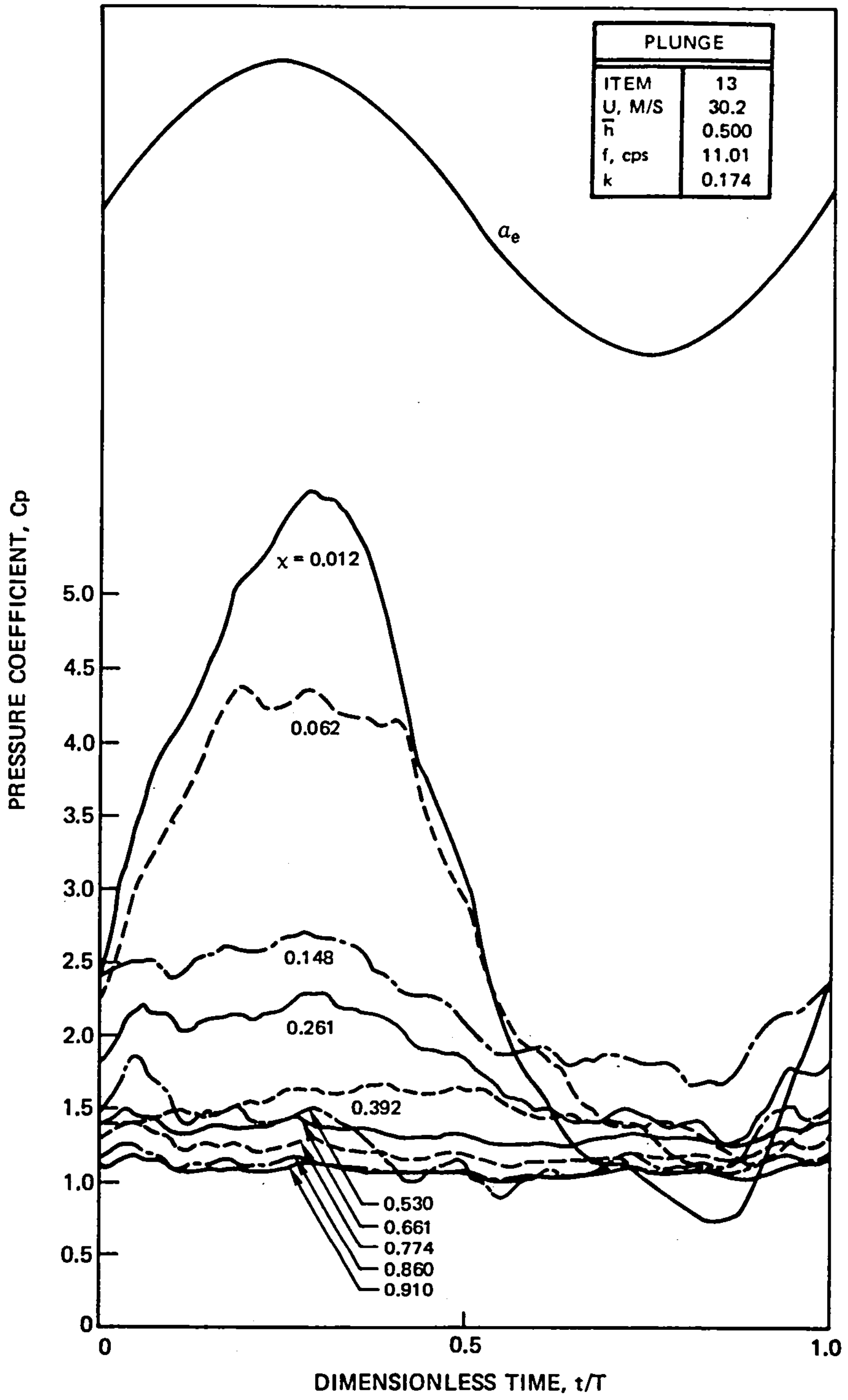

**Figure 50** (continued)
b) Plunge Time History

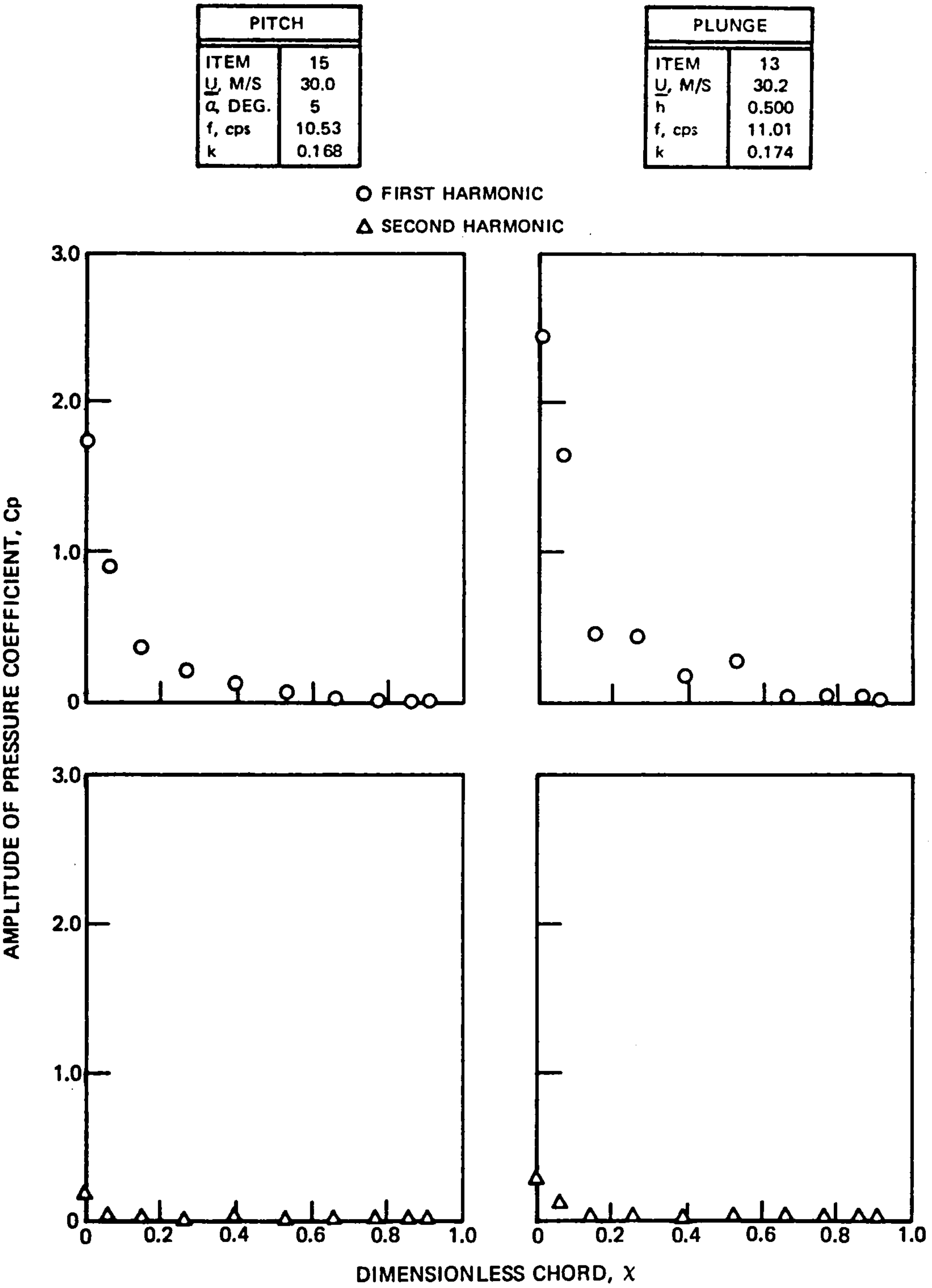

Figure 50 (continued)
c) Harmonic Amplitudes

| PITCH | |
|---|---|
| ITEM | 15 |
| U, M/S | 30.0 |
| α, DEG. | 5 |
| f, cps | 10.53 |
| k | 0.168 |

| PLUNGE | |
|---|---|
| ITEM | 13 |
| U, M/S | 30.2 |
| h | 0.500 |
| f, cps | 11.01 |
| k | 0.174 |

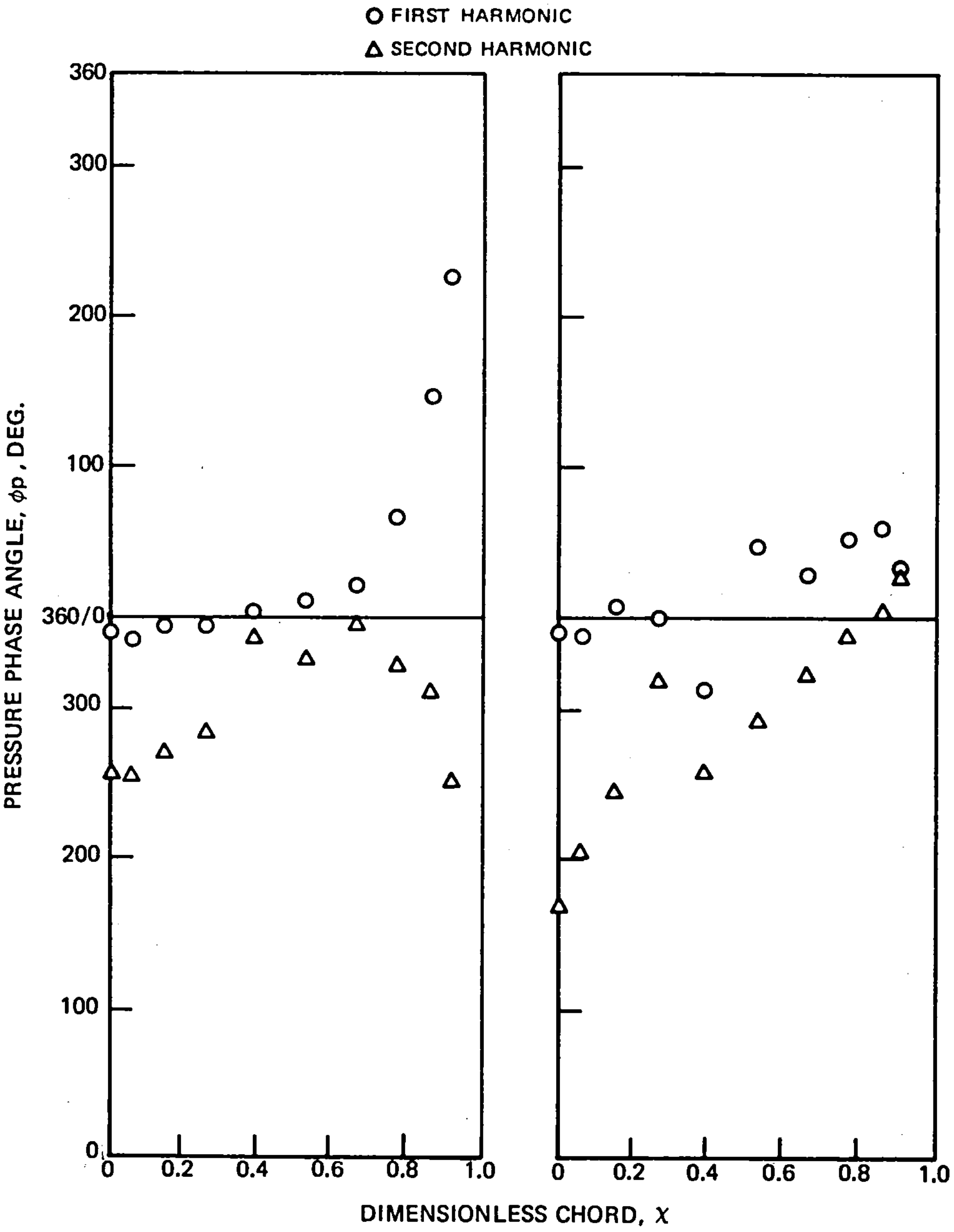

**Figure 50 (concluded)**
**d) Harmonic Phase Angles**

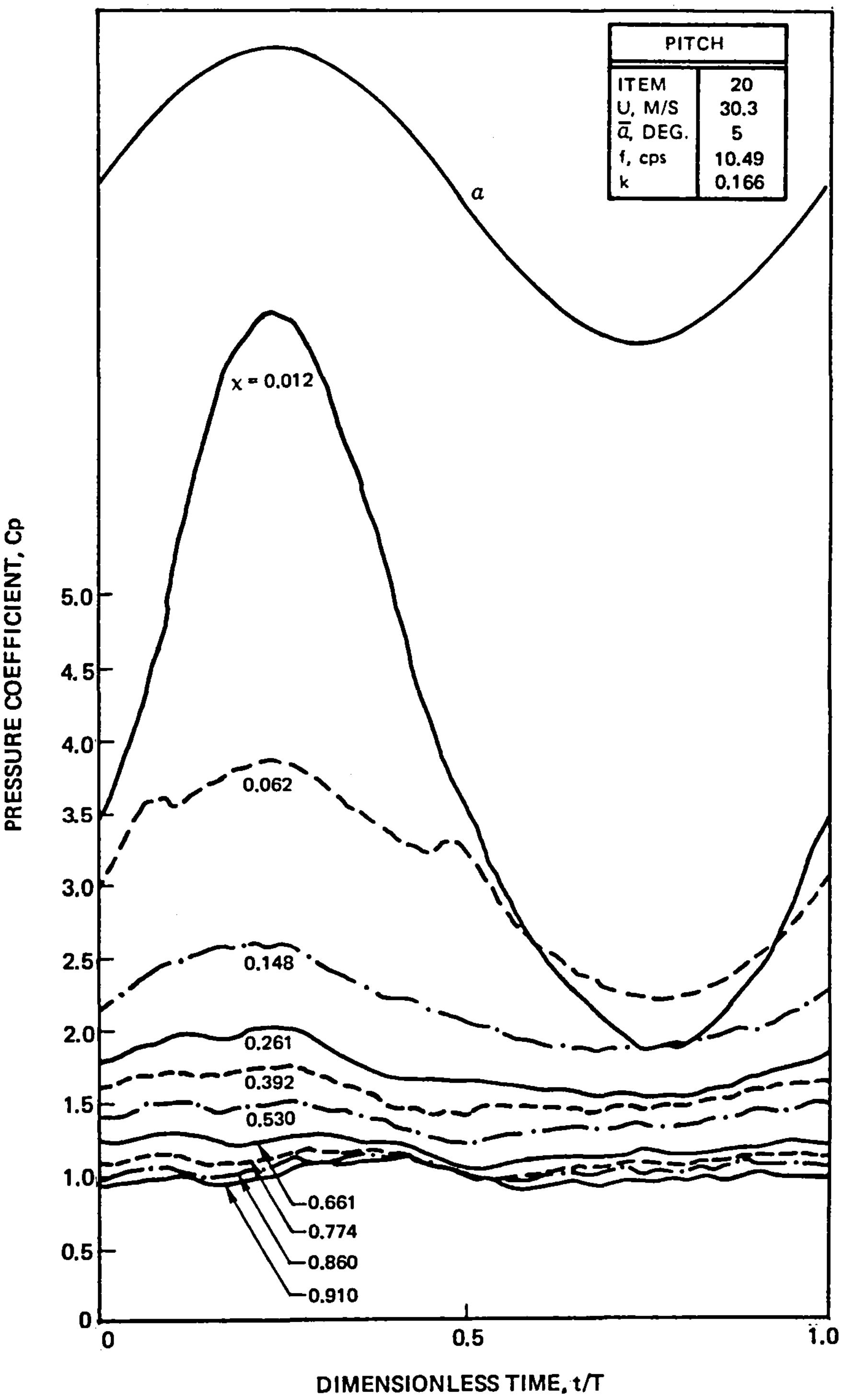

**Figure 51 Pressure Comparisons for $\alpha = 12 \pm 5°$ at k ≅ 0.17**
**a) Pitch Time History**

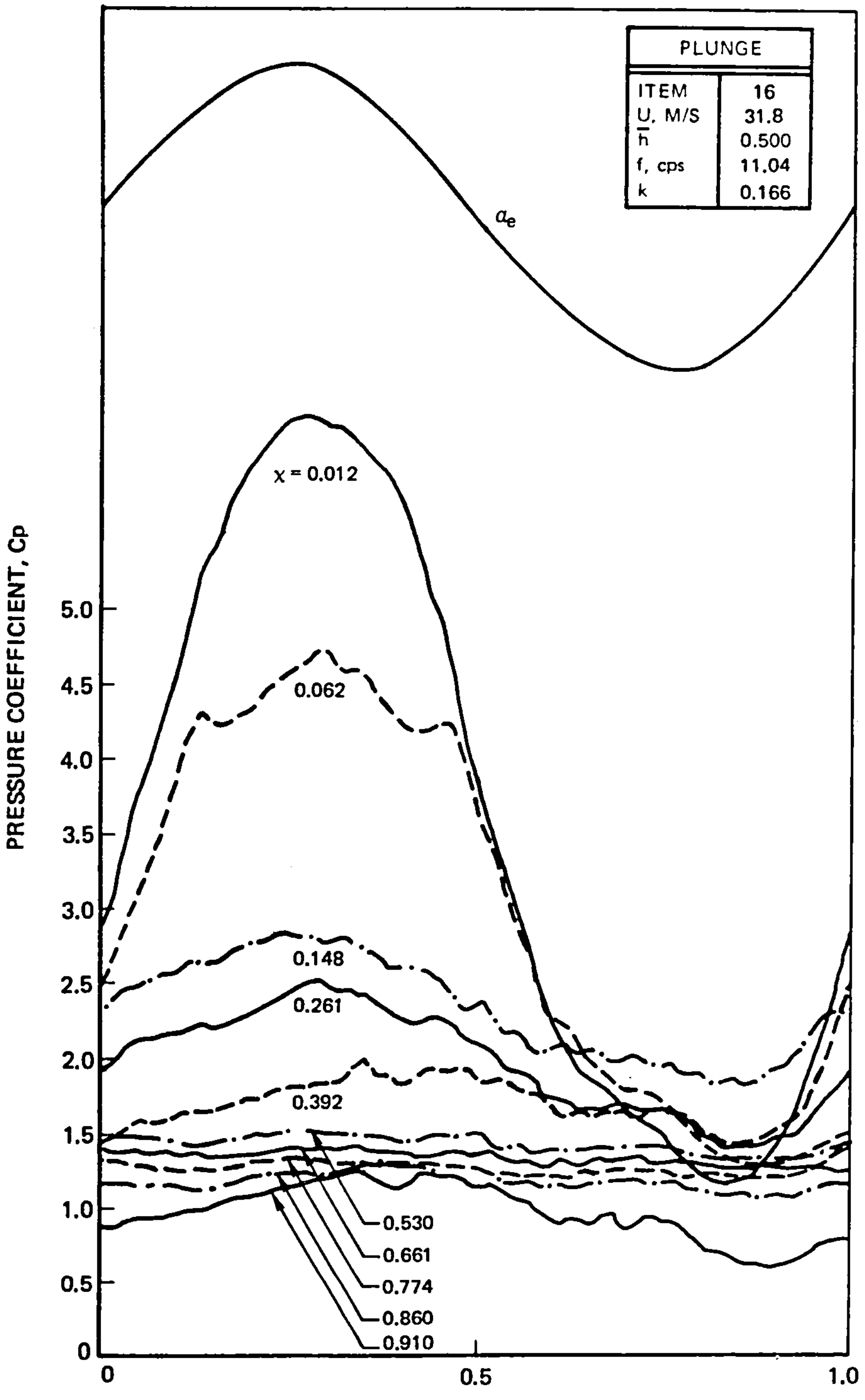

**Figure 51** (continued)
b) Plunge Time History

| PITCH | |
|---|---|
| ITEM | 20 |
| U, M/S | 30.3 |
| $\overline{\alpha}$, DEG. | 5 |
| f, cps | 10.49 |
| k | 0.166 |

| PLUNGE | |
|---|---|
| ITEM | 16 |
| U, M/S | 31.8 |
| $\overline{h}$ | 0.500 |
| f, cps | 11.04 |
| k | 0.166 |

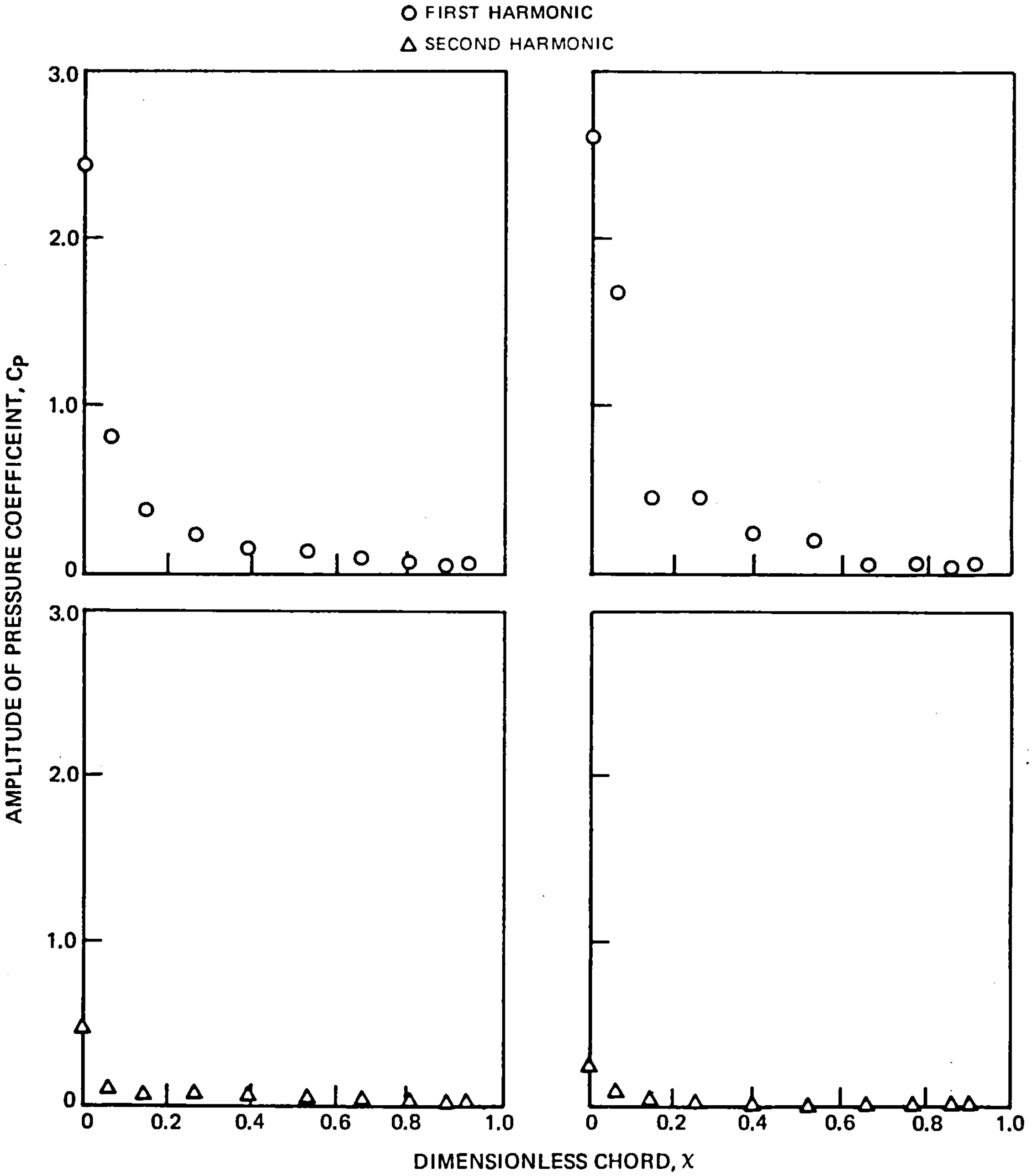

Figure 51 (continued)
c) Harmonic Amplitudes

| PITCH | |
|---|---|
| ITEM | 20 |
| U, M/S | 30.3 |
| $\bar{\alpha}$, DEG. | 5 |
| f, cps | 10.49 |
| k | 0.166 |

| PLUNGE | |
|---|---|
| ITEM | 16 |
| U, M/S | 31.8 |
| $\bar{h}$ | 0.500 |
| f, cps | 11.04 |
| k | 0.166 |

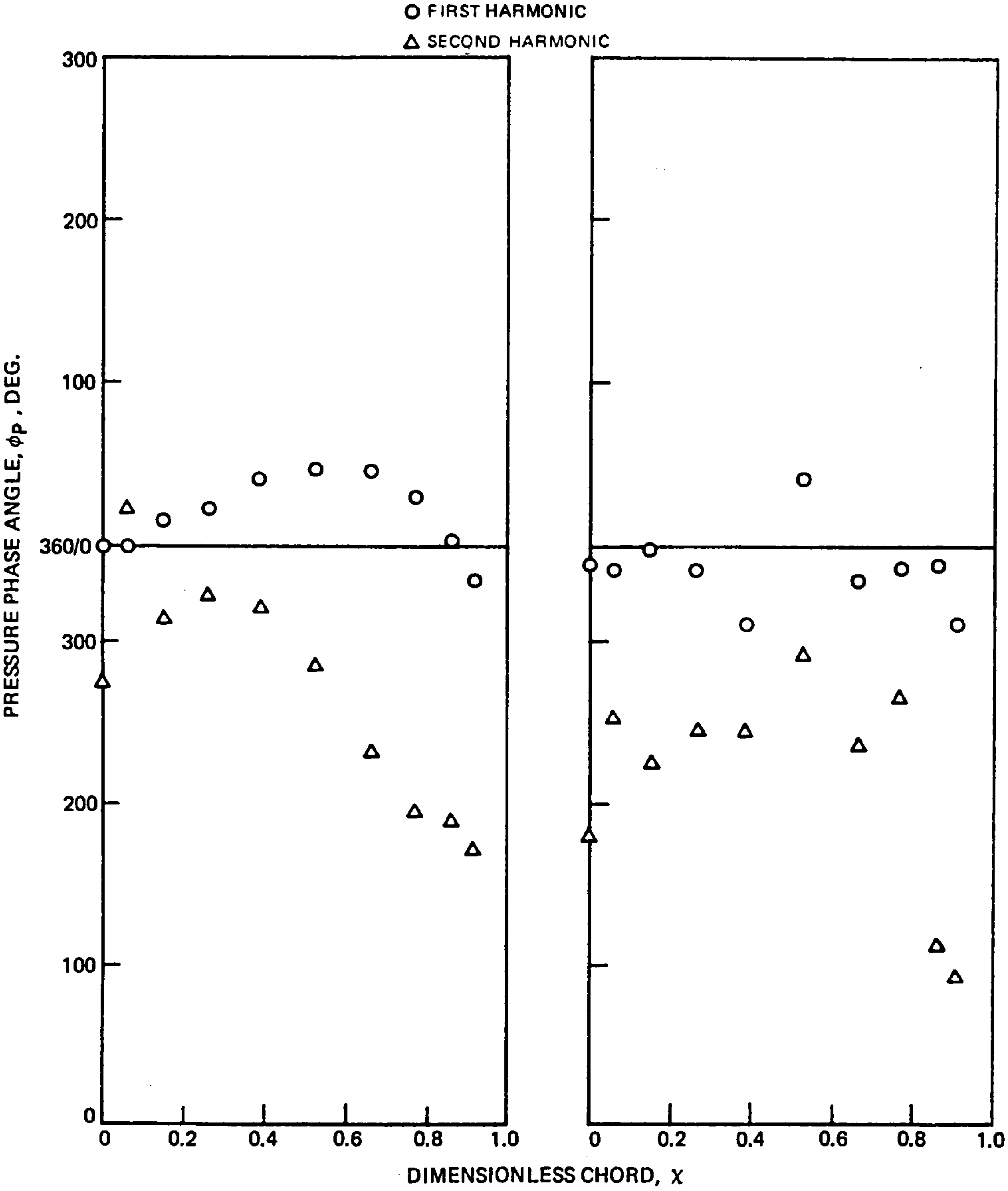

**Figure 51 (concluded)**
**d) Harmonic Phase Angles**

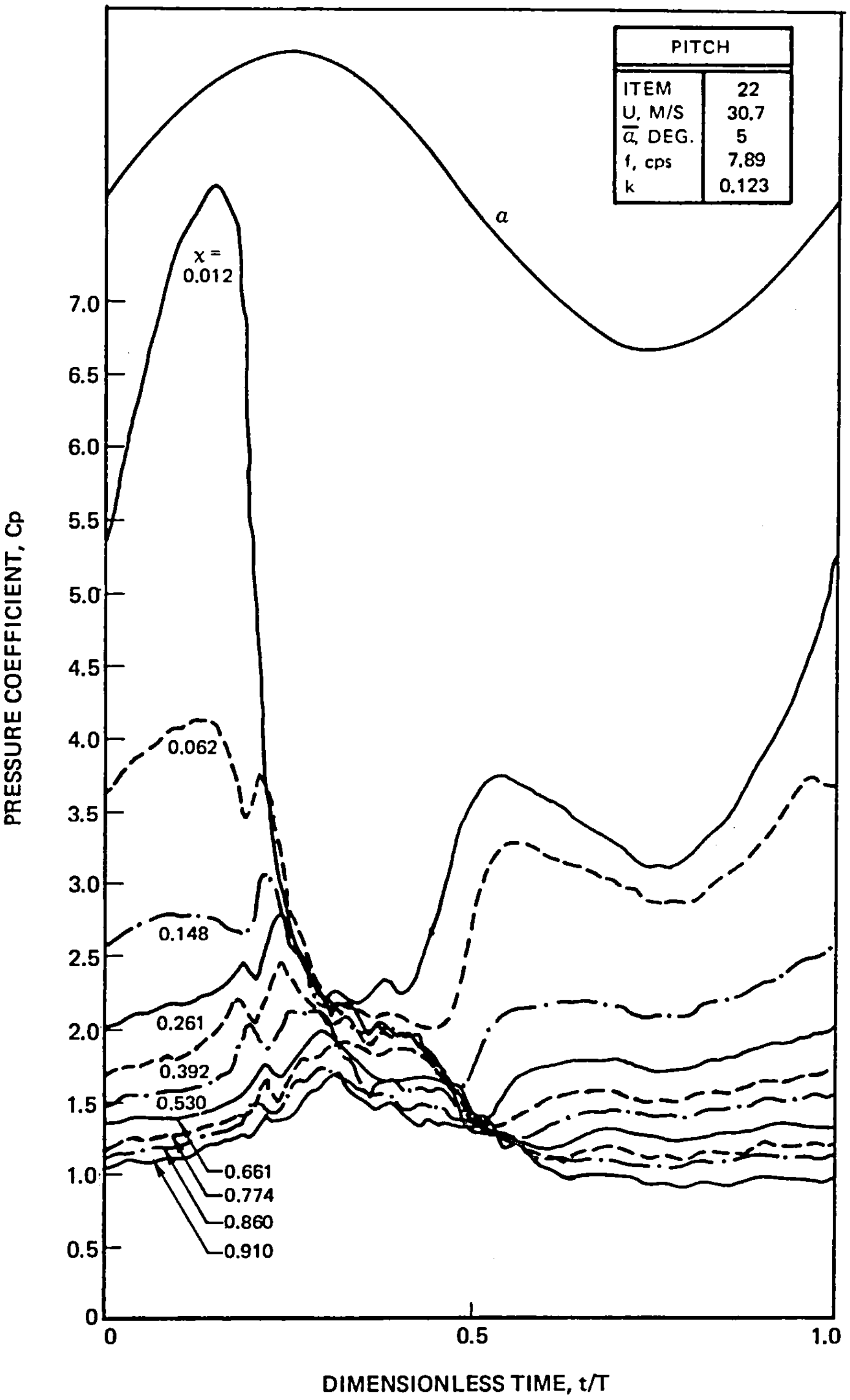

**Figure 52** Pressure Comparisons for $\alpha = 15 \pm 5°$ at $k \cong 0.12$
a) Pitch Time History

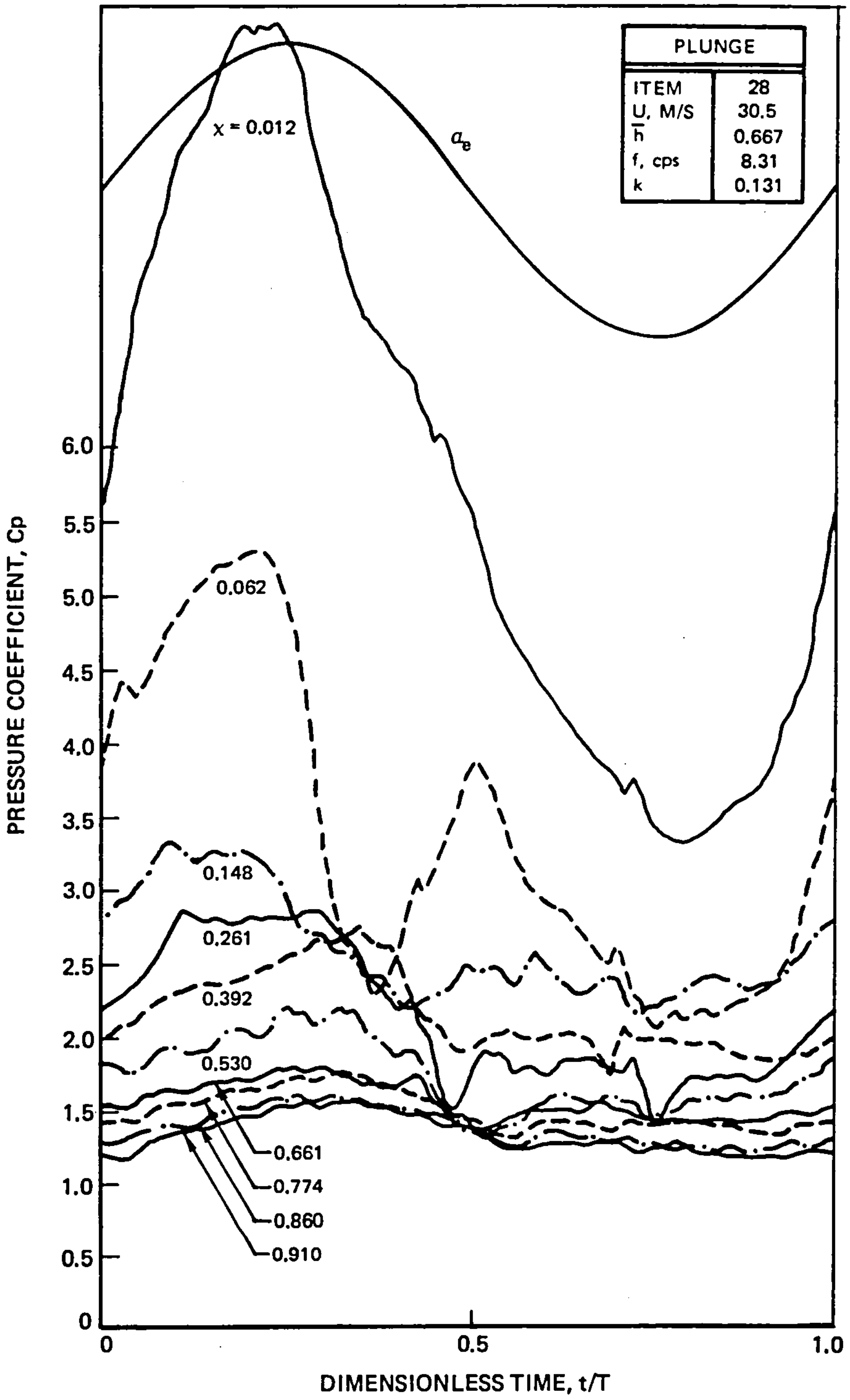

**Figure 52** (continued)
b) Plunge Time History

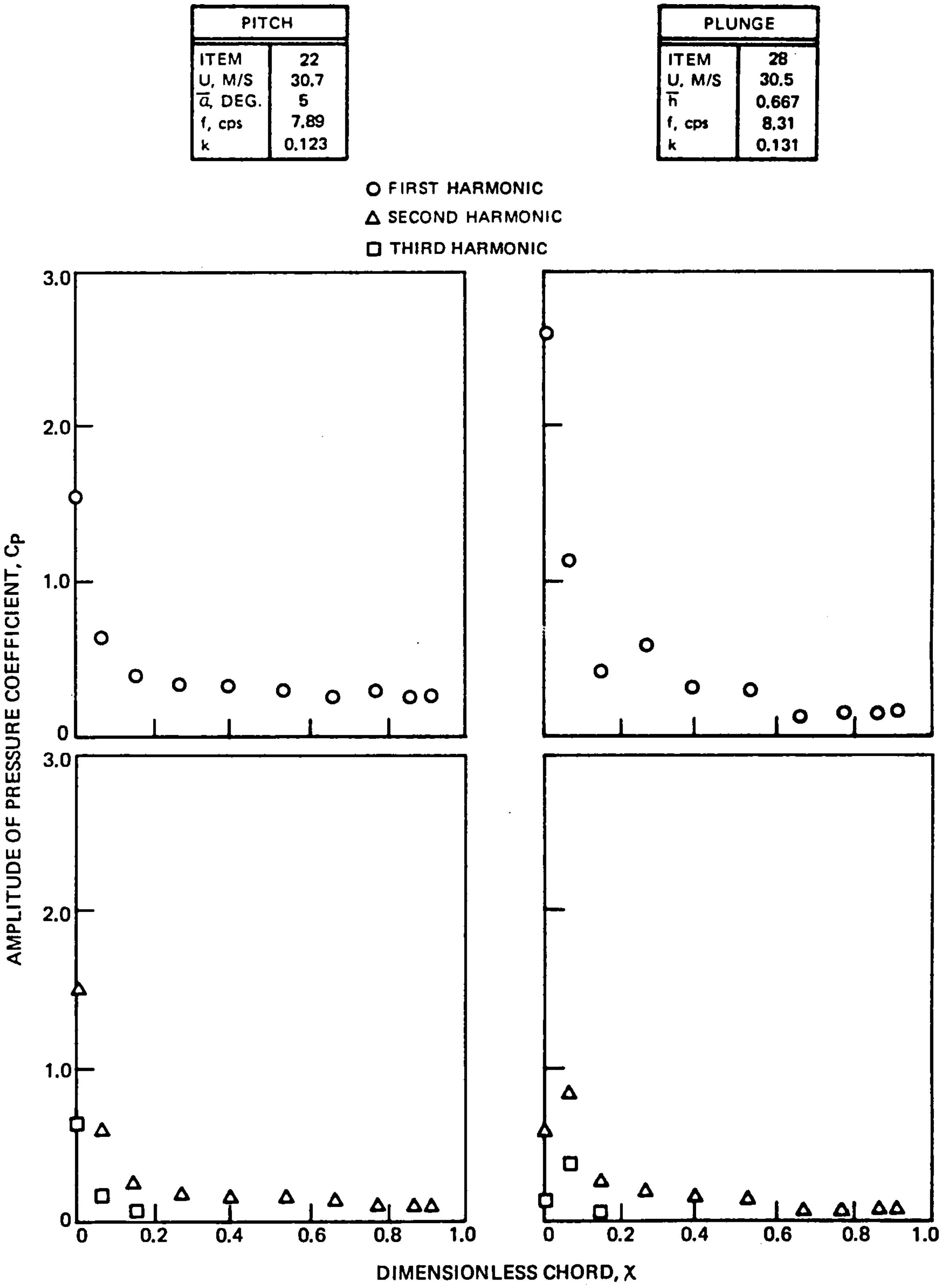

**Figure 52 (continued)**
**c) Harmonic Amplitudes**

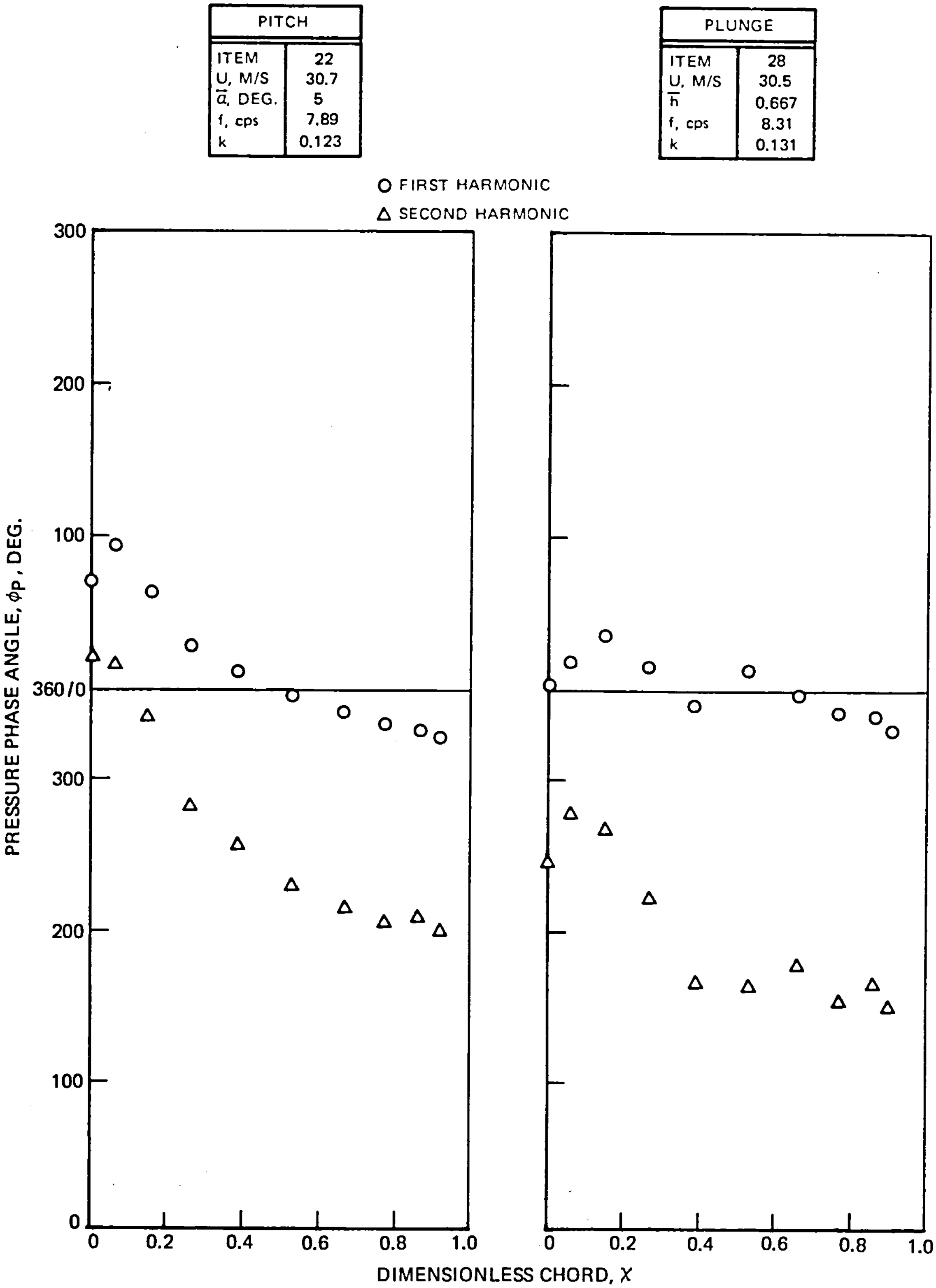

**Figure 52 (concluded)**
**d) Harmonic Phase Angles**

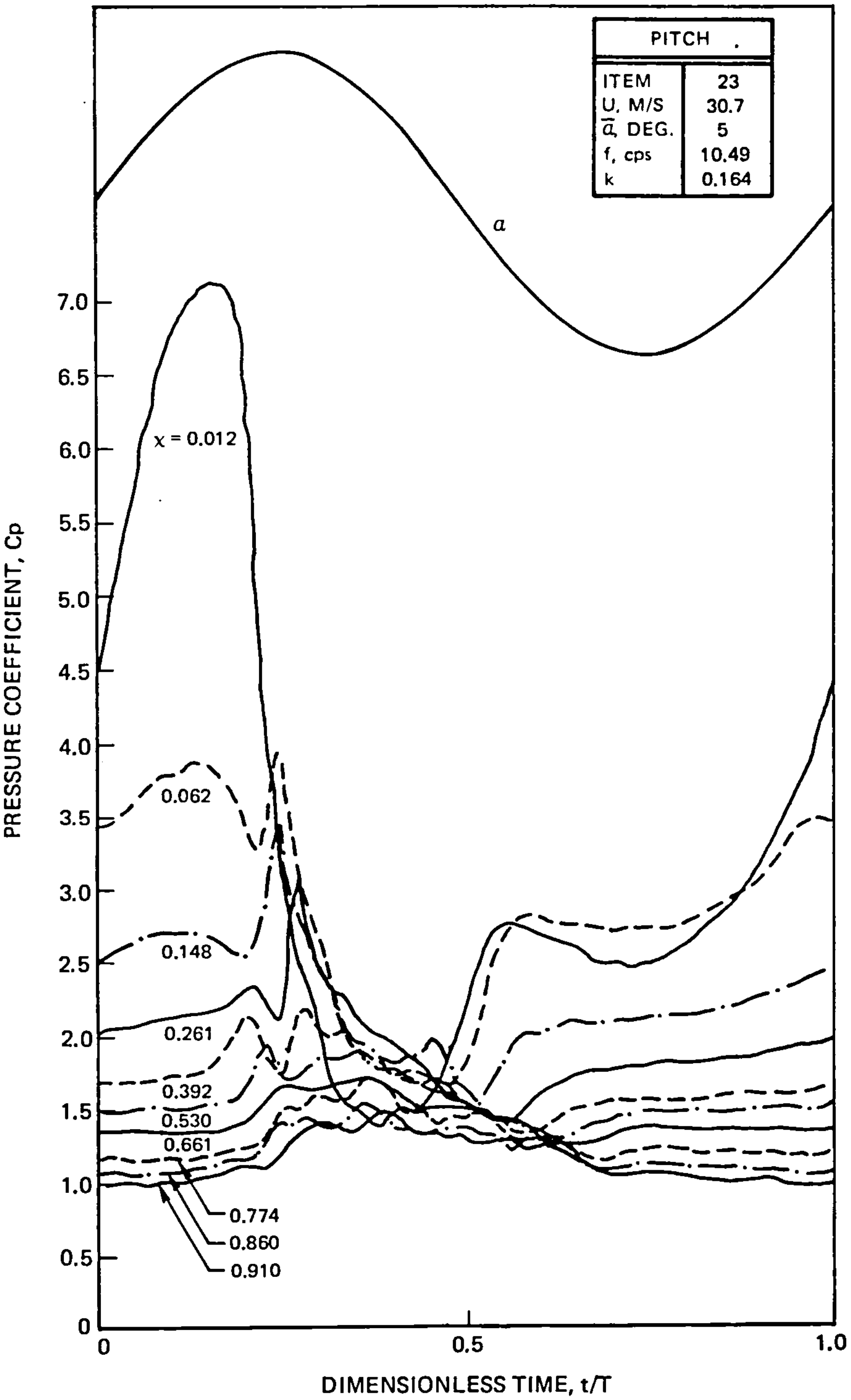

**Figure 53** Pressure Comparisons for $\alpha = 15 \pm 5°$ at $k \cong 0.17$
a) Pitch Time History

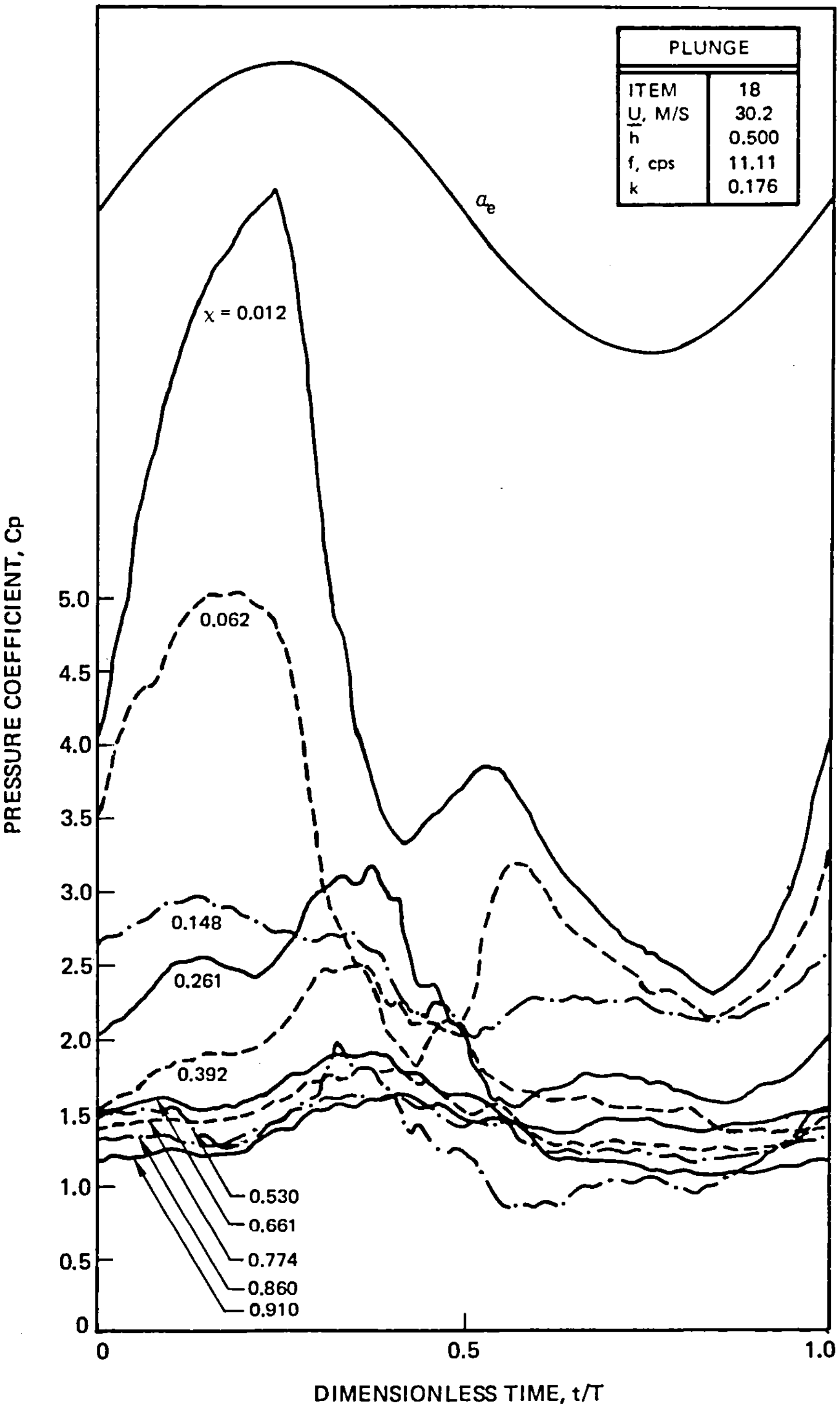

**Figure 53** **(continued)**
**b) Plunge Time History**

| PITCH | |
|---|---|
| ITEM | 23 |
| U, M/S | 30.7 |
| $\bar{\alpha}$, DEG. | 5 |
| f, cps | 10.49 |
| k | 0.164 |

| PLUNGE | |
|---|---|
| ITEM | 18 |
| U, M/S | 30.2 |
| $\bar{h}$ | 0.500 |
| f, cps | 11.11 |
| k | 0.176 |

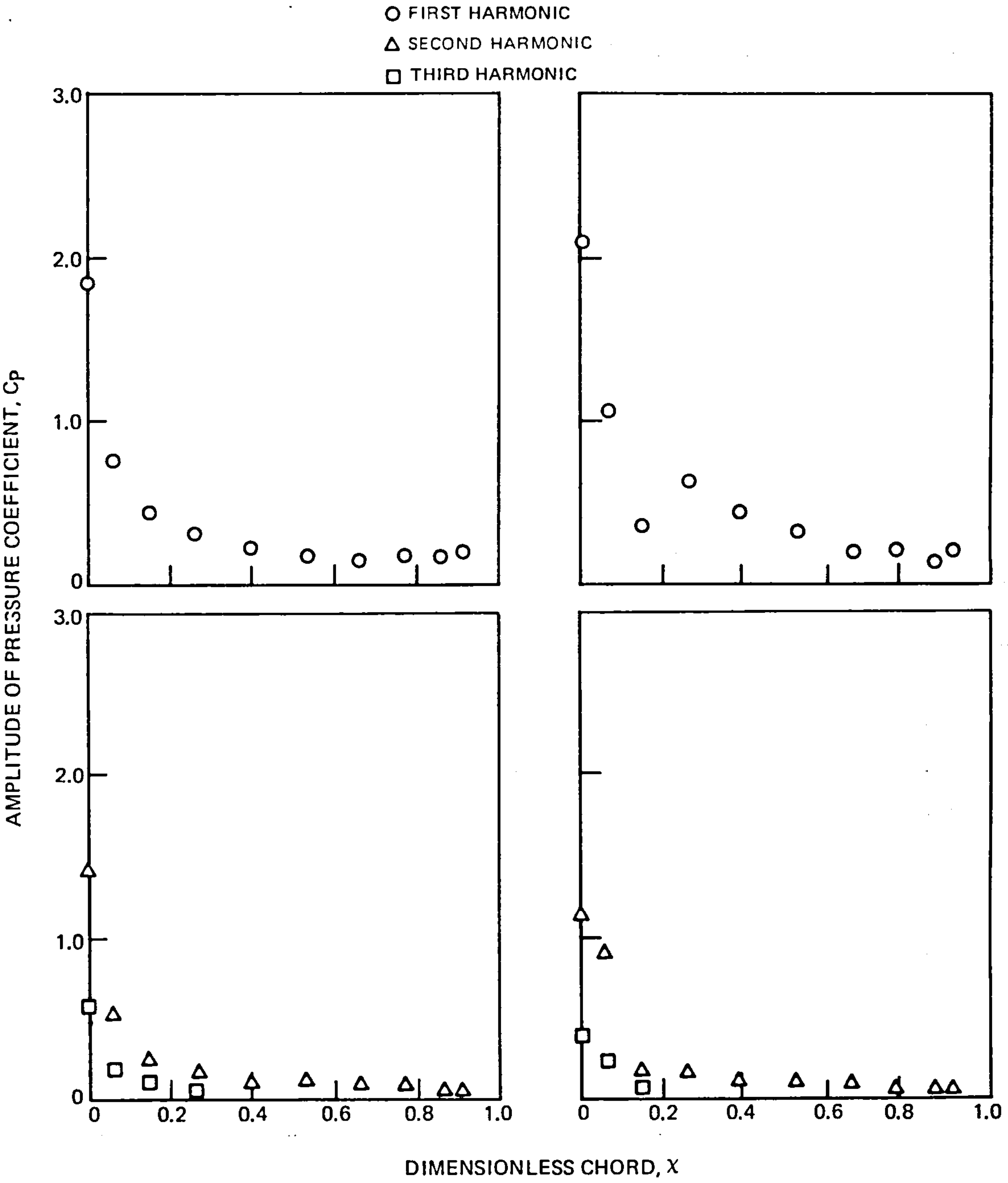

**Figure 53 (continued)**
**c) Harmonic Amplitudes**

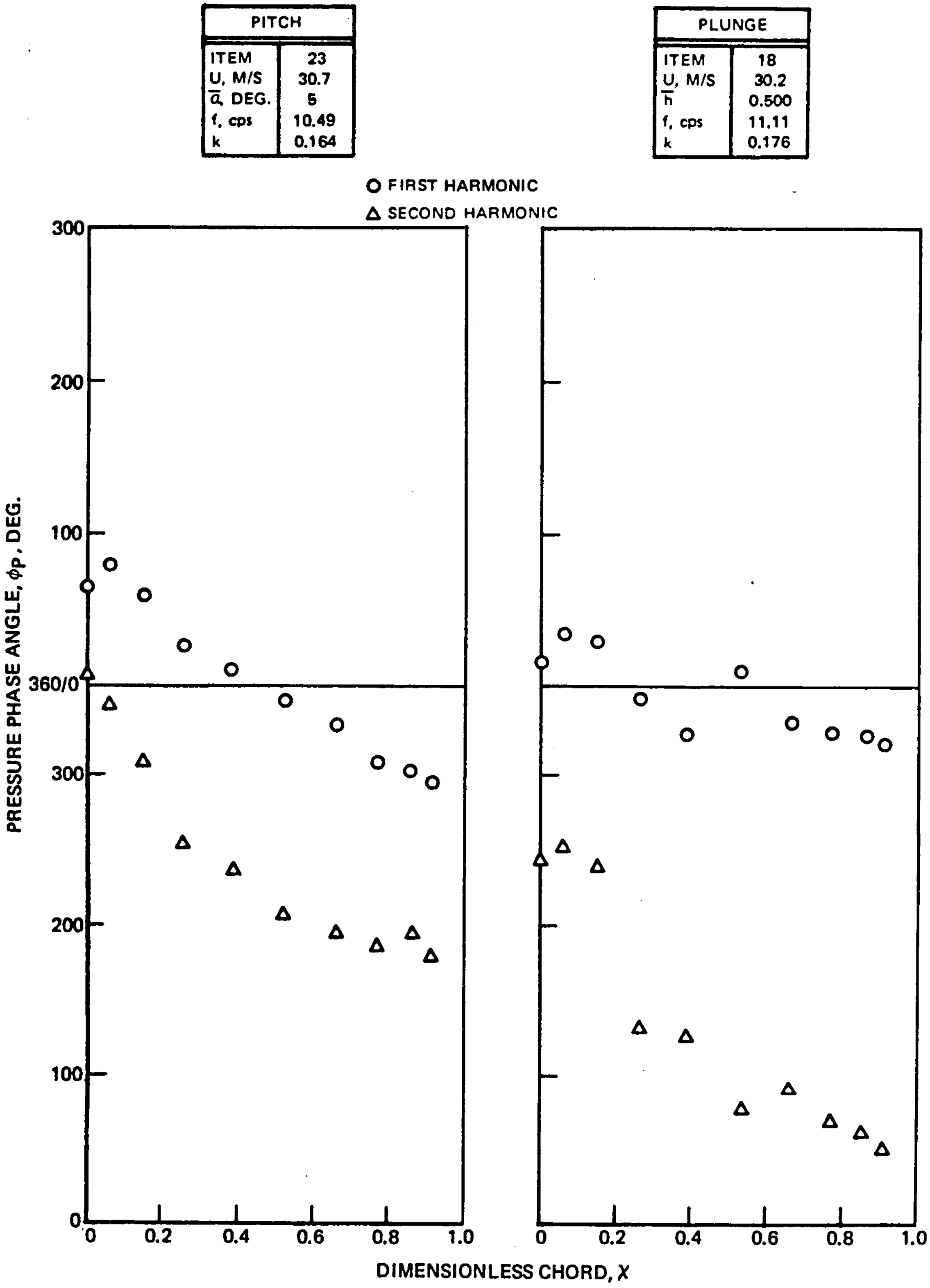

**Figure 53 (concluded)**
**d) Harmonic Phase Amplitudes**

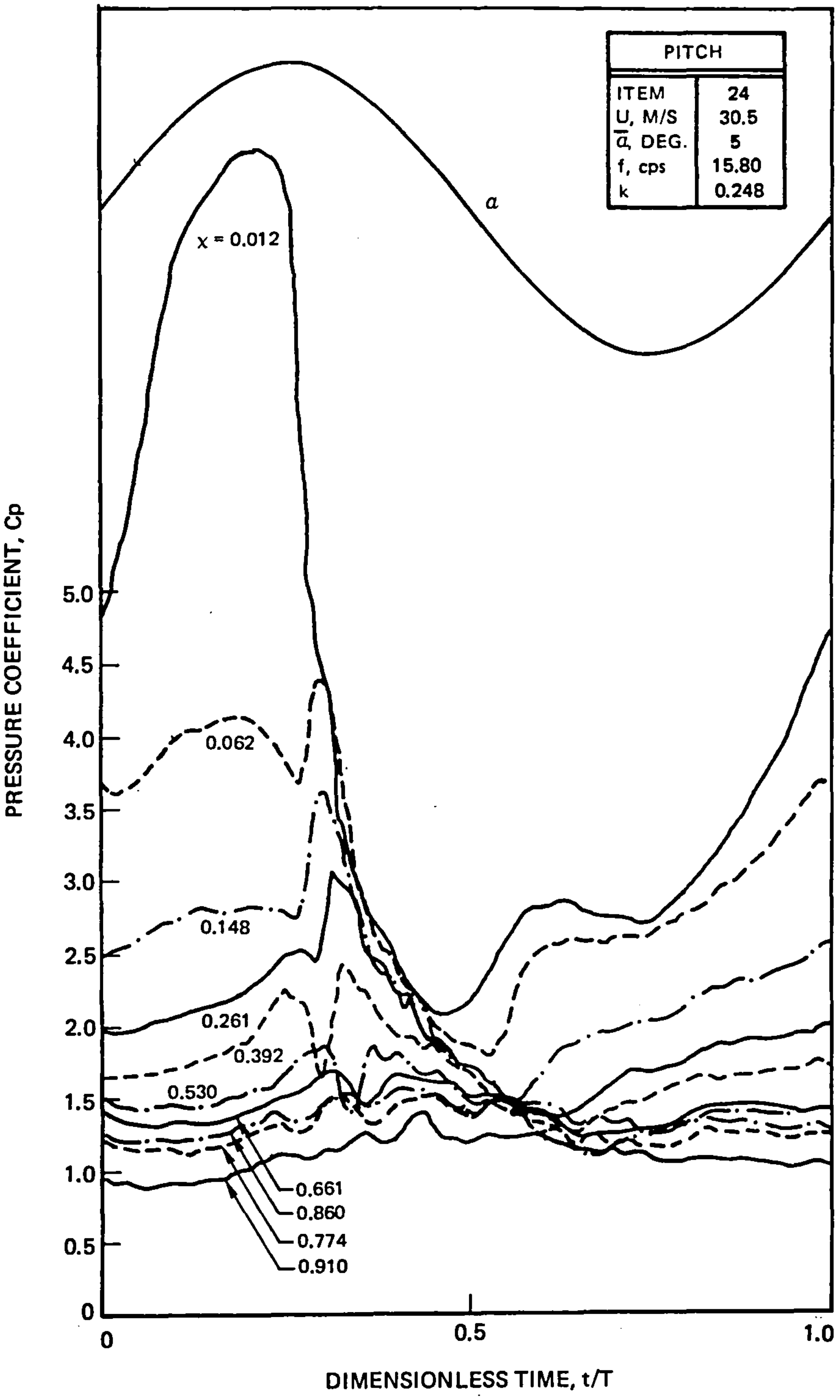

**Figure 54** Pressure Comparisons for $\alpha = 15 \pm 5°$ at $k \cong 0.25$
a) Pitch Time History

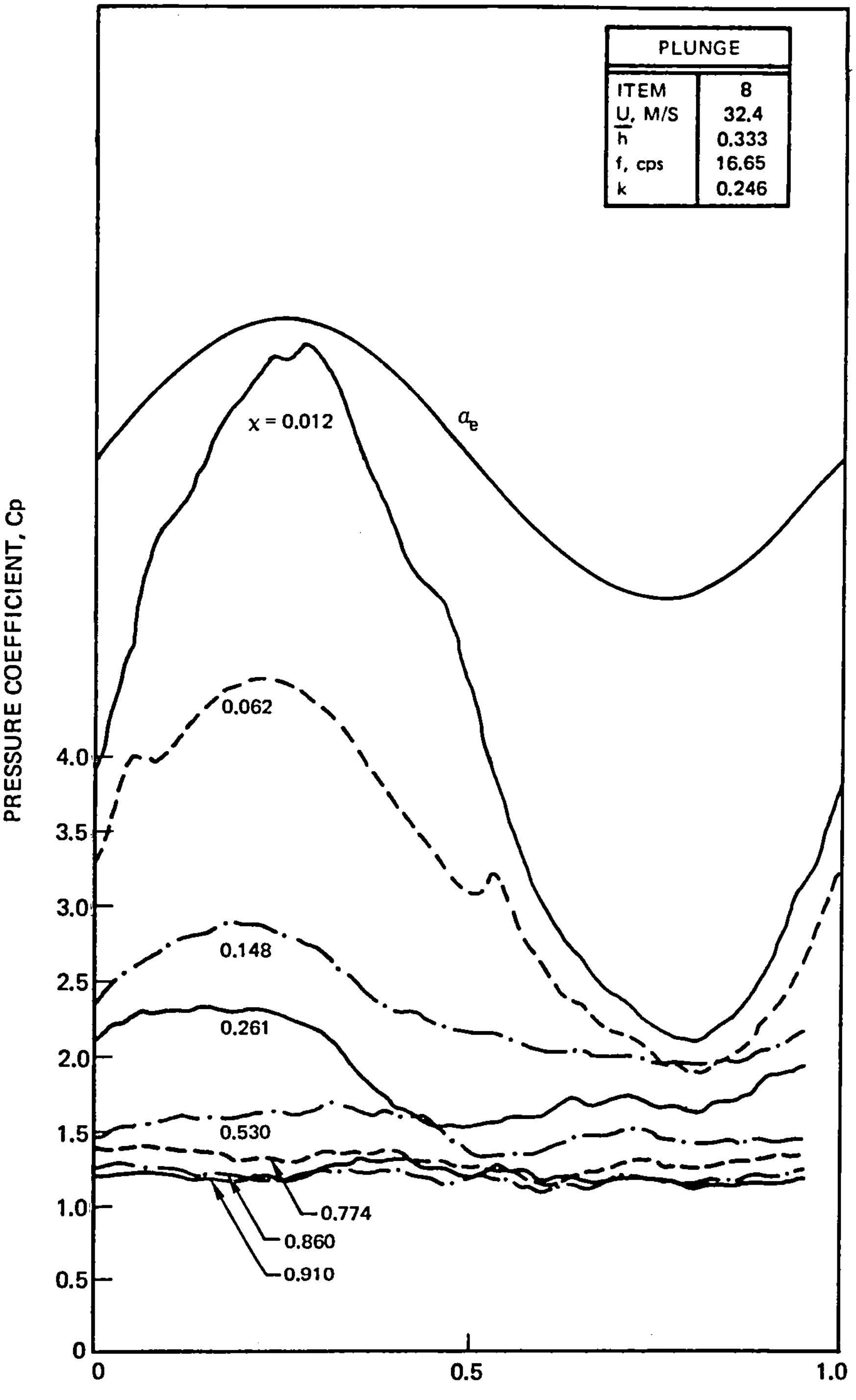

Figure 54 (continued)
b) Plunge Time History

| PITCH | |
|---|---|
| ITEM | 24 |
| U, M/S | 30.5 |
| $\bar{\alpha}$, DEG. | 5 |
| f, cps | 15.80 |
| k | 0.248 |

| PLUNGE | |
|---|---|
| ITEM | 8 |
| U, M/S | 32.4 |
| $\bar{h}$ | 0.333 |
| f, cps | 16.65 |
| k | 0.246 |

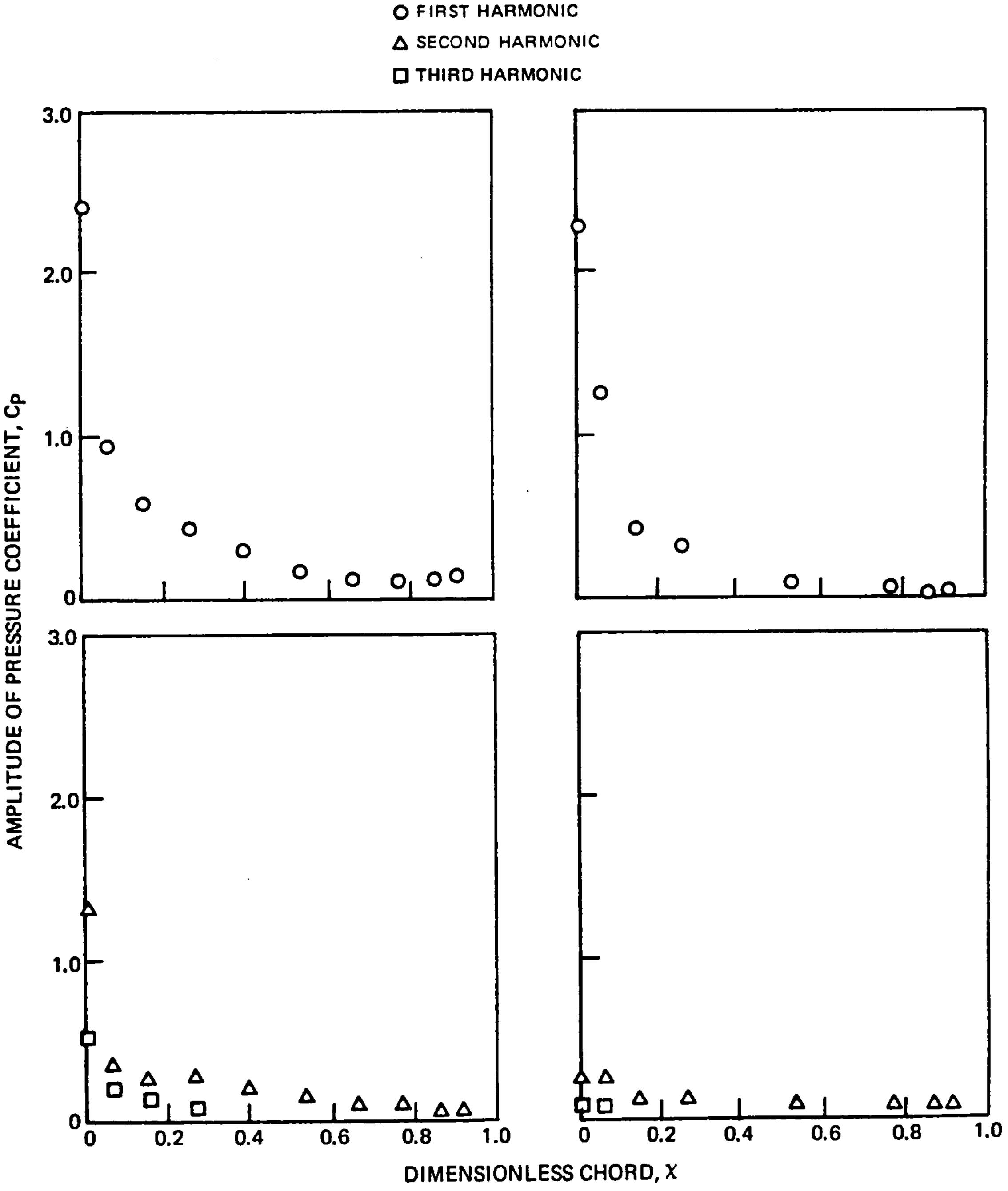

Figure 54 (continued)
c) Harmonic Amplitudes

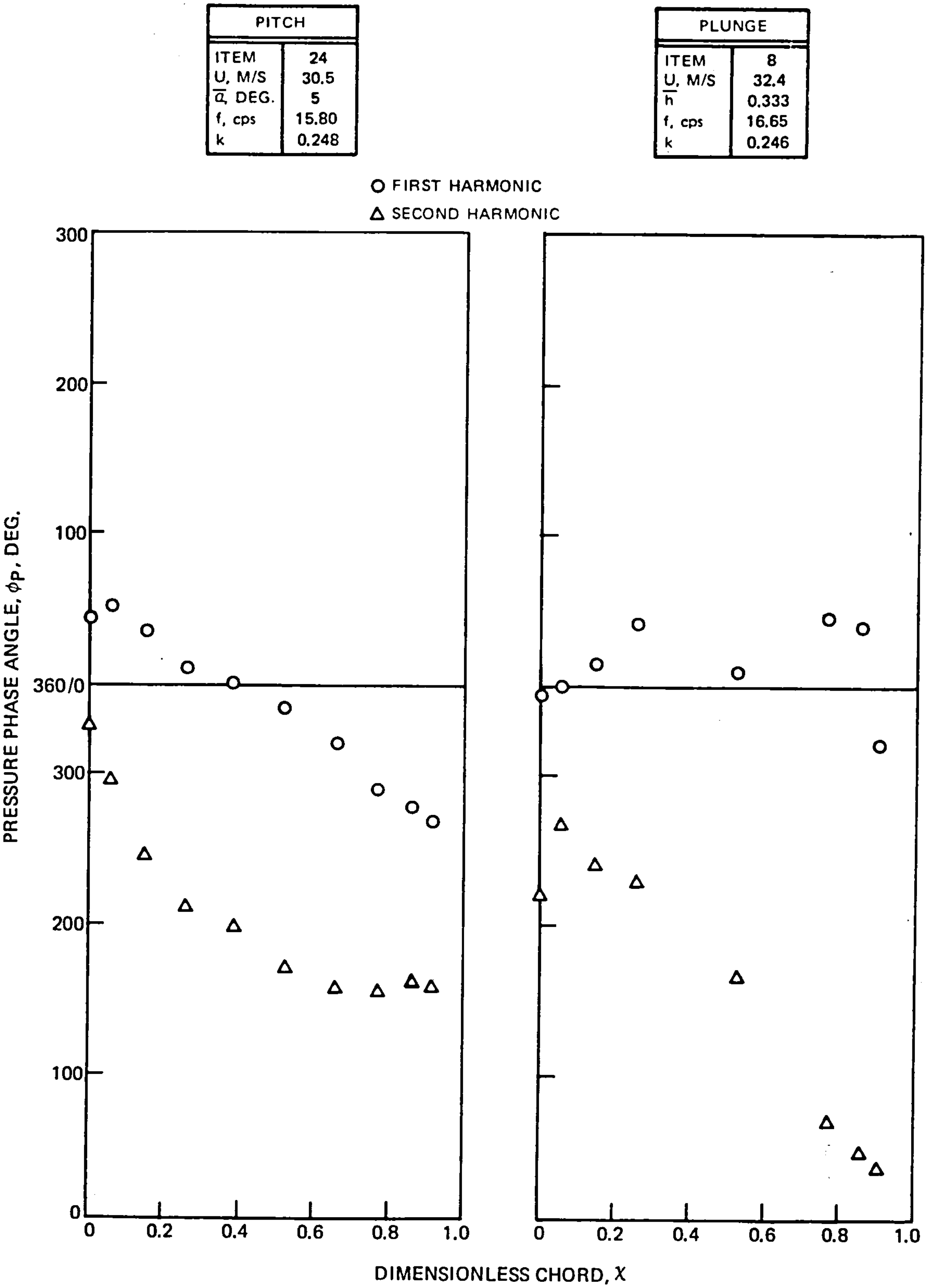

| PITCH | |
|---|---|
| ITEM | 24 |
| U, M/S | 30.5 |
| $\overline{\alpha}$, DEG. | 5 |
| f, cps | 15.80 |
| k | 0.248 |

| PLUNGE | |
|---|---|
| ITEM | 8 |
| U, M/S | 32.4 |
| $\overline{h}$ | 0.333 |
| f, cps | 16.65 |
| k | 0.246 |

Figure 54 (concluded)
d) Harmonic Phase Angles

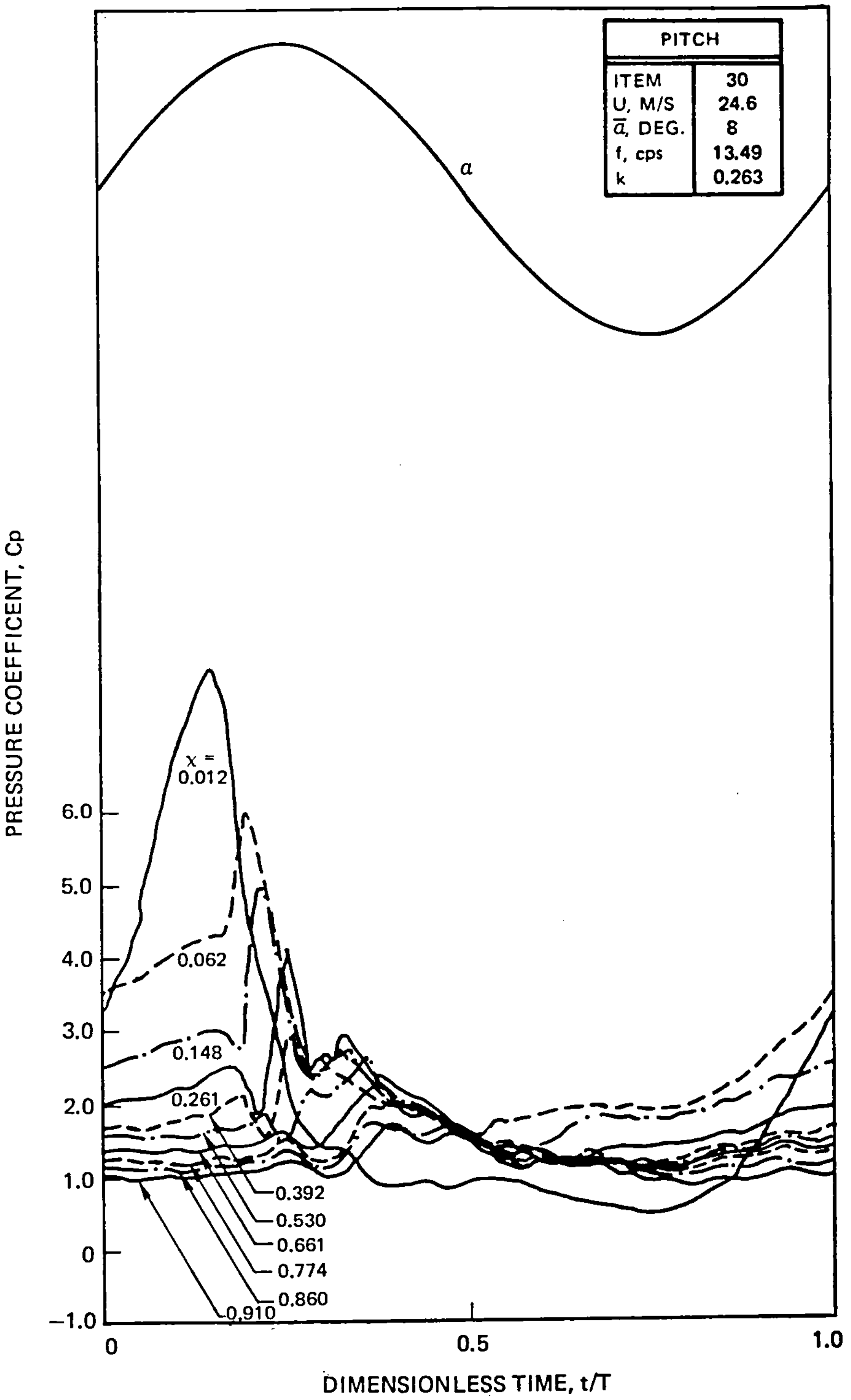

Figure 55 Pressure Comparisons for $\alpha$ = 15 ± 8° at k ≅ 0.26
a) Pitch Time History

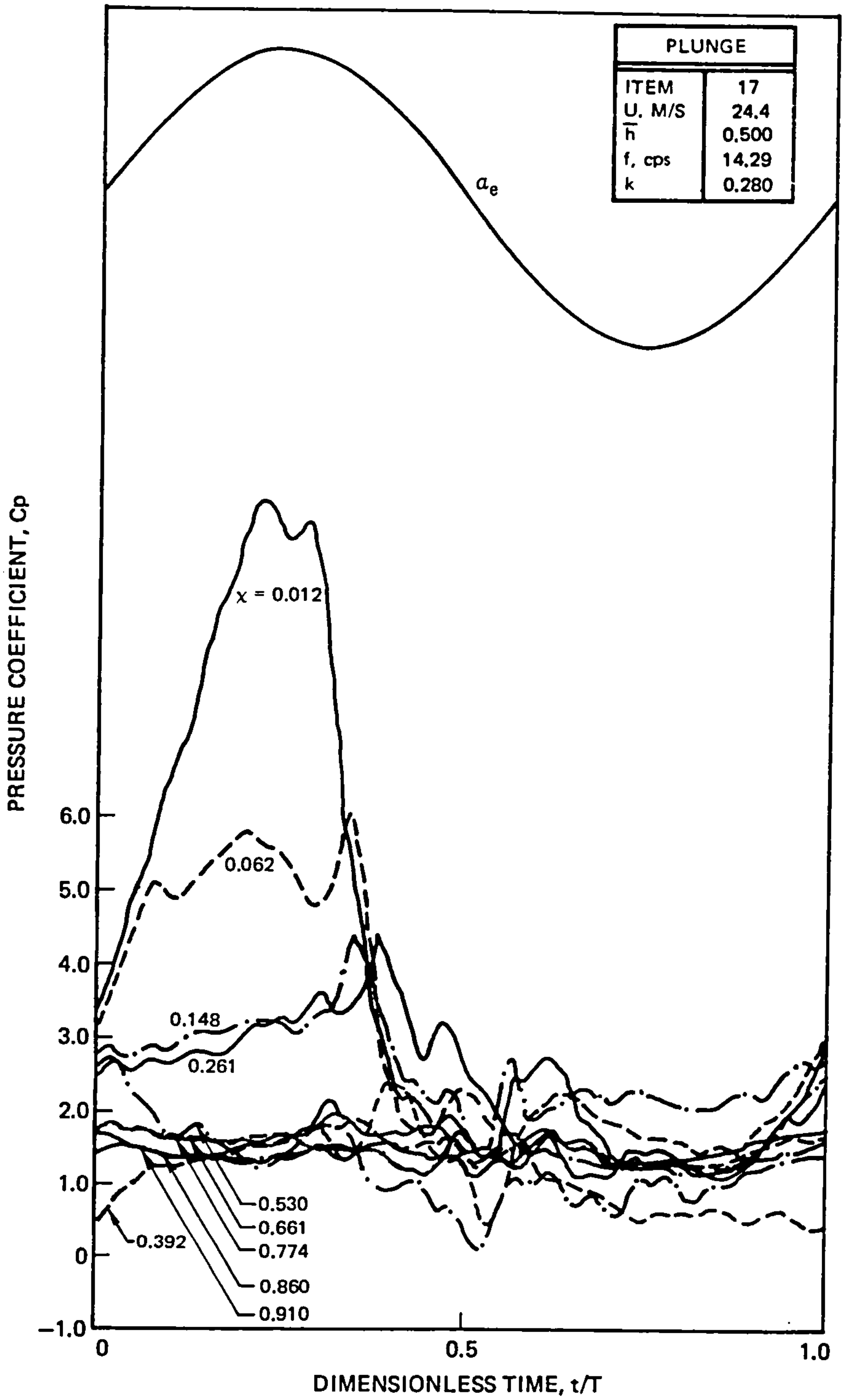

Figure 55 (continued)
b) Plunge Time History

| PITCH | |
|---|---|
| ITEM | 30 |
| U, M/S | 24.6 |
| $\overline{\alpha}$, DEG. | 8 |
| f, cps | 13.49 |
| k | 0.263 |

| PLUNGE | |
|---|---|
| ITEM | 17 |
| U, M/S | 24.4 |
| $\overline{h}$ | 0.500 |
| f, cps | 14.29 |
| k | 0.280 |

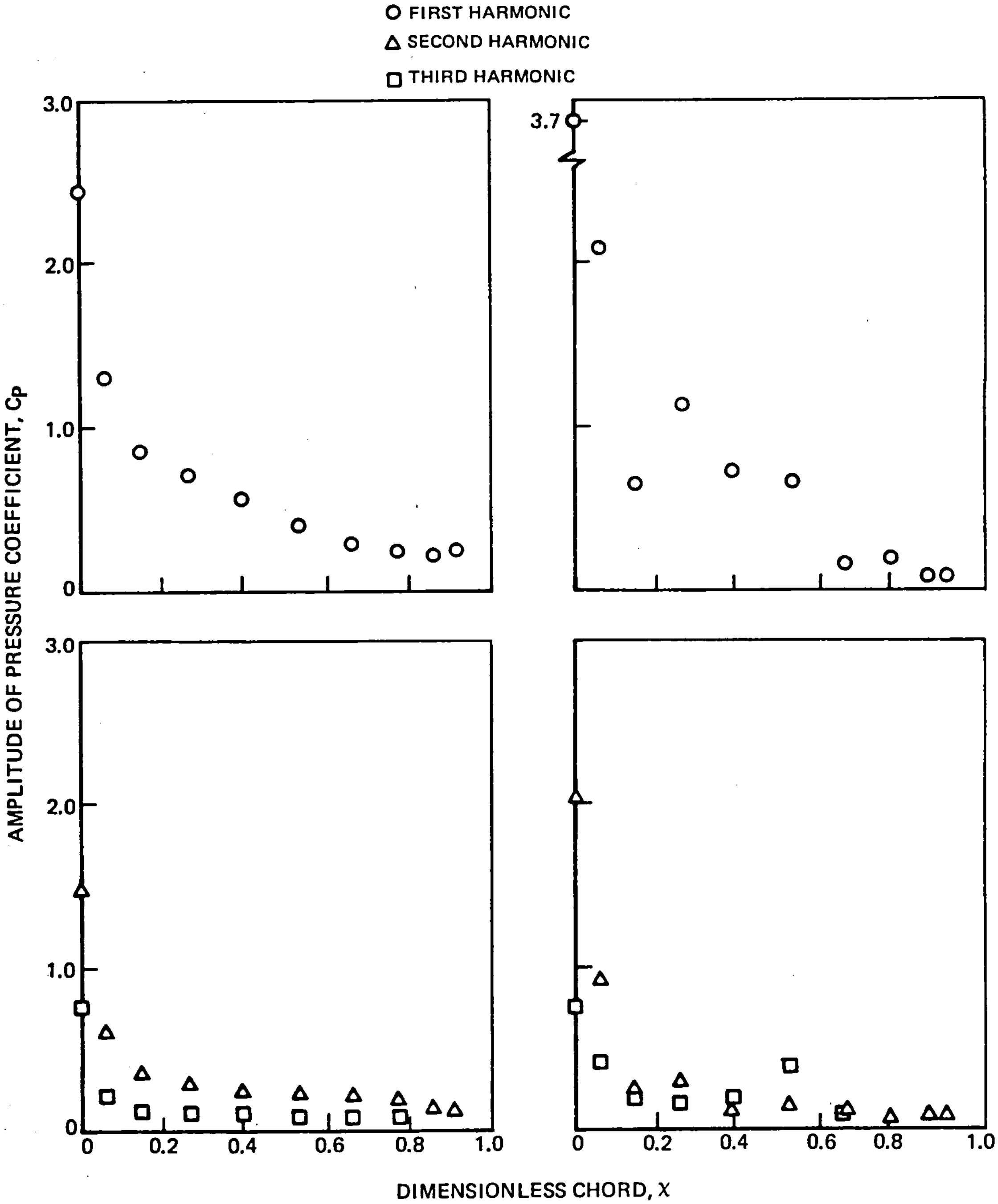

Figure 55 (continued)
c) Harmonic Amplitudes

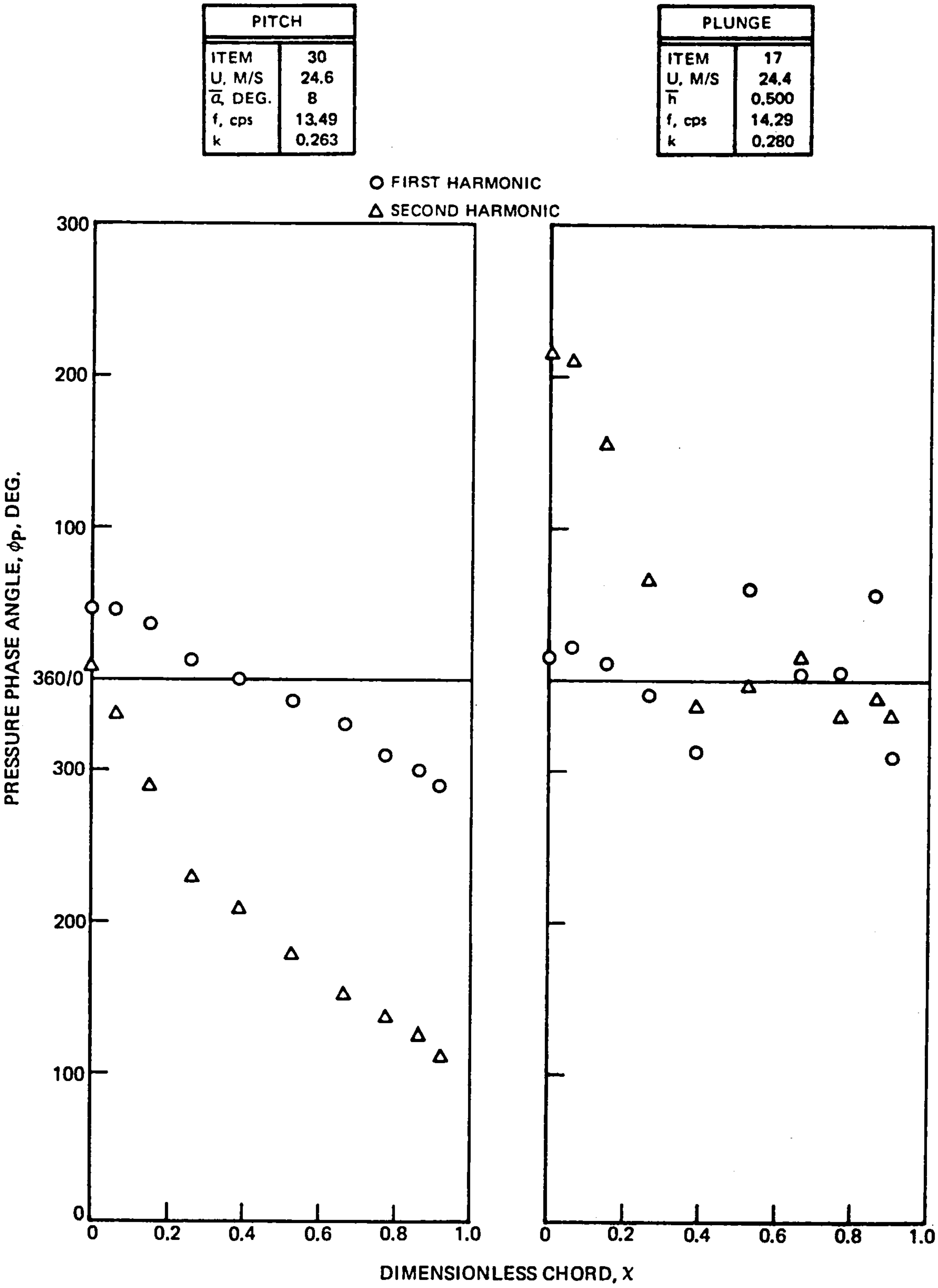

**Figure 55 (concluded)**
**d) Harmonic Phase Angles**

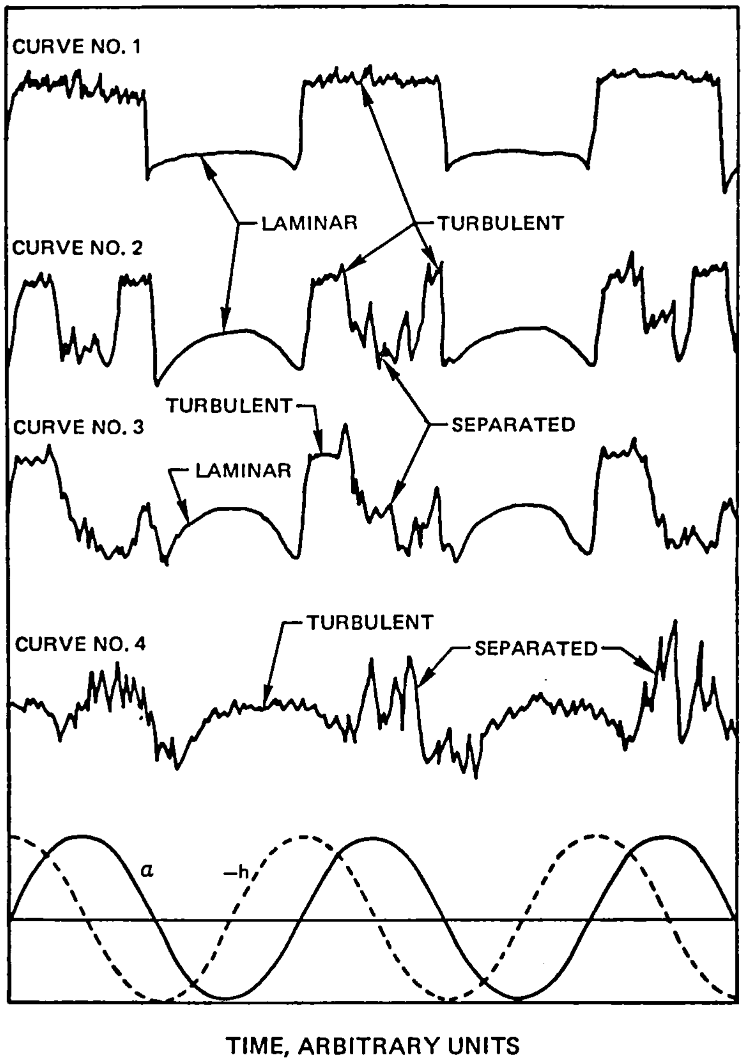

Figure 56 Schematic of Hot Film Response

| PITCH | |
|---|---|
| ITEM | 20 |
| U, M/S | 30.3 |
| $\bar{\alpha}$, DEG. | 5 |
| f, cps | 10.49 |
| k | 0.166 |

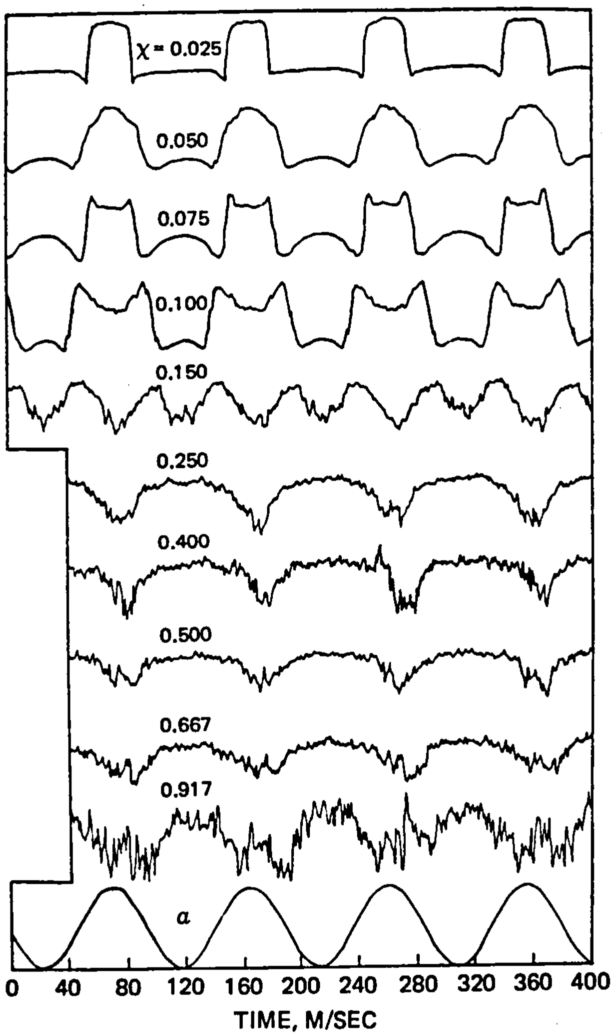

**Figure 57 Hot Film Response for $\alpha = 12 \pm 5°$ at k $\cong$ 0.17**
**a) Pitch Time History**

| PLUNGE | |
|---|---|
| ITEM | 16 |
| U, M/S | 31.8 |
| $\bar{h}$ | 0.500 |
| f, cps | 11.04 |
| k | 0.166 |

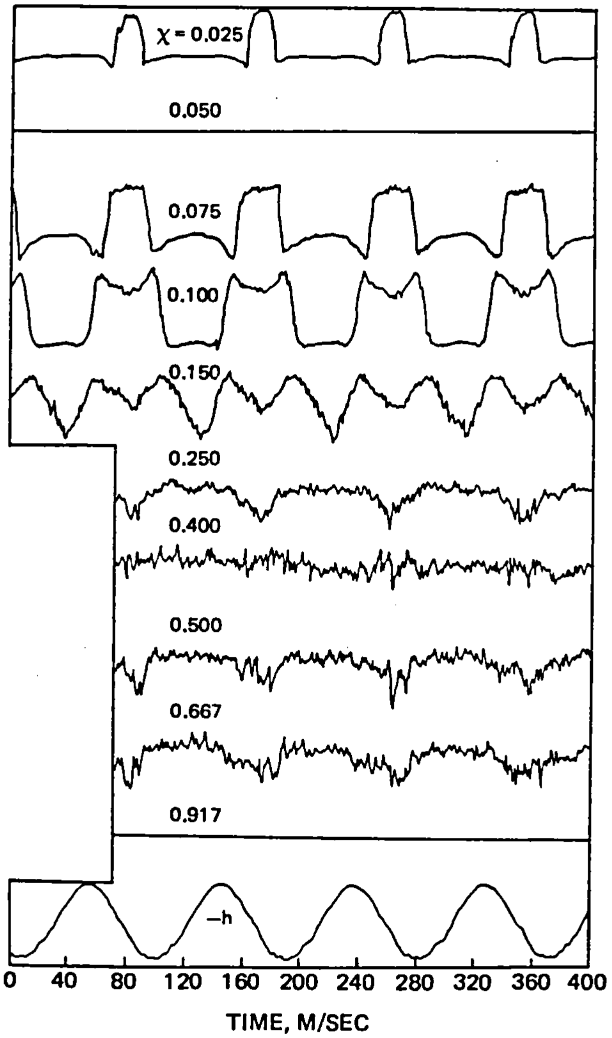

Figure 57 (concluded)
b) Plunge Time History

| PITCH | |
|---|---|
| ITEM | 22 |
| U, M/S | 30.7 |
| $\bar{\alpha}$, DEG. | 5 |
| f, cps | 7.89 |
| k | 0.123 |

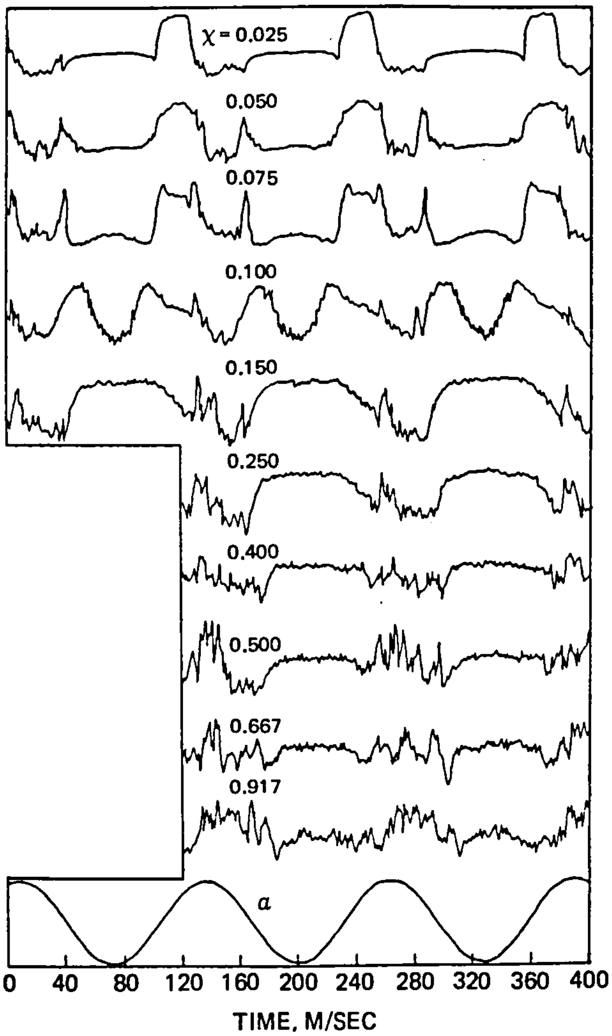

**Figure 58 Hot Film Response for $\alpha = 15 \pm 5°$ at $k \cong 0.12$**
**a) Plunge Time History**

| PLUNGE | |
|---|---|
| ITEM | 28 |
| U, M/S | 30.5 |
| $\bar{h}$ | 0.667 |
| f, cps | 8.31 |
| k | 0.131 |

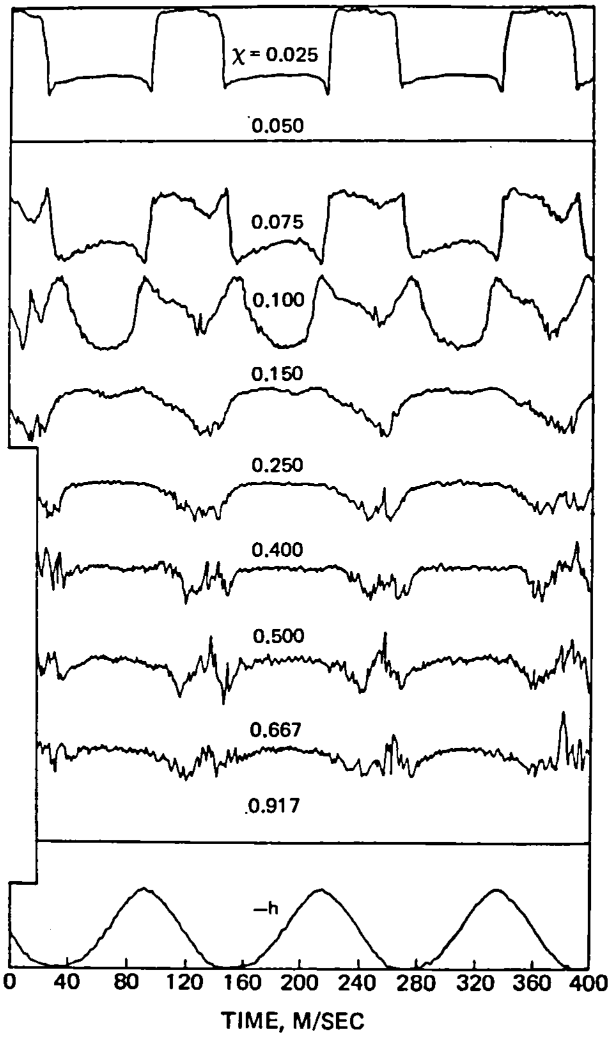

**Figure 58** (concluded)
b) Plunge Time History

| PITCH | |
|---|---|
| ITEM | 23 |
| U, M/S | 30.7 |
| $\bar{\alpha}$, DEG. | 5 |
| f, cps | 10.49 |
| k | 0.164 |

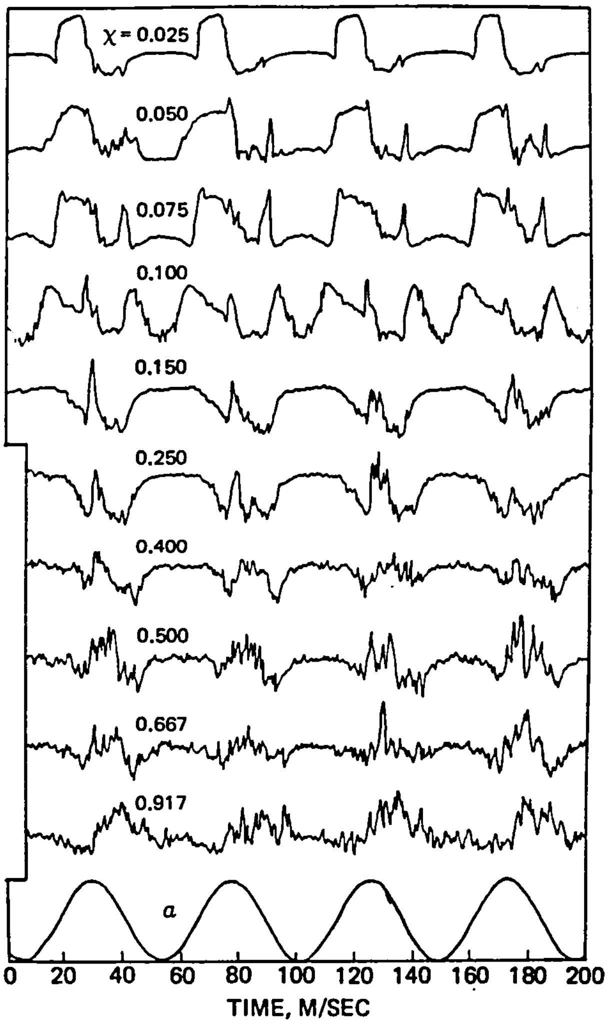

Figure 59 Hot Film Response for $\alpha = 15 \pm 5°$ at k ≅ 0.17
a) Pitch Time History

| PLUNGE | |
|---|---|
| ITEM | 18 |
| U, M/S | 30.2 |
| $\bar{h}$ | 0.500 |
| f, cps | 11.11 |
| k | 0.176 |

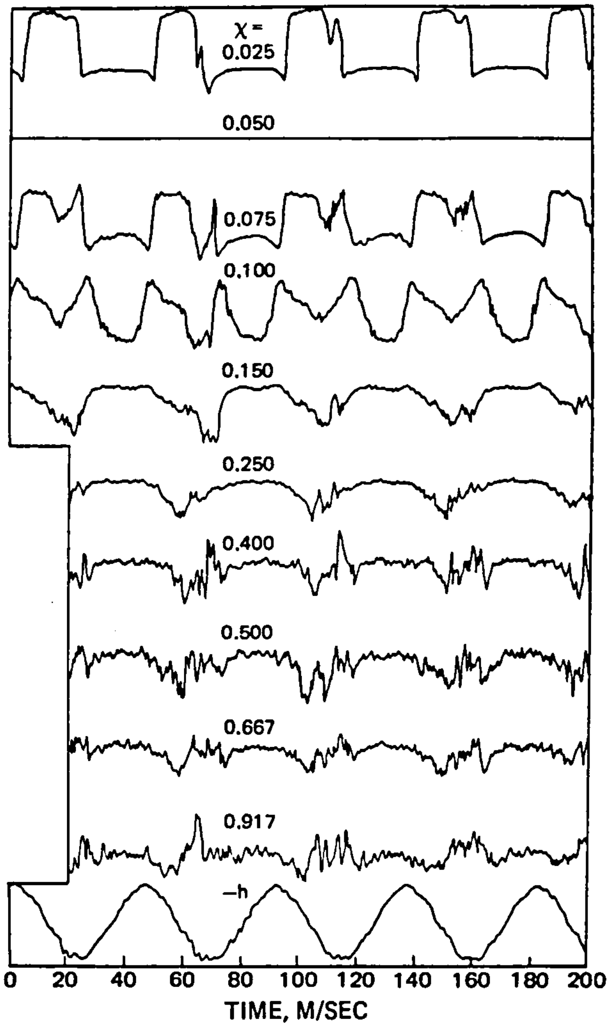

**Figure 59 (concluded)**
**b) Plunge Time History**

| PITCH | |
|---|---|
| ITEM | 24 |
| U, M/S | 30.5 |
| $\overline{\alpha}$, DEG. | 5 |
| f, cps | 15.8 |
| k | 0.248 |

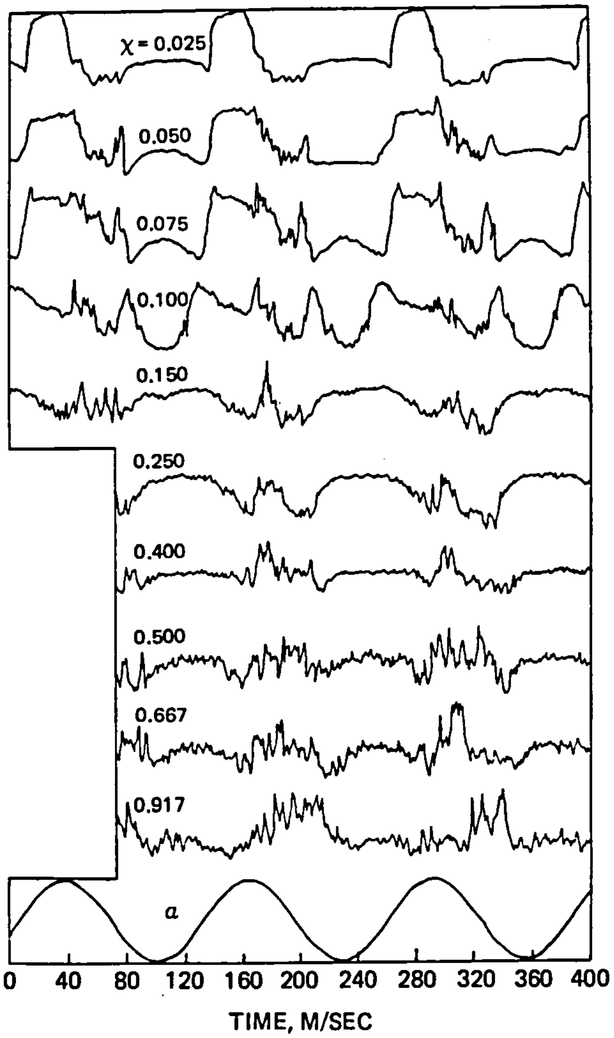

Figure 60 Hot Film Response for $\alpha$ = 15 ± 5° at k ≅ 0.25
a) Pitch Time History

| PLUNGE | |
|---|---|
| ITEM | 8 |
| U, M/S | 32.4 |
| $\bar{h}$ | 0.333 |
| f, cps | 16.65 |
| k | 0.246 |

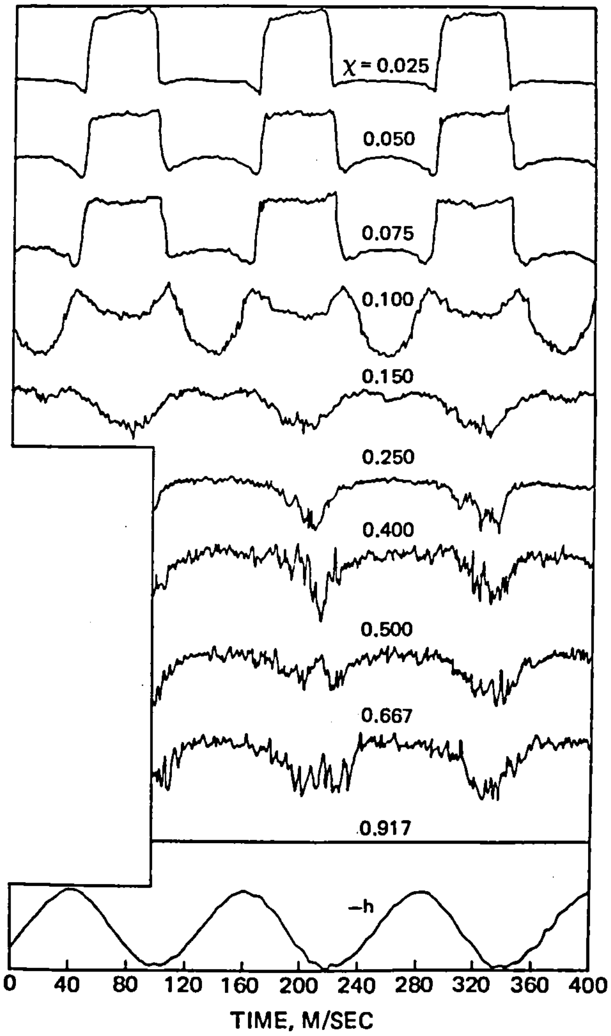

**Figure 60 (concluded)**
**b) Plunge Time History**

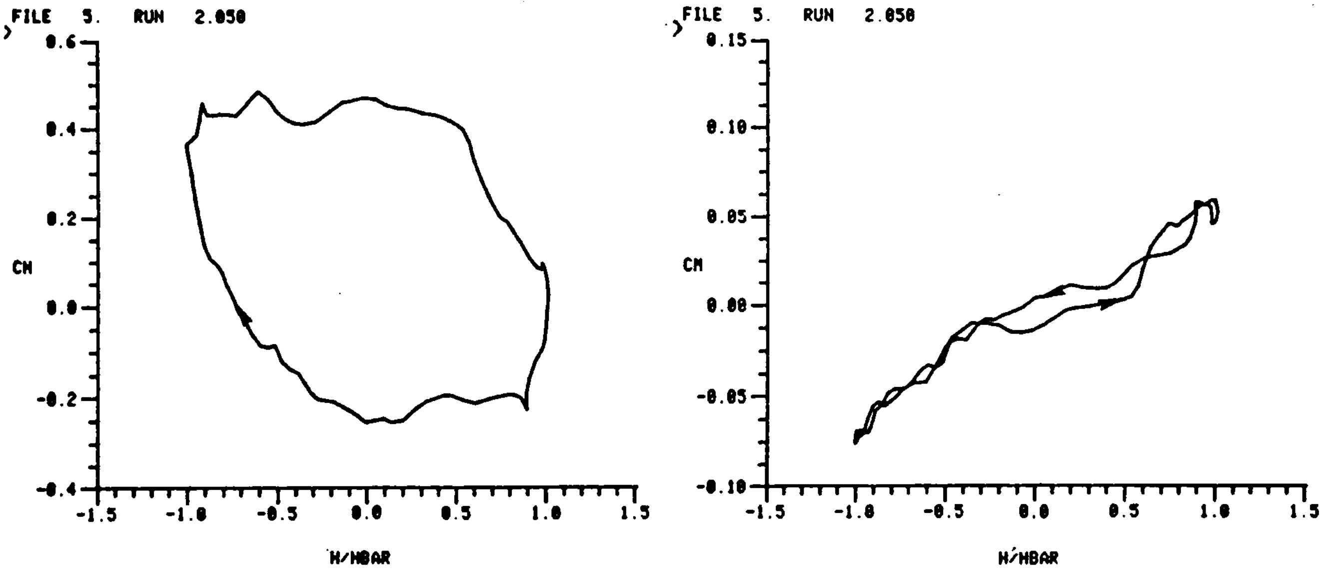

PITCH-PLUNGE EXPERIMENT: PLUNGING DATA VELOCITY = 98.1
MEAN INCIDENCE = 2.0 PLUNGING AMPLITUDE = .3
FREQUENCY = 16.960 (K = .2717)

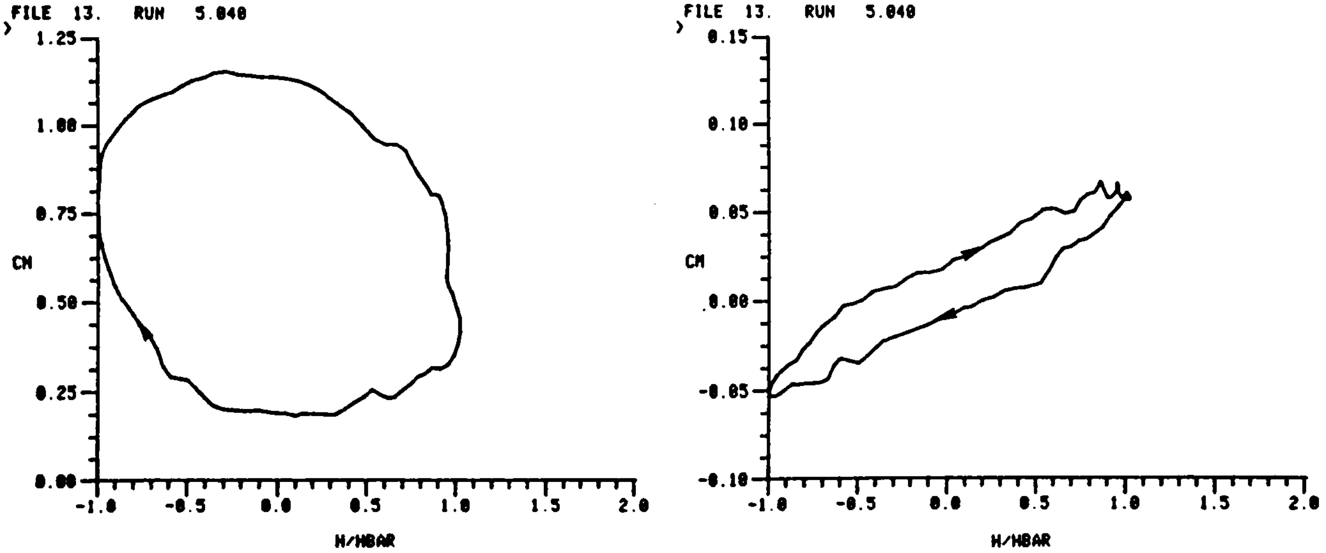

PITCH-PLUNGE EXPERIMENT: PLUNGING DATA VELOCITY = 100.1
MEAN INCIDENCE = 9.0 PLUNGING AMPLITUDE = .3
FREQUENCY = 16.715 (K = .2623)

**Figure 61 Plunging Loops**

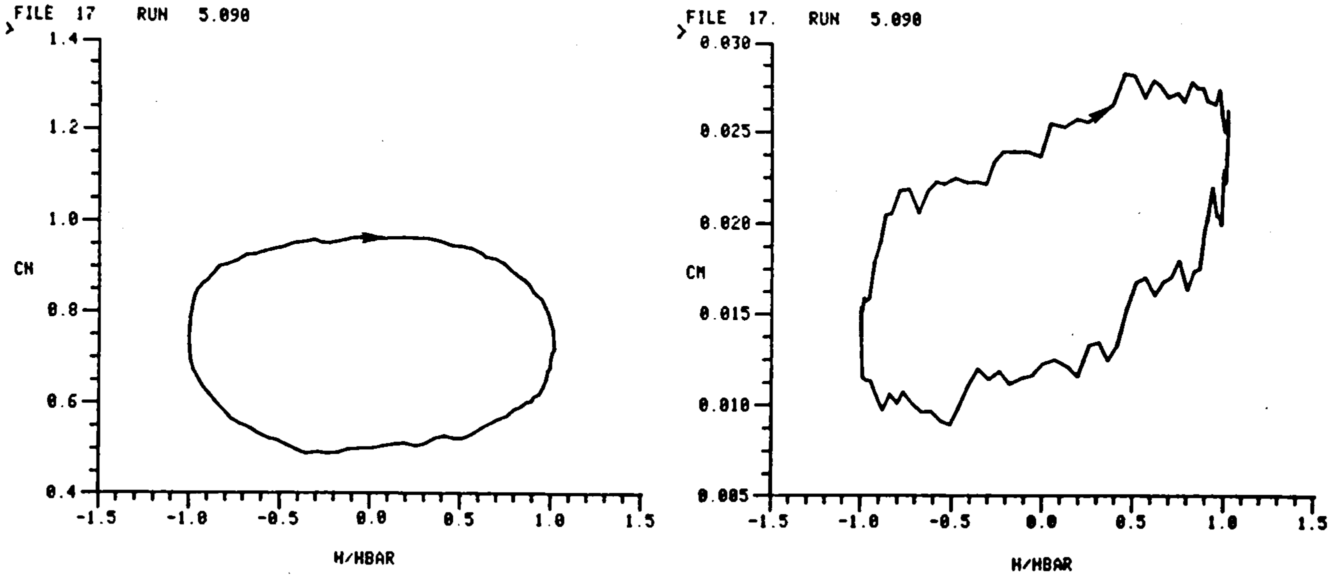

PITCH-PLUNGE EXPERIMENT: PLUNGING DATA VELOCITY = 152.4
MEAN INCIDENCE = 9.0 PLUNGING AMPLITUDE = .3
FREQUENCY = 9.993 (K = .1030)

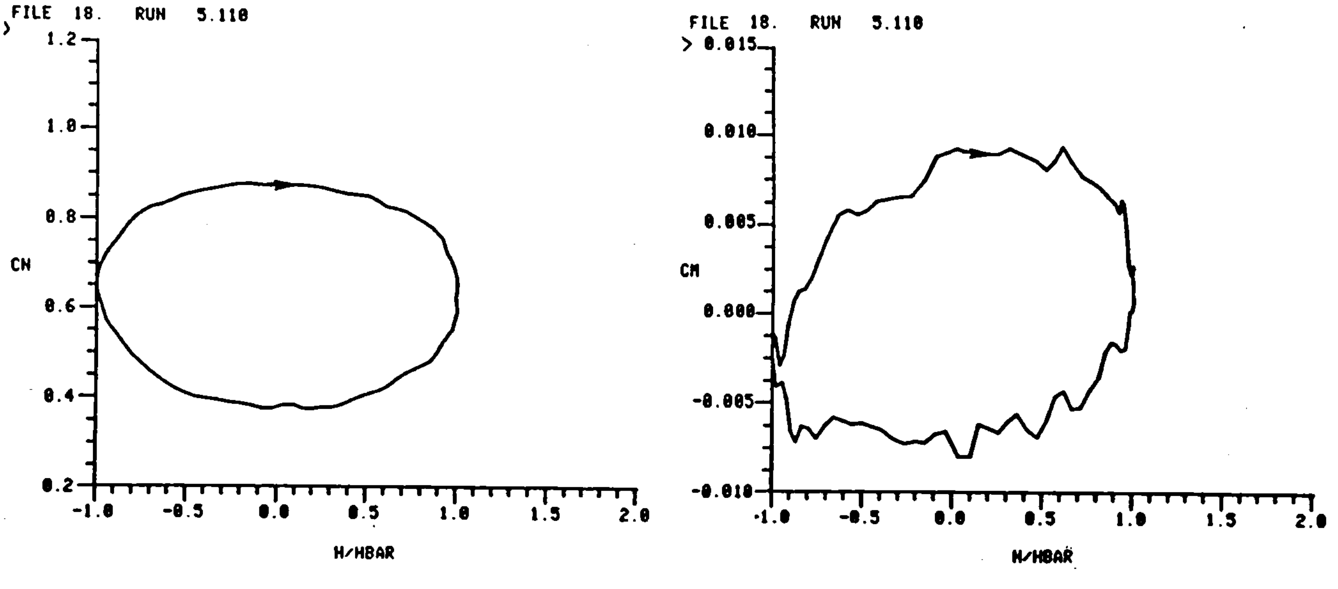

PITCH-PLUNGE EXPERIMENT: PLUNGING DATA VELOCITY = 203.4
MEAN INCIDENCE = 9.0 PLUNGING AMPLITUDE = .3
FREQUENCY = 13.187 (K = .1010)

Figure 62 Plunging Loops

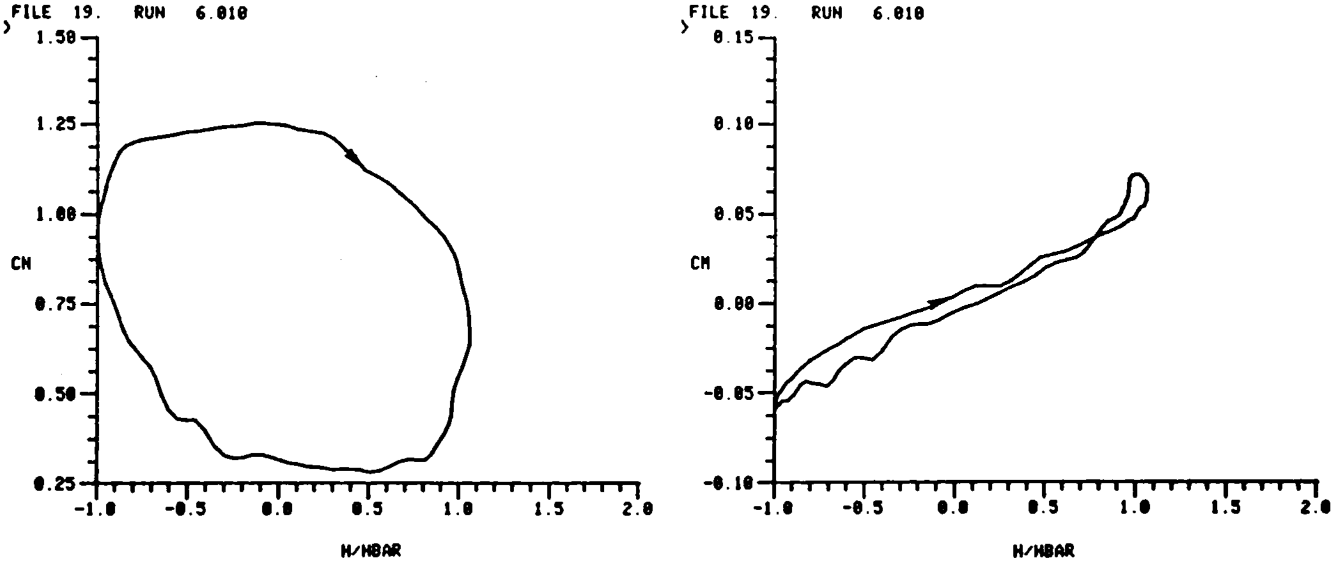

PITCH-PLUNGE EXPERIMENT: PLUNGING DATA VELOCITY = 100.3
MEAN INCIDENCE = 12.0 PLUNGING AMPLITUDE = .3
FREQUENCY = 16.680 (K = .2612)

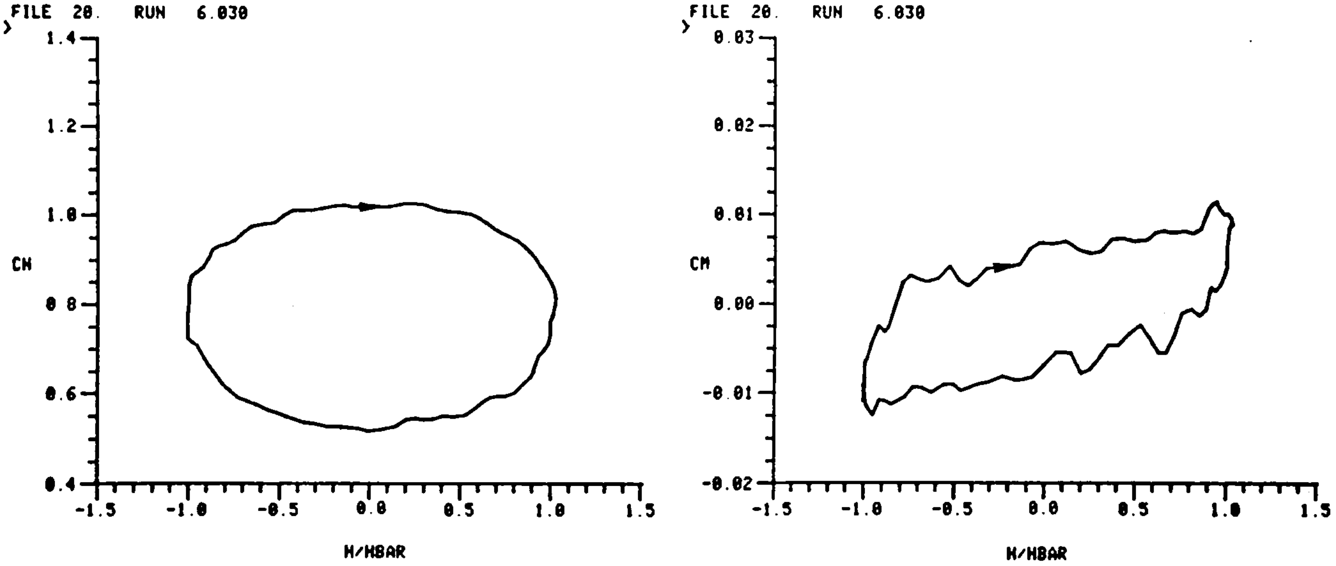

PITCH-PLUNGE EXPERIMENT: PLUNGING DATA VELOCITY = 152.7
MEAN INCIDENCE = 12.0 PLUNGING AMPLITUDE = .3
FREQUENCY = 10.092 (K = .1038)

Figure 63 Plunging Loops

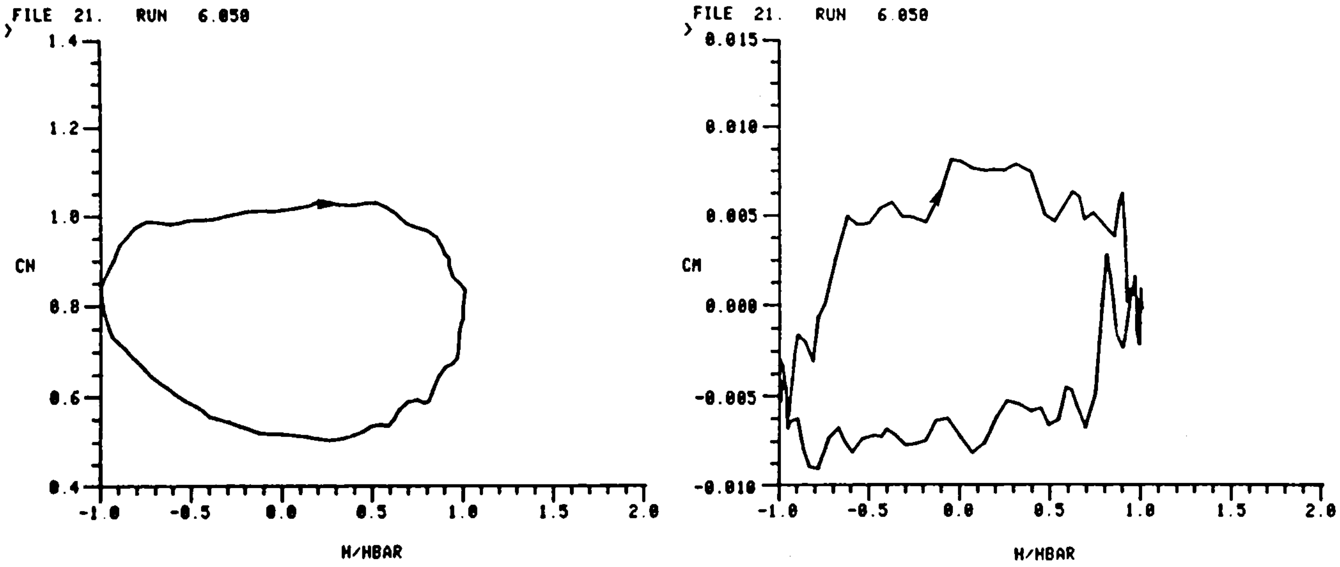

PITCH-PLUNGE EXPERIMENT: PLUNGING DATA VELOCITY = 201.1
MEAN INCIDENCE = 12.0 PLUNGING AMPLITUDE = .3
FREQUENCY = 13.214 (K = .1032)

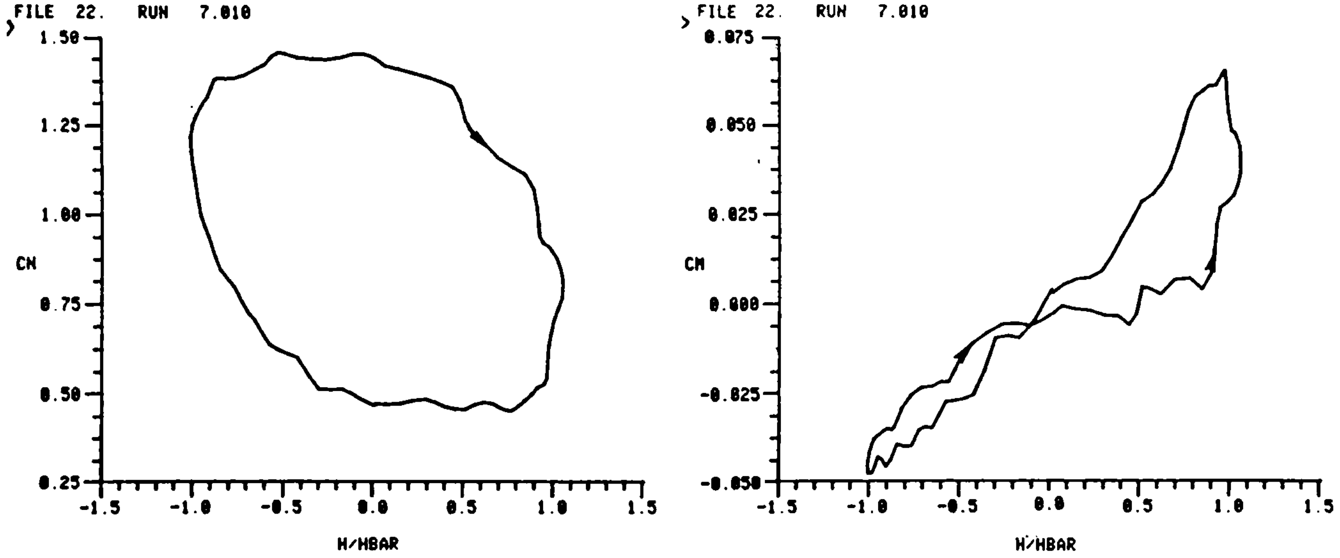

PITCH-PLUNGE EXPERIMENT: PLUNGING DATA VELOCITY = 106.3
MEAN INCIDENCE = 15.0 PLUNGING AMPLITUDE = .3
FREQUENCY = 16.628 (K = .2457)

Figure 64 Plunging Loops

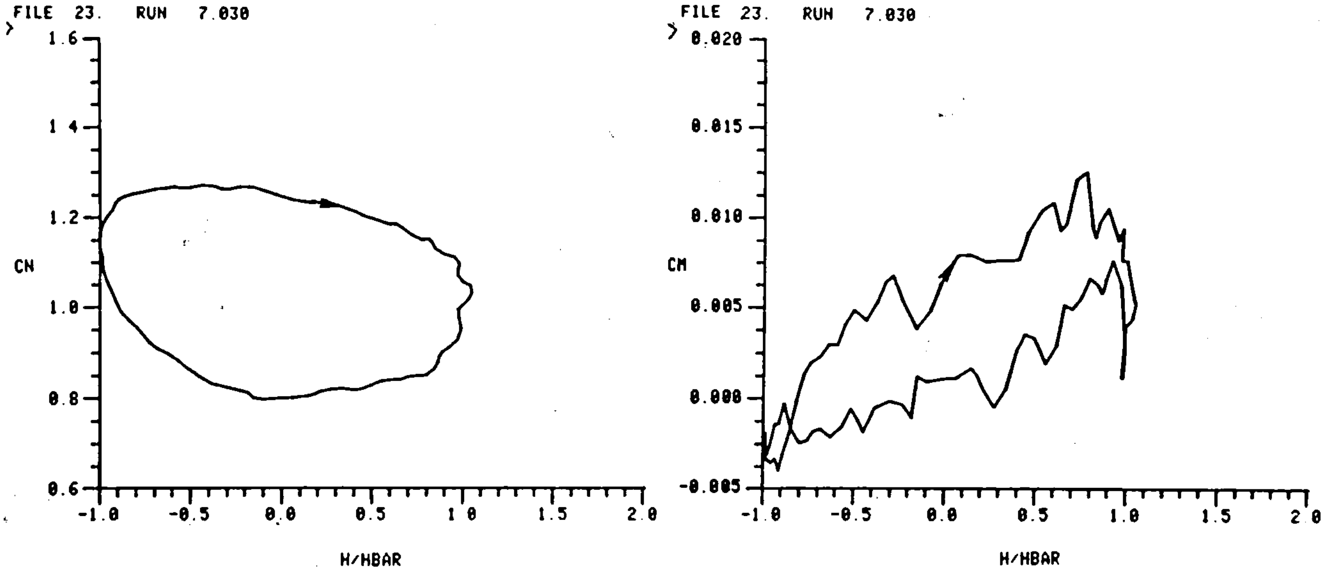

PITCH-PLUNGE EXPERIMENT: PLUNGING DATA VELOCITY = 155.6
MEAN INCIDENCE = 15.0 PLUNGING AMPLITUDE = .3
FREQUENCY = 10.010 (K = .1010)

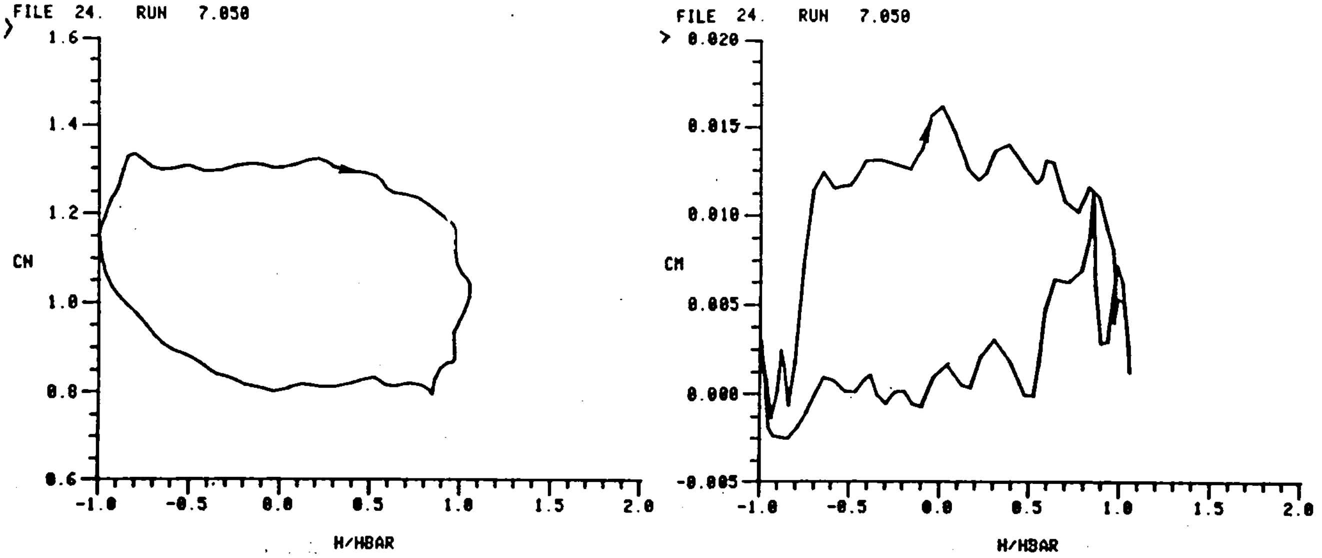

PITCH-PLUNGE EXPERIMENT: PLUNGING DATA VELOCITY = 201.4
MEAN INCIDENCE = 15.0 PLUNGING AMPLITUDE = .3
FREQUENCY = 13.287 (K = .1036)

Figure 65 Plunging Loops

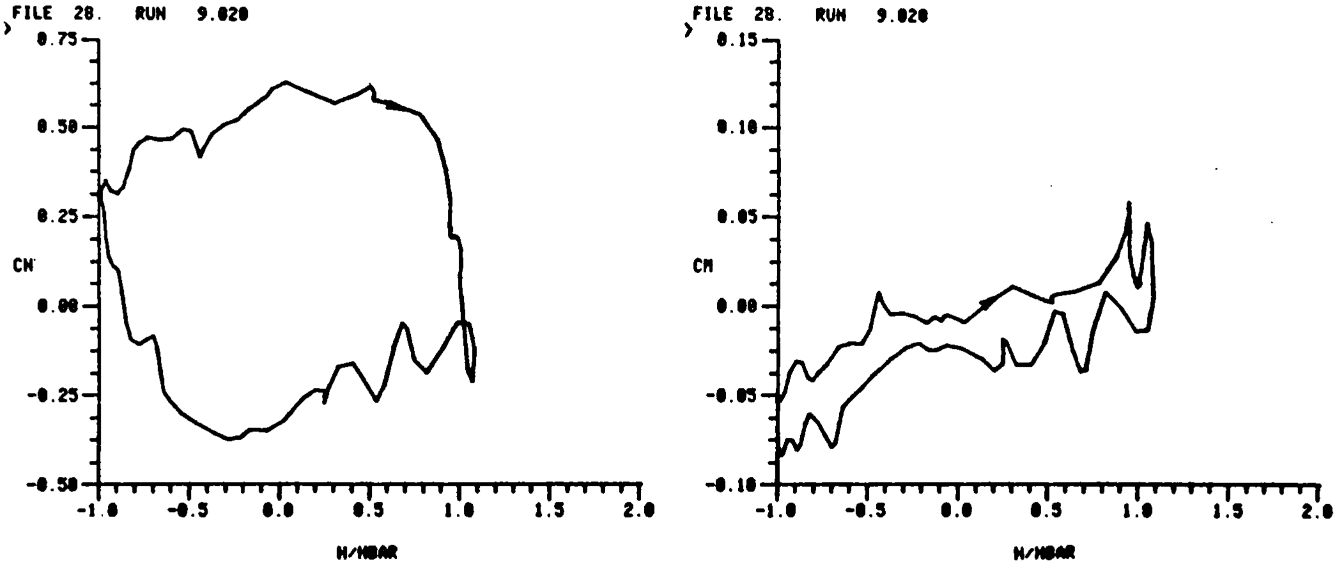

PITCH-PLUNGE EXPERIMENT: PLUNGING DATA VELOCITY = 125.4
MEAN INCIDENCE = 2.0 PLUNGING AMPLITUDE = .5
FREQUENCY = 13.104 (K = 1651)

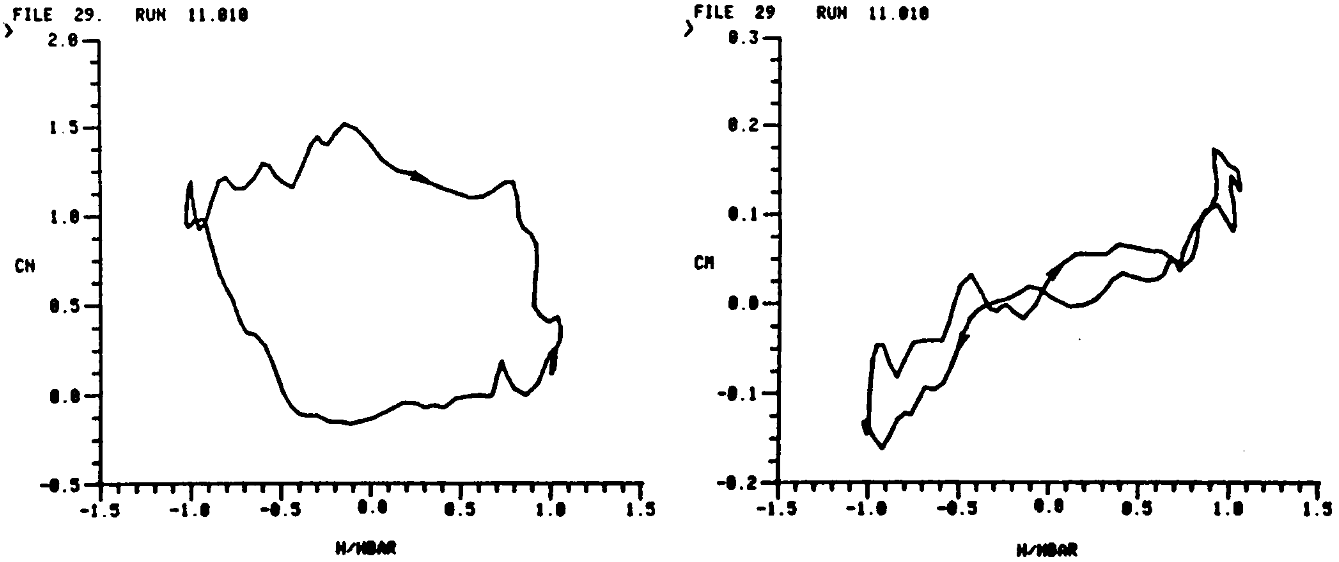

PITCH-PLUNGE EXPERIMENT: PLUNGING DATA VELOCITY = 85.1
MEAN INCIDENCE = 9.0 PLUNGING AMPLITUDE = .5
FREQUENCY = 14.220 (K = .2626)

Figure 66 Plunging Loops

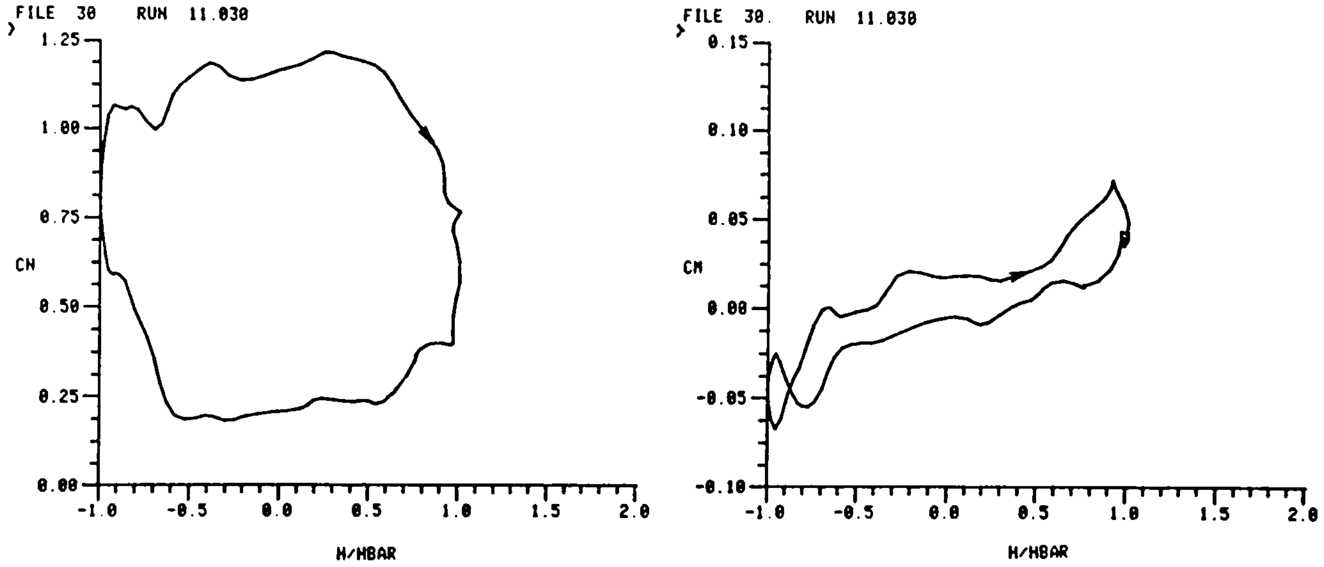

PITCH-PLUNGE EXPERIMENT: PLUNGING DATA VELOCITY = 99.2
MEAN INCIDENCE = 9.0 PLUNGING AMPLITUDE = .5
FREQUENCY = 11.010 (K = .1743)

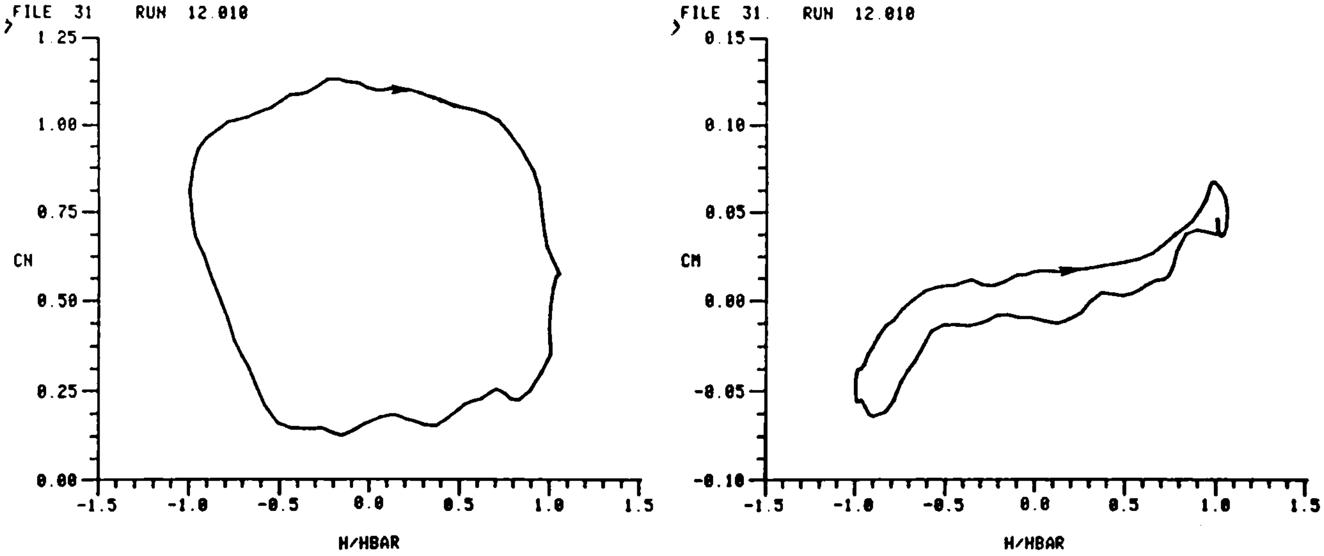

PITCH-PLUNGE EXPERIMENT: PLUNGING DATA VELOCITY = 122.1
MEAN INCIDENCE = 9.0 PLUNGING AMPLITUDE = .5
FREQUENCY = 13.433 (K = .1728)

Figure 67 Plunging Loops

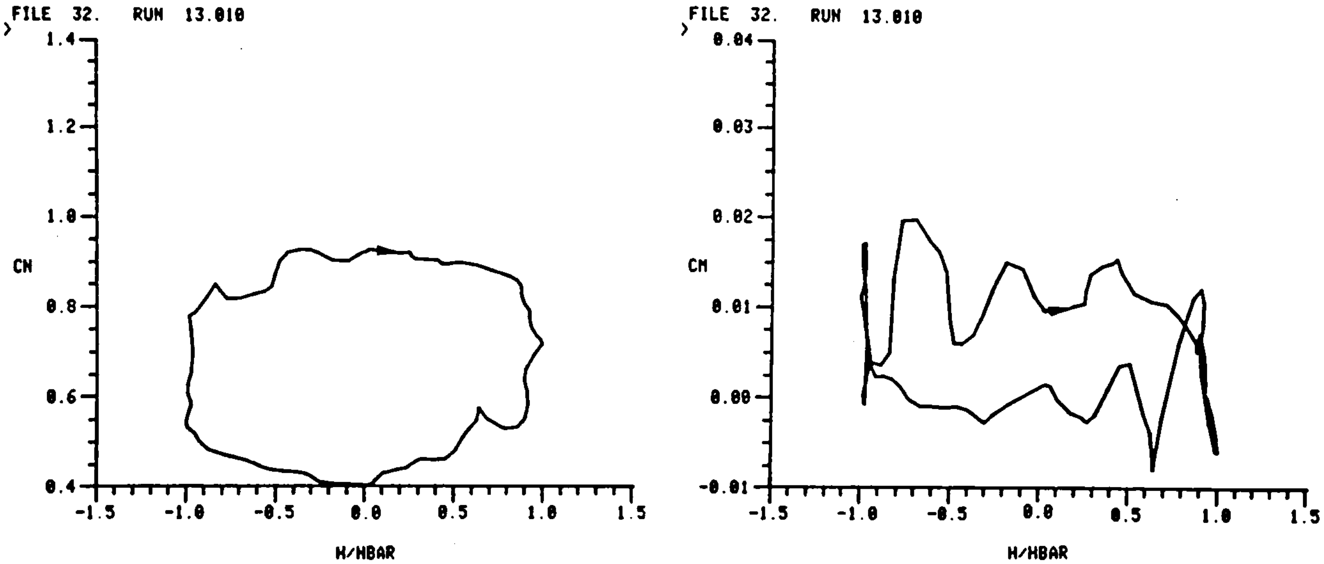

PITCH-PLUNGE EXPERIMENT: PLUNGING DATA VELOCITY = 197.6
MEAN INCIDENCE = 9.0 PLUNGING AMPLITUDE = .5
FREQUENCY = 8.901 (K = .0708)

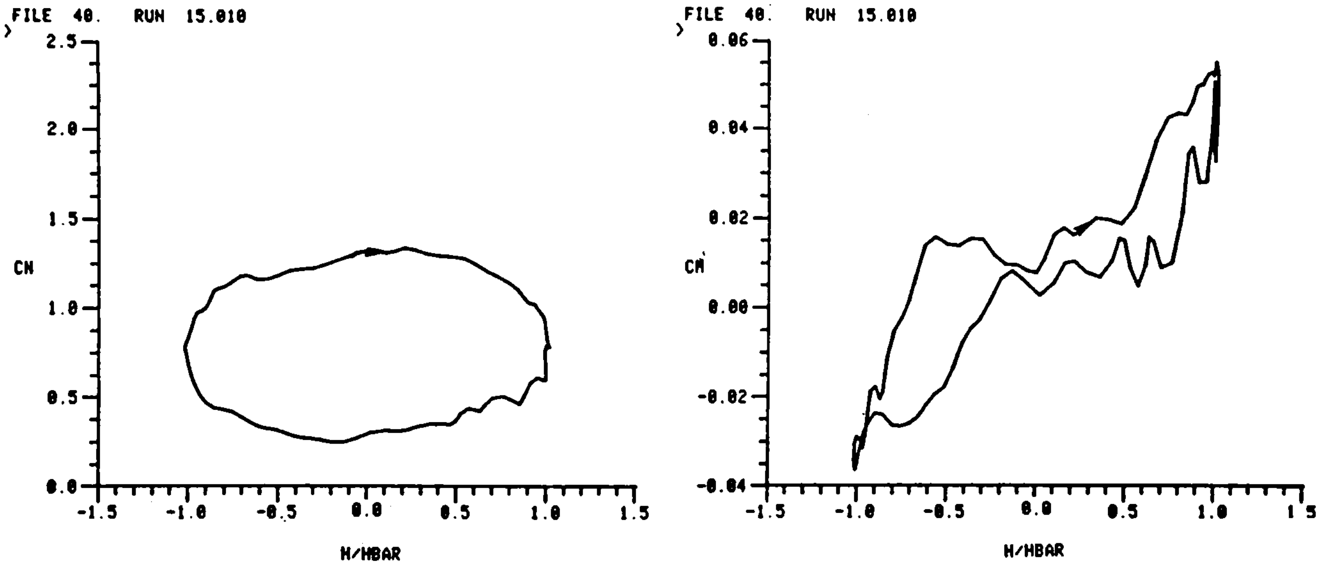

PITCH-PLUNGE EXPERIMENT: PLUNGING DATA VELOCITY = 104.3
MEAN INCIDENCE = 12.0 PLUNGING AMPLITUDE = .5
FREQUENCY = 11.037 (K = .1662)

Figure 68 Plunging Loops

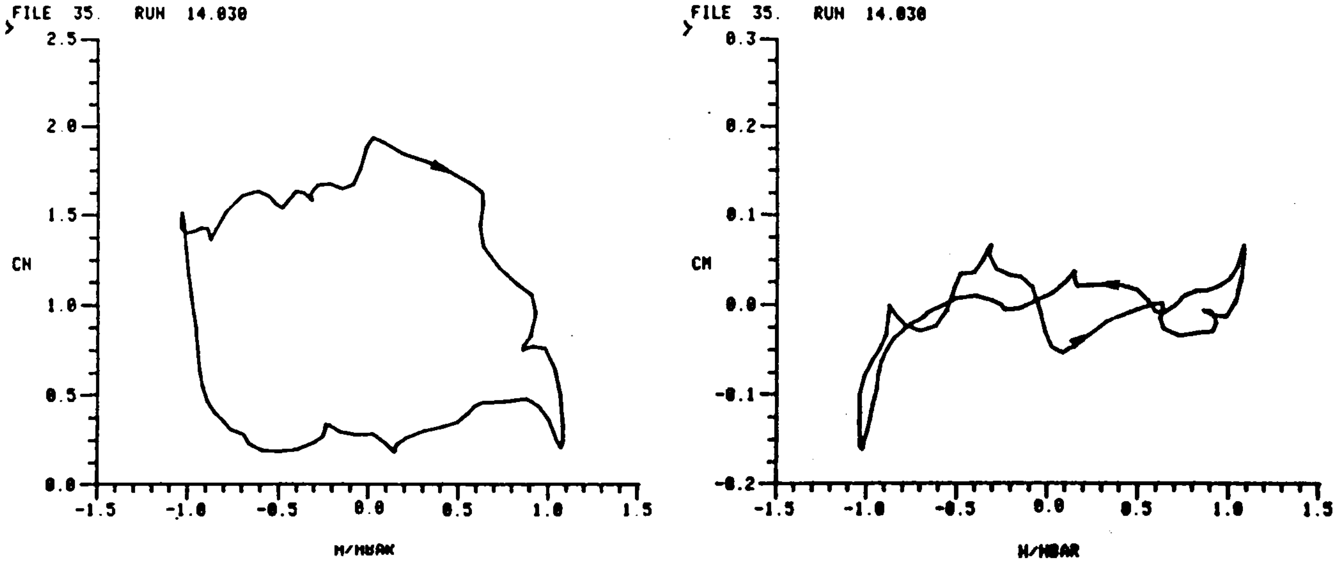

PITCH-PLUNGE EXPERIMENT: PLUNGING DATA VELOCITY = 80.2
MEAN INCIDENCE = 15.0 PLUNGING AMPLITUDE = .5
FREQUENCY = 14.207 (K = .2798)

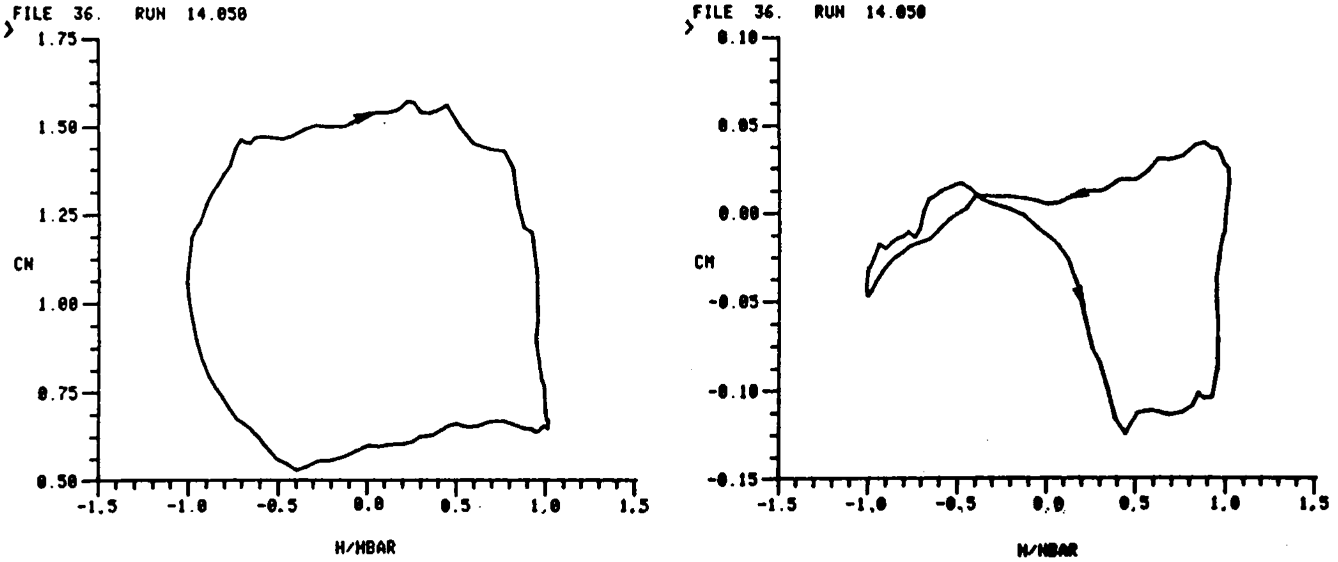

PITCH-PLUNGE EXPERIMENT: PLUNGING DATA VELOCITY = 99.2
MEAN INCIDENCE = 15.0 PLUNGING AMPLITUDE = .5
FREQUENCY = 11.114 (K = .1760)

**Figure 69 Plunging Loops**

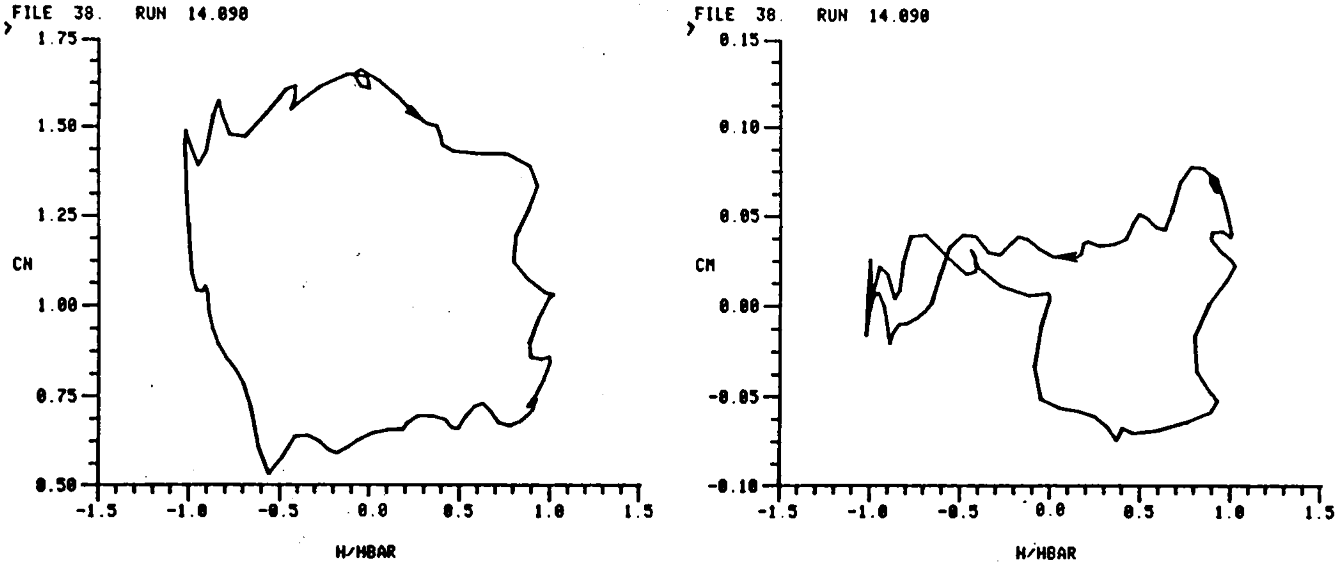

PITCH-PLUNGE EXPERIMENT: PLUNGING DATA VELOCITY = 120.9
MEAN INCIDENCE = 15.0 PLUNGING AMPLITUDE = .5
FREQUENCY = 13.290 (K = 1727)

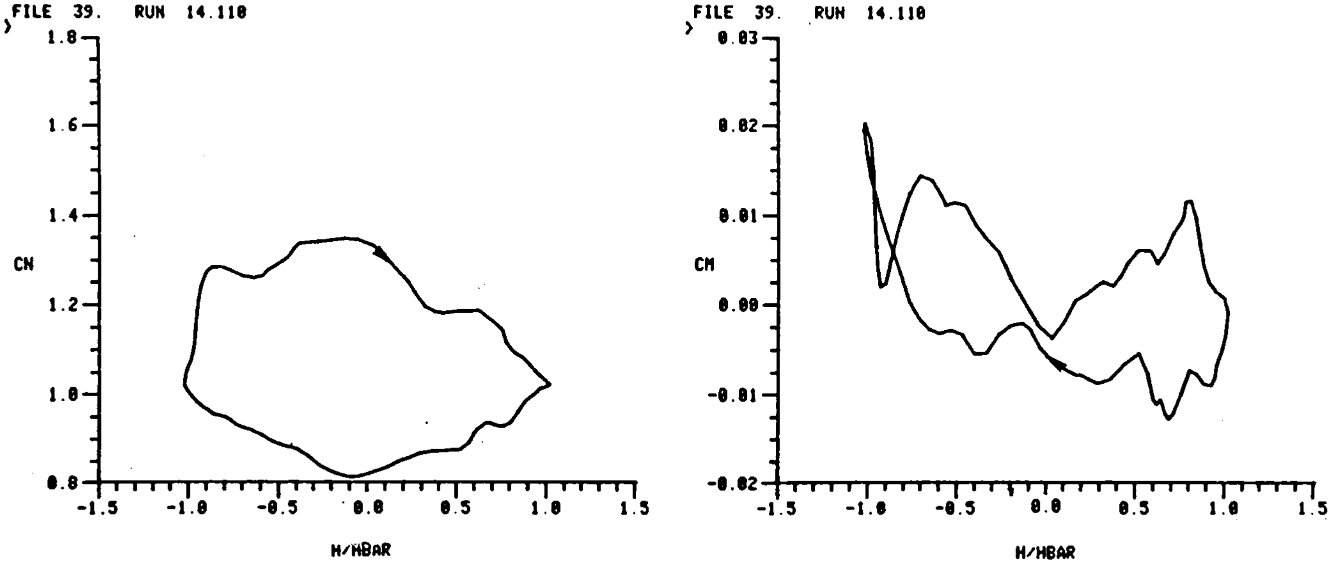

PITCH-PLUNGE EXPERIMENT: PLUNGING DATA VELOCITY = 199.6
MEAN INCIDENCE = 15.0 PLUNGING AMPLITUDE = .5
FREQUENCY = 8.936 (K = .0703)

Figure 70 Plunging Loops

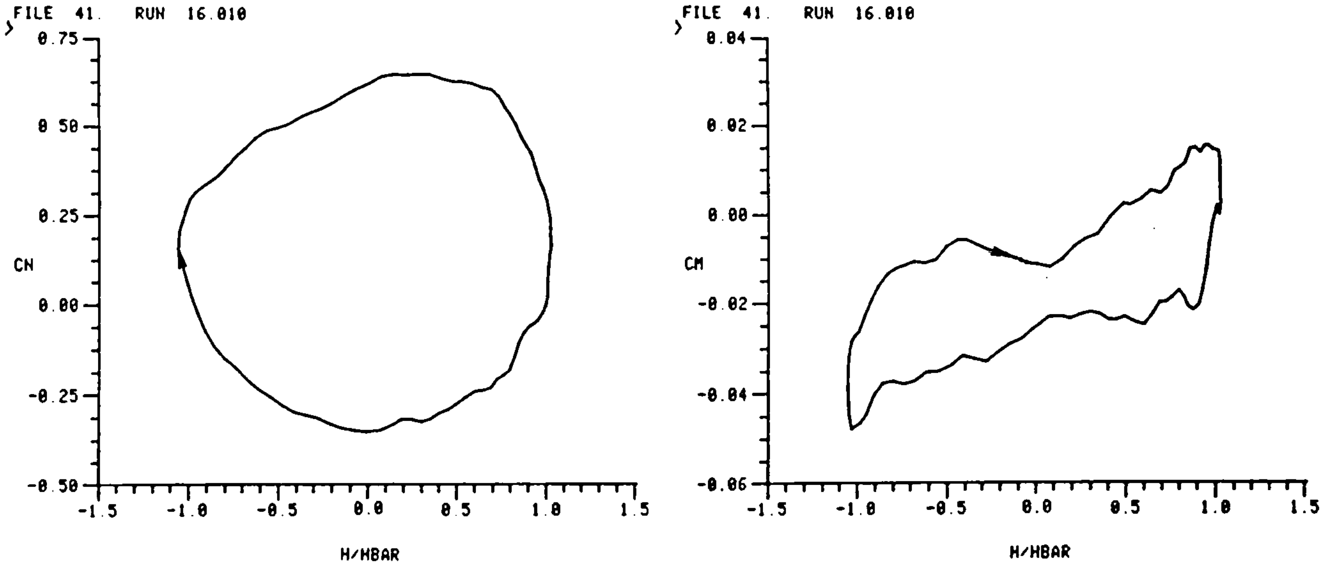

PITCH-PLUNGE EXPERIMENT: PLUNGING DATA VELOCITY = 101.9
MEAN INCIDENCE = 2.0 PLUNGING AMPLITUDE = .7
FREQUENCY = 8.336 (K = .1285)

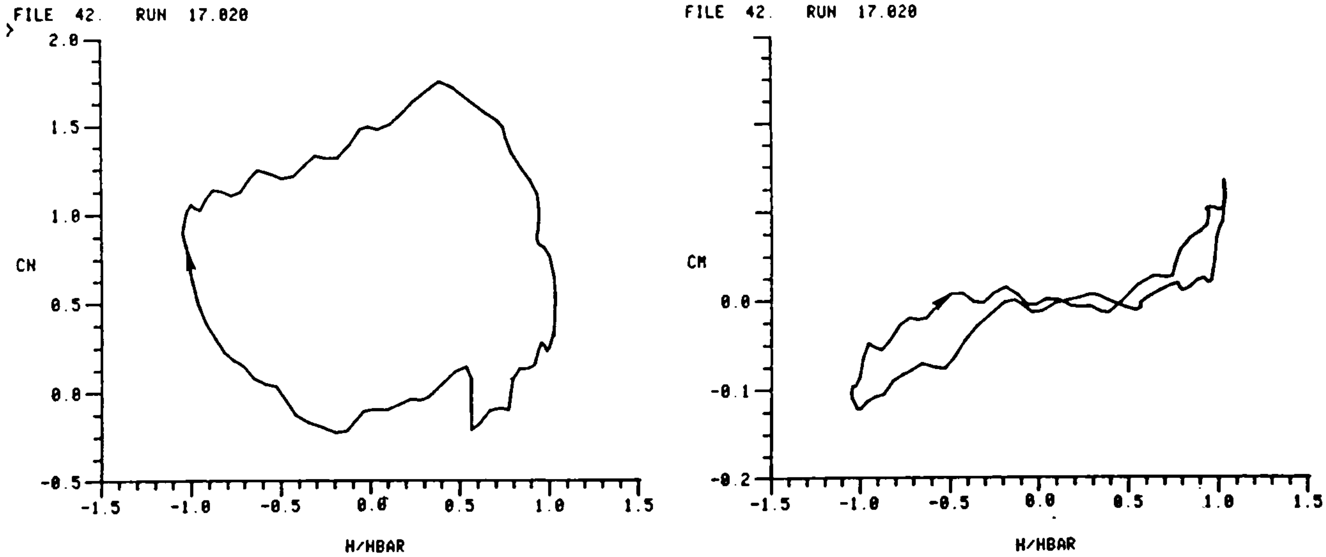

PITCH-PLUNGE EXPERIMENT: PLUNGING DATA VELOCITY = 77.4
MEAN INCIDENCE = 9.0 PLUNGING AMPLITUDE = .7
FREQUENCY = 10.728 (K = .2177)

Figure 71 Plunging Loops

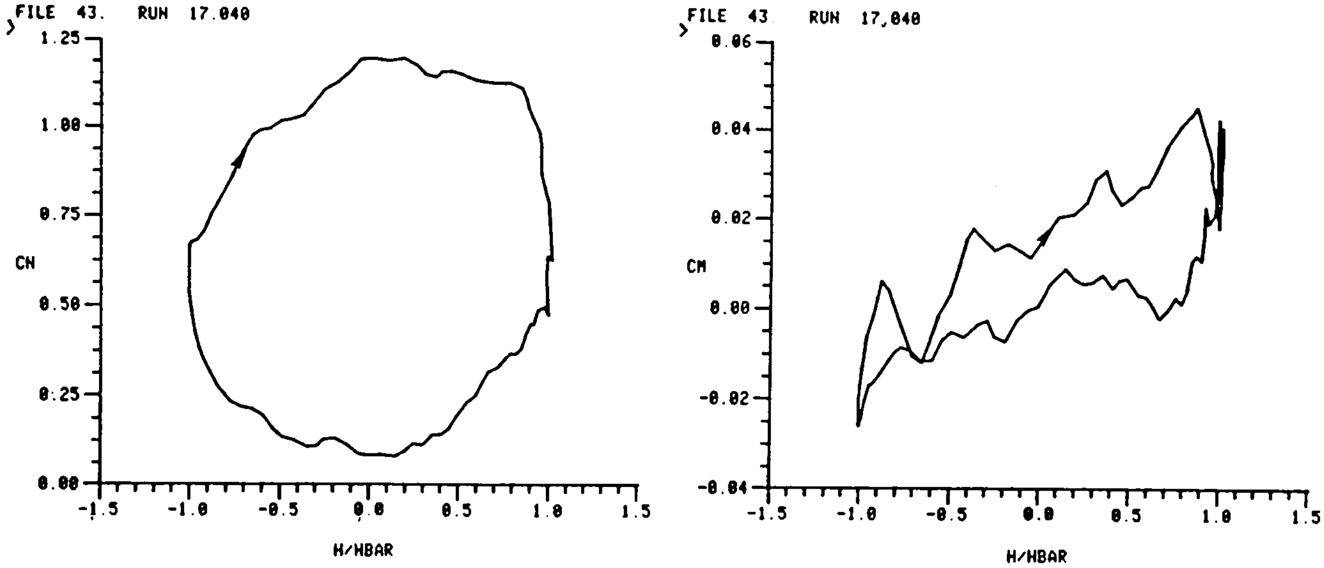

PITCH-PLUNGE EXPERIMENT: PLUNGING DATA VELOCITY = 100.2
MEAN INCIDENCE = 9.0 PLUNGING AMPLITUDE = .7
FREQUENCY = 8.297 (K = .1301)

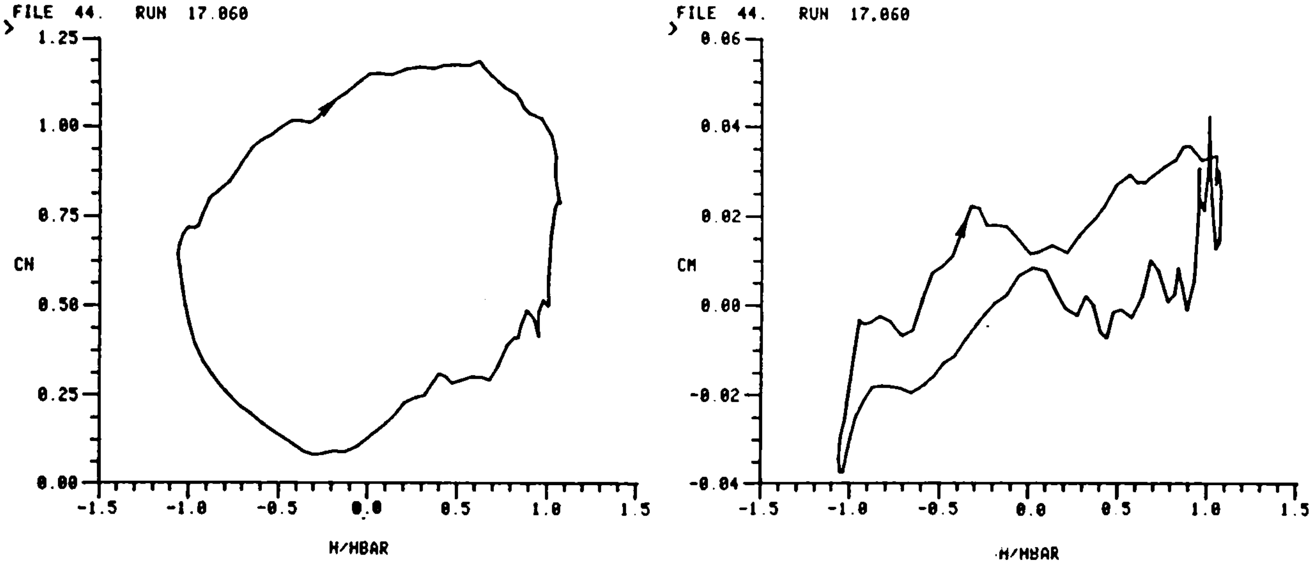

PITCH-PLUNGE EXPERIMENT: PLUNGING DATA VELOCITY = 122.5
MEAN INCIDENCE = 9.0 PLUNGING AMPLITUDE = .7
FREQUENCY = 10.823 (K = .1285)

Figure 72 Plunging Loops

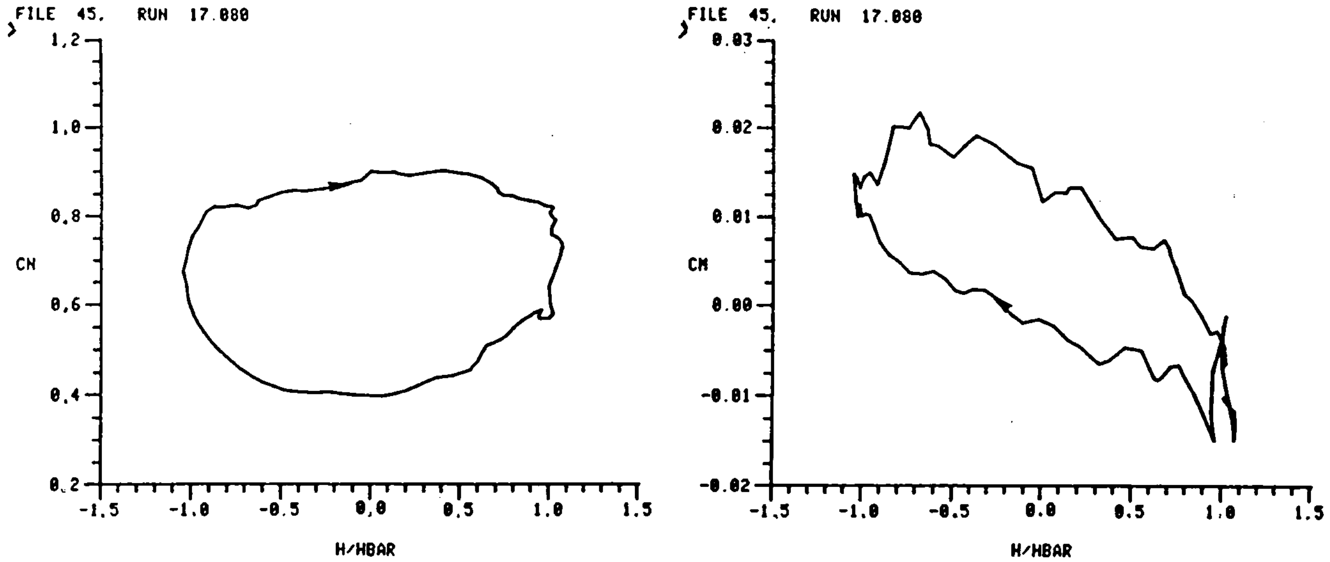

PITCH-PLUNGE EXPERIMENT: PLUNGING DATA VELOCITY = 204.5
MEAN INCIDENCE = 9.0 PLUNGING AMPLITUDE = .7
FREQUENCY = 6.619 (K = .0508)

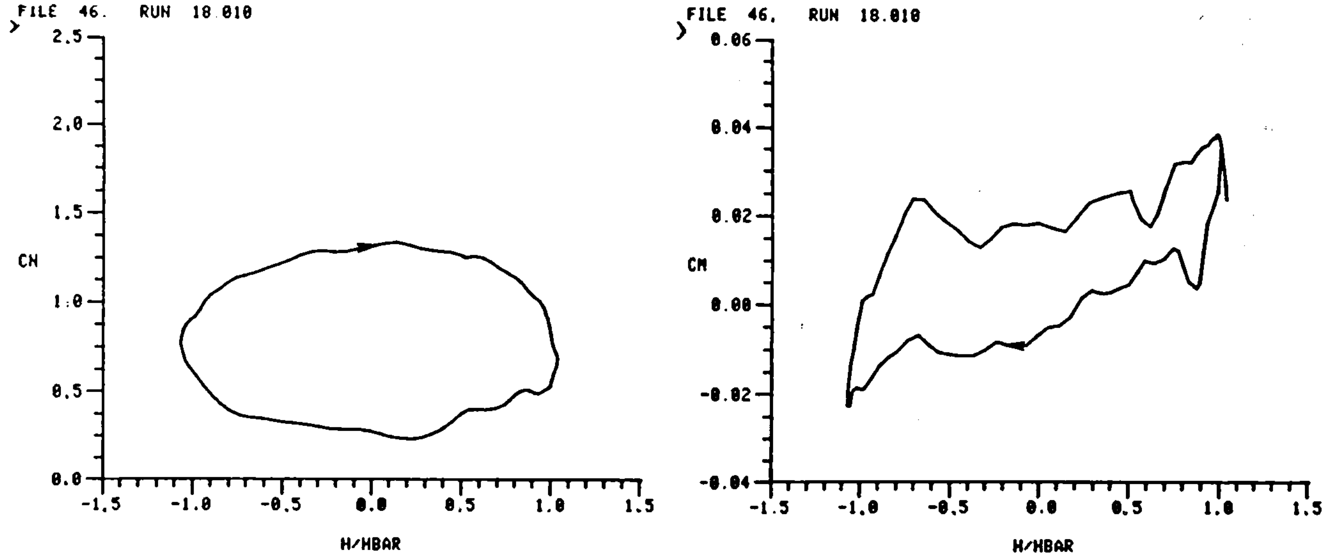

PITCH-PLUNGE EXPERIMENT: PLUNGING DATA VELOCITY = 100.2
MEAN INCIDENCE = 12.0 PLUNGING AMPLITUDE = .7
FREQUENCY = 8.282 (K = .1298)

Figure 73 Plunging Loops

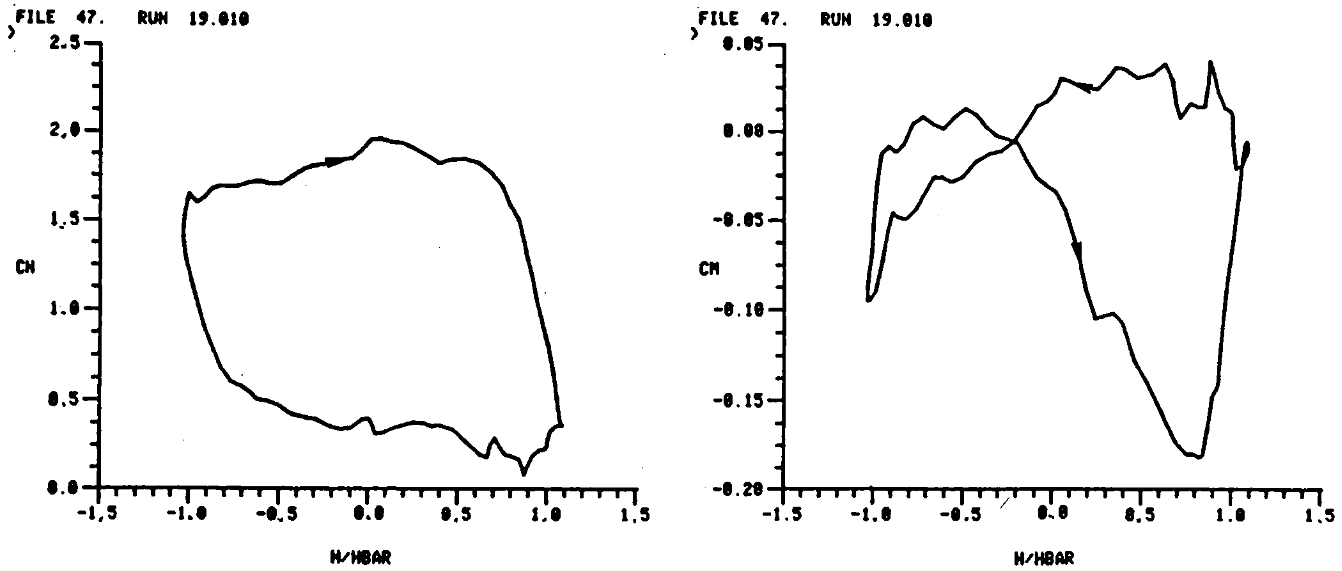

PITCH-PLUNGE EXPERIMENT: PLUNGING DATA VELOCITY = 79.1
MEAN INCIDENCE = 15.0 PLUNGING AMPLITUDE = .7
FREQUENCY = 10.730 (K = .2131)

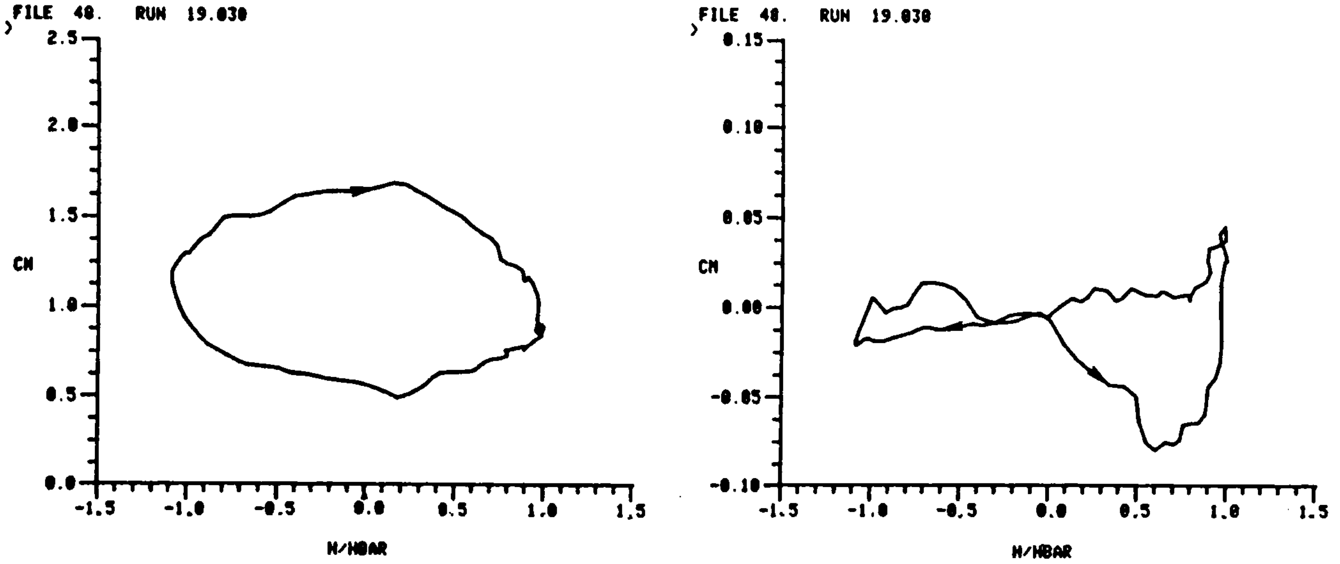

PITCH-PLUNGE EXPERIMENT: PLUNGING DATA VELOCITY = 100.0
MEAN INCIDENCE = 15.0 PLUNGING AMPLITUDE = .7
FREQUENCY = 8.312 (K = .1306)

**Figure 74 Plunging Loops**

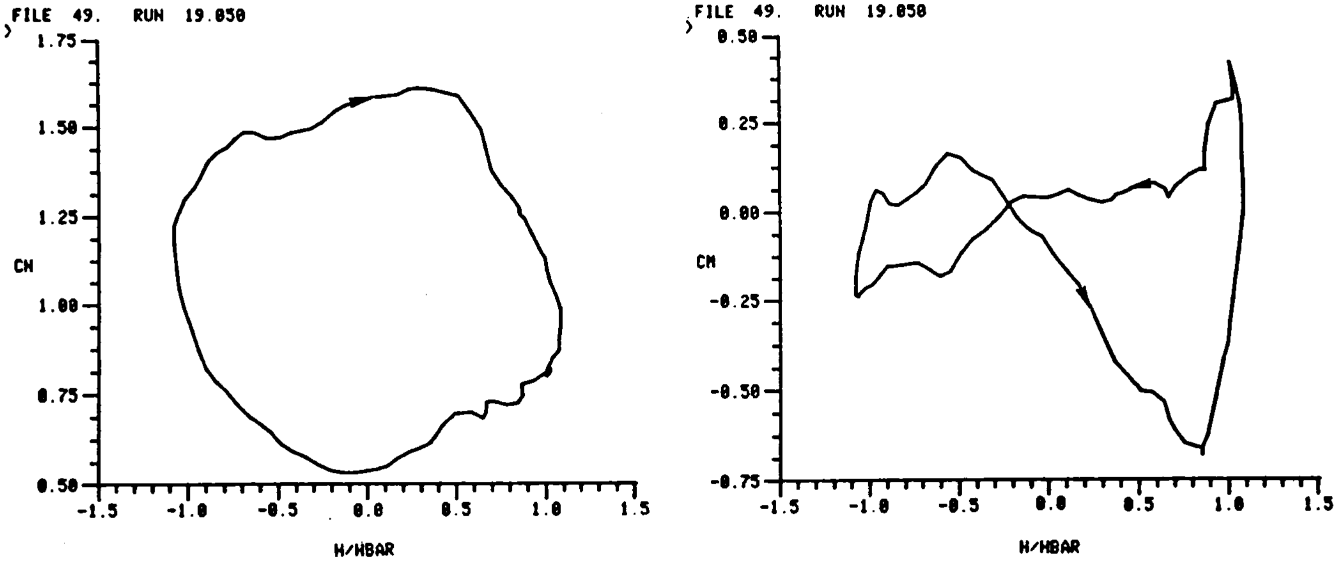

PITCH-PLUNGE EXPERIMENT: PLUNGING DATA VELOCITY = 122.6
MEAN INCIDENCE = 15.0 PLUNGING AMPLITUDE = .7
FREQUENCY = 9.989 (K = .1280)

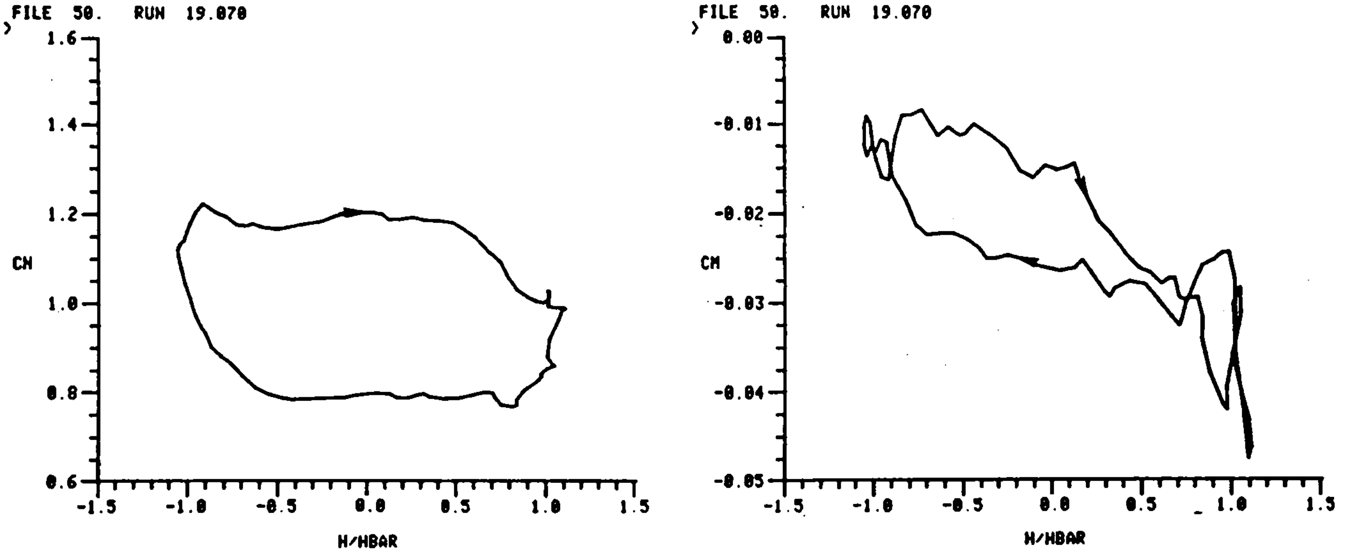

PITCH-PLUNGE EXPERIMENT: PLUNGING DATA VELOCITY = 202.7
MEAN INCIDENCE = 15.0 PLUNGING AMPLITUDE = .7
FREQUENCY = 6.658 (K = .0516)

**Figure 75 Plunging Loops**

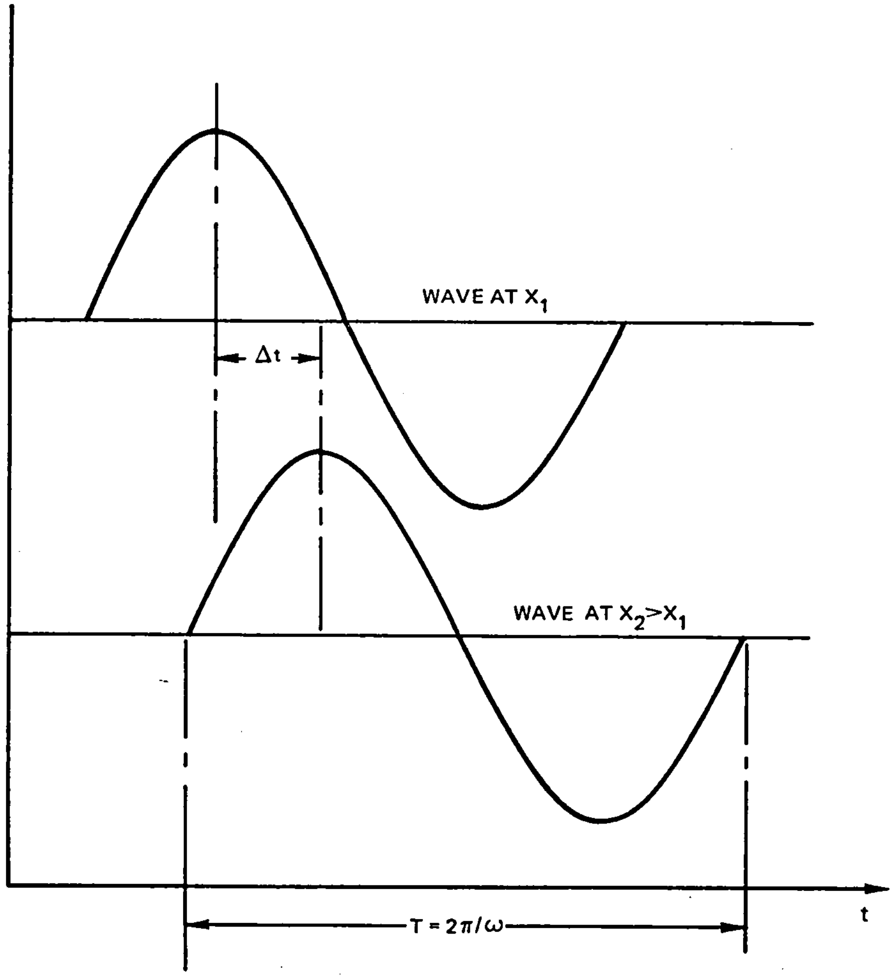

Figure 76 Schematic for Chordwise Wave Propagation

*U.S. GOVERNMENT PRINTING OFFICE: 1979 - 635-004/30

1. Report No.
NASA CR-3172

2. Government Accession No.

3. Recipient's Catalog No.

4. Title and Subtitle
A Comparison of the Pitching and Plunging Response of an Oscillating Airfoil

5. Report Date
October 1979

6. Performing Organization Code

7. Author(s)
Franklin O. Carta

8. Performing Organization Report No.

9. Performing Organization Name and Address
United Technologies Research Center
Silver Lane
East Hartford, Conn. 06108

10. Work Unit No.

11. Contract or Grant No.
NAS1-14012

12. Sponsoring Agency Name and Address
National Aeronautics and Space Administration
Washington, D.C. 20546

13. Type of Report and Period Covered
Contractor Report

14. Sponsoring Agency Code

15. Supplementary Notes
Langley Technical Monitor: Warren H. Young, Jr.
Final Report

16. Abstract
Unsteady aerodynamic experiments were conducted on an oscillating SC1095 airfoil model in rigid body single-degree-of-freedom pitch about its quarter chord, and also in rigid body single-degree-of-freedom plunge, to evaluate the ability of pitching data to model plunging motions. A one-to-one correspondence was established between pairs of pitching and plunging motions according to the potential flow transformation formula $\alpha = ikh$. The imposed variables of the experiment were mean incidence angle, amplitude of motion, free stream velocity, and oscillatory frequency.

The main objective of this program was to determine whether or not pitching and plunging data obtained according to the potential flow transformation formula were interchangeable via that formula. Over the range of parameters tested, it was found that significant differences exist between the aerodynamic responses to the two motions, particularly at high load conditions. This evaluation of the two motions was carried out by a direct comparison of force and moment loops, aerodynamic damping parameter variations, pressure time histories, pressure harmonic content, and hot film time histories.

The major finding of this study was that at high load conditions the normal force for equivalent pitch is significantly greater than that for true pitch at the same geometric incidence angle. In addition, the $C_N$ loops for equivalent pitch have higher slopes than those for true pitch. It appears that these differences are chordwise pressure manifestations of a major difference in the way in which stall flow breakdown occurs.

17. Key Words (Suggested by Author(s))

| | |
|---|---|
| Aerodynamic Testing | Pitching Oscillations |
| Dynamic Stall | Plunging Oscillations |
| Pitch-Plunge Comparison | Unsteady Aerodynamics |

18. Distribution Statement
Unclassified-Unlimited

Subject Category 02

| | | | |
|---|---|---|---|
| 19. Security Classif. (of this report) | 20. Security Classif. (of this page) | 21. No. of Pages | 22. Price* |
| Unclassified | Unclassified | 155 | $8.00 |

---

* For sale by the National Technical Information Service, Springfield, Virginia 22161

National Aeronautics and
Space Administration

Washington, D.C.
20546

NASA